Thermodynamic Uncertainty Relation for Stochastic Field Theories

General Formulation and Application to the Kardar-Parisi-Zhang Equation

Von der Fakultät Mathematik und Physik der Universität Stuttgart zur Erlangung der Würde eines Doktors der Naturwissenschaften (Dr. rer. nat.) genehmigte Abhandlung

vorgelegt von

Oliver Niggemann

aus Würzburg

Hauptberichter : Prof. Dr. Udo Seifert
Mitberichter : Prof. Dr. Siegfried Dietrich
Vorsitzender : Prof. Dr. Ronny Nawrodt

Tag der Einreichung : 02. Februar 2022
Tag der mündlichen Prüfung : 09. Mai 2022

II. Institut für Theoretische Physik der Universität Stuttgart

2022

Contents

List of Figures

List of Tables

Publications

Parts of this thesis have been published in:

[1] O. Niggemann and U. Seifert, 'Field-Theoretic Thermodynamic Uncertainty Relation – General Formulation Exemplified with the Kardar-Parisi-Zhang Equation',
J Stat Phys 178:1142-1174 (2020).
Parts of Chapter 3, Chapter 4 and parts of Chapter 5 are based on this publication.

[2] O. Niggemann and U. Seifert, 'Numerical Study of the Thermodynamic Uncertainty Relation for the KPZ-Equation',
J Stat Phys 182:25 (2021).
Chapter 3 and Chapter 7 are partly based on this publication.

[3] O. Niggemann and U. Seifert, 'The Two Scaling Regimes of the Thermodynamic Uncertainty Relation for the KPZ-Equation',
J Stat Phys 186:3 (2022).
Parts of Chapter 3, parts of Chapter 5, Chapter 6 and parts of Chapter 7 are based on this publication.

Zusammenfassung

Stochastische Feldtheorien zur Beschreibung von komplexem physikalischem Verhalten bilden ein wichtiges Themengebiet der statistischen Physik. Sie umfassen die Modellierung beispielsweise von Fluid-Turbulenz durch die Navier-Stokes Gleichungen sowie von nichtlinearem Oberflächenwachstum anhand der Kardar-Parisi-Zhang (KPZ) Gleichung. Beide Modelle waren und sind Gegenstand intensiver Forschung, sowohl vonseiten der statistischen Physik als auch der angewandten Mathematik. Trotz des beachtlichen Fortschritts und der Tatsache, dass beide Modelle seit geraumer Zeit bekannt sind, im Fall der KPZ Gleichung seit über dreißig Jahren und im Fall der Fluid-Turbulenz seit mehr als einem Jahrhundert, gibt es noch immer eine Vielzahl ungelöster Herausforderungen. Eine dieser Herausforderungen besteht in der jeweiligen Formulierung einer exakten, allgemeingültigen Lösung beider Gleichungen. Dennoch konnten mithilfe der dynamischen Renormalisierungsgruppentheorie in Verbindung mit der Theorie kritischer Phänomene und Skaleninvarianz Vorhersagen bezüglich des Verhaltens der Modelle auf großen Skalen und für lange Zeiten getroffen werden. Diese konnten sowohl numerisch als auch experimentell bestätigt werden.

Insbesondere in den letzten Jahren hat sich ein weiteres sehr aktives Forschungsgebiet in der statistischen Physik etabliert. Es beschreibt die thermodynamische Behandlung einzelner Trajektorien, die von stochastischen dynamischen Systemen erzeugt werden, und ist unter der Bezeichnung stochastische Thermodynamik bekannt. Im Rahmen der stochastischen Thermodynamik können beispielsweise Begriffe wie Wärme, Arbeit, innere Energie und Entropie entlang der zufälligen Trajektorie eines Brownschen Teilchens in einem Wärmebad definiert werden. Das Teilchen kann dabei dem Einfluss von konservativen wie auch nicht-konservativen Kräften ausgesetzt sein. Der Einfluss des Wärmebads wird über weißes Gaußches Rauschen (thermisches Rauschen) modelliert. Die Beschreibung eines solchen Systems erfolgt über Langevin Gleichungen. In Fällen, in denen die Trägheit des Teilchens von Bedeutung ist, spricht man von unterdämpften Langevin Gleichungen, wohingegen überdämpfte Langevin Gleichungen diese Trägheit außer Acht lassen. Das Beispiel des Brownschen Teilchens fällt unter die große Klasse von Modellen, die kein intrinsisches Gedächtnis besitzen. Man sagt auch, dass sie die Markov-Eigenschaft erfüllen. Statt mittels überdämpfter Langevin Gleichung können sie alternativ auch über eine Fokker-Planck Gleichung beschrieben werden. Deren Lösung liefert die Wahrscheinlichkeitsdichte für das Auffinden des Teilchens an einem bestimmten Ort zu einer gegebenen Zeit. Diese Wahrscheinlichkeitsdichte konvergiert unter bestimmten Voraussetzungen im Langzeitlimes entweder gegen eine stationäre Gleichgewichts-

oder Nichtgleichgewichts-Verteilung. Für eine überdämpfte Langevin-Dynamik wurde in [*Journal of Physics A: Mathematical and Theoretical* 50, 184004 (2017)] bewiesen, dass die sog. thermodynamische Unschärferelation (TUR) gilt. Sie wurde in [*Phys. Rev. Lett.* 114, 158101 (2015)] im Rahmen von Markov-Dynamiken in diskreten Netzwerken postuliert und verbindet die Präzision eines zufälligen Prozesses mit den thermodynamischen Kosten, die aufgebracht werden müssen, um diese Präzision zu garantieren. Das Produkt aus der Präzision des Prozesses und den thermodynamischen Kosten ist immer größer oder gleich zwei. Hierbei ist die Präzision definiert als das Quadrat des Variationskoeffizienten zeitintegrierter stromähnlicher Observablen und die Kosten über die totale Entropieproduktion.
Im Rahmen dieser Thesis wird eine Verbindung zwischen den Themengebieten der Feldtheorie und der stochastischen Thermodynamik hergestellt, indem die TUR für eine generische stochastische Feldtheorie verallgemeinert wird. Als Beispiel dieser allgemeinen Formulierung dient die KPZ Gleichung. Die Gültigkeit der TUR für die eindimenionale KPZ Gleichung wird analytisch gezeigt, wobei sich allerdings ergibt, dass die TUR nicht saturiert werden kann. Konkret bedeutet dies, dass das oben definierte Produkt aus Präzision und thermodynamischen Kosten immer strikt größer als zwei ist. In der Thesis wird nachgewiesen, dass dieses Produkt tatsächlich immer größer oder gleich fünf ist. Darüber hinaus wird die Abhängigkeit der TUR von der Stärke der Kopplung der Nichtlinearität sowohl analytisch also auch numerisch untersucht. In einem geeigneten Skalenbereich wird schließlich die TUR der KPZ Gleichung in höheren Raumdimensionen bestimmt, wobei gezeigt werden kann, dass sie für wachsende Dimensionen gegen ihre Saturierung strebt.

***Kapitel 2*:** Dieses Kapitel beinhaltet eine kurze Einführung in das Gebiet der stochastischen Thermodynamik. Insbesondere werden die Grundlagen zur Definition von Wärme, Arbeit, innerer Energie und Entropie längs einer Trajektorie, beschrieben durch eine überdämpfte Langevin Gleichung, erläutert. Auch die wahrscheinlichkeitstheoretische Beschreibung einer Langevin Gleichung, sowohl über das Pfadgewicht einer Trajektorie als auch über die korrespondierende Fokker-Planck Gleichung, werden beleuchtet. Von besonderer Bedeutung ist die stationäre Lösung der Fokker-Planck Gleichung sowie die Unterscheidung von stationären Gleichgewichts- und Nichtgleichgewichts-Zuständen. Die trajektorienabhängige Beschreibung der Entropie ist im weiteren Verlauf entscheidend für die Formulierung der TUR. Nach Einführung des Begriffs einer stromähnlichen Observablen wird die TUR formuliert.

***Kapitel 3*:** Ein weiteres wichtiges Konzept für diese Thesis ist das Skalenverhalten der KPZ Gleichung auf einem endlich ausgedehnten Substrat. Als Grundlage hierfür stellt dieses Kapitel zunächst einige Basisinformationen über die KPZ Gleichung zusammen, bezüglich ihrer allgemeinen Formulierung, physikalischen Bedeutung sowie ihres Phasenübergangs und ihrer Verbindung zu anderen, wohlbekannten stochastischen Feld-

theorien. Anschließend werden die Korrelationslängen der linearen (Edwards-Wilkinson (EW) Gleichung) und nichtlinearen Gleichung erläutert. Hierbei ist die sogenannte Oberflächenstärke eine wichtige Größe. Sie misst die Fluktuationen der KPZ Oberfläche um ihr räumliches Mittel. Ihr Skalenverhalten in Abhängigkeit von den jeweiligen Korrelationslängen wird erklärt und zur Einführung dreier Zeitskalen herangezogen, nämlich der 'EW nach KPZ'-Übergangszeit, der EW-Korrelationszeit sowie der KPZ-Korrelationszeit. Alle drei Zeiten sind essentiell zur Beschreibung der Varianz des räumlich gemittelten Höhenfeldes der KPZ Gleichung, welche wiederum eine wichtige Rolle in der feldtheoretischen KPZ-TUR spielt.
In den Anhängen dieses Kapitels werden einige für die folgende Analysis nützliche mathematische Werkzeuge dargestellt. Außerdem werden Fragen zur Regularität der KPZ Gleichung kurz behandelt.

***Kapitel 4*:** Im ersten Teil dieses Kapitels wird die Verallgemeinerung der Bestandteile der TUR von Kapitel 2 hin zu einer feldtheoretischen Formulierung vorgestellt. Sie basiert auf Analogien zu den Begrifflichkeiten, die zur TUR für endlich dimensionale Langevin Gleichungen benötigt werden. Als Abschluss dieses ersten Teils wird die TUR für eine generische stochastische Feldtheorie formuliert.
Eine Anwendung der allgemeinen Darstellung des ersten Teils auf ein einfaches Beispielsystem erfolgt im zweiten Teil dieses Kapitels. Es besteht aus der EW Gleichung, welche von einer konstanten, externen 'Kraft' aus ihrem Gleichgewichtszustand getrieben wird (FEW). Anhand der FEW Gleichung wird detailliert das Vorgehen zur Berechnung aller Anteile der feldtheoretischen TUR dargelegt. Die Saturierung der FEW-TUR ist von Bedeutung in Kapitel 5, in dem gezeigt wird, dass die KPZ-TUR nicht saturiert.

***Kapitel 5*:** Dieses Kapitel befasst sich mit der Berechnung der TUR für die KPZ Gleichung selbst. Im ersten Teil wird eine sehr allgemeine Herangehensweise zur Darstellung der feldtheoretischen KPZ-TUR vorgestellt, welche auch auf andere stochastische Feldtheorien übertragbar ist. Dieses Vorgehen beinhaltet eine perturbative Approximation der KPZ Lösung bezüglich des Kopplungsparameters der Nichtlinearität und eine anschließende Berechnung der TUR Anteile in niedrigster, nicht verschwindender Ordnung. Die resultierende TUR wird im Grenzfall schwacher Kopplung verwendet, und es wird gezeigt, dass sie nicht saturiert werden kann.
Im zweiten Teil wird eine Vorgehensweise herangezogen, die auf der Annahme der sogenannten Quasinormalität beruht. Diese Annahme begrenzt die generelle Anwendbarkeit, kann aber für den Fall der KPZ Gleichung gerechtfertigt werden. Auf diesem Weg wird die Berechnung höherer Ordnungen deutlich vereinfacht, was die Darstellung der TUR in höherer Perturbationsordnung ermöglicht. Beide Herangehensweisen sind allerdings auf den linearen Skalenbereich der KPZ Gleichung beschränkt.
Im letzten Teil werden anhand der stationären Wahrscheinlichkeitsverteilung der eindimensionalen KPZ Gleichung gleichzeitige Korrelationsfunktionen im stationären Zustand

berechnet. Dieses Vorgehen ist in allen Skalenbereichen der KPZ Gleichung gültig. Da die KPZ-TUR zum Teil aus solchen Korrelationsfunktionen aufgebaut ist, kann hier ein exaktes Zwischenergebnis angegeben werden. Dieses hängt nur noch von einem nicht exakt bekannten Anteil ab, nämlich der Varianz des räumlich gemittelten Höhenfeldes. Da sie mittels einer zeitlichen Zweipunkt-Korrelation berechnet wird, kann sie nicht nach dem soeben beschriebenen, exakten Vorgehen erhalten werden. Im nächsten Kapitel wird sie für alle Skalenbereiche der KPZ Gleichung approximiert.
Die Anhänge dieses Kapitels enthalten Detailrechnungen zu den hier vorgestellten Ergebnissen, sowie weitere relevante Kommentare zur Regularität der KPZ Gleichung.

***Kapitel 6*:** Hier wird die Erweiterung der KPZ-TUR von Kapitel 5, gültig im EW Skalenbereich, hin zu einer Formulierung der TUR in allen Skalenbereichen dargestellt. Aus dem letzten Kapitel ist bekannt, dass einzig die Varianz des räumliche gemittelten Höhenfeldes noch nicht im genuinen KPZ Skalenbereich vorliegt. Mittels dynamischer Renormalisierungsgruppentheorie und der Äquivalenz zwischen der KPZ und stochastischen Burgers Gleichung (siehe Kapitel 3) kann auch die Varianz in allen Skalenbereichen der KPZ Gleichung angegeben werden. Ein Zwischenergebnis dieser Vorgehensweise ist eine explizite Approximation der Zweipunkt-Korrelationsfunktion für die eindimensionale Burgers Gleichung im Impulsraum.

***Kapitel 7*:** Der Vergleich zwischen direkter numerischer Simulation und theoretischen Vorhersagen aus den Kapiteln 5, 6 bezüglich der TUR der eindimensionalen KPZ Gleichung ist Gegenstand dieses Kapitels.
Zunächst wird das verwendete numerische Vorgehen erläutert. Bezüglich der zeitlichen Diskretisierung kommt ein stochastisches Heun Schema zum Einsatz. Mit Blick auf die räumliche Diskretisierung bedarf es einiger Vorsicht. Es ist bekannt, dass, aufgrund der schlechten Regularitätseigenschaften der KPZ Lösung, verschiedene literaturbekannte Diskretisierungen der Nichtlinearität zu stark unterschiedlichen Ergebnissen führen. Daher wird die am besten geeignete Diskretisierung ausgewählt und im Weiteren angewendet.
Im zweiten Teil des Kapitels wird das Skalenverhalten der theoretischen Ausdrücke auf die für die Numerik relevanten Größen übertragen.
Der letzte Teil umfasst den eigentlichen Vergleich der Numerik mit der Theorie. Er ist gegliedert in einen ersten Abschnitt, der sich mit der Simulation der KPZ Gleichung im EW Skalenbereich und dem Grenzfall schwacher Kopplung befasst. An den Stellen, an denen die theoretischen Ausdrücke exakt bekannt sind, wird dieser Abschnitt außerdem als Test für die Approximationseigenschaften des numerischen Verfahrens herangezogen. Der zweite Abschnitt beinhaltet numerische Ergebnisse in beiden Skalenbereichen der KPZ Gleichung, welche wieder mit den theoretischen Angaben aus den Kapiteln 5, 6 verglichen werden.
Es lässt sich eine zufriedenstellende Übereinstimmung zwischen der Numerik und den

theoretischen Vorhersagen in allen Bereichen feststellen. Jedoch ergibt sich, selbst für die oben erwähnte beste räumliche Diskretisierung der Nichtlinearität, eine systematische Unterschätzung der Entropieproduktion und damit der TUR selbst. In den Anhängen wird gezeigt, dass diese Unterschätzung eine intrinsische Eigenschaft der Diskretisierungen der Nichtlinearität darstellt.

***Kapitel 8*:** Das letzte Kapitel befasst sich mit der Berechnung der KPZ-TUR in höheren Dimensionen. Dazu werden Informationen über den KPZ Phasenübergang (siehe Kapitel 3) mit der Methodik der dynamischen Renormalisierungsgruppe aus Kapitel 6 kombiniert. Letztere ist nur unterhalb der Phasenseparationslinie anwendbar. In diesem linearen Skalenbereich wird eine von der Raumdimension abhängige TUR hergeleitet. Im Grenzfall schwacher Kopplung wird gezeigt, dass sich die TUR für wachsende Dimension dem Wert zwei von oben annähert.

Summary

A very prominent area in statistical physics is the stochastic field-theoretic description of physically complex behavior. It encompasses the modeling of, e.g., fluid turbulence via the Navier-Stokes equation and non-linear surface growth via the Kardar-Parisi-Zhang (KPZ) equation. Both of these models have been and are still subject to very extensive studies in the statistical physics community as well as from the side of applied mathematics. Despite the considerable progress made and the fact that the models are known for quite some time, in the case of the KPZ equation, for over thirty years and, in the case of fluid turbulence, for over a century, there are still quite a few open problems. For example, the derivation of a general exact solution to either of these equations is still a highly discussed topic. However, especially with the aid of dynamic renormalization group theories combined with the theory of critical phenomena and scale-invariance, asymptotic large-scale, long-time predictions of these models have been made and verified by means of numerical simulations as well as direct experimental measurements.
Another highly active field in statistical physics, especially in recent years, is the thermodynamic treatment of single trajectories generated by stochastic dynamical systems. It has become known by the name stochastic thermodynamics. To give an example, stochastic thermodynamics yields a tool to define notions like heat, work, internal energy and entropy along a single trajectory of a Brownian particle possibly subject to conservative and non-conservative forces in a heat bath. The influence of the heat bath is modeled via Gaussian white noise with zero mean (thermal noise). Such a system is described by a Langevin equation, which may either be underdamped, i.e., the inertia of the particle enters explicitly, or overdamped, i.e., inertia is neglected in the equation of motion. The example of a Brownian particle is representative of a wide class of models that have no intrinsic memory, i.e., they obey Markovian dynamics. Instead via an overdamped Langevin equation, they may equivalently be described by a Fokker-Planck equation, which yields the probability density function to find the particle at a certain position for a given time. Under suitable assumptions this probability density function converges in the long-time limit either to an equilibrium or to a so-called non-equilibrium steady state distribution. For overdamped Markovian Langevin dynamics in a non-equilibrium steady state, it has been proven in [*Journal of Physics A: Mathematical and Theoretical* 50, 184004 (2017)] that the so-called thermodynamic uncertainty relation (TUR) holds. It was first proposed in [*Phys. Rev. Lett.* 114, 158101 (2015)] for Markovian dynamics on a discrete set of states and links the precision at which a certain process operates to the thermodynamic cost necessary to guarantee this precision. The

product of the precision, defined as the squared variational coefficient of time-integrated current-like variables, with the thermodynamic cost, measured by the total entropy production, is always greater or equal than two.
In this thesis, a link between field theory and stochastic thermodynamics is established by formulating an extension of the TUR to a generic stochastic field theory. This general framework is then applied to the KPZ equation. It is shown analytically, that the TUR holds for the KPZ equation in one spatial dimension, however, it cannot be saturated, i.e., the above defined product of precision and thermodynamic cost is always strictly greater than two. In fact, it is shown to have a value of at least five. Further, the dependence of the TUR product on the scaling behavior of the KPZ equation is analyzed analytically as well as numerically. Finally, the field theoretic TUR of the KPZ equation in higher spatial dimensions is studied in an appropriate scaling regime. It is shown that the TUR product tends to saturation for growing spatial dimension.

***Chapter 2*:** In this chapter, a brief introduction to the field of stochastic thermodynamics is given. It focuses on the basic concepts needed to define thermodynamic notions like heat, entropy, internal energy and work on the level of a single trajectory described by an overdamped Langevin equation. Further, the probabilistic description of such a Langevin equation is discussed, both via the path-weight of a single trajectory as well as via the Fokker-Planck equation corresponding to the Langevin equation. In particular, the stationary solution of the Fokker-Planck equation and the distinction between equilibrium and non-equilibrium stationary states is discussed.
The trajectory-dependent formulation of notions like the entropy production is crucial for the formulation of the TUR. This relation is stated for current-like variables, which are also defined in this chapter. Finally, some general remarks on the extension of the above notions to higher dimensional systems are given.

***Chapter 3*:** Another important topic in this thesis is the scaling behavior of the KPZ equation on a finite substrate. To discuss this matter, the chapter first provides some basic background on the KPZ equation in terms of its general formulation, its physical interpretation and phase transition as well as the relation to other well-known stochastic field theories. Subsequently, the correlation lengths of both the linear (Edwards-Wilkinson (EW) equation) and non-linear equation is explained. In this aspect, a quantity of particular interest is the so-called surface width, which measures the fluctuations of the KPZ surface height around its spatial mean. Its scaling behavior in dependence on the respective correlation lengths is presented. Using this scaling behavior, three characteristic time-scales are introduced, the EW to KPZ crossover time, the EW correlation time and the KPZ correlation time. These three times are crucial for the description of the variance of the spatially averaged KPZ height field, which itself turns out to be an integral part of the field-theoretic TUR for the KPZ equation.
In the appendices of this chapter, some mathematical tools useful in the subsequent

analysis are introduced and, further, comments on the regularity of the KPZ equation are made.

***Chapter 4*:** The first part of this chapter is devoted to the generalization of the quantities constituting the TUR from Chapter 2 to the case of a TUR for stochastic field theories. The definitions in this chapter are based on the analogy to the formulation of the TUR for finite-dimensional Langevin equations. At the end of the first part, the field-theoretic thermodynamic uncertainty relation is stated.
The second part of this chapter shows the application of the general formulation to a model system that is simple enough to be still instructive, namely, the EW equation driven out of equilibrium by a constant external 'force' (FEW). In particular, all steps necessary in the derivation of the constituents of the field-theoretic TUR are demonstrated in detail. The result that the TUR for the FEW is saturated, plays an important role in Chapter 5, where it is shown that the KPZ-TUR cannot saturate.

***Chapter 5*:** This chapter deals with establishing the TUR for the KPZ equation itself. In the first part, a very general approach to the derivation of a field-theoretic TUR, which may also be applied to other stochastic field theories, is discussed and exemplified with its application to the KPZ equation. This approach constitutes a perturbative approximation of the KPZ-solution with respect to the coupling parameter of the non-linearity and a subsequent calculation of the TUR constituents to lowest non-vanishing order. The resulting TUR is used in the weak-coupling limit and it is demonstrated that the KPZ-TUR cannot be saturated.
In the second part, a more tractable approach is shown, which relies on the key assumption of so-called quasi-normality. This assumption limits its applicability. However, for the case of the KPZ equation, it may be justified. Using this approach, approximations of the TUR to higher orders are feasible and are calculated explicitly. It has to be noted, however, that, as shown in this chapter, both of the prior approximations are inherently limited to the linear scaling regime of the KPZ equation.
The last part of this chapter uses the explicit knowledge of the stationary probability distribution for the one-dimensional KPZ equation to calculate equal-time steady state correlations exactly in all scaling regimes. Since the TUR is partly built via such equal-time correlations, an intermediate exact result for the KPZ-TUR is given. It still depends on only one, exactly unknown, quantity, namely, the variance of the spatially averaged height field. As this is obtained via a two-time correlation function, which cannot be evaluated in the above framework, it is determined in the next chapter.
The appendices contain detailed calculations for the derivation of the key results in this chapter as well as further comments on regularity issues of the KPZ equation.

***Chapter 6*:** In this chapter, the TUR for the KPZ equation is extended from the linear (EW) scaling regime to arbitrary scaling regimes, in particular to the non-linear

(KPZ) one. Since it was shown in the last part of Chapter 5 that the variance of the spatially averaged height field is so far known in the EW regime only, it will be calculated in this chapter in the KPZ regime. To this end, a dynamic renormalization group procedure and the equivalence of the one-dimensional KPZ equation to the noisy Burgers equation, discussed in Chapter 3, is employed. An intermediate result of this approach is an explicit approximate form of the two-point correlation function in wavenumber space for the one-dimensional Burgers equation. It allows for stating the TUR in the KPZ scaling regime.

***Chapter 7*:** Having derived the thermodynamic uncertainty relation for the one-dimensional KPZ equation in both its linear and non-linear scaling regimes in Chapters 5 and 6, respectively, a comparison between the theoretical predictions and direct numerical simulations is presented in this chapter.
In the first part, the numerical scheme for the direct simulation of the one-dimensional KPZ equation is explained. A stochastic Heun method is used for the time discretization. Regarding the spatial discretization care has to be taken when discretizing the non-linearity. As is well known, due to the poor regularity of the KPZ-solution, different popular discretizations may lead to significantly different results. An optimal discretization is identified and employed.
In the second part, the scaling forms of the theoretical predictions in terms of the numerical parameters are derived.
The last part of this chapter contains the actual comparison of the numerical data to the theoretical predictions. It is split into a first section dealing with simulations of the KPZ equation in its linear scaling regime, especially in the weak-coupling limit. This section is also used as a test of accuracy of the employed numerical scheme for those cases where the analytically obtained scaling forms are known to be exact. The second section shows numerical results in both scaling regimes, which are again compared to the corresponding theoretical predictions from Chapters 5 and 6.
The numerical simulations show an overall convincing agreement with the analytical predictions. However, even for the optimal discretization from above, a systematic underestimation of the entropy production and consequently of the TUR itself remains. Via an analytical argument it is shown in the appendices that this underestimation is an intrinsic property of the discretizations of the non-linearity.

***Chapter 8*:** The last chapter is aimed at calculating the TUR for the KPZ equation in higher dimensions. To this end, the knowledge of the phase transition of the KPZ equation from Chapter 3 and the dynamic renormalization group technique from Chapter 6 are combined. The applicability of the dynamic renormalization group is limited to the region below the phase-separation line of the KPZ roughening transition. In this linear scaling regime, a TUR depending on the spatial dimension is derived and it is shown that the value of the TUR product in the weak-coupling limit tends to two from above for growing space dimension.

1 Introduction

During the 19th century, classical equilibrium thermodynamics has been developed, at least at the beginning inspired by the invention of steam engines some decades earlier. Since then, classical thermodynamics has provided a framework to quantify the change of variables like heat, work, internal energy and entropy when a system transitions from one equilibrium state to another. Prominent applications of this theory since the late 19th century were heat engines like the Otto or Diesel engine. Equilibrium thermodynamics allows for the macroscopic description of a system via some externally measurable quantities without any knowledge of the underlying microscopic dynamics. In the case of, e.g., a heat engine, the actual processes taking place between the single gas particles in its cylinder, which drive the working piston, are unknown.
A description on the level of these single particles was devised in the late 19th and early 20th century. It became known under the name of statistical mechanics or, equivalently, statistical thermodynamics. This framework uses a multi-particle Hamiltonian formalism, where the full Hamiltonian encompasses all possible microscopic configurations that the system may assume. With each individual energetic configuration one associates a statistical weight, the Boltzmann weight. Summing all allowed weights over the complete configuration space leads to the so-called partition function. The logarithm of the partition function is linked to the Helmholtz free energy of the system, which is a notion from classical thermodynamics. Hence, this relation provides a bridge between the microscopic and macroscopic description of a system. Once the free energy is known, further macroscopic variables can be obtained, solely using the formalism of classical thermodynamics. The Hamiltonian framework provides swift insight into the microscopic physics leading to the macroscopic observations in classical thermodynamics, when particle interactions can be neglected. While the general approach stays viable in more complex cases, where particle interactions, chemical reactions and changes in particle number are relevant, the necessity of having to know all energetic consequences of every single interaction somewhat limits its practicability.
In recent years, a third thermodynamic approach has become popular, which is neither on the macroscopic nor microscopic scale but rather on a mesoscopic scale. Such a mesostate may, for example, be the trajectory of a colloidal particle in a liquid medium at a certain temperature.
Instead of keeping track of every single interaction of the particle with the particles in the medium, one can model these interactions via a thermal noise. The equation of motion of the particle is then given by the so-called Langevin equation, introduced in

1908 by P. Langevin. Intrinsically, a Langevin equation models Markovian dynamics, i.e., the configuration of a system at a certain time does not depend on the history of its evolution. In cases where inertia is of importance, the corresponding Langevin equation is called underdamped, whereas in situations for which inertia may be neglected in the equation of motion, the Langevin equation is called overdamped. In either case, the particle position in this mesoscopic description via Langevin equations is a stochastic quantity. This is the trade-off one has to accept when choosing to simplify the microscopic description with its numerous individual interactions via a Langevin description.
While modeling the dynamics of Brownian motion has been known since the early 20th century, the link to thermodynamics was established not earlier than in 1998 by K. Sekimoto in his work on 'Langevin Equation and Thermodynamics' [4]. He presented a way to calculate changes in work, heat and internal energy, when a Brownian particle, confined by a potential and embedded in a heat bath, moves along its trajectory. This thermodynamic picture was further developed by U. Seifert, who introduced in 2005 the notion of total entropy production along a single stochastic trajectory [5]. The thermodynamic description on a trajectory (mesoscopic) level has become known under the term stochastic thermodynamics. In contrast to the first two thermodynamic frameworks from above, stochastic thermodynamics is not a strict equilibrium theory, but is also valid for systems in genuine non-equilibrium states.
One of the many possible applications of stochastic thermodynamics in its continuous Langevin framework is the thermodynamic description of active Brownian particles. Applications are also plentiful in the case of a discrete set of mesostates like, e.g., Markovian networks, molecular motors and biochemical oscillators.
In 2015 A.C. Barato and U. Seifert postulated a relation connecting entropy production with precision of current-like variables, defined via their squared variational coefficient, in a non-equilibrium steady state for Markovian networks [6]. In particular, this relation, now known as the thermodynamic uncertainty relation (TUR), states that the product of the entropy production with the precision is always greater or equal to two. From a physical point of view, the TUR indicates a trade-off between a certain amount of precision and the associated thermodynamic cost to maintain that precision in form of the entropy production. The postulated relation has been proven for Markovian networks in [7] by T.R. Gingrich, J.M. Horowitz et al. and extended to overdamped Langevin dynamics in [8] by T.R. Gingrich, G.M. Rotskoff and J.M. Horowitz. The proof uses large deviation theory to derive the lower bound of two. Since its introduction, the thermodynamic uncertainty relation has been subject to considerable attention in the statistical physics community. For recent reviews on this topic see, e.g., [9–11] and the references therein.

Another highly active field of interest, albeit being around since 1986, is the Kardar-Parisi-Zhang (KPZ) equation [12] and its universality class. It is one of the most prominent examples of stochastic field theories and critical out-of-equilibrium behavior. For his contribution to this field of theoretical physics, G. Parisi was awarded the Nobel prize

in physics in 2021. In its original intent, the KPZ equation models non-linear surface growth on a substrate via the time evolution of a height field. For example, widely used models for the description of molecular beam epitaxy rely on the KPZ equation [13] and variations of it [14]. Due to the non-linear nature of the KPZ equation, analytical treatment is a rather involved matter. One of the most-employed techniques is the dynamic renormalization group approach combined with scaling theory, which led to analytic results for the critical exponents characterizing the KPZ universality class. In more recent years, another characterization of the KPZ universality class has become possible via a probability density functional of the height field derived by C.A. Tracy and H. Widom [15–17], which has been experimentally observed by T. Iwatsuka, T. Fukai and K.A. Takeuchi, see [18] and references therein.
Of particular interest is on one hand the scaling behavior of the KPZ equation in one spatial dimension on a finite substrate, which displays two distinct scaling regimes. One is the linear scaling regime associated with the linearized KPZ equation, namely the Edwards-Wilkinson (EW) equation [19]. It is characterized by the critical EW exponents. The second scaling regime is the genuine non-linear KPZ scaling regime with critical exponents according to the non-linear theory.
On the other hand, for higher dimensions, the KPZ roughening phase transition and its implications on the analytical treatment within the dynamic renormalization group framework is another crucial aspect. For reviews covering the wide field of the KPZ equation and its universality class see, e.g., [20–22].

The aim of this thesis is to connect field theory with stochastic thermodynamics by extending the framework of the TUR for overdamped Langevin equations to a generic stochastic field theory. This general concept is then applied to the KPZ equation using three different analytical approaches, depending on the particular setting, i.e., whether the KPZ equation is analyzed in its linear or non-linear scaling regime. Within all of the approaches, it is shown that the TUR holds for the KPZ equation on a finite substrate. Furthermore, for the case of one spatial dimension, it is demonstrated that the TUR cannot be saturated. To be more specific, the TUR for the one-dimensional KPZ equation turns out to be greater or equal to five instead of two. The exact value is linked directly to the coupling strength of the KPZ non-linearity. To show this link, dynamic renormalization group techniques are employed to calculate an explicit approximate expression for the stationary scaling function of the KPZ equation.
Still in the one-dimensional case, the analytically obtained scaling forms of the constituents of the TUR as well as for the TUR product itself are compared to direct numerical simulations of the KPZ equation in the linear and non-linear scaling regime. For the former case, where two of the scaling forms of the individual constituents are shown to be exact, the comparison between the analytical and numerical results additionally serves as a test of accuracy of the numerical scheme. It is found that the numerical scheme intrinsically underestimates the TUR product. The cause of this underestimation is analyzed and explained analytically. Ultimately, very satisfying agreement between

the analytical and numerical results are observed.
Finally, an approach to tackle the TUR for the KPZ equation in higher spatial dimensions is presented using dynamic renormalization group calculations. Due to the fixed-point structure in the phase diagram of the KPZ roughening transition, it can be demonstrated that those calculations apply to the linear scaling regime only. In this regime, an analytic expression is derived for the TUR product depending on the spatial dimension. A numerical evaluation of this expression suggests that for growing spatial dimensions the value of the TUR product tends to two from above, i.e., for infinitely large dimension the TUR will be saturated.

2 Background on Stochastic Thermodynamics

This chapter is meant to give a brief introduction to the wide topic of stochastic thermodynamics, which deals with the dynamics of mesoscopic physical systems in contact with a heat bath. The random interaction between the system and the heat bath generates a stochastic trajectory of the system. This dynamics may in the continuous case be described via a Langevin equation. For the most parts of this chapter, we will focus on the notions and concepts that are necessary for the analysis in the subsequent chapters. In particular, we give an introduction to the framework of stochastic energetics, which defines analogs to the classical thermodynamic quantities like heat, work, internal energy and entropy at the level of a single stochastic trajectory. Anticipating the nature of the systems studied in the subsequent chapters, we restrict ourselves to trajectories generated by an overdamped Langevin equation. Furthermore, the thermodynamic uncertainty relation for current-like observables will be introduced. For the sake of brevity, we refrain from discussing, e.g., work relations (see, e.g., [23]), which make up a significant part of stochastic thermodynamics, however, have no direct influence on the topics discussed in this thesis.

2.1 Some Notions Concerning Stochastic Energetics

2.1.1 A Basic Approach to Stochastic Heat, Work and the First Law

As a first step, we establish the first law of thermodynamics for a generic overdamped Langevin equation following the arguments from [4, 24]. Consider the position x of a particle confined in a potential $U(x, \lambda)$, with λ an external control parameter, placed in a heat bath of temperature T. Then the overdamped dynamics of such a particle is described by

$$\gamma \frac{d\,x}{dt} = -\frac{\partial\, U(x, \lambda)}{\partial x} + \eta(t), \tag{2.1}$$

where γ denotes a friction coefficient and $\eta(t)$ represents thermal noise, i.e.,

$$\langle \eta(t) \rangle = 0\,, \qquad \big\langle \eta(t)\, \eta(t') \big\rangle = \Delta_0 \delta(t - t'), \tag{2.2}$$

with Δ_0 measuring the noise strength. Let us rearrange (2.1) as

$$0 = -\gamma \frac{d\,x}{dt} + \eta(t) - \frac{\partial\, U(x, \lambda)}{\partial x}, \tag{2.3}$$

and identify the respective terms in this balance of forces. The first two terms on the r.h.s. of (2.3) together, represent the force exerted by the heat bath on the particle, where the first represents the systematic force and the second one denotes the fluctuating force. The third term describes the force caused by the potential U. Multiplying (2.3) by $-dx$, yields the energy balance

$$0 = \left(\gamma \frac{d\,x}{dt} - \eta(t)\right) dx + \frac{\partial\, U(x,\lambda)}{\partial x}\, dx, \tag{2.4}$$

where the external parameter λ has been held fixed. The force in the brackets on the r.h.s. of (2.4) is interpreted as the reaction force of the particle to the influence of the heat bath. We identify the work done by this reaction force along dx as the heat increment $đq$ dissipated by the system into the heat bath,

$$đq \equiv \left(\gamma \frac{d\,x}{dt} - \eta(t)\right) dx. \tag{2.5}$$

Note, that the sign of the dissipated heat is opposite to the sign convention in classical thermodynamics, where heat transfer from the system to the environment has a negative sign. In other words, we view heat from the perspective of the heat bath, since the amount of dissipated heat from the system leads to an increase in entropy of the environment. Assuming that the external parameter λ of the potential U is changed according to some prescribed protocol, the differential dU may be completed, $dU = \partial_x U dx + \partial_\lambda U d\lambda$. Adding the second contribution to both sides of (2.4) leads with (2.5) to the energy balance

$$đq + dU = đw. \tag{2.6}$$

In (2.6), we identified the work applied to the system as

$$đw \equiv \frac{\partial\, U(x,\lambda)}{\partial \lambda}\, d\lambda. \tag{2.7}$$

The relation in (2.6) is the first law of thermodynamics on trajectory level. Hence, for a setting as in (2.1), the only way work can be applied to the system is via altering the potential U through its control parameter λ. For the work in (2.7) the usual sign convention applies, i.e., work applied to the system has a positive sign and work done by the system a negative sign. In the subsequent sections we will allow for non-conservative forces in the Langevin equation, which will cause an additional contribution to (2.7).

2.1.2 Including Non-Conservative Forces in the Langevin Equation

We now discuss a more general case of overdamped Langevin equation compared to (2.1), in particular (see, e.g., [10, 25]),

$$\frac{d\,x}{dt} = \mu\, F(x,\lambda) + \eta(t)\,, \qquad F(x,\lambda) \equiv -\frac{\partial\, U(x,\lambda)}{\partial x} + f(x,\lambda), \tag{2.8}$$

with η correlated according to (2.2), μ as a mobility constant and $f(x,\lambda)$ as a non-conservative force. Note, that the noise strength Δ_0 and the mobility μ are related via the Einstein relation,

$$\Delta_0 = 2\, k_B\, T\, \mu, \tag{2.9}$$

where k_B is Boltzmann's constant. In the following, we set k_B to unity to allow for a dimensionless formulation of entropy, see (2.43) and, e.g., [4, 24, 25].
The introduction of the non-conservative force f leads to an additional contribution to the work applied to the system [25], i.e.,

$$đw = \frac{\partial\, U(x,\lambda)}{\partial \lambda}\, d\lambda + f(x,\lambda)\, dx. \tag{2.10}$$

Thus, with the first law from (2.6) and (2.10), the dissipated heat into the medium, or heat bath, now reads [25]

$$đq = đw - dU = -\frac{\partial\, U(x,\lambda)}{\partial x}\, dx + f(x,\lambda)\, dx = F(x,\lambda)\, dx. \tag{2.11}$$

Using (2.10) and (2.11), we find for the work performed on the system along a single trajectory in the time-interval $[0,\tau]$,

$$w[x(\tau)] = \int_0^\tau dt \left(\frac{\partial\, U(x,\lambda)}{\partial \lambda}\, \frac{d\,\lambda}{dt} + f(x,\lambda)\, \frac{d\,x}{dt} \right), \tag{2.12}$$

and equivalently for the amount of heat dissipated into the medium along the same trajectory during the time-interval $[0,\tau]$,

$$q[x(\tau)] = \int_0^\tau dt\, F(x,\lambda)\, \frac{d\,x}{dt}. \tag{2.13}$$

Before continuing with the probabilistic description of (2.8), we illustrate the above concepts for a simple exemplary system.

Example: Overdamped Stochastic Harmonic Oscillator Driven by a Non-Conservative Force

We consider the model system of a single overdamped oscillator, which is driven by a non-conservative force f_0 and an additional stochastic force $\eta(t)$, correlated according to (2.2),

$$\frac{d\,x}{dt} = \frac{1}{\gamma}\, (-K\, x + f_0) + \eta(t)\,, \qquad x(0) = 0, \tag{2.14}$$

with friction coefficient γ and K the spring constant. In terms of (2.8), $\mu = 1/\gamma$ and $F = -Kx + f_0$. The energy balance corresponding to (2.14) in the spirit of (2.5) and (2.13) is given by

$$q[x(t)] = -K\, \frac{x^2(t)}{2} + \int_0^t dt'\, f_0\, \frac{d\,x}{dt'} = \int_0^t dt' \left(-\frac{d\,U(x)}{dx} + f_0 \right) \frac{d\,x}{dt'}. \tag{2.15}$$

We identify the first term on the r.h.s. of (2.15) as the potential energy, $U(x) = Kx^2/2$, the second term as the work applied to the system via the external force f_0 along the trajectory $x(t'=0) \to x(t'=t)$, $w = \int_{x(0)}^{x(t)} dx\, f_0$, and the term on the l.h.s. as the net amount of heat $q[x(t)] = \int_{x(0)}^{x(t)} đq$ dissipated along the trajectory into the heat bath.
It is instructive to analyze this example in more detail. For simplicity, we choose $f_0 =$ const. The solution of the SDE (2.14) is given by

$$x(t) = \frac{f_0}{K}\left(1 - e^{-\frac{K}{\gamma}t}\right) + \int_0^t dt'\, e^{-\frac{K}{\gamma}(t-t')}\eta(t'), \tag{2.16}$$

where the integral term is understood as a stochastic convolution with a Wiener process $W(t)$, $\int_0^t dW(t')\, e^{-\frac{K}{\gamma}(t-t')}$ (see Appendix 3.A.3). We will evaluate the individual terms in (2.15) and test this balance by calculating the respective expectation values. To this end, we first state the expressions for mean and variance of $x(t)$,

$$\langle x(t)\rangle = \frac{f_0}{K}\left(1 - e^{-\frac{K}{\gamma}t}\right), \tag{2.17}$$

and

$$\mathrm{var}[x(t)] = \left\langle x^2(t)\right\rangle - \langle x(t)\rangle^2 = \frac{\Delta_0\,\gamma}{2\,K}\left(1 - e^{-2\frac{K}{\gamma}t}\right). \tag{2.18}$$

Here, $\langle\cdot\rangle$ denotes the average with respect to the noise history. Then the expectation value of the potential difference $U(x(t)) - U(x(0))$ along the trajectory is given by

$$\langle U\rangle = \frac{f_0^2}{2\,K}\left(1 - e^{-\frac{K}{\gamma}t}\right)^2 + \frac{\Delta_0\,\gamma}{4}\left(1 - e^{-2\frac{K}{\gamma}t}\right), \tag{2.19}$$

the mean work applied to the system by

$$\langle w\rangle = \frac{f_0^2}{K}\left(1 - e^{-\frac{K}{\gamma}t}\right), \tag{2.20}$$

and the net amount of dissipated heat into the environment by

$$\langle q\rangle = \left(\frac{f_0^2}{2\,K} - \frac{\Delta_0\,\gamma}{4}\right)\left(1 - e^{-2\frac{K}{\gamma}t}\right). \tag{2.21}$$

Hence, we have $\langle q\rangle + \langle U\rangle = \langle w\rangle$, which satisfies (2.15) in the mean and therefore the first law from (2.6) as well. As is to be expected for consistency reasons, for $\Delta_0 = 0$ the expressions for $\langle U\rangle$, $\langle w\rangle$ and $\langle q\rangle$ reduce to their respective expressions for the deterministic equation of motion.
In the limit of large times t, we obtain for $\langle U\rangle$ from (2.19) and $\langle q\rangle$ from (2.21),

$$U_\infty = \frac{f_0^2}{2\,K} + \frac{\Delta_0\,\gamma}{4}, \qquad q_\infty = \frac{f_0^2}{2\,K} - \frac{\Delta_0\,\gamma}{4}, \tag{2.22}$$

where the respective first terms stem from the deterministic dynamics and the second terms represent the noise contribution. Thus, the deterministic potential energy is increased by the thermal energy provided by the heat bath, whereas the pure mechanical dissipation is reduced correspondingly. Using the Einstein relation from (2.9) leads to

$$U_\infty = \frac{f_0^2}{2\,K} + \frac{1}{2}\,k_B\,T\,, \qquad q_\infty = \frac{f_0^2}{2\,K} - \frac{1}{2}\,k_B\,T\,, \tag{2.23}$$

where the respective second terms are in accordance with the equipartition theorem (for one degree of freedom corresponding to one-dimensional motion). This indicates that for $t \to \infty$ the particle reaches an equilibrium steady state (see also Section 2.2.2).
We conclude this example with the observation that the l.h.s. of (2.15) may also be written as

$$q[x(t)] = \int_0^t dt' \left(\gamma \frac{d\,x}{dt'} - \widetilde{\eta}(t')\right) \frac{d\,x}{dt'}\,, \tag{2.24}$$

which is the integral equivalent of (2.5) ($\widetilde{\eta} = \gamma\eta$). It is important to note that (2.24) cannot be split up into two separate terms as might be expected by deriving a term-wise energy balance from (2.14). This is due to the fact that each individual term becomes singular (see, e.g., [24]) as can be seen by evaluating $\left\langle \int_0^t dt' \gamma\,(\dot{x})^2 \right\rangle$ and $\left\langle \int_0^t dt' \widetilde{\eta}(t')\dot{x}(t') \right\rangle$, respectively, along the same lines as above.

2.2 Probabilistic Description of a Langevin Equation

2.2.1 Path-Weight of a Trajectory

With a single trajectory described by (2.8) a path weight given by

$$p[x(t)|x_0] = \frac{1}{\mathcal{N}}\, e^{-\mathcal{S}[x(t),\lambda(t)]}, \tag{2.25}$$

is associated, where $x_0 = x(0)$ is the initial condition of the trajectory, $\mathcal{N}$ a path-independent normalization constant of p and $\mathcal{S}$ the stochastic action. The latter is given by

$$\mathcal{S}[x(t),\lambda(t)] = \int_0^t dt' \left[\frac{(\dot{x} - \mu\,F(x,\lambda))^2}{2\,\Delta_0} + \frac{\mu}{2}\,\frac{\partial\,F(x,\lambda)}{\partial x} \right]. \tag{2.26}$$

The second term in (2.26) arises from the 'variable' change from $\eta(t)$ to $x(t)$, if the Stratonovich discretization is used (see, e.g., [10,25,26]), which will be assumed throughout.
Using this path-weight, expectation values of an arbitrary observable $O[x(t)]$, conditioned on a certain initial configuration, may be written via path-integral formalism as (see, e.g., [10, 25, 26])

$$\langle O[x(t)]|x_0\rangle = \int dx_0 \int \mathcal{D}[x(t)]\, O[x(t)]\, p[x(t)|x_0]\, p(x_0,0), \tag{2.27}$$

where $p(x_0, 0)$ describes the probability to have the initial configuration x_0 at time $t = 0$. This probability is given by the solution of the Fokker-Planck equation.

2.2.2 Fokker-Planck Equation and Non-Equilibrium Steady State

The Fokker-Planck equation equivalent to (2.8) reads [10, 25–27]

$$\frac{\partial p(x,t)}{\partial t} = -\partial_x \left(\mu F(x,\lambda)\, p(x,t) - \frac{\Delta_0}{2} \frac{\partial p(x,t)}{\partial x} \right), \tag{2.28}$$

where its solution $p(x, t)$ yields the probability to observe the particle at position x at time t. Introducing the probability current $j_p(x, t)$, given by

$$j_p(x,t) = \mu F(x,\lambda)\, p(x,t) - \frac{\Delta_0}{2} \frac{\partial p(x,t)}{\partial x}, \tag{2.29}$$

we may rewrite the Fokker-Planck equation as a continuity equation

$$\partial_t p(x,t) = -\partial_x j_p(x,t). \tag{2.30}$$

In a stationary state, the l.h.s. of (2.28) vanishes and one has

$$\frac{\partial j_p^s(x)}{\partial x} = 0, \tag{2.31}$$

with

$$j_p^s(x) = \mu F(x,\lambda)\, p^s(x) - \frac{\Delta_0}{2} \frac{\partial p^s(x)}{\partial x}, \tag{2.32}$$

where $p^s(x)$ denotes the stationary probability distribution. For the case of an equilibrium stationary state, the condition in (2.31) is fulfilled trivially, as $j_p^s = 0$. The case, where (2.31) is fulfilled but $j_p^s \neq 0$ is called non-equilibrium stationary state (NESS) (see, e.g., [10, 25–27]). In the following chapters, we are concerned only with systems that display a genuine NESS.
Before we continue, let us briefly come back to the example of a single overdamped oscillator from the above section. Since (2.14) is linear and the noise Gaussian, we expect the probability distribution of the particle position to be Gaussian as well. With the results for $\langle x \rangle$ and var$[x]$ from (2.17) and (2.18), respectively, in the long time limit,

$$p^s(x) \sim \exp\left[-\frac{K}{\Delta_0\, \gamma} \left(x - \frac{f_0}{K} \right)^2 \right]. \tag{2.33}$$

This assumption is readily confirmed by inserting (2.33) into (2.32) using

$$\frac{\partial p^s(x)}{\partial x} = -\frac{2K}{\Delta_0\, \gamma} \left(x - \frac{f_0}{K} \right) p^s(x), \tag{2.34}$$

which leads to

$$j_p^s(x) = \left[\frac{1}{\gamma}\,(-K\,x + f_0) + \frac{\Delta_0}{2}\,\frac{2\,K}{\Delta_0\,\gamma}\left(x - \frac{f_0}{K}\right)\right] p^s(x) = 0. \tag{2.35}$$

Hence, the stationary probability current vanishes identically, which implies an equilibrium stationary state with (2.33) as the stationary probability distribution.

2.3 Entropy Production

The total entropy production along a single trajectory contains two contributions. One is the entropy associated with the heat dissipated into the medium, the change in medium entropy Δs_m,

$$\Delta s_m = \frac{q[x(t)]}{T}, \tag{2.36}$$

with q according to (2.13). The second originates in the change of the so-called stochastic entropy, Δs, given by

$$\Delta s = -\ln p(x(t'), t')\Big|_0^t, \tag{2.37}$$

where the solution of the Fokker-Planck equation, $p(x,t)$, is evaluated along the stochastic trajectory $x(t)$, e.g., [10,25,28]. Note that on average, the expression for the stochastic entropy becomes the ensemble definition of system entropy,

$$\langle s \rangle = -\int dx\, p(x,t)\, \ln p(x,t), \tag{2.38}$$

i.e., the Gibbs entropy.
Regarding the medium entropy from (2.36), the heat $q[x(t)]$ may, alternatively to (2.13), be evaluated using the path weight (2.25) for a single trajectory and its time-reversed counterpart. With $x(\tau)$ as the forward trajectory starting for $\tau = 0$ at $x = 0$ and ending for $\tau = t$ at $x(t)$, we define the backward trajectory as $\widetilde{x}(\tau)$ with $\widetilde{x}(\tau) = x(t-\tau)$, i.e., $\widetilde{x}$ starts with $\widetilde{x}(0) = x(t)$ at $\tau = 0$ and ends at $\widetilde{x}(t) = x(0)$ for $\tau = t$. Correspondingly, the backward protocol for the control parameter λ reads $\widetilde{\lambda}(\tau) = \lambda(t-\tau)$. Then we have for the forward trajectory $x(\tau)$ and control parameter $\lambda(\tau)$, $\tau \in [0,t]$, with (2.26)

$$\mathcal{S}[x(\tau), \lambda(\tau)] = \int_0^t d\tau \left[\frac{(\dot{x} - \mu\,F)^2}{2\,\Delta_0} + \frac{\mu}{2}\,\partial_x F\right], \tag{2.39}$$

and for the backward trajectory

$$\widetilde{\mathcal{S}}[\widetilde{x}(\tau), \widetilde{\lambda}(\tau)] = \int_0^t d\tau \left[\frac{(\dot{x} + \mu\,F)^2}{2\,\Delta_0} + \frac{\mu}{2}\,\partial_x F\right]. \tag{2.40}$$

The integrand in (2.40) has been re-expressed in terms of x and λ again. Subtracting (2.39) from (2.40), where only the time-antisymmetric parts survive, yields

$$\widetilde{\mathcal{S}}[\widetilde{x}(\tau),\widetilde{\lambda}(\tau)] - \mathcal{S}[x(\tau),\lambda(\tau)] = \frac{2\,\mu}{\Delta_0}\int_0^t d\tau\, F[x(\tau),\lambda(\tau)]\,\dot{x}(\tau) = \frac{2\,\mu}{\Delta_0}\, q[x(\tau),\lambda(\tau)]. \quad (2.41)$$

Here we used (2.13) in the last step [5,25]. Therefore, with (2.25), it is found that

$$q[x(t),\lambda(t)] = \frac{\Delta_0}{2\,\mu}\,\ln\frac{p[x(t),\lambda(t)]}{\widetilde{p}[\widetilde{x}(t),\widetilde{\lambda}(t)]}, \quad (2.42)$$

where it is understood that $p[x(t),\lambda(t)] = p[x(t)|x_0,\lambda(t)]$ and $\widetilde{p}$ denotes the path weight of the backward trajectory. Hence, with (2.36) and the Einstein relation from (2.9), the entropy dissipated into the medium is given by [5,25],

$$\Delta s_m = \ln\frac{p[x(t),\lambda(t)]}{\widetilde{p}[\widetilde{x}(t),\widetilde{\lambda}(t)]}. \quad (2.43)$$

With (2.37) and (2.43), the total entropy production Δs_{tot} reads

$$\Delta s_{\text{tot}} = \Delta s_m + \Delta s = \ln\frac{p[x(t),\lambda(t)]}{\widetilde{p}[\widetilde{x}(t),\widetilde{\lambda}(t)]} - \ln p(x(t'),t')\Big|_0^t = \ln\frac{p[x(t),\lambda(t)]\,p(x(0),0)}{\widetilde{p}[\widetilde{x}(t),\widetilde{\lambda}(t)]\,p(x(t),t)}. \quad (2.44)$$

To exemplify, let us consider the overdamped oscillator from above. For the sake of simplicity, we here assume that the initial state of the oscillator at $t = 0$ is drawn from the stationary distribution $p^s(x)$ from (2.33). Then, the change in stochastic entropy along a trajectory is given by

$$\Delta s = -\ln p^s(x)\Big|_0^t = \frac{K}{2\,T}\left(x^2(t) - x^2(0)\right) - \frac{f_0}{T}\left(x(t) - x(0)\right), \quad (2.45)$$

where we used the Einstein relation from (2.9). With (2.36), we readily obtain for the entropy dissipated into the medium,

$$\Delta s_m = \frac{1}{T}\int_0^t dt'\, F\,\dot{x} = -\frac{K}{2\,T}\left(x^2(t) - x^2(0)\right) + \frac{f_0}{T}\left(x(t) - x(0)\right). \quad (2.46)$$

Thus, with (2.44) we find

$$\Delta s_{\text{tot}} = \Delta s_m + \Delta s = 0, \quad (2.47)$$

which, of course, is to be expected in a genuine equilibrium state. Generally speaking, every equilibrium trajectory has an identically vanishing total entropy production Δs_{tot}, e.g., [10].

A non-equilibrium relation for Δs_{tot} is given in the following.

2.3.1 Fluctuation Theorem and Second Law of Thermodynamics

A dimensionless observable $O[x(t)]$ depending on the trajectory $x(t)$ is said to fulfill an integral fluctuation theorem if

$$\left\langle e^{-O[x(t)]} \right\rangle = 1, \tag{2.48}$$

with $\langle \cdot \rangle$ according to (2.27). Due to the convexity of the exponential function, the relation in (2.48) implies with Jensen's inequality

$$\langle O[x(t)] \rangle \geq 0. \tag{2.49}$$

A dimensionless observable $O[x(t)]$ satisfying (2.48) is the total entropy production Δs_{tot}, since

$$\begin{aligned}\left\langle e^{-\Delta s_{\text{tot}}} \right\rangle &= \int dx(0) \int \mathcal{D}[x(t)]\, e^{-\Delta s_{\text{tot}}}\, p[x(t)|x(0)]p(x(0),0) \\ &= \int dx(t) \int \mathcal{D}[\widetilde{x}(t)]\, \widetilde{p}[\widetilde{x}(t), \widetilde{\lambda}(t)]\, p(x(t),t) = 1,\end{aligned} \tag{2.50}$$

where the second step uses the expression for Δs_{tot} from (2.44) and the last holds for properly normalized distribution $p(x(t),t)$ (see [5, 25]). Hence, with (2.49), we have the second law-like form

$$\langle \Delta s_{\text{tot}} \rangle \geq 0, \tag{2.51}$$

where equality only holds in equilibrium (see also the example at end of the above section). The total entropy production from (2.44) is one constituent of the so-called thermodynamic uncertainty relation, which is stated in the following section.

2.4 Thermodynamic Uncertainty Relation

In [6], a thermodynamic uncertainty relation (TUR) for current-like observables was proposed in the setting of discrete Markovian networks. It has been proven in [7] using large deviation theory and extended to Langevin dynamics described by (2.8) in [8]. Roughly speaking, the TUR represents a trade-off relation between the precision at which a system operates versus the thermodynamic costs that are necessary to ensure that precision. Before we state the TUR, we have to clarify what is meant by current-like observable and precision.

We begin by introducing a fluctuating generalized current $j_d(t)$ via

$$j_d(t) \equiv d\,\dot{x}(t), \tag{2.52}$$

where, in general, $d = d(x(t), t)$ represents an arbitrary weight function and the product between d and $\dot{x}(t)$ is interpreted in the Stratonovich sense (see, e.g., [8, 11, 29–31]).

The current $j_d(t)$ may also be written as the time derivative of the so-called fluctuating output, or, equivalently, the time-integrated current $\Psi_d(t)$, i.e.,

$$j_d(t) = \partial_t \, \Psi_d(t). \tag{2.53}$$

If the system is in a NESS, it holds that (e.g., [11])

$$\lim_{t\to\infty} \langle \partial_t \, \Psi_d(t) \rangle = \lim_{t\to\infty} \frac{\langle \Psi_d(t) \rangle}{t} \equiv J_d, \tag{2.54}$$

with J_d the stationary generalized current and $\langle \cdot \rangle$ denoting averages with respect to the noise history. Hence, in the NESS

$$\langle \Psi_d(t) \rangle = J_d \, t, \tag{2.55}$$

and similarly, it holds that

$$\langle \Delta s_{\mathrm{tot}} \rangle = \sigma \, t, \tag{2.56}$$

with σ the total entropy production rate.

A measure for the precision of the fluctuating system output $\Psi_d(t)$ is defined via its squared coefficient of variation,

$$\epsilon^2 \equiv \frac{\left\langle \left(\Psi_d(t) - \langle \Psi_d(t) \rangle \right)^2 \right\rangle}{\langle \Psi_d(t) \rangle^2}, \tag{2.57}$$

with ϵ interpreted as the amplitude of the fluctuations related to their mean (see, e.g., [6,11]). In other words, ϵ quantifies the uncertainty of the system output and its accuracy is proportional $1/\epsilon$. For a system in a NESS, ϵ^2 may be rewritten as

$$\epsilon^2 = \frac{\left\langle \left(\Psi_d(t) - J_d \, t \right)^2 \right\rangle}{(J_d \, t)^2}. \tag{2.58}$$

Now we are able to state the TUR for a system in a non-equilibrium steady state as

$$\mathcal{Q} \equiv \langle \Delta s_{\mathrm{tot}} \rangle \, \epsilon^2 \geq 2, \tag{2.59}$$

where we defined $\mathcal{Q}$ as the TUR product $\langle \Delta s_{\mathrm{tot}} \rangle \, \epsilon^2$ for later convenience, e.g., [6–9, 11]. The higher the precision, i.e., the smaller ϵ^2, the more $\langle \Delta s_{\mathrm{tot}} \rangle$ is generated, i.e., the higher the thermodynamic cost.

Defining the diffusivity according to

$$D_d = \lim_{t\to\infty} \frac{\left\langle \left(\Psi_d(t) - J_d \, t \right)^2 \right\rangle}{2\, t}, \tag{2.60}$$

see, e.g., [11], and using (2.55), (2.56) the TUR product from (2.59) becomes

$$\frac{D_d\,\sigma}{J_d^2} \geq 1, \tag{2.61}$$

e.g., [6–9, 11]. In the equivalent form, $\sigma \geq J_d^2/D_d$, it states that the stationary fluctuations of the system output are bounded from above by the entropy production.
There are quite a few variants of (2.59). The first is a generalization to the case of periodically driven systems, see [32] and references therein. Another variant is a formulation of a TUR for unidirectional transitions, see [33]. As a last example, we mention the so-called generalized TUR, derived via the detailed fluctuation theorem of the entropy production rate [34].

2.5 Extension to Higher Degrees of Freedom

For simplicity, we considered in the preceding sections the dynamics of a particle at the one-dimensional position $x(t)$ moving in $\mathbb{R}^1$ (i.e., with one degree of freedom). However, all of the above concepts and notions may be straightforwardly extended to arbitrary higher dimensions d (i.e., with d coupled degrees of freedom). For finite d, the position of the particle then becomes a d-dimensional vector $\mathbf{r}(t) = (x_1(t), \ldots, x_d(t))^\top$ moving along a trajectory $t \mapsto \mathbf{r}(t)$ in $\mathbb{R}^d$. Even an extension to fields, e.g., the scalar surface-height field at position $\mathbf{r}$ at time t, $h(\mathbf{r}, t)$, of the Kardar-Parisi-Zhang equation, works. It may be understood as a 'point' in an infinitely ($d = \infty$) dimensional abstract function space moving on a trajectory $t \mapsto h(\mathbf{r}, t)$ in this space. At any given time-instant t, the 'point' $h(\mathbf{r}, t)$, which is identical with the height profile at time t, is an element of this function space. For further details on this function space of the Kardar-Parisi-Zhang equation, see Appendices 3.A.5 and 5.C. Similarly, a further generalization to vector fields may be established (see Chapter 4 and [28]).
This generalizations come with the need for suitable replacements, e.g., for finite d, the scalar quantities F and η from the Langevin equation (2.8) have to be replaced by $\mathbf{F} = (F_1(\mathbf{r}, \lambda), \ldots, F_d(\mathbf{r}, \lambda))^\top$ and $\boldsymbol{\eta} = (\eta_1(t), \ldots, \eta_d(t))^\top$. Accordingly, μ and Δ_0 become linear operators represented by their corresponding matrices. In the field theoretic case, these linear operators are integral operators represented by their kernel functions, e.g., $\Delta_0 K(\mathbf{r} - \mathbf{r}')$, with $K(\mathbf{r} - \mathbf{r}') = \delta^d(\mathbf{r} - \mathbf{r}')$ representing spatial white noise (see also Appendices 3.A.4 and 3.A.5 and Chapter 4).
Naturally, also the Fokker-Planck equation changes. Written as continuity equation, the Fokker-Planck equation reads for finite d, e.g., [27],

$$\frac{\partial\, p(\mathbf{r}, t)}{\partial t} = -\nabla \cdot \mathbf{j}_p(\mathbf{r}, t) = -\sum_{i=1}^{d} \partial_{x_i}\, j_{p,i}(\mathbf{r}, t), \tag{2.62}$$

with $\nabla\cdot$ the divergence operator. In the field theoretic case, with, e.g., $h(\mathbf{r},t)$ from above, we have, e.g., [20, 21, 35–37],

$$\frac{\partial\, p[h,t]}{\partial t} = -\int d\mathbf{r}\, \frac{\delta j_p[h,t]}{\delta h}, \tag{2.63}$$

i.e., the partial derivative ∂_{x_i} from (2.62) has to be replaced by the functional derivative $\delta/\delta h$ in (2.63) and the discrete sum of the divergence becomes a spatial integral.
Finally, the following correspondences are frequently used. The product of real numbers $f, g \in \mathbb{R}$, extends to the scalar product of real vectors, $\mathbf{f}\cdot\mathbf{g} = \sum_i f_i g_i$, $\mathbf{f},\mathbf{g} \in \mathbb{R}^d$, which extends to the inner product ($\mathcal{L}_2$-product) of real functions $f(\mathbf{r})$, $g(\mathbf{r})$ given by $\int d\mathbf{r}\, f(\mathbf{r})\, g(\mathbf{r})$.
These extensions will be made more precise in Chapter 4. Prior to that, we introduce the field theoretic model which the above concepts will be exemplified with at a later stage of this thesis.

3 Background on the Kardar-Parisi-Zhang Equation

In this chapter, we introduce the celebrated Kardar-Parisi-Zhang equation and present an overview of some of its plentiful facets, which will be of importance to the subsequent analysis. Besides its physical properties, we also discuss technical and methodological aspects in order to explain the approach taken in the chapters below.

3.1 The Kardar-Parisi-Zhang Equation

In 1986, M. Kardar, G. Parisi and Y.-C. Zhang introduced a surface-growth model [12], which has since then become one of the most widely studied field-theoretic problems. It reads

$$\begin{aligned} \partial_t \, h(\mathbf{r},t) &= \nu \, \nabla^2 h(\mathbf{r},t) + \frac{\lambda}{2} \left(\nabla h(\mathbf{r},t)\right)^2 + \eta(\mathbf{r},t) \, , \\ \langle \eta(\mathbf{r},t) \rangle &= 0 \, , \\ \big\langle \eta(\mathbf{r},t) \, \eta(\mathbf{r}',t') \big\rangle &= \Delta_0 \, \delta^d(\mathbf{r}-\mathbf{r}') \, \delta(t-t') \, . \end{aligned} \tag{3.1}$$

Here the field $h(\mathbf{r},t)$ denotes the surface height at the spatial coordinate $\mathbf{r} \in \mathbb{R}^d$ and time t in d spatial dimensions. The diffusive linear term on the right hand side of (3.1) represents the mechanism of surface tension with 'viscosity' parameter ν. The statistical uncertainty of the growth process is modeled by a Gaussian noise field $\eta(\mathbf{r},t)$ with zero mean and autocorrelation according to (3.1), where Δ_0 measures the noise strength (space-time white noise). With these components a surface growth model was already proposed by S.F. Edwards and D.R. Wilkinson, the Edwards-Wilkinson (EW) model [19], namely

$$\partial_t \, h(\mathbf{r},t) = \nu \, \nabla^2 h(\mathbf{r},t) + \eta(\mathbf{r},t), \tag{3.2}$$

with noise correlations according to (3.1). The intriguing additional feature of the KPZ equation is its non-linearity, which allows for the description of growth locally normal to the surface. The coupling strength of the non-linearity is given by the coupling parameter λ, which should be understood as an independent external parameter [21].

For the most part of this thesis, we will deal with the KPZ equation from (3.1) in one

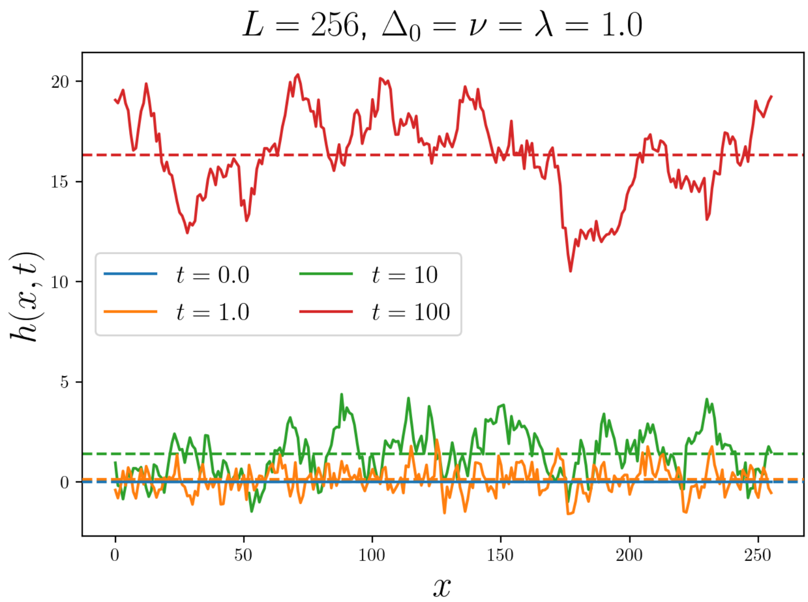

Figure 3.1: Surface height $h(x, t)$ on a discrete substrate with $x \in [0, 256]$ for four distinct times t. The dashed lines represent the spatial mean of $h(x, t)$. This graphic was obtained via numerical simulation according to Section 7.1.

spatial dimension. In particular, we have

$$\begin{aligned}\partial_t h(x,t) &= \nu\, \partial_x^2 h(x,t) + \frac{\lambda}{2}\left(\partial_x h(x,t)\right)^2 + \eta(x,t)\,,\\ \langle \eta(x,t)\rangle &= 0\,,\\ \left\langle \eta(x,t)\,\eta(x',t')\right\rangle &= \Delta_0\, \delta(x-x')\,\delta(t-t')\,.\end{aligned} \tag{3.3}$$

Here we restrict ourselves to a finite spatial interval $x \in [0, b]$, $b > 0$, for reasons that will become clear in the following. We further assume periodic boundary conditions, namely, $h(0, t) = h(b, t)$, and further flat initial condition, $h(x, 0) = 0$. In Figure 3.1, we show the temporal evolution of the surface height $h(x, t)$ from (3.3) with $x \in [0, L = 256]$. The data of $h(x, t)$ is obtained by the numerical scheme described in Chapter 7. We further show as dashed lines the value of $L^{-1} \int_0^L dx\, h(x, t)$, i.e., the spatial mean of the height field, at the respective times t. This quantity will be of importance in the following.
Besides its modeling of surface growth, the KPZ equation is closely related to numerous other models. Among these are the Sivashinsky equation [38] that describes the propagation of flame fronts and a model discussed in [39], which governs density fluctuations in driven diffusive systems. Further, the KPZ equation can be mapped to models for fluid dynamics and directed polymers, which are discussed below.

3.1.1 Relation to Stochastic Burgers Equation

The relation to fluid dynamics, in particular the stochastic or noisy Burgers equation, is obtained by taking the spatial derivative on both sides of (3.1), which yields

$$\partial_t \nabla h(\mathbf{r},t) = \nu \nabla^3 h(\mathbf{r},t) + \lambda \nabla h(\mathbf{r},t) \nabla^2 h(\mathbf{r},t) + \nabla \eta(\mathbf{r},t). \tag{3.4}$$

Setting $\mathbf{u}(\mathbf{r},t) \equiv -\nabla h(\mathbf{r},t)$ and $\lambda = 1$ leads to

$$\partial_t \mathbf{u}(\mathbf{r},t) + \mathbf{u}(\mathbf{r},t) \cdot \nabla \mathbf{u}(\mathbf{r},t) = \nu \nabla^2 \mathbf{u}(\mathbf{r},t) - \nabla \eta(\mathbf{r},t), \tag{3.5}$$

which is known as the stochastic Burgers equation (see, e.g., [12, 40–42]) excited by a noise field $\mathbf{f}(\mathbf{r},t) \equiv -\nabla \eta(\mathbf{r},t)$ with $\eta(\mathbf{r},t)$ from (3.1). As long as (3.5) describes a vorticity-free (i.e., $\nabla \times \mathbf{u}(\mathbf{r},t) = \mathbf{0}$), randomly stirred fluid, the noisy Burgers equation is equivalent to the KPZ equation, e.g., [43], with h being the potential of $\mathbf{u}$ (potential flow). For the case of the one-dimensional versions of the KPZ equation (3.3) and noisy Burgers equation (3.5), respectively, the equivalence holds generally. In Chapter 6 we will use this equivalence to perform dynamic renormalization group calculations for the KPZ equation.

3.1.2 Relation to Directed Polymers

Another intriguing mapping of the KPZ equation is the one on the stochastic heat equation (SHE) via the Cole-Hopf transformation

$$W(\mathbf{r},t) = \exp\left[\frac{\lambda}{2\nu} h(\mathbf{r},t)\right]. \tag{3.6}$$

Applying the transformation from (3.6) to (3.1) yields

$$\partial_t W(\mathbf{r},t) = \nu \nabla^2 W(\mathbf{r},t) + \frac{\lambda}{2\nu} \eta(\mathbf{r},t) W(\mathbf{r},t), \tag{3.7}$$

i.e., the heat equation excited by a multiplicative noise, which models directed polymers in a random medium (see, e.g., [40, 41, 44–46]). Note that the transformation from (3.6) maps the non-linear KPZ equation from (3.1) to the linear SHE from (3.7) and changes the additive noise structure to a multiplicative noise, respectively. Besides its physical applications, the SHE is of great importance especially for the construction of a solution to (3.1) [21]. While the equivalence between (3.1) and (3.7) via (3.6) is on a formal level evident, there are serious difficulties in formulating a mathematically rigorous solution $h(\mathbf{r},t)$, which from a mathematical point of view is due to the 'ill-posedness' of (3.1) (see, e.g., [47–53] and also the discussion regarding the KPZ regularity in Appendices 3.A.5 and 5.C).

3.1.3 Dimensionless Form of the KPZ Equation

A technical but useful step is to rewrite the KPZ equation from (3.1) in its dimensionless form. We relate all physical quantities to suitable reference values so that the scaled quantities are dimensionless and that the equation is characterized by only one dimensionless parameter. In anticipation of the calculations below, we choose this parameter to represent a dimensionless effective coupling parameter λ_{eff}, that replaces the coupling constant λ from (3.1). To this end the following characteristic scales are introduced,

$$h = Hh_{\text{s}}\ ;\quad \eta = N\eta_{\text{s}}\ ;\quad \mathbf{r} = b\mathbf{r}_{\text{s}}\ ;\quad t = Tt_{\text{s}}, \tag{3.8}$$

where dimensionless quantities are designated by the subscript 's'. Here H is a characteristic scale for the height field, N a scale for the noise field, b is the characteristic length scale in space and T the time scale of the system.
Choosing the three respective scales according to

$$H = \sqrt{\frac{\Delta_0\, b^{2-d}}{\nu}},\quad N = \sqrt{\frac{\Delta_0\, \nu}{b^{2+d}}},\quad T = \frac{b^2}{\nu}, \tag{3.9}$$

leads to the dimensionless KPZ equation in the d-dimensional unit ball, $|\mathbf{r}_s| < 1$,

$$\partial_{t_{\text{s}}} h_{\text{s}}(\mathbf{r}_{\text{s}}, t_{\text{s}}) = \nabla^2_{\mathbf{r}_{\text{s}}} h_{\text{s}}(\mathbf{r}_{\text{s}}, t_{\text{s}}) + \frac{\lambda_{\text{eff}}}{2}\left(\nabla_{\mathbf{r}_{\text{s}}} h_{\text{s}}(\mathbf{r}_{\text{s}}, t_{\text{s}})\right)^2 + \eta_{\text{s}}(\mathbf{r}_{\text{s}}, t_{\text{s}}), \tag{3.10}$$

$$\langle \eta_{\text{s}}(\mathbf{r}_{\text{s}}, t_{\text{s}})\rangle = 0, \tag{3.11}$$

$$\big\langle \eta_{\text{s}}(\mathbf{r}_{\text{s}}, t_{\text{s}})\eta_{\text{s}}(\mathbf{r}'_{\text{s}}, t'_{\text{s}})\big\rangle = \delta^d(\mathbf{r} - \mathbf{r}')\,\delta(t_{\text{s}} - t'_{\text{s}}). \tag{3.12}$$

Here, the effective dimensionless coupling constant is given by

$$\lambda_{\text{eff}} = \sqrt{\frac{\Delta_0\, b^{2-d}}{\nu^3}}\,\lambda. \tag{3.13}$$

The effective coupling constant will be of importance in the subsequent discussion of the KPZ scaling behavior as well as for the perturbative and DRG calculations and is found in various works concerning the KPZ-Burgers equation; see, e.g., [40, 43, 54, 55].

3.2 Scaling Behavior of the 1D-KPZ Equation on a Finite Substrate

3.2.1 Edwards-Wilkinson and KPZ Correlation Lengths and Times

The Edwards-Wilkinson Case

An important measure for the scaling behavior of the KPZ equation on a finite substrate is the correlation length. It is instructive to first take a look at the origin and implication of the correlation length in the context of the Edwards-Wilkinson equation. In the following chapters, with the exception of Chapter 8, we will focus on the one-dimensional case and therefore analyze

$$\partial_t h(x,t) = \nu \, \partial_x^2 h(x,t) + \eta(x,t), \tag{3.14}$$

with noise correlations as in (3.2) and $x \in [0, b]$, $b > 0$. Representing the height field $h(x,t)$ and the noise $\eta(x,t)$ in terms of their respective Fourier series

$$\begin{aligned} h(x,t) &= \sum_k h_k(t) \, e^{2\pi i k x/b}, \\ \eta(x,t) &= \sum_k \eta_k(t) \, e^{2\pi i k x/b}, \end{aligned} \tag{3.15}$$

leads via (3.14) to the ordinary differential equation (ODE) for the k-th Fourier mode of the height field

$$\dot{h}_k(t) = -4\pi^2 \nu \frac{k^2}{b^2} h_k(t) + \eta_k(t). \tag{3.16}$$

Assuming flat initial condition for $h(x,t)$, i.e., $h(x,0) = 0$, this linear stochastic ODE is readily solved by formally applying the variation of constants formula and yields

$$h_k(t) = \int_0^t dt' \, e^{-4\pi^2 \nu k^2/b^2 (t-t')} \eta_k(t'). \tag{3.17}$$

Note, that (3.17) is a formal expression only. For a mathematically rigorous formulation see Appendix 3.A.
Of particular interest to the subsequent analysis is the surface width, $W(b,t)$, of the height field given by (see, e.g., [20, 56, 57])

$$W^2(b,t) = \left\langle \int_0^b \frac{dx}{b} \left(h(x,t) - \int_0^b \frac{dx}{b} \, h(x,t) \right)^2 \right\rangle. \tag{3.18}$$

Inserting the Fourier series representation from (3.15) into (3.18) and using the orthogonality relation,

$$\int_0^b dx e^{2\pi i x (k+k')/b} = b \, \delta_{k,-k'},$$

where $\delta_{i,j}$ denotes the Kronecker symbol, the (squared) surface width W^2 may be rewritten as

$$W^2(b,t) = \sum_{k \neq 0} \langle h_k(t) \, h_{-k}(t) \rangle = \sum_{k \neq 0} \Pi_k(t) \,, \quad \Pi_k(t) \equiv \langle h_k(t) \, h_{-k}(t) \rangle \,. \tag{3.19}$$

With (3.17) and

$$\left\langle \eta_k(t)\,\eta_{k'}(t')\right\rangle = \frac{\Delta_0}{b}\delta_{k,-k'}\delta(t-t'), \tag{3.20}$$

which is inferred from the general noise correlation in (3.2), the calculation of $\Pi_k(t)$ is straightforward and yields (see also [20])

$$\Pi_k(t) = \frac{\Delta_0}{2\,\nu\,b}\,\frac{1-e^{-2\nu(2\pi k/b)^2\,t}}{(2\pi k/b)^2}. \tag{3.21}$$

Hence, we find for the surface width

$$W^2(b,t) = \frac{\Delta_0}{\nu}\,b\sum_{k=1}^{\infty}\frac{1-e^{-2\nu\,t(2\pi k)^2/b^2}}{(2\pi k)^2}. \tag{3.22}$$

Substituting in (3.22) $2\pi k \to y$ and replacing the sum approximately by an integral leads to

$$W^2(b,t) \approx \frac{\Delta_0}{2\pi\,\nu}\,b\int_{2\pi}^{\infty} dy\,\frac{1-e^{-2\nu\,t/b^2\,y^2}}{y^2}. \tag{3.23}$$

At this point we identify the Edwards-Wilkinson correlation length for a one-dimensional system as

$$\xi_{\mathrm{EW}}(t) \equiv (2\,\nu\,t)^{1/2}\,, \tag{3.24}$$

which may generally also be written as $\xi_{\mathrm{EW}}(t) = (2\nu t)^{1/z}$, where $z = 2$ is the dynamical scaling exponent of the Edwards-Wilkinson equation (see, e.g., [20]). Inserting (3.24) into (3.23) leads to the well known scaling form of the surface width, namely the Family-Vicsek scaling law [56, 57]

$$W^2(b,t) \sim b\,f_{\mathrm{EW}}\left(\frac{\xi_{\mathrm{EW}}(t)}{b}\right), \quad f(x) = \int_{2\pi}^{\infty} dy\,\frac{1-e^{-(x\,y)^2}}{y^2}, \tag{3.25}$$

or, again in greater generality, $W^2 \sim b^{2\chi}f(\xi/b)$, with $\chi = (z-d)/2 = 1/2$ the roughness exponent of the Edwards-Wilkinson equation in one spatial dimension; $f(x)$ denotes a universal scaling function.

For the scaling function $f(x)$ in (3.25) two limiting behaviors are of interest. The first one occurs for values of $x \approx 1$, or equivalently $\xi_{\mathrm{EW}}(t) \approx b$, where $f(x)$ behaves like a numerical constant. The second one is found in the limit of $x \ll 1$, or equivalently $\xi_{\mathrm{EW}}(t) \ll b$, for which it holds that $f(x \ll 1) \sim x$. Hence,

$$f(x) \sim \begin{cases} \text{const.} & \text{for } x \approx 1, \\ x & \text{for } x \ll 1. \end{cases} \tag{3.26}$$

Accordingly, the one-dimensional scaling form of the Edwards-Wilkinson surface width reads (e.g., [20, 56, 57])

$$W^2 \sim \begin{cases} t^{1/2} \ (t^{2\chi/z}) & \text{for } \xi_{\mathrm{EW}} \ll b, \\ b \quad (b^{2\chi}) & \text{for } \xi_{\mathrm{EW}} \gtrapprox b. \end{cases} \tag{3.27}$$

Here the results in brackets denote the form in terms of the critical exponents for a general d-dimensional analysis [20]. As can be seen from (3.27), the correlation length is critical in the discussion of the scaling behavior of the surface width. For correlation lengths that are significantly smaller than the system size b, the EW system is in its transient regime and the surface width grows with $t^{1/2}$ (for $d = 1$). When the correlation length is of the order of the system size the system leaves the transient regime and the surface width becomes stationary and scales like b (for $d = 1$).
While the ad-hoc approximation of the sum in (3.22) via the integral in (3.23) yields the scaling relation (3.27) not only in one spatial dimension but is valid for higher dimensions as well, it does not lead to exact results. For the case of one spatial dimension it is possible to calculate the sum in (3.22) explicitly in the transient and stationary regime, respectively. We begin with the evaluation of (3.22) in the stationary regime. From (3.27) it can be inferred that for fixed system size b, stationarity is reached for $t \to \infty$, implying $\xi_{\mathrm{EW}}(t) \gg b$ (see (3.24)). Thus, the stationary limit of the surface width is given by (see also [20])

$$\begin{aligned} \lim_{t\to\infty} W^2(b,t) &= \frac{\Delta_0}{2\,\nu\, b} \lim_{t\to\infty} \sum_{k\neq 0} \frac{1 - e^{-4\pi^2(\xi_{\mathrm{EW}}(t)k/b)^2}}{(2\pi k/b)^2} \\ &= \frac{\Delta_0\, b}{8\pi^2\,\nu} \sum_{k\neq 0} \frac{1}{k^2} = \frac{\Delta_0\, b}{4\pi^2\,\nu}\,\zeta(2) \\ &= \frac{\Delta_0}{2\,\nu}\,\frac{b}{12}, \end{aligned} \tag{3.28}$$

where $\zeta(x)$ denotes the Riemann-Zeta function. For the transient regime we note again from (3.27) that the condition on the correlation length is given by $\xi_{\mathrm{EW}} \ll b$. Hence, with (3.24), for any fixed time t, the limit of $b \to \infty$ ensures that $\xi_{\mathrm{EW}} \ll b$. Therefore, the surface width in the transient regime reads

$$\begin{aligned} \lim_{b\to\infty} W^2(b,t) &= \frac{\Delta_0}{2\,\nu} \lim_{b\to\infty} \frac{1}{b} \sum_{k\neq 0} \frac{1 - e^{-4\pi^2(\xi_{\mathrm{EW}}(t)k/b)^2}}{(2\pi k/b)^2} \\ &= \frac{\Delta_0}{\nu} \int_0^\infty dx\, \frac{1 - e^{-4\pi^2\xi_{\mathrm{EW}}^2(t)x^2}}{4\pi^2\, x^2} \\ &= \frac{\Delta_0}{2\,\nu}\,\frac{\xi_{\mathrm{EW}}(t)}{\sqrt{\pi}}, \end{aligned} \tag{3.29}$$

where we substituted $k/b = x$. With (3.24) we then find [20]

$$\lim_{b\to\infty} W^2(b,t) = \frac{\Delta_0}{2\,\nu}\sqrt{\frac{2\,\nu}{\pi}}\,t^{1/2}. \tag{3.30}$$

Comparing the expressions in (3.28) and (3.30) to the respective prediction from the scaling arguments in (3.27), it can be seen that the dependence on b and t are of course that same. However, the explicit limits in (3.28) and (3.30) also yield the exact prefactors that are not accessible via the scaling argument. Note, that in the above calculations we restricted ourselves to the case $z = 2$ and $\chi = 1/2$. In [20], one can find a derivation for general z.

At this point, we are able to calculate the Edwards-Wilkinson correlation time t_c^EW at which the surface width transitions from the transient regime to the stationary regime. This may be done by demanding that at $t = t_\mathrm{c}^\mathrm{EW}$ the value of the surface width in the transient regime has to be equal to the value of the surface width in the stationary regime. Hence, with (3.28) and (3.30),

$$\frac{\Delta_0}{2\,\nu}\sqrt{\frac{2\,\nu}{\pi}}\,(t_\mathrm{c}^\mathrm{EW})^{1/2} \stackrel{!}{=} \frac{\Delta_0}{2\,\nu}\,\frac{b}{12}. \tag{3.31}$$

This leads to (e.g., [20])

$$t_\mathrm{c}^\mathrm{EW} = \frac{\pi}{288}\,\frac{b^2}{\nu}. \tag{3.32}$$

Inserting the result from (3.32) into (3.24) yields

$$\xi_\mathrm{EW}(t_\mathrm{c}^\mathrm{EW}) = \frac{\sqrt{\pi}}{12}\,b, \tag{3.33}$$

which implies that for correlation lengths larger than $b\sqrt{\pi}/12$ the EW behavior becomes stationary.

The Kardar-Parisi-Zhang Case

The construction of an explicit expression for the KPZ correlation length $\xi_\mathrm{KPZ}(t)$ and correlation time $t_\mathrm{c}^\mathrm{KPZ}$ is tied to three properties of the KPZ equation, where the first two only hold in one spatial dimension. The first is the knowledge of the stationary probability density functional $p^s[h]$, given by (e.g., [20, 21, 58])

$$p^s[h] \sim \exp\left[-\frac{\nu}{\Delta_0}\int dx\,(\partial_x h)^2\right], \tag{3.34}$$

which is equivalent to the stationary distribution of the Edwards-Wilkinson equation[1]. This implies that all equal-time stationary correlations for the KPZ equation are actually

[1] See also Chapters 4 and 5 for further remarks on the EW/KPZ stationary probability density functional.

given by the stationary correlations of the EW equation, hence, the linear theory [20]. The second is the existence of a fluctuation dissipation theorem, see, e.g., [20, 40, 43, 54, 59]. The last property follows from a tilt-invariance (Galilean invariance) of the KPZ equation, which implies the exponent identity (see, e.g., [20, 40, 43, 54, 59])

$$z + \chi = 2. \tag{3.35}$$

In a dynamic renormalization group context, the latter two properties implie that the coupling parameter λ in (3.1) and the ratio Δ_0/ν stay invariant under the change of length scales in the DRG scheme.
Thus we know that Δ_0/ν and λ are scale-independent. This is particularly important for the construction of a KPZ correlation length, which needs to be independent of the length scale at which the KPZ system is analyzed. One way of constructing such a correlation length is via a dimensional argument and the assumption that the general structure of the KPZ correlation length is the same as in the linear case, i.e. $\xi \sim t^{1/z}$ with z now according to the dynamics of the KPZ equation (in $d = 1$, $z = 3/2$). According to [20], the only solution under the above constraints for the correlation length $\xi_{\mathrm{KPZ}}(t)$ is given by

$$\xi_{\mathrm{KPZ}}(t) = \left[\left(\frac{\Delta_0}{2\,\nu} \right)^{1/2} \lambda\, t \right]^{2/3}, \tag{3.36}$$

where the factor of 2 in the denominator has been introduced for later convenience. Note, that in Chapter 6 we calculate correlations via DRG and recover this exact expression of the correlation length from (3.36) (see (6.28)).
To introduce a relationship between the surface width W^2 and the KPZ correlation length $\xi_{\mathrm{KPZ}}(t)$, we try to follow the same steps as in the EW case. From the EW equation we know that (see (3.21))

$$\lim_{t\to\infty} \Pi_k(t) = \frac{\Delta_0\, b}{2\,\nu} \frac{1}{(2\pi\, k)^2}. \tag{3.37}$$

Since the KPZ equation in one spatial dimension has the same stationary probability distribution as the EW equation, the expression in (3.37) is expected to hold for the KPZ equation as well. In the transient regime of the KPZ equation, however, there will certainly be differences between the EW and KPZ behavior. This is taken into account by defining

$$\Pi_k^{\mathrm{KPZ}}(t) = \frac{\Delta_0\, b}{2\,\nu} \frac{1}{(2\pi\, k)^2}\, g\left(\frac{\xi_{\mathrm{KPZ}}(t)}{b}\, 2\pi\, k \right), \tag{3.38}$$

where $g(x)$ denotes the KPZ scaling function for all times t, which is the equivalent to the numerator in (3.21), but is in general unknown [20][2]. The scaling function has

[2] In [60], an exact solution for the scaling function has been derived for the stationary state of the KPZ equation. In the above context, the scaling function is needed not only in the stationary case but for all times t.

to fulfill $g(0) = 0$ and $g(x) = 1$ for $x \to \infty$ (see also the explicit form of $g(x)$ for the EW case in (3.21)) [20]. With (3.38) we calculate the surface width in the transient KPZ regime in analogy to the calculation for the EW case above (see (3.29), (3.30) and, e.g., [20])

$$\begin{aligned}
\lim_{b\to\infty} W^2(b,t) &= \frac{\Delta_0}{2\,\nu} \lim_{b\to\infty} \frac{1}{b} \sum_{k\neq 0} \frac{g\left(\xi_{\mathrm{KPZ}}(t) 2\pi\, k/b\right)}{(2\pi\, k/b)^2} \\
&= \frac{\Delta_0}{\nu} \int_0^\infty dx\, \frac{g(2\pi\, \xi_{\mathrm{KPZ}}(t)\, x)}{(2\pi\, x)^2} \\
&= \frac{\Delta_0}{2\,\nu}\, \xi_{\mathrm{KPZ}}(t) \int_0^\infty \frac{dy}{\pi}\, \frac{g(y)}{y^2} \\
&= \frac{\Delta_0}{2\,\nu}\, \xi_{\mathrm{KPZ}}(t)\, c_2\,, \quad c_2 \equiv \int_0^\infty \frac{dy}{\pi}\, \frac{g(y)}{y^2}.
\end{aligned} \tag{3.39}$$

Here, we first substituted $k/b = x$ to rewrite the sum in terms of the integral and subsequently substituted $2\pi\xi_{\mathrm{KPZ}}(t)x = y$ to arrive at the final expression in (3.39). Note, that the analytical evaluation of the amplitude c_2 is not possible due to the lack of the exact knowledge of the KPZ scaling function $g(x)$. There are, however, numerical estimates for this amplitude, which yield $c_2 \approx 0.4$ [20, 61]. Inserting the explicit expression from (3.36) for the KPZ correlation length into (3.39) leads to the following expression for the surface width in the transient KPZ regime [20],

$$W^2(t) = c_2 \left[\left(\frac{\Delta_0}{2\,\nu} \right)^2 \lambda\, t \right]^{2/3} = c_2\, \frac{\Delta_0}{2\,\nu}\, \xi_{\mathrm{KPZ}}(t). \tag{3.40}$$

With the second step in (3.40), we have the complete analogy to (3.29).
Using (3.40), we may determine two distinct time scales. One is the time at which the KPZ system changes from the transient EW regime to the transient KPZ regime, the EW to KPZ crossover time $t^{\mathrm{EW}\to\mathrm{KPZ}}$, and the second is the KPZ correlation time $t_{\mathrm{c}}^{\mathrm{KPZ}}$ at which the transient KPZ regime becomes stationary [20]. The former is obtained by demanding that at $t = t^{\mathrm{EW}\to\mathrm{KPZ}}$ the value of the surface width in the transient EW regime has to be equal to the corresponding value in the transient KPZ regime. Hence, with (3.30) and (3.40),

$$\frac{\Delta_0}{2\sqrt{\pi}\,\nu} \left(2\,\nu\, t^{\mathrm{EW}\to\mathrm{KPZ}}\right)^{1/2} \stackrel{!}{=} c_2 \left[\left(\frac{\Delta_0}{2\,\nu} \right)^2 \lambda\, t^{\mathrm{EW}\to\mathrm{KPZ}} \right]^{2/3}, \tag{3.41}$$

which yields [20]

$$t^{\mathrm{EW}\to\mathrm{KPZ}} = \frac{32}{\pi^3\, c_2^6}\, \frac{\nu^5}{\Delta_0^2\, \lambda^4}. \tag{3.42}$$

The latter time, the KPZ correlation time t_c^{KPZ}, is found via the condition that at $t = t_c^{\mathrm{KPZ}}$ the value of the surface width in the transient KPZ regime has to be equal to the stationary value of the surface width in the EW regime. This is due to the fact that the steady state correlations of the one-dimensional KPZ equation are given by the steady state correlations of the EW equation. Thus, with (3.28) and (3.40),

$$c_2 \left[\left(\frac{\Delta_0}{2\,\nu} \right)^2 \lambda\, t_c^{\mathrm{KPZ}} \right]^{2/3} \stackrel{!}{=} \frac{\Delta_0}{2\,\nu} \frac{b}{12}, \tag{3.43}$$

which yields for t_c^{KPZ} [20]

$$t_c^{\mathrm{KPZ}} = \left(\frac{b}{12\, c_2} \right)^{3/2} \left(\frac{2\,\nu}{\Delta_0} \right)^{1/2} \lambda^{-1}. \tag{3.44}$$

Rearranging the l.h.s. of (3.43) in terms of the KPZ correlation length from (3.36) and solving for $\xi_{\mathrm{KPZ}}(t_c^{\mathrm{KPZ}})$ leads to [20]

$$\xi_{\mathrm{KPZ}}(t_c^{\mathrm{KPZ}}) = \frac{b}{12\, c_2}. \tag{3.45}$$

Hence, when the correlation length of the KPZ equation becomes larger than $b/(12c_2)$ the system changes from its transient behavior into its stationary state.
In the following, we discuss the influence of the coupling strength λ on the temporal scaling of the variance of the height field, which is critically depending on the time scales derived above.

3.2.2 Temporal Scaling of the Variance of the Spatially Averaged Height Field

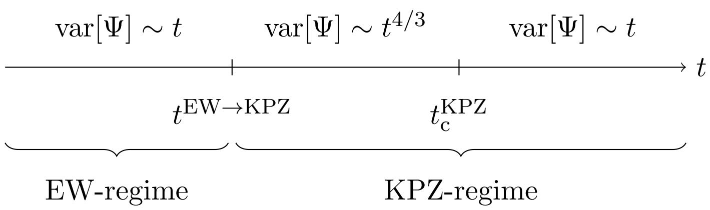

Figure 3.2: Schematic scaling behavior of var$[\Psi(t)]$ for the ‘normal’ ordering of time-scales, i.e., $t_c^{\mathrm{KPZ}} > t^{\mathrm{EW}\to\mathrm{KPZ}}$, for a finite KPZ system (see, e.g., [20]).

The KPZ equation on a one-dimensional finite substrate of size b shows intriguing behavior regarding the scaling properties of certain observables, e.g., the surface width from above. A related observable is the so-called center of mass dispersion W_c^2, which is given by [20]

$$W_c^2 \equiv \frac{1}{b^2} \left\langle \left(\int_0^b dx\, h(x,t) - \left\langle \int_0^b dx\, h(x,t) \right\rangle \right)^2 \right\rangle, \tag{3.46}$$

and describes the variance of the spatial mean of the height field $h(x,t)$ from (3.3). Its scaling behavior reads [20, 39, 62–64]

$$W_c^2 \sim \begin{cases} t^{4/3}/b & \text{for } \xi_{\mathrm{KPZ}} \ll b, \\ t/b^{1/2} & \text{for } \xi_{\mathrm{KPZ}} \gg b, \end{cases} \tag{3.47}$$

with ξ_{KPZ} from (3.36). One remarkable feature of (3.47) is the superdiffusive behavior in the transient regime $\xi_{\mathrm{KPZ}} \ll b$. In Chapter 6 we derive this scaling behavior including the respective system-parameter dependent amplitudes via a DRG scheme. In anticipation of the physical observables needed for the subsequent analysis, we will not discuss the scaling behavior of (3.46) but rather that of

$$\mathrm{var}[\Psi(t)] \equiv \left\langle \left(\int_0^b dx\, h(x,t) - \left\langle \int_0^b dx\, h(x,t) \right\rangle \right)^2 \right\rangle = b^2\, W_c^2, \tag{3.48}$$

with $\Psi(t) \equiv \int_0^b dx h(x,t)$, see Chapter 4. In the following, we focus on highlighting the scaling behavior of (3.48) in dependence of the effective coupling parameter from (3.13). To this end, it is instructive to have a look at the time-scales at which changes in the scaling behavior of $\mathrm{var}[\Psi(t)]$ occur. In the case of a large[3] coupling parameter λ_{eff} from (3.13), these time-scales are the EW to KPZ crossover time $t^{\mathrm{EW}\to\mathrm{KPZ}}$, given by (3.42) and the KPZ correlation time $t_{\mathrm{c}}^{\mathrm{KPZ}}$, given by (3.44). In Figure 3.2, we show schematically the behavior of the variance of $\Psi(t)$ if $t_{\mathrm{c}}^{\mathrm{KPZ}} > t^{\mathrm{EW}\to\mathrm{KPZ}}$. For times $t < t^{\mathrm{EW}\to\mathrm{KPZ}}$ the system is in the so-called Edwards-Wilkinson regime, characterized by the critical exponent $z = 2$ of the linear theory. In this scaling regime, the variance of $\Psi(t)$ is expected to scale linearly in time t [20]. For times in the range $t^{\mathrm{EW}\to\mathrm{KPZ}} < t < t_{\mathrm{c}}^{\mathrm{KPZ}}$, the system is in its transient regime. This regime belongs to the KPZ scaling-regime, characterized by the KPZ critical exponent $z = 3/2$. While in the transient regime, the variance is predicted via scaling arguments to scale with $t^{4/3}$, i.e., it displays superdiffusive behavior [20]. For times $t > t_{\mathrm{c}}^{\mathrm{KPZ}}$ the system enters the KPZ stationary regime, where the variance is again expected to scale linearly in time t. However, due to the superdiffusive behavior in the transient regime, the proportionality factor is larger in the stationary KPZ regime than in the EW scaling regime [20][4]. In the following we will refer to the above described behavior as the behavior for the 'normal' ordering of time-scales, namely

[3] What is meant by 'large' will be made precise in (3.52).

[4] This time behavior of $\mathrm{var}[\Psi(t)]$ can be clearly observed in Figure 7.6.

$t_{\mathrm{c}}^{\mathrm{KPZ}} > t^{\mathrm{EW}\to\mathrm{KPZ}}$.
Before we discuss the case of $t^{\mathrm{EW}\to\mathrm{KPZ}} > t_{\mathrm{c}}^{\mathrm{KPZ}}$ let us reformulate the two time-scales in (3.42) and (3.44) by expressing both in terms of the effective coupling parameter λ_{eff} from (3.13). To this end we introduce a dimensionless time $t_s = t/T$ with the diffusive time scale $T = b^2/\nu$ from (3.9). This yields for the EW to KPZ crossover time

$$t_s^{\mathrm{EW}\to\mathrm{KPZ}} = \frac{32}{\pi^3\, c_2^6} \frac{\nu^6}{\Delta_0^2\, b^2} \frac{1}{\lambda^4} = \frac{32}{\pi^3\, c_2^6} \frac{1}{\lambda_{\mathrm{eff}}^4}, \tag{3.49}$$

and for the KPZ correlation time

$$t_{\mathrm{c},s}^{\mathrm{KPZ}} = \sqrt{\frac{2}{(12\, c_2)^3}} \left(\frac{\nu^3}{\Delta_0\, b}\right)^{1/2} \frac{1}{\lambda} = \sqrt{\frac{2}{(12\, c_2)^3}} \frac{1}{\lambda_{\mathrm{eff}}}. \tag{3.50}$$

The form of (3.49) and (3.50) indicates the existence of a critical effective coupling parameter $\lambda_{\mathrm{eff}}^{\mathrm{c}}$ below which the 'normal' ordering of time-scales breaks down, that is, $t_s^{\mathrm{EW}\to\mathrm{KPZ}} > t_{\mathrm{c},s}^{\mathrm{KPZ}}$. One may think of this as shrinking the transient regime in Figure 3.2 to zero, and thus, equating (3.49) with (3.50) and solving for λ_{eff} yields

$$\lambda_{\mathrm{eff}}^{\mathrm{c}} = \frac{8}{\pi} \sqrt{\frac{3}{2\, c_2^3}}\,. \tag{3.51}$$

Note, that in Chapters 6 and 7 we will use the approximation $c_2 \approx 0.4$ from [20, 61] when needing the numerical values of the crossover time $t^{\mathrm{EW}\to\mathrm{KPZ}}$ from (3.42), (3.49), the correlation time $t_{\mathrm{c}}^{\mathrm{KPZ}}$ from (3.44), (3.50) as well as the critical effective coupling constant from (3.51).
In dependence of the critical effective coupling parameter we have

$$\begin{aligned} t_s^{\mathrm{EW}\to\mathrm{KPZ}} &< t_{\mathrm{c},s}^{\mathrm{KPZ}} \quad \text{for} \quad \lambda_{\mathrm{eff}} > \lambda_{\mathrm{eff}}^{\mathrm{c}}, \\ t_s^{\mathrm{EW}\to\mathrm{KPZ}} &> t_{\mathrm{c},s}^{\mathrm{KPZ}} \quad \text{for} \quad \lambda_{\mathrm{eff}} < \lambda_{\mathrm{eff}}^{\mathrm{c}}. \end{aligned} \tag{3.52}$$

Hence, the behavior of $\mathrm{var}[\Psi(t)]$ sketched in Figure 3.2 is valid as long as $\lambda_{\mathrm{eff}} > \lambda_{\mathrm{eff}}^{\mathrm{c}}$.
We now turn to the behavior of the variance of $\Psi(t)$ for $\lambda_{\mathrm{eff}} < \lambda_{\mathrm{eff}}^{\mathrm{c}}$. In this case we have $t_s^{\mathrm{EW}\to\mathrm{KPZ}} > t_{\mathrm{c},s}^{\mathrm{KPZ}}$, which is physically not sensible as this implies that the system would have to become stationary in the KPZ regime before even crossing over from the EW to the KPZ regime. This situation is resolved by taking the EW correlation time $t_{\mathrm{c}}^{\mathrm{EW}}$ into account. With the result from (3.32),

$$t_{\mathrm{c},s}^{\mathrm{EW}} = \frac{\pi}{288}. \tag{3.53}$$

As can easily be seen, $\lambda_{\mathrm{eff}} < \lambda_{\mathrm{eff}}^{\mathrm{c}}$ implies that $t_{\mathrm{c},s}^{\mathrm{EW}} < t_s^{\mathrm{EW}\to\mathrm{KPZ}}$, hence the system becomes stationary in the EW scaling regime. Therefore, if $\lambda_{\mathrm{eff}} \ll \lambda_{\mathrm{eff}}^{\mathrm{c}}$, its dynamical behavior

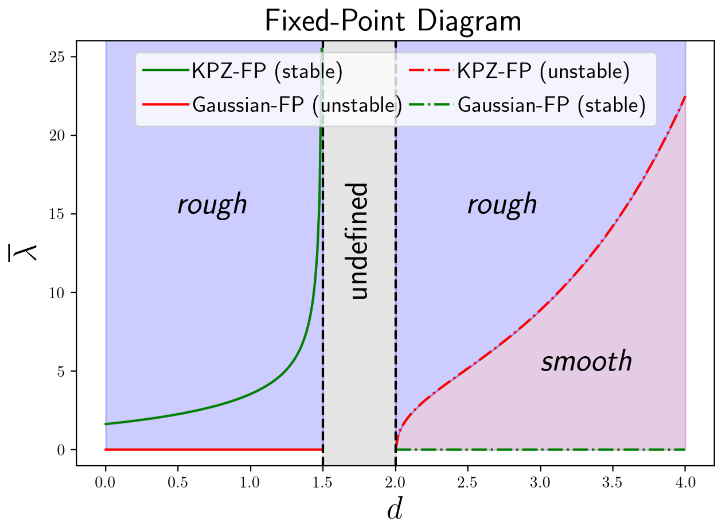

Figure 3.3: Fixed-point diagram of the d-dimensional KPZ equation. The fixed-points are calculated using one-loop DRG, see (8.6).

will be governed for all times t by the critical exponent $z = 2$ of the linear theory. For $\lambda_{\text{eff}} \uparrow \lambda_{\text{eff}}^{\text{c}}$ the behavior of the variance will change from the one in the linear theory to the one predicted for the KPZ equation and should be accessible by a perturbation expansion in λ_{eff} up to $\lambda_{\text{eff}} \approx \lambda_{\text{eff}}^{\text{c}}$. This approach will be taken in Chapter 5. Note, that when we state λ_{eff} 'small', we mean $\lambda_{\text{eff}} < \lambda_{\text{eff}}^{\text{c}}$.

3.3 Phase Transition of the Kardar-Parisi-Zhang Equation

Another important feature of the KPZ equation is the so-called roughening transition, which occurs only for spatial dimensions $d > 2$. A concise analytical treatment of the roughening transition will be given in Chapter 8. To understand this transition, the fixed-point structure of the KPZ equation with respect to the effective coupling parameter $\overline{\lambda}$ (see (8.5)) is of importance. In Chapter 8 we derive this fixed-point structure by means of a one-loop dynamic renormalization group (DRG) approach (see (8.4) and (8.6)). For the purpose of this section, the technical details are not important and thus we simply plot the resulting fixed-point structure from (8.6) in $\overline{\lambda}$ as a function of the spatial dimension d in Figure 3.3. As can be seen, there are two distinct fixed-points. One is the so-called Gaussian fixed-point ($\overline{\lambda}_* = 0$, see (8.6)) and the second one is the so-called KPZ fixed-point ($\overline{\lambda}_* = \sqrt{4d(d-2)/((2d-3)K_d)}$, see (8.6)) or also strong-coupling fixed-point. For dimensions $d < 3/2$, the Gaussian fixed-point is unstable and the KPZ fixed-point stable, hence the RG flow is from the Gaussian to the KPZ fixed-point. In $d = 1$, the

KPZ fixed-point is characterized by the critical exponents $z = 3/2$ and $\chi = 1/2$, which fulfills the exponent identity $z + \chi = 2$ (see, e.g., [12, 54, 59]). As $\chi = 1/2 > 0$ for $d = 1$, the KPZ system is in its rough phase. The calculations in Chapter 6 are performed at this fixed-point. As can be seen from Figure 3.3, the only existing phase for $d < 3/2$ is the rough phase of the KPZ equation (see also [54, 59, 65–67]). Note that the gap between $3/2 < d < 2$ is due to the one-loop order DRG approach and can be filled by a two-loop calculation [54]. In particular, the divergence of the KPZ fixed-point is shifted from $d = 3/2$ in the one-loop case to $d = 2$ in the two-loop case. The general fixed-point structure, however, remains the same for the one- and two-loop calculations.

For dimensions $d > 2$ the stability of the fixed-points is reversed, i.e., the KPZ fixed-point becomes unstable and the Gaussian fixed-point stable, see Figure 3.3. Since the KPZ fixed-point is unstable, the RG flow now points away from this fixed-point for every $d > 2$. For all $\overline{\lambda}$ that lie below the KPZ fixed-point value, the system is thus driven to the stable Gaussian, or weak-coupling fixed-point. For all $\overline{\lambda}$ that are greater than the KPZ fixed-point value, the RG flow drives the system to a stable fixed-point at infinity, the strong-coupling fixed-point. This implies that the perturbative DRG approach is not feasible in this case (see, e.g., [54, 68]). There are approaches to the strong-coupling regime using mode-coupling theory, see, e.g., [69, 70], non-perturbative DRG, see, e.g., [71] and weak-noise approximations, see, e.g., [65]. The light-red shaded region in Figure 3.3 is the only domain for $d > 2$, where the perturbative DRG approach is applicable. This is the region relevant in Chapter 8. Using the results in (8.13) with (8.12) and (8.14) as well as the general scaling form for the correlation function (see, e.g., [12, 54, 57, 59] and replace $u = -\nabla h$),

$$C(q, \omega) = q^{-(d+2\chi+z-2)} \Phi \left(\frac{\omega}{q^z} \right), \tag{3.54}$$

with Φ a universal scaling function, we infer that for all $d > 2$ the dynamical scaling exponent $z = 2$ and the roughness exponent $\chi = 1 - d/2 < 0$. Note, that at the Gaussian fixed-point the exponent identity $z + \chi = 2$ is not fulfilled. Hence, with $\chi < 0$ for $d > 2$, the light-red shaded region in Figure 3.3 represents a smooth phase of the KPZ system. In the light-blue shaded region in Figure 3.3, which is the region of $\overline{\lambda}$-values driven to the strong-coupling fixed-point, the exponent identity $z + \chi = 2$ is expected to hold. As the strong-coupling KPZ fixed-point is characterized by $z < 2$, the exponent identity dictates $\chi > 0$ and thus the light blue shaded region in Figure 3.3 represents a rough phase of the KPZ system. Therefore, for $d > 2$, the KPZ fixed-point as a function of spatial dimension d acts as a phase-separation line between the smooth and rough state of the KPZ system. On this phase-separation line, the critical exponents read $z = 2$ and $\chi = 0$.

From the above discussion, it becomes apparent that $d = 2$ is a critical dimension, called the lower critical dimension of the KPZ equation. The existence and value of an upper critical dimension is, to our knowledge, still not answered satisfactorily (see, e.g., [65–67, 69–76]). Such an upper critical dimension would appear in the rough phase and denote a dimension above which $z = 2$ and $\chi = 0$.

Appendix 3.A Mathematical Prerequisites Regarding the KPZ Equation

3.A.1 Expansion in Terms of Eigenfunctions

In, e.g., Section 3.2.1 we have seen that the representation of the height and noise fields via their respective Fourier series (see (3.15)) is a convenient tool in treating SPDEs like (3.14) and, as will be shown below, for the full KPZ equation itself. The Fourier expansion can be understood in a more general sense. For the case of periodic boundary conditions, the differential operator $\hat{L} = \nu\,\partial_x^2$ possesses the eigenfunctions $\{\phi_k(x)\}$,

$$\phi_k(x) \equiv \frac{1}{\sqrt{b}} e^{2\pi i k x/b} \qquad k \in \mathbb{Z}, \tag{3.55}$$

and corresponding eigenvalues $\{\mu_k\}$,

$$\mu_k \equiv -4\,\pi^2\,\frac{\nu}{b^2}\,k^2 \qquad k \in \mathbb{Z}. \tag{3.56}$$

In terms of the dimensionless representation, we have

$$\phi_{s,\,k}(x_s) = e^{2\pi i k x_s}, \tag{3.57}$$

and

$$\mu_{s,\,k} = -4\,\pi^2\,k^2. \tag{3.58}$$

It is well-known that the set $\{\phi_k(x)\}$ constitutes a complete orthonormal system in the Hilbert space $\mathcal{L}_2(0, b)$ of all square-integrable functions on $(0, b)$, equipped with the usual $\mathcal{L}_2$-product $(\cdot,\cdot)_0 = \int_0^b dx\ \cdot(x)\cdot(x)$. Thus, the expansions

$$\begin{aligned} h(x,t) &= \sum_{k\in\mathbb{Z}} h_k(t)\phi_k(x), \\ \eta(x,t) &= \sum_{k\in\mathbb{Z}} \eta_k(t)\phi_k(x), \end{aligned} \tag{3.59}$$

$h_k(t)$, $\eta_k(t) \in \mathbb{C}$, hold and the Fourier-expansion can also be interpreted as an expansion in the eigenfunctions of the operator $\hat{L}$. A similar proceeding was used in [77–80]. With this interpretation, (3.17) also holds when in the EW equation (3.14) the operator $\hat{L} = \nu\,\partial_x^2$ is replaced by $\hat{L}_p \equiv (-1)^{p+1}\partial_x^{2p}$, with $p \in \mathbb{N}$ and adjusted eigenvalues $\{\mu_k^p\}$. The choice $p = 2$ has been used for the description of surface growth in [14, 81].

3.A.2 Spectral Form of the KPZ Equation

We formulate (3.3) on the one-dimensional spatial interval $[0, b]$, $b > 0$, with Gaussian white noise $\eta(x,t)$

$$\begin{aligned} \frac{\partial\, h(x,t)}{\partial t} &= \hat{L}\, h(x,t) + \frac{\lambda}{2}\left(\frac{\partial\, h(x,t)}{\partial x}\right)^2 + \eta(x,t) \\ \langle \eta(x,t)\rangle &= 0 \\ \big\langle \eta(x,t)\, \eta(x',t')\big\rangle &= \Delta_0 \delta(x-x')\delta(t-t'), \end{aligned} \tag{3.60}$$

with vanishing initial condition $h(x,0) = 0$, $x \in [0,b]$ (i.e., the growth process starts with a flat profile). Here $\hat{L}$ is the standard diffusion operator with periodic boundary conditions. Like above in (3.3), Δ_0 denotes a constant noise strength, and λ the coupling constant of the non-linearity. We will apply the eigenfunction-expansion of the height field $h(x,t)$ and the stochastic driving force $\eta(x,t)$ from (3.59) to (3.60), which yields

$$\begin{aligned} &\sum_{k\in\mathbb{Z}} \dot{h}_k(t)\phi_k(x) \\ &= \sum_{k\in\mathbb{Z}} h_k(t)\hat{L}\phi_k(x) + \frac{\lambda}{2}\sum_{l,m\in\mathbb{Z}} h_l(t)h_m(t)\partial_x\phi_l(x)\partial_x\phi_m(x) + \sum_{k\in\mathbb{Z}} \eta_k(t)\phi_k(x) \\ &= \sum_{k\in\mathbb{Z}} h_k(t)\mu_k\phi_k(x) - 2\pi^2\frac{\lambda}{b^2}\sum_{l,m\in\mathbb{Z}} l\, m\, h_l(t)h_m(t)\phi_l(x)\phi_m(x) \\ &\quad + \sum_{k\in\mathbb{Z}} \eta_k(t)\phi_k(x). \end{aligned}$$

For the $\{\phi_k(x)\}$ the relation $\phi_l(x)\phi_m(x) = \phi_{l+m}(x)/\sqrt{b}$ holds and thus the double-sum in the eigenfunction-expansion of the KPZ equation can be rewritten in convolution form setting $k = l + m$. This yields

$$\begin{aligned} &\sum_{k\in\mathbb{Z}} \dot{h}_k(t)\phi_k(x) \\ &= \sum_{k\in\mathbb{Z}} h_k(t)\mu_k\phi_k(x) - 2\pi^2\frac{\lambda}{b^{5/2}}\sum_{k,l\in\mathbb{Z}} l(k-l)h_l(t)h_{k-l}(t)\phi_k(x) \\ &\quad + \sum_{k\in\mathbb{Z}} \eta_k(t)\phi_k(x), \end{aligned} \tag{3.61}$$

which implies ordinary differential equations for the coefficients $h_k(t)$,

$$\dot{h}_k(t) = \mu_k h_k(t) - 2\pi^2\frac{\lambda}{b^{5/2}}\sum_{l\in\mathbb{Z}} l(k-l)h_l(t)h_{k-l}(t) + \eta_k(t). \tag{3.62}$$

The above ODEs (3.62) are readily 'solved' by the variation-of-constants formula, which leads for flat initial condition $h_k(0) \equiv 0$ to

$$h_k(t) = \int_0^t dt' e^{\mu_k(t-t')} \left[\eta_k(t') - 2\pi^2 \frac{\lambda}{b^{5/2}} \sum_{l \in \mathbb{Z}\setminus\{0\}} l(k-l) h_l(t') h_{k-l}(t') \right], \tag{3.63}$$

$k \in \mathbb{Z}$. With (3.63), a non-linear integral equation for the k-th Fourier coefficient has been derived. In Section 5.1, the solution to (3.63) will be constructed by means of an expansion in a small coupling parameter λ.

3.A.3 Stochastic Convolution and Mild Solution

Equation (3.63) has been derived on a purely formal level. In particular, the integral $\int dt' e^{\mu_k(t-t')} \eta_k(t')$ has to be given a meaning. In a strict mathematical formulation, this integral has to be written as

$$\int_0^t e^{\mu_k(t-t')} dW_k(t'), \tag{3.64}$$

which is called a stochastic convolution (see e.g. [82–85])[5]. This has its origin in the fact that the noise $\eta(x,t)$ in (3.60) is, mathematically speaking, a generalized time-derivative of a Wiener process $W(x,t)$ (see also Appendix 3.A.5, (3.67)). In this spirit, (3.63) with the first integral on the right hand side replaced by (3.64) may be called the mild form of the KPZ equation (in its spectral representation) and $h(x,t) = \sum_{k\in\mathbb{Z}} h_k(t)\phi_k(x)$, $h_k(t)$ solution of equation (3.63), is then called a mild solution of the KPZ equation. In mathematical literature, proofs of existence and uniqueness of such a mild solution to the KPZ-Burgers equation can be found for various assumptions on the spatial regularity of the noise (see e.g. [84, 86, 87] and references therein). These assumptions generally exclude space-time white noise. Therefore, some form of regularization is needed (see also Appendix 3.A.5).

3.A.4 Remarks on the Noise Structure

Besides the complex Fourier expansion in (3.59) with coefficients $h_k(t) \in \mathbb{C}$, the real expansion $h(x,t) = \sum_{k\in\mathbb{Z}} \widetilde{h}_k(t)\gamma_k(x)$, $\widetilde{h}_k(t) \in \mathbb{R}$ (e.g. [84]) and

$$\gamma_0 = \frac{1}{\sqrt{b}}, \quad \gamma_k = \sqrt{\frac{2}{b}} \sin 2\pi k \frac{x}{b}, \quad \gamma_{-k} = \sqrt{\frac{2}{b}} \cos 2\pi k \frac{x}{b} \quad k \in \mathbb{N}, \tag{3.65}$$

will be used, for convenience, in this section. The relationship between $h_k(t)$ and $\widetilde{h}_k(t)$ reads

$$h_k(t) = \frac{\widetilde{h}_{-k}(t) - i\widetilde{h}_k(t)}{\sqrt{2}}, \qquad h_{-k}(t) = \frac{\widetilde{h}_{-k}(t) + i\widetilde{h}_k(t)}{\sqrt{2}} = \overline{h_k}(t), \tag{3.66}$$

[5] Due to the deterministic integrand of (3.64), the integral can optionally be interpreted in the Ito or Stratonovitch sense, respectively [82]

with $\overline{h_k}(t)$ as the complex conjugate.
The noise $\eta(x,t)$ is given by a generalized time-derivative of a Wiener process $W(x,t) \in \mathbb{R}$ [82–84, 88], i.e.,

$$\eta(x,t) = \sqrt{\Delta_0}\,\frac{\partial\, W(x,t)}{\partial t}. \tag{3.67}$$

Such a Wiener process $W(x,t)$ can be written as (e.g., [82, 84])

$$W(x,t) = \sum_{k\in\mathbb{Z}} \alpha_k \beta_k(t) \gamma_k(x). \tag{3.68}$$

Here $\{\alpha_k\} \in \mathbb{R}$ are arbitrary expansion coefficients that may be used to introduce a spatial regularization of the Wiener process, $\{\beta_k(t)\} \in \mathbb{R}$ are stochastically independent standard Brownian motions and $\{\gamma_k(x)\}$ from (3.65). A well-known result for the two-point correlation function of two stochastically independent Brownian motions $\beta_k(t)$ reads [82]

$$\big\langle \beta_k(t)\, \beta_l(t') \big\rangle = (t \wedge t')\, \delta_{k,l}, \tag{3.69}$$

with $(t \wedge t') = \min(t, t')$.
In the following it will be shown that the noise η defined by (3.67) and (3.68) possesses the autocorrelation

$$\big\langle \eta(x,t)\, \eta(x',t') \big\rangle = K(x-x')\delta(t-t'), \tag{3.70}$$

which for $K(x-x') = \Delta_0\delta(x-x')$ results in space-time white noise. Furthermore, an explicit expression of the kernel $K(x-x')$ by means of the Fourier coefficients $\{\alpha_k\}$ of $W(x,t)$ from (3.68) will be given.
To this end, first an expression for the two-point correlation function of the Wiener process itself can be derived according to

$$\begin{aligned}\big\langle W(x,t)\, W(x',t') \big\rangle = \frac{t\wedge t'}{b}\Bigg[&\alpha_0^2 + \sum_{k\in\mathbb{N}} \left[\alpha_{-k}^2 + \alpha_k^2\right] \cos 2\pi k \frac{x-x'}{b} \\ &+ \sum_{k\in\mathbb{N}} \left[\alpha_{-k}^2 - \alpha_k^2\right] \cos 2\pi k \frac{x+x'}{b}\Bigg].\end{aligned} \tag{3.71}$$

To represent the noise structure dictated by (3.70), the expression in (3.71) has to be an even, translationally invariant function in space. Thus, the following relation has to be fulfilled

$$\alpha_{-k} = \alpha_k \quad \forall\, k \in \mathbb{N}. \tag{3.72}$$

Then the two-point correlation function of the Wiener process is given by

$$\big\langle W(x,t)\, W(x',t') \big\rangle = \frac{t\wedge t'}{b}\left[\alpha_0^2 + 2\sum_{k\in\mathbb{N}} \alpha_k^2 \cos 2\pi k \frac{x-x'}{b}\right]. \tag{3.73}$$

With $W(x,t) = \sum_{k\in\mathbb{Z}} W_k(t)\phi_k(x)$, $\phi_k(x)$ from (3.55), equation (3.73) implies for the two-point correlation function of the Fourier coefficients $W_k(t)$

$$\big\langle W_k(t)\, W_l(t')\big\rangle = \alpha_k\, \alpha_l\, (t\wedge t')\, \delta_{k,-l}, \qquad k,l\in\mathbb{Z}. \tag{3.74}$$

This result leads immediately to

$$\big\langle \eta_k(t)\, \eta_l(t')\big\rangle \equiv \Delta_0 \frac{\partial^2\, \langle W_k(t)\, W_l(t')\rangle}{\partial t\, \partial t'} = \Delta_0 \alpha_k\, \alpha_l\, \delta_{k,-l}\, \delta(t-t'), \qquad k,l\in\mathbb{Z}, \tag{3.75}$$

using $\partial_t\partial_{t'}(t\wedge t') = \delta(t-t')$.
For the relation between (3.73) and the noise from (3.70), we differentiate (3.73) with respect to t and t' yielding

$$\begin{aligned}\big\langle \eta(x,t)\, \eta(x',t')\big\rangle &= \Delta_0 \frac{\partial^2\, \langle W(x,t)\, W(x',t')\rangle}{\partial t\, \partial t'} \\ &= \frac{\Delta_0}{b}\left[\alpha_0^2 + 2\sum_{k\in\mathbb{N}} \alpha_k^2\, \cos 2\pi k \frac{x-x'}{b}\right]\delta(t-t').\end{aligned} \tag{3.76}$$

The following identification can be made

$$K(x-x') = \frac{\Delta_0}{b}\left[\alpha_0^2 + 2\sum_{k\in\mathbb{N}} \alpha_k^2\, \cos 2\pi k \frac{x-x'}{b}\right] = K(|x-x'|), \tag{3.77}$$

which structurally represents the standard implicit assumption that $K(x-x')$ is translationally invariant, positive definite and even. Note, that the regularity of the noise-kernel $K(|x-x'|)$ is given by the behavior of the set of $\{\alpha_k\}$ for $k\to\infty$, where $\{\alpha_k\}$ are the dimensionless Fourier coefficients of the underlying Wiener process from (3.68) for all k. For the case of $\alpha_k = 1\ \forall\ k\in\mathbb{Z}$, spatially white noise is obtained.
Thus, the derivation via the Wiener process has indeed led to a translationally invariant real-valued two-point correlation function for $\eta(x,t)$, given by (3.70), with $K(|x-x'|)$ from (3.77), which describes white in time and spatially colored Gaussian noise. In the following, we will use (3.77) to approximate spatially white noise to meet the required form in (3.60).

3.A.5 Regularity of the KPZ Equation and its Implications

The solution $h(x,t)$ to the KPZ equation from (3.3) is a very rough function for all times t. The spatial regularity of $h(x,t)$ cannot be higher than that of the solution to the corresponding Edwards-Wilkinson equation, $h^{(0)}(x,t)$, i.e., the KPZ equation with a vanishing coupling constant, $\lambda = 0$ in (3.3) (see, e.g., [89–91]). For $h^{(0)}(x,t)$ it can be checked that for all $t>0$

$$\left\langle \left\| h^{(0)}(x,t)\right\|_{H^s}^2 \right\rangle < \infty \quad \text{for} \quad s < 1/2, \tag{3.78}$$

where H^s denotes the Sobolev space of order $s \in \mathbb{R}$ of 1-periodic functions,

$$H^s = \left\{ f \;\middle|\; f(x) = \sum_{k\in\mathbb{Z}} f_k e^{2\pi i k x} \text{ and } \|f\|^2_{H^s} \equiv \sum_{k\in\mathbb{Z}} (1+k^2)^s |f_k|^2 < \infty \right\}. \tag{3.79}$$

This implies that $h^{(0)}(x,t) \in H^s$ with $s < 1/2$, and thus $h^{(0)}(x,t) \in \mathcal{L}_2$, however $h^{(0)}(x,t) \notin H^1$. Therefore, $\langle \|\partial_x h^{(0)}\|^2_{\mathcal{L}_2} \rangle = \langle \int dx\, (\partial_x h^{(0)})^2 \rangle$, is not a well-defined quantity. This means that the solution $h(x,t)$ is not regular enough to give a mathematically sound meaning to the KPZ non-linearity $(\partial_x h(x,t))^2$. Thus, the KPZ equation is mathematically ill-defined. In order to avoid divergent terms, some form of regularization is needed. This may be done by either choosing a more regular colored noise by means of the Fourier coefficients $\{\alpha_k\}$ from (3.68) or, alternatively, by introducing a cutoff Λ of the Fourier spectrum. Throughout this thesis, the latter is chosen.
Such a cutoff amounts to an orthogonal projection of the full eigenfunction expansion of (3.60) to a finite-dimensional subspace spanned by the eigenfunctions $\phi_{-\Lambda}(x), \ldots, \phi_{\Lambda}(x)$. Mathematically, this projection may be represented by a linear projection operator $\mathcal{P}_\Lambda$, which maps the Hilbert space $\mathcal{L}_2(0,b)$ to $\mathrm{span}\{\phi_{-\Lambda}(x), \ldots, \phi_{\Lambda}(x)\}$, acting on (3.61). In terms of the noise representation from Appendix 3.A.4 this implies that we choose $\alpha_k = 1$ for $k \in \mathfrak{R}$, with

$$\mathfrak{R} \equiv [-\Lambda, \Lambda]. \tag{3.80}$$

and $\alpha_k = 0$, otherwise. Hence, the noise kernel from (3.77) now reads

$$K(x-x') = \frac{\Delta_0}{b}\left[1 + 2\sum_{k=1}^{\Lambda} \cos 2\pi k \frac{x-x'}{b}\right] = \Delta_0 \delta(x-x')\Big|_{\mathrm{span}\{\phi_{-\Lambda},\ldots,\phi_\Lambda\}}, \tag{3.81}$$

and its dimensionless form is given by

$$K_\mathrm{s}(x_\mathrm{s} - x'_\mathrm{s}) = 1 + 2\sum_{k=1}^{\Lambda} \cos 2\pi k (x_\mathrm{s} - x'_\mathrm{s}). \tag{3.82}$$

Also, the choice of $\alpha_k = 1 \;\forall\, k \in \mathfrak{R}$ implies for the correlation function of the Fourier coefficients $\eta_k(t)$ from (3.75)

$$\langle \eta_k(t)\eta_l(t') \rangle = \Delta_0 \delta_{k,-l} \delta(t-t') \qquad k,l \in \mathfrak{R}, \tag{3.83}$$

or, in dimensionless form

$$\langle \eta_{s,k}(t_\mathrm{s})\eta_{s,l}(t'_\mathrm{s}) \rangle = \delta_{k,-l} \delta(t_\mathrm{s} - t'_\mathrm{s}) \qquad k,l \in \mathfrak{R}. \tag{3.84}$$

This mapping, however, causes a problem in the non-linear term of (3.61), where by mode coupling the k-th Fourier mode ($-\Lambda \le k \le \Lambda$) is influenced also by modes with $|l| > \Lambda$.

This issue can be resolved by choosing Λ large enough, for modes with $h_l(t) \sim \exp[\mu_l t]$, μ_l from (3.56), (3.58), $|l| > \Lambda$ will be damped out rapidly so that the bias introduced by limiting l to the interval $\mathfrak{R}$ is small. Note that the restriction to $h \in \mathrm{span}\{\phi_{-\Lambda}, \ldots, \phi_{\Lambda}\}$ also implies the introduction of restricted summation boundaries in the convolution term in (3.63), namely

$$\sum_{l\in\mathbb{Z}} l(k-l)h_l h_{k-l} \quad \longrightarrow \quad \sum_{l\in\mathfrak{R}_k\setminus\{0,k\}} l(k-l)h_l h_{k-l}, \qquad k \in \mathfrak{R},$$

with $\mathfrak{R}_k$ defined by

$$\mathfrak{R}_k \equiv [\max(-\Lambda, -\Lambda+k), \min(\Lambda, \Lambda+k)]\,, \qquad k \in \mathfrak{R}. \tag{3.85}$$

To end this section, a noise operator $\hat{K}$ describing spatial noise correlations will be introduced as

$$\hat{K}(\cdot) \equiv \int_0^b dx' K(x-x')(\cdot)(x'), \tag{3.86}$$

with kernel $K(x-x')$ from (3.81) and its inverse $\hat{K}^{-1}$ given by

$$\hat{K}^{-1}(\cdot) = \int_0^b dx' K^{-1}(x-x')(\cdot)(x'), \tag{3.87}$$

where its kernel reads $K^{-1}(x-x') = \Delta_0^{-1}\delta(x-x')\Big|_{\mathrm{span}\{\phi_{-\Lambda},\ldots,\phi_{\Lambda}\}}$. It can be checked that

$$\hat{K}(\phi_k(x)) = \alpha_k^2\,\phi_k(x)\,, \qquad \forall k \in \mathbb{Z}, \tag{3.88}$$

with $\phi_k(x)$ from (3.57) and α_k from (3.68), which will be of use in Section 4.2. In dimensionless form, the noise operators defined in (3.86), (3.87), respectively, read

$$\hat{K}_{\mathrm{s}}(\cdot) = \int_0^1 dx'_{\mathrm{s}}\, K_{\mathrm{s}}(x_{\mathrm{s}} - x'_{\mathrm{s}})(\cdot)(x'_{\mathrm{s}}), \tag{3.89}$$

and

$$\hat{K}_{\mathrm{s}}^{-1}(\cdot) = \int_0^1 dx'_{\mathrm{s}}\, K_{\mathrm{s}}^{-1}(x_{\mathrm{s}} - x'_{\mathrm{s}})(\cdot)(x'_{\mathrm{s}}), \tag{3.90}$$

with $K_{\mathrm{s}}(x_{\mathrm{s}} - x'_{\mathrm{s}})$ from (3.82) and $K_{\mathrm{s}}^{-1}(x_{\mathrm{s}} - x'_{\mathrm{s}})$ is defined via the integral-relation $\int dy_{\mathrm{s}}\, K_{\mathrm{s}}(x_{\mathrm{s}} - y_{\mathrm{s}}) K_{\mathrm{s}}^{-1}(y_{\mathrm{s}} - z_{\mathrm{s}}) = \delta(x_{\mathrm{s}} - z_{\mathrm{s}})$.

4 Field–Theoretic Thermodynamic Uncertainty Relation

4.1 General Formulation

In this section, we will present a generalization of the thermodynamic uncertainty relation introduced in Section 2.4 to a field theory. Consider a generic field theory of the form

$$\begin{aligned} \partial_t \Phi_\gamma(\mathbf{r},t) &= F_\gamma\left[\{\Phi_\mu(\mathbf{r},t)\}\right] + \eta_\gamma(\mathbf{r},t), \\ \langle \eta_\gamma(\mathbf{r},t)\rangle &= 0, \\ \left\langle \eta_\gamma(\mathbf{r},t)\eta_\kappa(\mathbf{r}',t')\right\rangle &= K(\mathbf{r}-\mathbf{r}')\delta_{\gamma,\kappa}\delta(t-t'). \end{aligned} \tag{4.1}$$

Here $\Phi_\gamma(\mathbf{r},t)$ is a scalar field or the γ-th component of a vector field ($\gamma \in \mathbb{N}$) with $\mathbf{r} \in \Omega \subset \mathbb{R}^d$, $F_\gamma\left[\{\Phi_\mu(\mathbf{r},t)\}\right]$ represents a (possibly non-linear) functional of Φ_μ and $\eta_\gamma(\mathbf{r},t)$ denotes Gaussian noise, which is white in time, and with $K(\mathbf{r}-\mathbf{r}')$ as spatial noise correlations. Prominent examples of (4.1) are the stochastic Navier-Stokes equation for turbulent flow (see e.g. [88]) or the Kardar-Parisi-Zhang equation for non-linear growth processes [12] to name only two. The latter will be treated in the subsequent chapters within the framework established in the following.

Let us begin with the introduction of some notions. A natural choice of a local fluctuating current $\mathbf{j}(\mathbf{r},t)$ is

$$\mathbf{j}(\mathbf{r},t) \equiv \partial_t \mathbf{\Phi}(\mathbf{r},t), \tag{4.2}$$

with $\mathbf{\Phi}(\mathbf{r},t) = (\Phi_1(\mathbf{r},t),\ldots,\Phi_n(\mathbf{r},t))^\top$. The local current $\mathbf{j}(\mathbf{r},t)$ is fluctuating around its mean, i.e.

$$\mathbf{j}(\mathbf{r},t) = \langle \mathbf{j}(\mathbf{r},t)\rangle + \delta\mathbf{j}(\mathbf{r},t), \tag{4.3}$$

with $\delta\mathbf{j}(\mathbf{r},t)$ denoting the fluctuations. Given that the system (4.1) possesses a NESS, the long-time behavior of the local current (4.2) can be described as

$$\mathbf{j}(\mathbf{r},t) = \mathbf{J}(\mathbf{r}) + \delta\mathbf{j}(\mathbf{r},t), \tag{4.4}$$

with $\delta\mathbf{j}(\mathbf{r},t)$ being now a stationary stochastic process with zero mean and with

$$\mathbf{J}(\mathbf{r}) = \lim_{t\to\infty} \langle \partial_t \mathbf{\Phi}(\mathbf{r},t)\rangle = \lim_{t\to\infty} \frac{\langle \mathbf{\Phi}(\mathbf{r},t)\rangle}{t}. \tag{4.5}$$

Here $\langle\cdot\rangle$ denotes averages with respect to the noise history. Thus, in a NESS, the local current $\mathbf{j}(\mathbf{r},t) = \partial_t \mathbf{\Phi}(\mathbf{r},t)$ is in a statistically stationary state, i.e. becomes a stationary stochastic process with mean $\mathbf{J}(\mathbf{r})$.
The thermodynamic uncertainty relation in a Markovian network is formulated for some form of integrated currents, see, e.g., (2.52). In the spirit of (2.52), we define the projection of the local current onto an arbitrarily directed weight function $\mathbf{g}(\mathbf{r})$ as

$$j_g(t) \equiv \int_\Omega d\mathbf{r}\, \mathbf{j}(\mathbf{r},t)\cdot\mathbf{g}(\mathbf{r}). \tag{4.6}$$

The integral in (4.6) represents the usual $\mathcal{L}_2$-product of the two vector fields $\mathbf{j}(\mathbf{r},t)$ and $\mathbf{g}(\mathbf{r})$ with $\mathbf{j}(\mathbf{r},t)\cdot\mathbf{g}(\mathbf{r}) = \sum_k j_k(\mathbf{r},t) g_k(\mathbf{r})$ as the scalar product between $\mathbf{j}$ and $\mathbf{g}$. With the projected current $j_g(t)$ from (4.6), we associate a fluctuating 'output'

$$\Psi_g(t) \equiv \int_\Omega d\mathbf{r}\, \mathbf{\Phi}(\mathbf{r},t)\cdot\mathbf{g}(\mathbf{r}). \tag{4.7}$$

Hence $j_g(t) = \partial_t \Psi_g(t)$ and in the NESS

$$J_g \equiv \lim_{t\to\infty} \frac{\langle \Psi_g(t)\rangle}{t}. \tag{4.8}$$

The fluctuating output $\Psi_g(t)$ provides us with the means to define a measure of the precision of the system output, namely the squared variational coefficient ϵ^2, as (see (2.57))

$$\epsilon^2 \equiv \frac{\left\langle \left(\Psi_g(t) - \langle\Psi_g(t)\rangle\right)^2 \right\rangle}{\langle\Psi_g(t)\rangle^2}. \tag{4.9}$$

If the system is in its non-equilibrium steady state, we can rewrite (4.9) as

$$\epsilon^2 = \frac{\left\langle \left(\Psi_g(t) - J_g\, t\right)^2 \right\rangle}{(J_g\, t)^2}. \tag{4.10}$$

Let us now connect the variance of the output $\Psi_g(t)$ to the Green-Kubo diffusivity given by

$$D_g \equiv \int_0^\infty dt\ \langle \delta j_g(t)\, \delta j_g(0)\rangle\,. \tag{4.11}$$

Using (4.6) and (4.2), it is straightforward to verify that

$$\int_0^t dt'\, \delta j_g(t') = \widetilde{\Psi}_g(t) - \left\langle \widetilde{\Psi}_g(t)\right\rangle, \qquad \widetilde{\Psi}_g(t) \equiv \Psi_g(t) - \Psi_g(0).$$

Thus,

$$\left\langle \left(\widetilde{\Psi}_g(t) - \left\langle\widetilde{\Psi}_g(t)\right\rangle\right)^2 \right\rangle = \int_0^t dr \int_0^t ds\ \langle \delta j_g(r)\delta j_g(s)\rangle\,. \tag{4.12}$$

By dividing both sides of (4.12) by $2t$ and taking the limit of $t \to \infty$ it is found in analogy to [92], that

$$\lim_{t\to\infty} \frac{\int_0^t dr \int_0^t ds \, \langle \delta j_g(r) \delta j_g(s) \rangle}{2t} = D_g,$$

with D_g from (4.11) and therefore

$$D_g = \lim_{t\to\infty} \frac{\left\langle \left(\widetilde{\Psi}_g(t) - \left\langle \widetilde{\Psi}_g(t) \right\rangle \right)^2 \right\rangle}{2t}. \tag{4.13}$$

Since in the NESS $\Psi_g(t)$ is stochastically independent of the initial configuration $\Psi_g(0)$, we can simplify the expression for the diffusivity in the NESS according to

$$D_g = \lim_{t\to\infty} \frac{\left\langle (\Psi_g(t) - \langle \Psi_g(t) \rangle)^2 \right\rangle}{2t}. \tag{4.14}$$

With the result of (4.14) and ϵ^2 from (4.9), an alternative formulation of the precision in a NESS is

$$\epsilon^2 = \frac{\left\langle (\Psi_g(t) - \langle \Psi_g(t) \rangle)^2 \right\rangle}{\langle \Psi_g(t) \rangle^2} = 2 \frac{D_g}{J_g^2} \frac{1}{t}. \tag{4.15}$$

We proceed with expressing the total entropy production Δs_{tot}. The total entropy production is given by the sum of the entropy dissipated into the medium along a single trajectory, Δs_{m}, and the stochastic entropy, Δs, of such a trajectory; see e.g. [25]. The medium entropy is given by,

$$\Delta s_{\mathrm{m}} \equiv \ln \frac{p[\mathbf{\Phi}(\mathbf{r},t)|\mathbf{\Phi}(\mathbf{r},t_0)]}{p[\widetilde{\mathbf{\Phi}}(\mathbf{r},t)|\widetilde{\mathbf{\Phi}}(\mathbf{r},t_0)]}, \tag{4.16}$$

see (2.43). Here $p[\mathbf{\Phi}(\mathbf{r},t)|\mathbf{\Phi}(\mathbf{r},t_0)]$ denotes the functional probability density of the entire vector field $\mathbf{\Phi}(\mathbf{r},t)$, i.e. the field configuration after some time t has elapsed since a starting-time $t_0 < t$, conditioned on an initial value $\mathbf{\Phi}(\mathbf{r},t_0)$, i.e. a certain field configuration at the starting time t_0. In contrast, $p[\widetilde{\mathbf{\Phi}}(\mathbf{r},t)|\widetilde{\mathbf{\Phi}}(\mathbf{r},t_0)]$ is the conditioned probability density of the time reversed process, i.e. starting in the final configuration at time t_0 and ending up in the original one at time t. For the sake of simplicity, we will write in the following $p[\mathbf{\Phi}]$ and $p[\widetilde{\mathbf{\Phi}}]$ instead of $p[\mathbf{\Phi}(\mathbf{r},t)|\mathbf{\Phi}(\mathbf{r},t_0)]$ and $p[\widetilde{\mathbf{\Phi}}(\mathbf{r},t)|\widetilde{\mathbf{\Phi}}(\mathbf{r},t_0)]$, respectively. The functional probability density can be expressed via a so-called action functional, $\mathcal{S}[\mathbf{\Phi}]$, according to

$$p[\mathbf{\Phi}] \propto \exp\left[-\mathcal{S}[\mathbf{\Phi}]\right]. \tag{4.17}$$

For the system (4.1), the action functional (see, e.g., [25, 26, 35, 55, 59, 93–96] and references therein) is given by (see (2.26))

$$\begin{aligned}\mathcal{S}[\mathbf{\Phi}] = \frac{1}{2}\sum_{\gamma}\int_{t_0}^{t} dt' \int d\mathbf{r}\, \Big(\dot{\Phi}_\gamma(\mathbf{r},t') - F_\gamma[\{\Phi_\mu(\mathbf{r},t')\}]\Big) \\ \times \int d\mathbf{r}'\, K^{-1}(\mathbf{r}-\mathbf{r}')\Big(\dot{\Phi}_\gamma(\mathbf{r}',t') - F_\gamma[\{\Phi_\mu(\mathbf{r}',t')\}]\Big),\end{aligned} \tag{4.18}$$

where $K^{-1}(\mathbf{r}-\mathbf{r}')$ is the inverse of the noise correlation kernel $K(\mathbf{r}-\mathbf{r}')$ from (4.1). The two integral kernels fulfill

$$\int d\mathbf{r}''\, K(\mathbf{r}-\mathbf{r}'')K^{-1}(\mathbf{r}''-\mathbf{r}') = \delta^d(\mathbf{r}-\mathbf{r}'). \tag{4.19}$$

Before we proceed with the calculation of the medium entropy, let us give the following general remarks. Throughout the paper, stochastic integrals are interpreted in the Stratonovitch sense, i.e. mid-point discretization is used. This is essential for the calculation of the medium entropy Δs_{m} via (4.16), where Ito discretization may lead to incompatibilities. Using Stratonovitch discretization, however, gives rise to an additional term in the action functional (4.18), which is given by the functional derivative of the generalized force term F from (4.1) with respect to the field $\mathbf{\Phi}$. This contribution stems from the Jacobian ensuing from the variable transformation from the noise field to the field $\mathbf{\Phi}$ in the functional integral used for calculating expectation values of path dependent observables. As this addition to the action functional does not contribute to the medium entropy (cf. [25, 28]) it is neglected in (4.18).
Inserting (4.17), (4.18) into (4.16) and noticing that only the time-antisymmetric part of the action functional (4.18) and its time-reversed counterpart survives, leads to (see also [25, 28, 97])

$$\Delta s_{\mathrm{m}} = 2\sum_{\gamma}\int_{t_0}^{t} dt' \int d\mathbf{r} \int d\mathbf{r}'\, \dot{\Phi}_\gamma(\mathbf{r},t')K^{-1}(\mathbf{r}-\mathbf{r}')F_\gamma[\{\Phi_\mu(\mathbf{r}',t')\}]. \tag{4.20}$$

Δs_{m} is a measure of the energy dissipated into the medium during the time interval $[t_0,\, t]$, in analogy to the Langevin case. The stochastic entropy change Δs for the same trajectory, is given by (see (2.37) and also [28])

$$\Delta s \equiv -\ln p[\mathbf{\Phi}(\mathbf{r},\tau)]\Big|_{t_0}^{t}. \tag{4.21}$$

Thus, the total entropy production Δs_{tot} reads

$$\begin{aligned}\Delta s_{\mathrm{tot}} = 2\sum_{\gamma}\int_{t_0}^{t} dt' \int d\mathbf{r} \int d\mathbf{r}'\, \dot{\Phi}_\gamma(\mathbf{r},t')K^{-1}(\mathbf{r}-\mathbf{r}')F_\gamma[\{\Phi_\mu(\mathbf{r}',t')\}] \\ -\ln p[\mathbf{\Phi}(\mathbf{r},\tau)]\Big|_{t_0}^{t}.\end{aligned} \tag{4.22}$$

With (4.22) we may also define the rate of total entropy production σ in a NESS according to

$$\sigma = \lim_{t\to\infty} \frac{\langle \Delta s_{\mathrm{tot}} \rangle}{t}. \tag{4.23}$$

The expressions stated in (4.9) and (4.22) provide us with the necessary ingredients to formulate the field-theoretic thermodynamic uncertainty relation as (see (2.61))

$$\langle \Delta s_{\mathrm{tot}} \rangle \, \epsilon^2 = \frac{2\, D_g\, \sigma}{J_g^2} \geq 2, \tag{4.24}$$

with σ from (4.23), D_g from (4.13) and J_g from (4.8). The higher the precision, i.e., the smaller ϵ^2, the stronger the total entropy production $\langle \Delta s_{\mathrm{tot}} \rangle$, i.e., the higher the thermodynamic cost. Or, in other words, in order to sustain a certain NESS current J_g, a minimal entropy production rate $\sigma \geq J_g^2/D_g$ is required.

4.2 Example: Edwards-Wilkinson Equation Driven by a Constant Force

We demonstrate the above introduced concept of a field-theoretic thermodynamic uncertainty relation on a simple model system, which displays a non-trivial steady state current and entropy production. In particular, we use the one-dimensional Edwards-Wilkinson equation in its dimensionless form on a spatial interval $x \in [0, 1]$ driven out of equilibrium by a constant 'force' v_0, i.e.,

$$\begin{aligned} \partial_t\, h(x,t) &= \partial_x^2\, h(x,t) + v_0 + \eta(x,t), \\ \langle \eta(x,t) \rangle &= 0, \\ \big\langle \eta(x,t)\, \eta(x',t') \big\rangle &= K(x-x')\, \delta(t-t'), \end{aligned} \tag{4.25}$$

where $K(x-x')$ denotes the spatial noise correlations [1] and $h(x,t)$ the dimensionless surface height. We further assume periodic boundary conditions, i.e., $h(0,t) = h(1,t)$ as well as vanishing initial condition, i.e., $h(x,0) = 0$. In relation to the general formulation in (4.1) we have $\Phi_\gamma(\mathbf{r},t) = h(x,t)$ and $F[\{h(x,t)\}] = \partial_x^2\, h(x,t) + v_0$. In the following, we will refer to (4.25) as the forced Edwards-Wilkinson equation (FEW). This model is chosen for the reason that it may well be seen as a simplified version of the non-linear KPZ equation, where the KPZ non-linearity is replaced by the constant force v_0. This simplification preserves the existence of a NESS and benefits from a more straightforward analytical treatment compared to the full KPZ equation.

As a first step we will derive the stationary probability density $p^s[h]$ via the functional

[1] To demonstrate the general procedure, spatially colored noise is admitted. We are, however, primarily interested in spatial white noise, $K(x-x') = \delta(x-x')$, in the following chapters.

Fokker-Planck equation of the FEW model, which is given by (see (2.63) and, e.g., [20, 21, 35–37])

$$\partial_t\, p[h] = -\int dx\, \frac{\delta}{\delta h}\left[\left(\partial_x^2\, h + v_0\right) p[h] - \frac{\hat{K}}{2}\frac{\delta p[h]}{\delta h}\right]. \tag{4.26}$$

Here we use the notation introduced in (3.89) for the scaled, dimensionless noise operator $\hat{K}$. In the stationary state, the left hand side of (4.26) vanishes and the stationary probability density $p^s[h]$ is described by

$$0 = \int dx\, \frac{\delta}{\delta h}\left[\left(\partial_x^2\, h + v_0\right) p^s[h] - \frac{\hat{K}}{2}\frac{\delta p^s[h]}{\delta h}\right]. \tag{4.27}$$

the expression in the squared brackets of (4.26) is the stationary probability current $j_p^s[h]$, i.e., the analog to (2.32). To solve (4.27) we make the ansatz

$$p^s[h] \sim \exp\left[-\int dx\, \partial_x\, h\left(\hat{K}^{-1}(\partial_x\, h)\right)\right], \tag{4.28}$$

where $\hat{K}^{-1}$ is the inverse of the noise operator $\hat{K}$ according to (3.90). We proceed by analyzing the probability current $j_p^s[h]$, where the functional derivative of (4.28) reads for periodic boundary conditions

$$\frac{\delta p^s[h]}{\delta h} = 2\, \partial_x \left(\hat{K}^{-1}(\partial_x\, h)\right) p^s[h]. \tag{4.29}$$

Hence, we get

$$\begin{aligned} j_p^s[h] &= \left(\partial_x^2\, h + v_0\right) p^s[h] - \frac{\hat{K}}{2}\frac{\delta p^s[h]}{\delta h} \\ &= v_0\, p^s[h] + \left(\partial_x^2\, h - \hat{K}\left(\partial_x\left(\hat{K}^{-1}(\partial_x\, h)\right)\right)\right) p^s[h]. \end{aligned} \tag{4.30}$$

At this stage it proves useful to switch to the Fourier series representation of $h(x,t)$ according to (3.59) and (3.57), as then it is straightforward to explicitly evaluate expressions like the second term on the right hand side of (4.30). In particular, we have, e.g.,

$$\hat{K}\,(\partial_x\, h) = 2\pi i\, \hat{K} \sum_{k\in\mathbb{Z}} k\, h_k\, \phi_k(x) = 2\pi\, i \sum_{k\in\mathbb{Z}} k\, h_k\, \alpha_k^2 \phi_k(x), \tag{4.31}$$

where we used in the second step that $\hat{K}\phi_k = \alpha_k^2\phi_k$, see (3.88). As a consequence of $\hat{K}^{-1}$ being the inverse of $\hat{K}$ we know that

$$\hat{K}^{-1}\,(\partial_x\, h) = 2\pi\, i \sum_{k\in\mathbb{Z}} k\, h_k\, \alpha_k^{-2} \phi_k(x), \tag{4.32}$$

and therefore

$$\hat{K}\left(\partial_x\left(\hat{K}^{-1}\left(\partial_x h\right)\right)\right) = \hat{K}\sum_{k\in\mathbb{Z}}\mu_k\, h_k\, \alpha_k^{-2}\phi_k(x) = \sum_{k\in\mathbb{Z}}\mu_k\, h_k\, \phi_k(x), \tag{4.33}$$

with $\mu_k = -4\pi^2\, k^2$ from (3.58). The expression on the right hand side of (4.33) is the Fourier series representation of $\partial_x^2\, h$ and thus we have shown that the second term on the right hand side of (4.30) is identically zero. This result implies that the stationary probability current of the FEW model is given by

$$j_p^s[h] = v_0\, p^s[h]. \tag{4.34}$$

Hence, to validate the ansatz in (4.28), we have to show that

$$v_0 \int dx\, \frac{\delta p^s[h]}{\delta h} = 2\, v_0\, p^s[h] \int dx\, \partial_x\, \left(\hat{K}^{-1}(\partial_x\, h)\right) \stackrel{!}{=} 0. \tag{4.35}$$

Switching again to the Fourier series representation and using (4.32) yields

$$\begin{aligned}\int dx\, \partial_x\, \left(\hat{K}^{-1}(\partial_x\, h)\right) &= \sum_{k\in\mathbb{Z}}\mu_k\, h_k\, \alpha_k^{-2}\int_0^1 dx\, \phi_k(x) = \sum_{k\in\mathbb{Z}}\mu_k\, h_k\, \alpha_k^{-2}\, \delta_{0,k} \\ &= \mu_0\, h_0\, \alpha_0^{-2} \\ &= 0 \quad \Leftrightarrow \quad \alpha_0 \neq 0.\end{aligned} \tag{4.36}$$

Thus we have shown that (4.35) holds and therefore that (4.28) is indeed the stationary probability density of the FEW model.
Having shown that (4.25) possesses a NESS (see Section 2.2.2) with stationary probability density given by (4.28), we are able to explicitly calculate the precision ϵ^2 from (4.10) and $\langle\Delta s_{\mathrm{tot}}\rangle$ from (4.22). To this end we also have to know the explicit form of the Fourier coefficients $h_k(t)$, which, in analogy to (3.63), reads

$$h_k(t) = \int_0^t dt'\, e^{\mu_k(t-t')}\left[\eta_k(t') + v_0\, \delta_{0,k}\right], \tag{4.37}$$

where $\eta_k(t)$ denotes the k-th Fourier coefficient of the noise $\eta(x,t)$ from (4.25). With the general definition of the fluctuating output from (4.7), where we assume $g \in \mathcal{L}_2(0,1)$, and the result from (4.37) we see immediately that

$$\langle\Psi_g(t)\rangle = \sum_{k\in\mathbb{Z}}\overline{g}_k\, \langle h_k(t)\rangle = g_0\, v_0\, t. \tag{4.38}$$

Here $\overline{g}_k$ denotes the complex conjugate of the k-th Fourier coefficient of the weight function $g(x)$ from (4.6). To prevent (4.38) from becoming zero, we only allow weight functions that have a non-vanishing spatial mean. Further, we have in the long-time limit, using (3.75),

$$\begin{aligned}\left\langle \Psi_g^2(t) \right\rangle &= \sum_{k,l\in\mathbb{Z}} \overline{g}_k \overline{g}_l \left\langle h_k(t) h_l(t) \right\rangle \\ &= g_0^2\, v_0^2\, t^2 + \sum_{k,l\in\mathbb{Z}} \overline{g}_k \overline{g}_l \int_0^t dt' \int_0^t dt''\, e^{\mu_k (t-t')}\, e^{\mu_l (t-t'')} \left\langle \eta_k(t')\, \eta_l(t'') \right\rangle \\ &= g_0^2\, v_0^2\, t^2 + \sum_{k,l\in\mathbb{Z}} \overline{g}_k \overline{g}_l \alpha_k \alpha_l \int_0^t dt' \int_0^t dt''\, e^{\mu_k (t-t')}\, e^{\mu_l (t-t'')} \delta_{k,-l} \delta(t'-t'') \\ &= g_0^2\, v_0^2\, t^2 + \sum_{k\in\mathbb{Z}} \overline{g}_k \overline{g}_{-k} \alpha_k \alpha_{-k} \frac{e^{2\mu_k t} - 1}{2\mu_k}.\end{aligned} \tag{4.39}$$

Hence, with (4.38),

$$\mathrm{var}[\Psi_g(t)] = \left\langle \Psi_g^2(t) \right\rangle - \left\langle \Psi_g(t) \right\rangle^2 \simeq g_0^2\, \alpha_0^2\, t\,, \qquad \text{for } t \gg 1, \tag{4.40}$$

and thus we have for the precision ϵ^2,

$$\epsilon^2 = \frac{\left\langle \Psi_g^2(t) \right\rangle - \left\langle \Psi_g(t) \right\rangle^2}{\left\langle \Psi_g(t) \right\rangle^2} = \frac{\alpha_0^2}{v_0^2\, t}\,, \qquad \text{for } t \gg 1. \tag{4.41}$$

Applying the general expression for the total entropy production from (4.22) to the FEW equation in its stationary state, we obtain with the aid of (4.28),

$$\begin{aligned}\Delta s_{\mathrm{tot}} &= 2 \int_0^t dt' \int_0^1 dx\, \dot{h}\, \hat{K}^{-1} \left(\partial_x^2 h + v_0 \right) + \int_0^1 dx\, \partial_x h\, \hat{K}^{-1} \left(\partial_x h \right) \\ &= 2 \int_0^t dt' \int_0^1 dx\, \dot{h}\, \hat{K}^{-1} \partial_x^2 h - \int_0^1 dx\, h \hat{K}^{-1} \left(\partial_x^2 h \right) + 2\, v_0 \int_0^t dt' \int_0^1 dx\, \hat{K}^{-1}\, \dot{h} \\ &= 2\, v_0 \int_0^t dt' \int_0^1 dx\, \hat{K}^{-1}\, \dot{h} = 2\, v_0 \int_0^1 dx\, \hat{K}^{-1}\, h.\end{aligned} \tag{4.42}$$

Here we used integration by parts and the periodic boundary conditions in the second step as well as the identity

$$\frac{d}{dt} \int_0^1 dx\, h\, \hat{K}^{-1} \left(\partial_x^2\, h \right) = 2 \int_0^1 dx\, \dot{h}\, \hat{K}^{-1} \left(\partial_x^2\, h \right),$$

and the vanishing initial condition in the third step. Hence, the expectation value of the total entropy production is given by

$$\left\langle \Delta s_{\mathrm{tot}} \right\rangle = 2\, v_0 \int_0^1 dx\, \left\langle \hat{K}^{-1}\, h(x,t) \right\rangle = 2\, v_0 \sum_{k\in\mathbb{Z}} \alpha_k^{-2} \left\langle h_k(t) \right\rangle\, \delta_{0,k} = 2\, v_0^2\, \alpha_0^{-2}\, t. \tag{4.43}$$

We thus arrive at the thermodynamic uncertainty product for the FEW model

$$\mathcal{Q} = \langle \Delta s_{\mathrm{tot}} \rangle \, \epsilon^2 = 2 \, v_0^2 \, \alpha_0^{-2} \, t \, \frac{\alpha_0^2}{v_0^2 \, t} = 2. \tag{4.44}$$

For the sake of completeness, we also state the results for the NESS-current, J_g^{FEW} (see (2.55) and (4.8), (4.38)),

$$J_g^{\mathrm{FEW}} = g_0 \, v_0, \tag{4.45}$$

the stationary state diffusivity, D_g^{FEW} (see (2.60) and (4.14), (4.38) and (4.39)),

$$D_g^{\mathrm{FEW}} = \frac{g_0^2 \, \alpha_0^2}{2}, \tag{4.46}$$

and the total entropy production rate in the stationary state, σ^{FEW} (see (4.23), (4.43)),

$$\sigma^{\mathrm{FEW}} = \frac{2 \, v_0^2}{\alpha_0^2}. \tag{4.47}$$

To summarize the results obtained for this example system, we have found that the TUR-product is saturated for all types of colored spatial noise with $\alpha_0 \neq 0$, including white noise ($\alpha_k = 1$, $\forall k$). The reason for that is that J_g^{FEW}, D_g^{FEW} and σ^{FEW} are in the long-time limit all dominated by the zeroth Fourier mode h_0 and further, that also the only non-vanishing Fourier component of the driving force v_0 is its zeroth-order mode. Why this is an interesting case will become clear when we analyze the full KPZ equation in the following chapter. Finally, it is stressed that the approach used in this example, namely the Fourier-series representation of the fields $h(x,t)$ and $\eta(x,t)$ as well as the derivation of the stationary probability distribution and non-trivial stationary probability current indicating a NESS, is very widely applicable. It can straightforwardly be carried over to more complex models than the FEW model. That said, especially the derivation of a stationary probability density p^s can prove to be a very challenging task. In fact, for most of the more involved field-theoretic systems like, e.g., the KPZ equation or Navier-Stokes equation, a general analytical expression for p^s is, if at all, only possible for a very limited number of special cases (see, e.g., [65, 66, 98, 99]).

5 Thermodynamic Uncertainty Relation for the 1D-KPZ Equation – Perturbative & Exact Results

We begin the explicit derivation of the KPZ-TUR by using a perturbation expansion in a small effective coupling parameter. In the first part of this chapter, we focus on the most general approach, namely rewriting all higher order expressions in terms of the zeroth order of the perturbation expansion, since the zeroth order can be calculated exactly. This path does, however, lead to rather lengthy and cumbersome expressions. Therefore we employ this technique only for approximations up to second order in the effective coupling parameter, where the expressions are still manageable. In the second part of this chapter, we aim to extend the perturbative results to fourth order in the effective coupling parameter. To circumvent the steeply increasing complexity of the calculations that would occur with the above approach, we will here rely on the so-called quasi-normality hypothesis, which is commonly used in the context of, e.g., turbulence theory. Moreover, a calculation is performed, which yields exact steady state results for the current and entropy production rate.

5.1 Expansion in a Small Coupling Parameter

We begin by constructing an approximate solution to the nonlinear integral equation of the k-th Fourier coefficient of the heights field, $h_k(t)$ from (3.63), now in its dimensionless form and with the restricted spectral range, $k \in \mathfrak{R}$, $\mathfrak{R} = [-\Lambda, \Lambda]$, given by

$$h_k(t) = \int_0^t dt' e^{\mu_k(t-t')} \left[\eta_k(t') - 2\pi^2 \lambda_{\text{eff}} \sum_{l \in \mathfrak{R}_k \setminus \{0,k\}} l(k-l) h_l(t') h_{k-l}(t') \right], \tag{5.1}$$

with $\{\mu_k\}$ from (3.58), $\mathfrak{R}_k$ from (3.85). Note, that the summation of the discrete convolution in (5.1) is chosen such that it respects the above introduced cutoff in l as well as $k-l$, i.e., $|l|$, $|k-l| \le \Lambda$. For small values of the coupling constant we expand the solution in powers of λ_{eff}, i.e.,

$$h_k(t) = h_k^{(0)}(t) + \lambda_{\text{eff}} h_k^{(1)}(t) + \lambda_{\text{eff}}^2 h_k^{(2)}(t) + O(\lambda_{\text{eff}}^3), \tag{5.2}$$

with

$$h_k^{(0)}(t) = \int_0^t e^{\mu_k(t-t')} dW_k(t'), \tag{5.3}$$

$$h_k^{(1)}(t) = -2\pi^2 \sum_{l\in\mathfrak{R}_k\setminus\{0,k\}} l(k-l) \int_0^t dt' e^{\mu_k(t-t')} h_l^{(0)}(t') h_{k-l}^{(0)}(t'), \tag{5.4}$$

$$\begin{aligned} h_k^{(2)}(t) = -2\pi^2 &\sum_{l\in\mathfrak{R}_k\setminus\{0,k\}} l(k-l) \int_0^t dt' e^{\mu_k(t-t')} \\ &\times \left(h_l^{(0)}(t') h_{k-l}^{(1)}(t') + h_l^{(1)}(t') h_{k-l}^{(0)}(t') \right) \end{aligned} \tag{5.5}$$

Thus every $h_k^{(n)}$, $n > 1$, can be expressed in terms of $h_m^{(0)}$, $m \in \mathfrak{R}$, i.e. the stochastic convolution according to (3.64), which is known to be Gaussian.
In the following calculations multipoint correlation functions have to be evaluated, which can be simplified by Wick's theorem, where a recurring term reads $\left\langle h_k^{(0)}(t) h_l^{(0)}(t') \right\rangle$. It is thus helpful to determine this correlation function in general once and use this result later on. With (3.84) and $k, l \in \mathbb{Z}$ (and therefore also for $k, l \in \mathfrak{R}$) it follows that:

$$\begin{aligned} \left\langle h_k^{(0)}(t) h_l^{(0)}(t') \right\rangle &= e^{\mu_k t} e^{\mu_l t'} \int_0^t dr \int_0^{t'} ds\, e^{-\mu_k r} e^{-\mu_l s} \left\langle \eta_k(r) \eta_l(s) \right\rangle \\ &= e^{\mu_k t} e^{\mu_l t'} \delta_{k,-l} \frac{1 - e^{-(\mu_k+\mu_l)(t\wedge t')}}{\mu_k + \mu_l} = \Pi_{k,l}(t,t') \delta_{k,-l}, \end{aligned}$$

with

$$\Pi_{k,l}(t,t') \equiv e^{\mu_k t} e^{\mu_l t'} \frac{1 - e^{-(\mu_k+\mu_l)(t\wedge t')}}{\mu_k + \mu_l}. \tag{5.6}$$

Since the zeroth order Fourier coefficients are equivalent to the Fourier coefficients of the linear theory, i.e., the EW equation from (3.2), the result in (5.6) is identical to the one derived for the EW equation in Section 3.2 and [20]. For the auxiliary expression $\Pi_{k,l}$ the symmetries

$$\Pi_{k,l}(t,t') = \Pi_{k,-l}(t,t') = \Pi_{-k,l}(t,t') = \Pi_{-k,-l}(t,t') \tag{5.7}$$

hold, and thus it is found that

$$\begin{aligned} \left\langle h_k^{(0)}(t) h_l^{(0)}(t') \right\rangle &= \left\langle \overline{h_k^{(0)}}(t) \overline{h_l^{(0)}}(t') \right\rangle = \Pi_{k,l}(t,t') \delta_{k,-l}; \\ \left\langle h_k^{(0)}(t) \overline{h_l^{(0)}}(t') \right\rangle &= \left\langle \overline{h_k^{(0)}}(t) h_l^{(0)}(t') \right\rangle = \Pi_{k,l}(t,t') \delta_{k,l}. \end{aligned} \tag{5.8}$$

5.2 Thermodynamic Uncertainty Relation in the EW Scaling Regime

We now have the necessary means to show that the thermodynamic uncertainty relation from (4.24) holds for the KPZ equation driven by Gaussian white noise in the weak-coupling regime. In particular, the small-λ_{eff} expansion from Section 5.1 will be employed.
To recapitulate, the two ingredients needed for the thermodynamic uncertainty relation are (i) the long time behavior of the squared variation coefficient or precision ϵ^2 of $\Psi_g(t)$ from (4.9); (ii) the expectation value of the total entropy production in the steady state, $\langle \Delta s_{\text{tot}} \rangle$ from (4.22).

5.2.1 Expectation and Variance for the Height Field

With (4.7) adapted to the KPZ equation, namely

$$\Psi_g(t) = \int_0^1 dx\, h(x,t) g(x), \tag{5.9}$$

with $g(x)$ as any real-valued $\mathcal{L}_2$-function fulfilling $\int_0^1 dx g(x) \neq 0$, i.e., $g(x)$ possessing non-zero mean (see (4.38)), we rewrite the variance as

$$\left\langle (\Psi_g(t) - \langle \Psi_g(t) \rangle)^2 \right\rangle = \left\langle (\Psi_g(t))^2 \right\rangle - \langle \Psi_g(t) \rangle^2 . \tag{5.10}$$

As is shown below, ϵ^2 can be evaluated for arbitrary time $t > 0$. However, the final interest is on the non-equilibrium steady state of the system. Therefore, the long-time asymptotics will be studied.

5.2.2 Evaluation of Expectation and Variance

In the small-λ_{eff} expansion, the expectation of the output $\Psi_g(t)$ from (5.9), with $h(x,t)$ solution of the dimensionless KPZ equation (3.10) - (3.12) reads:

$$\begin{aligned} \langle \Psi_g(t) \rangle &= \sum_{k,l \in \mathfrak{R}} \langle h_k(t) \rangle \, \overline{g_l} \left(e^{2\pi i k x}, e^{2\pi i l x} \right)_0 \\ &= \lambda_{\text{eff}} \sum_{k \in \mathfrak{R}} \overline{g_k} \left\langle h_k^{(1)}(t) \right\rangle + O(\lambda_{\text{eff}}^3), \end{aligned} \tag{5.11}$$

where g_k and $\overline{g_k}$ are the k-th Fourier coefficient of the weight function $g(x)$ and its complex conjugate, respectively. Here the result from (5.3) - (5.5) is used as well as the fact that odd moments of Gaussian random variables vanish identically. Replacing $h_k^{(1)}(t)$ by the expression derived in (5.4) and using (5.8) leads to

$$\begin{aligned} \left\langle h_k^{(1)}(t)\right\rangle &= -2\pi^2 e^{\mu_k t}\int_0^t dt'\, e^{-\mu_k t'} \sum_{l\in\mathfrak{R}_k\setminus\{0,k\}} l(k-l)\left\langle h_l^{(0)}(t')h_{k-l}^{(0)}(t')\right\rangle \\ &= -2\pi^2 \sum_{l\in\mathfrak{R}_k\setminus\{0,k\}} l(k-l)\left[\frac{e^{(\mu_l+\mu_{k-l})t}-e^{\mu_k t}}{(\mu_l+\mu_{k-l})(\mu_l+\mu_{k-l}-\mu_k)}\right. \\ &\qquad \left. -\frac{e^{\mu_k t}-1}{(\mu_l+\mu_{k-l})\mu_k}\right]\delta_{0,k}. \end{aligned} \tag{5.12}$$

Note, that in the case of $k=0$ the second term in the last line of (5.12) is evaluated in the limit $\mu_k \to 0$, which yields t. Since the interest is in the NESS-current, the long-time asymptotics of the two expressions in (5.12) above is studied. So, eq. (5.11) yields

$$\langle \Psi_g(t)\rangle \simeq \left[2\pi^2 g_0\lambda_{\text{eff}} \sum_{l\in\mathfrak{R}\setminus\{0\}} \frac{l^2}{2(-\mu_l)} + O(\lambda_{\text{eff}}^3)\right] t, \quad \text{for } t\gg 1, \tag{5.13}$$

where $g_k = g_{-k}\ \forall k$ as $g(x)\in\mathbb{R}$. Note, that the formulation of (5.13) reflects our claim, that $\langle\Psi_g(t)\rangle \sim t$ for $t \gg 1$ (see also Chapter 6). Using the explicit form of μ_k from (3.58), the expression in (5.13) can be simplified according to

$$\langle \Psi_g(t)\rangle = \left[g_0\frac{\lambda_{\text{eff}}}{2}\Lambda + O(\lambda_{\text{eff}}^3)\right] t, \quad \text{for } t\gg 1, \tag{5.14}$$

with Λ from (3.80). Equivalently, the steady state current from (4.8) reads

$$J_g = g_0\frac{\lambda_{\text{eff}}}{2}\Lambda + O(\lambda_{\text{eff}}^3). \tag{5.15}$$

The first term of the variance as defined in (5.10) reads in the small-λ_{eff} expansion

$$\begin{aligned} \left\langle (\Psi_g(t))^2\right\rangle &= \left\langle \sum_{k,l\in\mathfrak{R}} h_k(t)\overline{g_k}h_l(t)\overline{g_l}\right\rangle \\ &= \sum_{k,l\in\mathfrak{R}} \overline{g_k}\,\overline{g_l}\left[\left\langle h_k^{(0)}(t)h_l^{(0)}(t)\right\rangle + \lambda_{\text{eff}}^2\left(\left\langle h_k^{(1)}(t)h_l^{(1)}(t)\right\rangle\right.\right. \\ &\qquad \left.\left. + \left\langle h_k^{(0)}(t)h_l^{(2)}(t)\right\rangle + \left\langle h_k^{(2)}(t)h_l^{(0)}(t)\right\rangle\right) + O(\lambda_{\text{eff}}^4)\right], \end{aligned} \tag{5.16}$$

where moments proportional to λ_{eff} (and λ_{eff}^3) vanish due to (5.3) and (5.4) as the two-point correlation function $\left\langle h_k^{(0)}h_l^{(1)}\right\rangle$ and its complex conjugate are odd moments.

In Appendix 5.A, we present the rather technical derivation of

$$\begin{aligned}\left\langle (\Psi_g(t))^2 \right\rangle \simeq g_0^2 &\left[1 - 2(2\pi^2)^2 \lambda_{\mathrm{eff}}^2 \sum_{l \in \Re \setminus \{0\}} \frac{l^4}{4\,\mu_l^3} \right] t \\ &+ g_0^2 \lambda_{\mathrm{eff}}^2 \sum_{k \in \Re} \left| \left\langle h_k^{(1)}(t) \right\rangle \right|^2 + O(\lambda_{\mathrm{eff}}^4) \quad \text{for } t \gg 1.\end{aligned} \tag{5.17}$$

Subtraction of (5.13) squared from (5.17) leads to

$$\begin{aligned}&\left\langle (\Psi_g(t))^2 \right\rangle - \langle \Psi_g(t) \rangle^2 \\ &\simeq \left[g_0^2 \left(1 - 2(2\pi^2)^2 \lambda_{\mathrm{eff}}^2 \sum_{l \in \Re \setminus \{0\}} \frac{l^4}{4\,\mu_l^3} \right) + O(\lambda_{\mathrm{eff}}^4) \right] t, \quad \text{for } t \gg 1.\end{aligned} \tag{5.18}$$

Here, $\left\langle (\Psi_g(t))^2 \right\rangle - \langle \Psi_g(t) \rangle^2 \sim t$, $t \gg 1$ is expected (see also Chapter 6). Again, with μ_k from (3.58), the above expression in (5.18) can be reduced to

$$\left\langle (\Psi_g(t))^2 \right\rangle - \langle \Psi_g(t) \rangle^2 = \left[g_0^2 \left(1 + \frac{\lambda_{\mathrm{eff}}^2}{16\,\pi^2} \mathcal{H}_\Lambda^{(2)} \right) + O(\lambda_{\mathrm{eff}}^4) \right] t. \tag{5.19}$$

Here $\mathcal{H}_\Lambda^{(2)} = \sum_{l=1}^{\Lambda} 1/l^2$ is the so-called generalized harmonic number, which converges to the Riemann zeta-function $\zeta(2)$ for $\Lambda \to \infty$. Using (4.13), eq. (5.19) yields the diffusivity D_g,

$$D_g = \frac{g_0^2}{2} \left[1 + \frac{\lambda_{\mathrm{eff}}^2}{16\,\pi^2} \mathcal{H}_\Lambda^{(2)} \right] + O(\lambda_{\mathrm{eff}}^4). \tag{5.20}$$

With (5.19) and (5.14) squared, the first constituent of the thermodynamic uncertainty relation, $\epsilon^2 = \mathrm{Var}[\Psi_g(t)] / \langle \Psi_g(t) \rangle^2$ from (4.9), is given for large times by

$$\epsilon^2 \simeq \frac{4 + \lambda_{\mathrm{eff}}^2/(4\,\pi^2)\mathcal{H}_\Lambda^{(2)}}{\lambda_{\mathrm{eff}}^2\,\Lambda^2} \frac{1}{t}. \tag{5.21}$$

Note, since $\epsilon^2 \approx 4/(\lambda_{\mathrm{eff}}^2 t)$, the long time asymptotics of the second term has to scale as $\langle \Delta s_{\mathrm{tot}} \rangle \sim \lambda_{\mathrm{eff}}^2 t$ for the uncertainty relation to hold. Note further, that the result for the precision of the projected output $\Psi_g(t)$ in the NESS is independent of the choice of $g(x)$[1].

[1] In Appendix 6.A, an argument is presented that shows the independence of the precision ϵ^2 on the weight function $g(x)$ generally, without relying on perturbation expansions.

5.2.3 Alternative Formulation of the Precision

Before we continue with the calculation of the total entropy production, we would like to mention an intriguing observation. From the field-theoretic point of view, it seems natural to define the precision ϵ^2 as

$$\epsilon^2 \equiv \frac{\left\langle \|h(x,t) - \langle h(x,t)\rangle\|_0^2 \right\rangle}{\|\langle h(x,t)\rangle\|_0^2}. \tag{5.22}$$

This is due to the fact that the height field $h(x,t)$ is at every time instant an element of the Hilbert-space $\mathcal{L}_2([0,1])$ as mentioned in Appendix 3.A.5. Hence, the difference between $h(x,t)$ and its expectation is measured by its $\mathcal{L}_2$-norm. Also the expectation squared is in this framework given by the $\mathcal{L}_2$-norm squared. At a cursory glance, the definitions in (5.22) and (4.9) seem to be incompatible. However, for the case of the above calculations of ϵ^2 for the one-dimensional KPZ equation, it holds up to $O(\lambda_{\text{eff}}^3)$ in perturbation expansion that

$$\begin{aligned} \left\langle (\Psi_g(t) - \langle \Psi_g(t)\rangle)^2 \right\rangle &= g_0^2 \left\langle \|h(x,t) - \langle h(x,t)\rangle\|_0^2 \right\rangle \qquad \text{for } t \gg 1, \\ \langle \Psi_g(t)\rangle^2 &= g_0^2 \, \|\langle h(x,t)\rangle\|_0^2 . \end{aligned} \tag{5.23}$$

Thus, with (5.23), it is obvious that in terms of the perturbation expansion both definitions of the precision, as in (4.9) and (5.22), respectively, are equivalent in the long-time limit. Note, that a similar observation may be found in [20] based on scaling arguments. Equation (5.23) can be verified by direct calculation along the same lines as above in this section. By studying these calculations it is found perturbatively that the height field $h(x,t)$ is spatially homogeneous, which is reflected by $\langle h_k(t)h_l(t)\rangle \sim \delta_{k,-l}$ (see (5.8)) for the correlation of its Fourier-coefficients. Further, the long-time behavior is solely determined by the largest eigenvalue of the differential diffusion operator $\hat{L} = \partial_x^2$, namely by $\mu_0 = 0$ (see e.g. (5.13) and (5.18), the essential quantities for deriving (5.23)).

In the following, we would like to give some reasoning why the above two statements should also hold for a broad class of field-theoretic Langevin equations as in (4.1). For simplicity, we restrict ourselves in (4.1) to the case of one-dimensional scalar fields $\Phi(x,t)$ and $F[\Phi(x,t)] = \hat{L}\Phi(x,t) + \hat{N}[\Phi(x,t)]$. Here $\hat{L}$ denotes a linear differential operator and $\hat{N}$ a non-linear (e.g. quadratic) operator. $\hat{L}$ should be selfadjoint and possess a pure point spectrum with all eigenvalues $\mu_k \leq 0$ (e.g. $\hat{L} = (-1)^{p+1}\partial_x^{2p}$, $p \in \mathbb{N}$, i.e. an arbitrary diffusion operator subject to periodic boundary conditions). For this class of operators $\hat{L}$ there exists a complete orthonormal system of corresponding eigenfunctions $\{\phi_k\}$ in $\mathcal{L}_2(\Omega)$. If it is further known, that the solution $\Phi(x,t)$ of (4.1) belongs at every time t to $\mathcal{L}_2(\Omega)$, we can calculate e.g. the second moment of the projected output $\Psi_g(t)$ according to $\left\langle (\Psi_g(t))^2 \right\rangle = \left\langle (\int_\Omega dx\, \Phi(x,t)g(x))^2 \right\rangle$, where $g(x) \in \mathcal{L}_2(\Omega)$ as well. As is the case in e.g. equation (5.16), the second moment is determined by the Fourier-coefficients

$\Phi_k(t)$ of $\Phi(x,t)$ and g_k of $g(x)$, namely

$$\left\langle (\Psi_g(t))^2 \right\rangle = \sum_{k,l} \overline{g_k}\,\overline{g_l}\,\langle \Phi_k(t)\Phi_l(t)\rangle\,. \tag{5.24}$$

Like the KPZ equation, (4.1) is driven by spatially homogeneous Gaussian white noise $\eta(x,t)$ with two-point correlations of the Fourier-coefficients $\eta_k(t)$ given by $\langle \eta_k(t)\eta_l(t)\rangle \sim \delta_{k,-l}$. Therefore, we expect the solution to (4.1) subject to periodic boundary conditions to be spatially homogeneous as well, at least in the steady state, which implies

$$\langle \Phi_k(t)\Phi_l(t)\rangle \sim \delta_{k,-l}, \tag{5.25}$$

see e.g. [100, 101]. Hence, with (5.25), the expression in (5.24) becomes

$$\left\langle (\Psi_g(t))^2 \right\rangle = g_0^2 \left\langle (\Phi_0(t))^2 \right\rangle + \sum_{k\neq 0} |g_k|^2 \langle \Phi_k(t)\Phi_{-k}(t)\rangle\,. \tag{5.26}$$

Comparing (5.26) to $\left\langle \|\Phi(x,t)\|_0^2 \right\rangle$, which is given by

$$\left\langle \|\Phi(x,t)\|_0^2 \right\rangle = \sum_k \langle \Phi_k(t)\Phi_{-k}(t)\rangle = \left\langle (\Phi_0(t))^2 \right\rangle + \sum_{k\neq 0} \langle \Phi_k(t)\Phi_{-k}(t)\rangle\,, \tag{5.27}$$

we find in the NESS

$$\left\langle (\Psi_g(t))^2 \right\rangle \simeq g_0^2 \left\langle \|\Phi(x,t)\|_0^2 \right\rangle, \tag{5.28}$$

provided that the long-time behavior is dominated by the Fourier-mode with largest eigenvalue, i.e. $k = 0$ with $\mu_0 = 0$. Under the same condition, the first moment of the projected output reads in the NESS

$$\langle \Psi_g(t)\rangle = \sum_k \overline{g_k}\,\langle \Phi_k(t)\rangle \simeq g_0 \langle \Phi_0(t)\rangle\,, \tag{5.29}$$

and thus

$$(\langle \Psi_g(t)\rangle)^2 \simeq g_0^2 \left(\langle \Phi_0(t)\rangle\right)^2. \tag{5.30}$$

Similarly,

$$\|\langle \Phi(x,t)\rangle\|_0^2 = \sum_k |\langle \Phi_k(t)\rangle|^2 \simeq (\langle \Phi_0(t)\rangle)^2 \qquad \text{for } t \gg 1, \tag{5.31}$$

which implies

$$(\langle \Psi_g(t)\rangle)^2 \simeq g_0^2\, \|\langle \Phi(x,t)\rangle\|_0^2\,. \tag{5.32}$$

Note, that g_0 and $\Phi_0(t)$ have to be real throughout the argument (which is indeed the case for expansions with respect to the eigenfunctions of the general diffusion operators $\hat{L}$ from Appendix 3.A.1). Hence, under the assumption that the prior mentioned requirements are met, which, of course, would have to be checked for every individual system (as was done in this section for the KPZ equation), the asymptotic equivalence in (5.28) and (5.32) validates the statement in (5.23) (and therefore, in the NESS, also (5.22)) for a whole class of one-dimensional scalar SPDEs from (4.1).

5.2.4 Total Entropy Production for the KPZ Equation

The total entropy production for the KPZ equation is obtained by inserting $F_\gamma[h_\mu(\mathbf{r},t)] = \partial_x^2 h(x,t) + \frac{\lambda_{\text{eff}}}{2}(\partial_x h(x,t))^2$ and the explicit expression for the one-dimensional stationary probability distribution $p^s[h]$ into (4.22). The form of the latter is given in the following.

The Fokker–Planck Equation and its 1D Stationary Solution

Let us briefly recapitulate the Fokker-Planck equation and its stationary solution in one spatial dimension for the KPZ equation.
The Fokker-Planck equation corresponding to (3.10) for the functional probability distribution $p[h]$ reads in one spatial dimension, e.g., [20, 21, 35, 37, 58] (see also (4.26)),

$$\begin{aligned}\frac{\partial\, p[h]}{\partial t} &= -\int_0^1 dx \frac{\delta}{\delta h}\left[\left(\partial_x^2 h(x,t) + \frac{\lambda_{\text{eff}}}{2}(\partial_x h(x,t))^2\right) p[h] - \frac{1}{2}\frac{\delta p[h]}{\delta h}\right] \\ &= -\int_0^1 dx \frac{\delta j_p[h]}{\delta h},\end{aligned} \tag{5.33}$$

$$j_p[h] \equiv \left(\partial_x^2 h(x,t) + \frac{\lambda_{\text{eff}}}{2}(\partial_x h(x,t))^2\right) p[h] - \frac{1}{2}\frac{\delta p[h]}{\delta h}, \tag{5.34}$$

with $j_p[h]$ as the probability current.
It is well known that for the case of pure Gaussian white noise, a stationary solution, i.e. $\partial_t p^s[h] = 0$, to the Fokker-Planck equation is given by [20, 21, 58]

$$p^s[h] \sim \exp\left[-\left\|\partial_x h\right\|_0^2\right]. \tag{5.35}$$

This stationary solution is the same as the one for the linear case, namely for the Edwards-Wilkinson model (see, e.g., Section 4.2). Note that in (5.35) we denote by $\|\cdot\|_0^2$ the standard $\mathcal{L}_2$-norm.

Stationary Total Entropy Production

With (4.22), the total entropy production in the NESS for the KPZ equation reads

$$\begin{aligned}\Delta s_{\text{tot}} = \Delta s_m + \Delta s &= 2\int_0^t dt' \left(\dot h, \left[\partial_x^2 h + \frac{\lambda_{\text{eff}}}{2}(\partial_x h)^2\right]\right)_0 - \left(h, \partial_x^2 h\right)_0 \\ &= \left[2\int_0^t dt' \left(\dot h, \partial_x^2 h\right)_0 - \left(h, \partial_x^2 h\right)_0\right] + \lambda_{\text{eff}}\int_0^t dt' \left(\dot h, (\partial_x h)^2\right)_0.\end{aligned} \tag{5.36}$$

Using $\left(\dot h, \partial_x^2 h\right)_0 = \frac{1}{2}\frac{d}{dt}\left(h, \partial_x^2 h\right)_0$, and the initial condition $h(x,0) = 0$, the first term in (5.36) vanishes and thus

$$\Delta s_{\text{tot}} = \lambda_{\text{eff}}\int_0^t dt' \left(\dot h(x,t'), \left(\partial_x h(x,t')\right)^2\right)_0. \tag{5.37}$$

For Gaussian white noise, the expectation value of (5.37) is given by

$$\begin{aligned}\langle \Delta s_{\text{tot}} \rangle &= \lambda_{\text{eff}} \int_0^t dt' \left\langle \left(\dot{h}(x,t'), \left(\partial_x h(x,t')\right)^2 \right)_0 \right\rangle \\ &= \frac{\lambda_{\text{eff}}^2}{2} \int_0^t dt' \left\langle \left\| \left(\partial_x h(x,t')\right)^2 \right\|_0^2 \right\rangle .\end{aligned} \tag{5.38}$$

For a derivation of this result see Appendix 5.B. Note that (5.38) and its derivation remains true for $h \in \operatorname{span}\{\phi_{-\Lambda}, \ldots, \phi_{\Lambda}\}$. More generally, the expectation of the total entropy production may also be written as

$$\langle \Delta s_{\text{tot}} \rangle = \frac{\lambda_{\text{eff}}^2}{2} \int_0^t dt' \left\langle \left(\left(\partial_x h(x,t')\right)^2, \hat{K}^{-1} \left(\partial_x h(x,t')\right)^2 \right)_0 \right\rangle , \tag{5.39}$$

with $\hat{K}^{-1}$ from (3.90).

Evaluating the Expectation of the Stationary Total Entropy Production

Above, an expression for the stationary total entropy production Δs_{tot} and its expectation value were derived (see eq. (5.38)). Inserting the Fourier representation from (3.59) and (3.57) into (5.38) leads to

$$\begin{aligned}&\langle \Delta s_{\text{tot}} \rangle \\ &= (4\pi^2)^2 \frac{\lambda_{\text{eff}}^2}{2} \int_0^t dt' \int_0^1 dx \sum_{k \in \mathfrak{R}} \sum_{m \in \mathfrak{R}} e^{2\pi i x (k-m)} \\ &\quad \times \left\langle \sum_{l \in \mathfrak{R}_k \setminus \{0,k\}} l(k-l) h_l(t') h_{k-l}(t') \sum_{n \in \mathfrak{R}_m \setminus \{0,m\}} n(m-n) \overline{h_n}(t') \overline{h_{m-n}}(t') \right\rangle \\ &= (4\pi^2)^2 \frac{\lambda_{\text{eff}}^2}{2} \int_0^t dt' \sum_{k \in \mathfrak{R}} \sum_{l,n \in \mathfrak{R}_k \setminus \{0,k\}} l(k-l) n(k-n) \\ &\quad \times \left\langle h_l(t') h_{k-l}(t') \overline{h_n}(t') \overline{h_{k-n}}(t') \right\rangle ,\end{aligned} \tag{5.40}$$

with $\mathfrak{R}_k$ from (3.85). As (5.40) above is already of order λ_{eff}^2, it suffices to expand the Fourier coefficients $h_i(t')$ to zeroth order, which yields

$$\begin{aligned}\langle \Delta s_{\text{tot}} \rangle = (4\pi^2)^2 \frac{\lambda_{\text{eff}}^2}{2} \int_0^t dt' \sum_{k \in \mathfrak{R}} \sum_{l,n \in \mathfrak{R}_k \setminus \{0,k\}} l(k-l) n(k-n) \\ \times \left\langle h_l^{(0)}(t') h_{k-l}^{(0)}(t') \overline{h_n^{(0)}}(t') \overline{h_{k-n}^{(0)}}(t') \right\rangle + O(\lambda_{\text{eff}}^4),\end{aligned} \tag{5.41}$$

with $h_i^{(0)}(t')$ given by (5.3). Via a Wick contraction and using (5.8), the four-point correlation function in (5.41) reads

$$\begin{aligned}&\left\langle h_l^{(0)}(t')h_{k-l}^{(0)}(t')\overline{h_n^{(0)}}(t')\overline{h_{k-n}^{(0)}}(t')\right\rangle\\&=\Pi_{l,k-l}(t',t')\Pi_{-n,n-k}(t',t')\delta_{0,k}+\Pi_{l,-n}(t',t')\Pi_{k-l,n-k}(t',t')\delta_{l,n}\\&\quad+\Pi_{l,n-k}(t',t')\Pi_{k-l,-n}(t',t')\delta_{n,k-l}.\end{aligned}\tag{5.42}$$

Inserting (5.42) into (5.41) leads to the following form of the total entropy production in the NESS,

$$\begin{aligned}&\langle\Delta s_{\text{tot}}\rangle\\&=\left[(4\pi^2)^2\frac{\lambda_{\text{eff}}^2}{2}\left(\sum_{l,n\in\Re\setminus\{0\}}\frac{l^2n^2}{4\mu_l\mu_n}+2\sum_{k\in\Re}\sum_{l\in\Re_k\setminus\{0,k\}}\frac{l^2(k-l)^2}{4\mu_l\mu_{k-l}}\right)+O(\lambda_{\text{eff}}^4)\right]t.\end{aligned}\tag{5.43}$$

Note, $\langle\Delta s_{\text{tot}}\rangle\sim t$ for $t\gg 1$ is expected to hold (see also Chapter 6). Note further, that the long time behavior of $\langle\Delta s_{\text{tot}}\rangle$ is indeed of the form required, i.e. $\langle\Delta s_{\text{tot}}\rangle\sim\lambda_{\text{eff}}^2 t$ (see remark after (5.21)), for the uncertainty relation to hold. With μ_k from (3.58), the expression for the total entropy production from (5.43) reads

$$\langle\Delta s_{\text{tot}}\rangle=\left[\frac{\lambda_{\text{eff}}^2}{2}\left(\Lambda^2+\frac{3\Lambda^2-\Lambda}{2}\right)+O(\lambda_{\text{eff}}^4)\right]t.\tag{5.44}$$

Thus, with (4.23) and (5.44), the total entropy production rate becomes

$$\sigma=\frac{\lambda_{\text{eff}}^2}{2}\left[\Lambda^2+\frac{3\Lambda^2-\Lambda}{2}\right]+O(\lambda_{\text{eff}}^4).\tag{5.45}$$

With (5.21) and (5.44), or, equivalently, (5.15), (5.20) and (5.45), the constituents of the thermodynamic uncertainty relation are known. Hence, the product entering the TUR from (4.24) for the KPZ equation reads

$$\mathcal{Q}=\langle\Delta s_{\text{tot}}\rangle\,\epsilon^2=\frac{2\,D_g\,\sigma}{J_g^2}=2+\left(3-\frac{1}{\Lambda}\right)+O(\lambda_{\text{eff}}^2).\tag{5.46}$$

Note, that the result given in (5.46) holds strictly for 'almost' white noise only, i.e. for the truncated noise spectrum with cutoff Λ (see e.g. (3.81) and (3.83)). However, we choose $\Lambda=\Lambda_0$ large enough, such that all contributions from modes with $|k|>\Lambda_0$ are expected to be dominated by the diffusive term of the KPZ equation, hence, be effectively described by the unforced Edwards-Wilkinson equation (see further the comments below (3.85)). As for very large times t, the Edwards-Wilkinson model displays a genuine equilibrium, it does not contribute to the current (5.15) nor the entropy production rate

(5.45). Consequently, modes with $|k| > \Lambda_0$ do not affect the TUR in (5.46) and thus we expect it to hold also for 'fully' white noise, i.e., without the need to increase the cutoff parameter Λ.
Note further, that in (5.46) we deliberately refrain from writing $\mathcal{Q} = 5 - 1/\Lambda$ as this would mask the physics causing this result. This point will be discussed further in the following.
To give an interpretation of the two terms in (5.43) and consequently in (5.46), it is instructive to refer to the precision and total entropy production for the FEW model from Section 4.2. According to (4.45) - (4.47), we have for the case of Gaussian white noise, i.e., $\alpha_k = 1\ \forall\, k$,

$$J_g^{\mathrm{FEW}} = g_0 v_0, \qquad D_g^{\mathrm{FEW}} = \frac{g_0^2}{2}, \qquad \sigma^{\mathrm{FEW}} = 2\, v_0^2. \tag{5.47}$$

With (5.47), we can now give an interpretation of the two terms in (5.44) and (5.46). The first term in the inner brackets of (5.44) originates from the first term of (5.43), where the latter represents the action of all higher-order Fourier modes on the mode $k = 0$ (see (5.42)). To illustrate this point further, observe that, in the NESS, we get with the aid of (5.11) – (5.15) for the current:

$$J_g = 2\pi^2 g_0 \lambda_{\mathrm{eff}} \left(\sum_{l \in \mathfrak{R}\setminus\{0\}} \frac{l^2}{2(-\mu_l)} \right) = g_0 \frac{\lambda_{\mathrm{eff}}}{2} \Lambda, \tag{5.48}$$

and from the calculation above we see that it contains only the impact of Fourier modes $l \neq 0$ on the mode $k = 0$, which belongs to the constant eigenfunction $\phi_0(x) = 1$. In other words, the modes $l \neq 0$ act like a constant external excitation, just in the same manner as v_0 acts for FEW in (4.45). Comparing (5.48) to (4.45), we may set

$$v_0 = 2\pi^2 \lambda_{\mathrm{eff}} \left(\sum_{l \in \mathfrak{R}\setminus\{0\}} \frac{l^2}{2(-\mu_l)} \right) = \frac{\lambda_{\mathrm{eff}}}{2} \Lambda, \tag{5.49}$$

and get $J_g = g_0 v_0$ in both cases.
Following now the calculations for FEW, we would expect from (4.43) ($\alpha_k = 1\ \forall k$),

$$\langle \Delta s_{\mathrm{tot}} \rangle = 2 v_0^2\, t = (4\pi^2)^2 \frac{\lambda_{\mathrm{eff}}^2}{2} \left(\sum_{l \in \mathfrak{R}\setminus\{0\}} \frac{l^2}{2(-\mu_l)} \right)^2 t = \frac{\lambda_{\mathrm{eff}}^2}{2} \Lambda^2\, t, \tag{5.50}$$

which is in fact exactly the first term in the inner brackets from (5.43) and (5.44), respectively. Since with (5.49) also the expression for ϵ^2 from (4.41) coincides with the first summand on the r.h.s. of (5.21), it is clear that both cases result in the saturated

TUR. This explains the value 2 on the r.h.s. of (5.46).
Turning to the second term of (5.44), we see that it stems from the second term in (5.43). In contrast to the first λ_{eff}^2-term in (5.43), the second one does not only measure the effect of the modes on the $k = 0$ mode but also on all other modes $k \neq 0$. It further features interactions of the k and l modes among each other via mode coupling. Hence, the mode coupling seems responsible for the larger constant on the right hand side of (5.46), since by neglecting the mode coupling term in (5.44), the thermodynamic uncertainty relation was saturated also for the KPZ equation up to $O(\lambda_{\text{eff}}^2)$. To conclude this brief discussion, we give the respective relations of the KPZ current (5.15), diffusivity (5.20) and total entropy production rate (5.45) to FEW, namely

$$\begin{aligned} J_g^{\text{KPZ}} &= J_g^{\text{FEW}} + O(\lambda_{\text{eff}}^3), \\ D_g^{\text{KPZ}} &= D_g^{\text{FEW}} + g_0^2 \frac{\lambda_{\text{eff}}^2}{32\,\pi^2} \mathcal{H}_\Lambda^{(2)} + O(\lambda_{\text{eff}}^4), \\ \sigma^{\text{KPZ}} &= \sigma^{\text{FEW}} + \lambda_{\text{eff}}^2 \frac{3\Lambda^2 - \Lambda}{4} + O(\lambda_{\text{eff}}^4), \end{aligned} \tag{5.51}$$

with J_g^{FEW}, D_g^{FEW} and σ^{FEW} from (5.47). We see that the additional mode coupling term in KPZ leads to corrections in D_g^{KPZ} and σ^{KPZ} of at least second order in λ_{eff}. For the case of $\lambda_{\text{eff}} \downarrow 0$ the KPZ equation becomes the unforced ($v_0 = 0$) Edwards-Wilkinson equation (EW), namely $\partial_t h(x,t) = \partial_x^2 h(x,t) + \eta(x,t)$, which possesses a genuine equilibrium steady state. Therefore, for the standard EW we have $J_g^{\text{EW}} = 0$, $\sigma^{\text{EW}} = 0$ and $D_g^{\text{EW}} = g_0^2/2$. From (5.51) it follows that for $\lambda_{\text{eff}} \downarrow 0$, $(J_g, \sigma, D_g)_{\text{KPZ}} \to (J_g, \sigma, D_g)_{\text{FEW}}$ and from (5.47), (5.49) that $(J_g, \sigma, D_g)_{\text{FEW}} \to (J_g, \sigma, D_g)_{\text{EW}} = (0, 0, g_0^2/2)$. Hence, the non-zero expressions for J_g^{KPZ} and σ^{KPZ} result solely from the KPZ non-linearity. The impact of the latter on the $k = 0$ Fourier mode (i.e., the spatial mean of $h(x,t)$) results in contributions to J_g^{KPZ} and σ^{KPZ} that can be modeled exactly by FEW, the Edwards-Wilkinson equation driven by a constant force v_0 from (4.25) for Gaussian white noise. Note, that despite the limiting behavior of (J_g, σ, D_g) described above, for the TUR product $\mathcal{Q}$ itself, $\mathcal{Q} \downarrow 5$ for $\lambda_{\text{eff}} \downarrow 0$ and $\Lambda \gg 1$ holds. This is due to the fact that both terms contributing to σ^{KPZ}, namely, σ^{FEW} with v_0 from (5.49) as well as the additional mode coupling term, are of the same order $O(\lambda_{\text{eff}}^2)$ as is $(J_g^{\text{KPZ}})^2$. Hence, we have a singular limit for $\lambda_{\text{eff}} \downarrow 0$.
In Section 5.4, it will be shown that the expressions for J_g^{KPZ} and σ^{KPZ}, which have been constructed in this section perturbatively to lowest non-vanishing order, are in fact exact. Therefore, the first and third line from (5.51) hold without the respective $O(\cdot)$-term. This is also true for the expressions in (5.14), (5.15) as well as (5.44), (5.45). Furthermore, the $O(\lambda_{\text{eff}}^2)$-term in the TUR product presented in (5.46) can be made explicit as this term is now known to stem solely form the expansion of the diffusivity

in (5.20). The resulting refined TUR product reads

$$\mathcal{Q} = \langle \Delta s_{\mathrm{tot}} \rangle \, \epsilon^2 = \frac{2\, D_g\, \sigma}{J_g^2} \simeq 5 \left(1 + \lambda_{\mathrm{eff}}^2 \frac{\zeta(2)}{16\, \pi^2} + O(\lambda_{\mathrm{eff}}^4) \right) , \qquad \Lambda \gg 1 \,. \tag{5.52}$$

5.3 Higher Order Approximations

In this section, we focus on extending the results from Sections 5.1 and 5.2 to higher orders in perturbation theory. Beforehand, let us remark the following. In Section 5.2.2, we have shown perturbatively (see the comment at the end of Section 5.2.2) that the precision ϵ^2 built with the observable $\Psi_g(t)$ is independent of the choice of the weight function $g(x)$. This will be shown generally in Appendix 6.A without relying on perturbation expansions. Anticipating this result, we will restrict ourselves in the following chapters to the case $g(x) \equiv 1$, i.e., we will replace $\Psi_g(t)$ by

$$\Psi(t) \equiv \Psi_1(t) = \int_0^b dx\, h(x,t), \tag{5.53}$$

or, in scaled variables, $\Psi_s(t) = \int_0^1 dx_s h_s(x_s, t_s)$ representing the spatial mean of the scaled height field.

As the results from Section 5.2 for $\langle \Psi_g(t) \rangle = \langle \Psi(t) \rangle$, or $J_g(t) = J(t)$ and $\langle \Delta s_{\mathrm{tot}} \rangle$ or σ are, in fact, exact (see Section 5.4), we have to deal only with the expansion of var$[\Psi(t)]$ to higher order. To this end, we use the same ansatz as in Section 5.1 to now evaluate

$$\mathrm{var}[\Psi(t)] = \int_0^t dt' \int_0^t dt'' \left[\left\langle \dot{\Psi}(t') \dot{\Psi}(t'') \right\rangle - \left\langle \dot{\Psi}(t') \right\rangle \left\langle \dot{\Psi}(t'') \right\rangle \right] , \tag{5.54}$$

where

$$\dot{\Psi}(t) = \frac{\lambda_{\mathrm{eff}}}{2} \int_0^1 dx \left(\partial_x h(x,t) \right)^2 + \int_0^1 dx\, \eta(x,t). \tag{5.55}$$

Here, the one-dimensional form of (3.10) is integrated with respect to the spatial variable to obtain (5.55). We use (5.55) to calculate the two-time correlation function

$$\begin{aligned} \left\langle \dot{\Psi}(t')\, \dot{\Psi}(t'') \right\rangle &= \frac{\lambda_{\mathrm{eff}}^2}{4} \int_0^1 dx \int_0^1 dy \, \left\langle \left(\partial_x h(x,t') \right)^2 \left(\partial_y h(y,t'') \right)^2 \right\rangle + \delta(t'-t'') \\ &\equiv \frac{\lambda_{\mathrm{eff}}^2}{4} \, \mathcal{J}(t',t'') + \delta(t'-t''), \end{aligned} \tag{5.56}$$

where

$$\mathcal{J}(t',t'') = (2\pi)^4 \sum_{k,l \in \mathfrak{R} \setminus \{0\}} k^2\, l^2 \, \left\langle h_k(t') h_{-k}(t') h_l(t'') h_{-l}(t'') \right\rangle . \tag{5.57}$$

In principle any correlation of the Fourier coefficients h_k can eventually be expressed by correlations of $h_k^{(0)}$ from (5.3), which depend linearly on the Gaussian noise η and

thus allow for the application of Wick's theorem. In practice, however, this results in a steeply increasing complexity of the calculation for higher order approximations in λ_{eff}. A possible circumvention of this issue is the physical assumption of so-called quasi-normality. This assumption has been successfully used in turbulence theory [101, 102] and has been adopted in [62] for the height field $h(x,t)$ of the KPZ equation. The quasi-normality hypothesis states that all even moments of h are assumed to behave like they were normally distributed and thus Wick's theorem may directly be applied to (5.57). At least for large times t', t'' the assumption is supported by the fact that $h(x,t)$ is exactly Gaussian distributed in the NESS (see Section 5.4).
Hence, after applying Wick's theorem to (5.57), we have

$$\begin{aligned}
&\left\langle \dot{\Psi}(t')\,\dot{\Psi}(t'')\right\rangle - \left\langle \dot{\Psi}(t')\right\rangle \left\langle \dot{\Psi}(t'')\right\rangle \\
&= \delta(t'-t'') + (2\pi)^4 \frac{\lambda_{\text{eff}}^2}{4} \sum_{k,l\in\mathfrak{R}\setminus\{0\}} k^2\, l^2 \\
&\times \left[\left\langle h_k(t')h_l(t'')\right\rangle \left\langle h_{-k}(t')h_{-l}(t'')\right\rangle + \left\langle h_k(t')h_{-l}(t'')\right\rangle \left\langle h_{-k}(t')h_l(t'')\right\rangle\right].
\end{aligned} \tag{5.58}$$

Replacing the h_j's in (5.58) with the expansion from (5.2)-(5.5), integrating twice over time and following the same steps as in Section 5.2, one obtains for $t \gg 1$

$$\begin{aligned}
\operatorname{var}[\Psi(t)] \simeq t \,&\left[1 + \frac{\lambda_{\text{eff}}^2}{32\pi^2} \sum_{k\in\mathfrak{R}\setminus\{0\}} \frac{1}{k^2}\right. \\
&\left. - \frac{\lambda_{\text{eff}}^4}{256\pi^4} \sum_{k\in\mathfrak{R}\setminus\{0\}} \sum_{m\in\mathfrak{R}_k\setminus\{0,k\}} \frac{m}{k^3(k^2+(k-m)^2+m^2)} + O(\lambda_{\text{eff}}^6)\right] \\
&\equiv t\left[1 + \frac{\lambda_{\text{eff}}^2}{32\pi^2}\mathcal{S}_1(\Lambda) - \frac{\lambda_{\text{eff}}^4}{256\pi^4}\mathcal{S}_2(\Lambda) + O(\lambda_{\text{eff}}^6)\right],
\end{aligned} \tag{5.59}$$

which is calculated to one order higher than in Section 5.2 and $\mathcal{S}_{1,2}$ are simply abbreviations for the respective sums in the first line. Next we will evaluate $\mathcal{S}_{1,2}$ analytically in the limit of large Λ. For $\mathcal{S}_1$ we find

$$\mathcal{S}_1(\Lambda) = 2\mathcal{H}_\Lambda^{(2)} \quad \xrightarrow{\Lambda\gg 1} \quad 2\,\zeta(2), \tag{5.60}$$

where $\mathcal{H}_\Lambda^{(n)} = \sum_{k=1}^{\Lambda} 1/k^n$ is again the generalized harmonic number of order n and ζ the Riemann-Zeta function. For $\mathcal{S}_2$ we find after some straightforward algebraic manipulation

$$\begin{aligned}\mathcal{S}_2(\Lambda) &= \sum_{k\in\mathfrak{R}\setminus\{0\}} \left[\sum_{m\in\mathfrak{R}_k} \frac{m}{k^3(k^2+(k-m)^2+m^2)} - \frac{1}{2\,k^4} \right] \\ &= 2\sum_{k=1}^{\Lambda} \frac{1}{k^3} \sum_{m=-\Lambda+k}^{\Lambda} \frac{m}{k^2+(k-m)^2+m^2} - \mathcal{H}_\Lambda^{(4)}.\end{aligned} \tag{5.61}$$

The inner sum over m in the second line in (5.61) may be approximated for large values of Λ by

$$\int_{-\Lambda+k}^{\Lambda} dx\, \frac{x}{k^2+(k-x)^2+x^2} = \frac{1}{\sqrt{3}} \arctan \frac{2\Lambda-k}{\sqrt{3}\,k} \equiv \mathcal{G}_\Lambda(k). \tag{5.62}$$

Plotting the function $\mathcal{G}_\Lambda(k)$ suggests that it may well be approximated by the linear expression

$$\begin{aligned}\mathcal{G}_\Lambda(k) &\approx \mathcal{G}_\Lambda(0) - \frac{\mathcal{G}_\Lambda(0)-\mathcal{G}_\Lambda(\Lambda)}{\Lambda}\, k = \frac{\pi}{2\sqrt{3}} - \frac{1}{\sqrt{3}} \frac{\pi/2-\arctan(1/\sqrt{3})}{\Lambda}\, k \\ &\approx 0.9069 - \frac{0.6046}{\Lambda}\, k,\end{aligned} \tag{5.63}$$

and thus we have

$$\sum_{m=-\Lambda+k}^{\Lambda} \frac{m}{k^2+(k-m)^2+m^2} \approx 0.9069 - \frac{0.6046}{\Lambda}\, k. \tag{5.64}$$

Inserting (5.64) into (5.61) and taking $\Lambda \gg 1$ leads to

$$2\sum_{k=1}^{\Lambda} \frac{1}{k^3} \sum_{m=-\Lambda+k}^{\Lambda} \frac{m}{k^2+(k-m)^2+m^2} - \mathcal{H}_\Lambda^{(4)} \quad \overset{\Lambda\gg1}{\longrightarrow} \quad 1.814\,\zeta(3) - \zeta(4). \tag{5.65}$$

Thus in the case of large Λ we have the following asymptotic behavior ($t \gg 1$) of the variance of Ψ,

$$\mathrm{var}[\Psi(t)] \simeq t\, \left[1 + \frac{\lambda_{\mathrm{eff}}^2}{16\pi^2}\,\zeta(2) - \frac{\lambda_{\mathrm{eff}}^4}{256\pi^4}\,(1.814\,\zeta(3)-\zeta(4)) + O(\lambda_{\mathrm{eff}}^6) \right], \tag{5.66}$$

or, in terms of the rescaled, dimensional variables

$$\mathrm{var}[\Psi(t)] \simeq \Delta_0\, b\, t \left[1 + \frac{\Delta_0 b\lambda^2}{16\pi^2\nu^3}\zeta(2) - \frac{\Delta_0^2 b^2\lambda^4}{256\pi^4\nu^6}\,(1.814\,\zeta(3)-\zeta(4)) + O(\lambda_{\mathrm{eff}}^6) \right]. \tag{5.67}$$

With (5.66), (5.67), the TUR product $\mathcal{Q}$ may now be written up to $O(\lambda_{\mathrm{eff}}^6)$. We expect the approximations in (5.66) and (5.67) to yield sound results for $\lambda_{\mathrm{eff}} \lessapprox \lambda_{\mathrm{eff}}^{\mathrm{c}}$ from (3.51). In Chapter 7, this will be checked by comparison with numerical simulations in the according parameter regime.

5.4 Exact Results

In the previous sections, we have derived perturbative approximations to the steady state current J, the steady state entropy production rate σ and diffusivity D. As already mentioned above, the results for J and σ obtained perturbatively to lowest non-vanishing order are in fact exact. This will be shown below in a non-perturbative way. To this end we make use of the exact knowledge of the stationary probability density functional of the one-dimensional KPZ equation and evaluate the expectation values of the current and entropy production rate via functional integration. This approach is, however, only valid for equal-time observables, like the current and entropy production rate, whereas the calculation of the variance, which is based on a two-time correlation, is not feasible in this approach.

5.4.1 Normalized Stationary Distribution

We recapitulate that for the $(1+1)$ dimensional KPZ equation the stationary probability density functional of the height field $h(x,t)$ is known exactly (e.g., [20,21,36]) and reads

$$p^s[h] \sim \exp\left[-\frac{\nu}{\Delta_0}\int_0^b dx\ (\partial_x h)^2\right]. \tag{5.68}$$

In the following, we want to use (5.68) to calculate equal-time steady-state correlation functions. Hence, (5.68) needs to be properly normalized. The normalization is obtained by expressing $h(x,t)$ in terms of its Fourier series (see, e.g., Appendix 3.A.1)

$$h(x,t) = \sum_{k\in\mathfrak{R}} h_k(t)\, e^{2\pi i k x/b}, \qquad \mathfrak{R} = [-\Lambda,\Lambda],\ \Lambda \in \mathbb{N}, \tag{5.69}$$

where $h_k(t) \in \mathbb{C}$, and inserting (5.69) into (5.68). The introduction of a finite Fourier-cutoff Λ ensures the normalizability of (5.68). A subsequent functional integration of (5.68) over h yields

$$\begin{aligned}
&\int \mathcal{D}[h]\ \exp\left[-\frac{\nu}{\Delta_0}\int_0^b dx\ (\partial_x h)^2\right] \\
&= \prod_{k=1}^{\Lambda}\int dh_{R,k}\ \exp\left[-\frac{8\pi^2\nu}{\Delta_0 b}k^2 h_{R,k}^2\right]\prod_{l=1}^{\Lambda}\int dh_{I,l}\ \exp\left[-\frac{8\pi^2\nu}{\Delta_0 b}l^2 h_{I,l}^2\right] \\
&= \left(\frac{\Delta_0\, b}{8\pi\,\nu}\right)^{\Lambda}\left(\frac{1}{\Lambda!}\right)^2,
\end{aligned} \tag{5.70}$$

where $h_{R/I,j}(t)$ represents the real/imaginary part of $h_j(t)$, respectively. Hence, the normalization of (5.68) reads

$$\mathcal{N} = \left(\frac{\Delta_0\, b}{8\pi\,\nu}\right)^{\Lambda}\left(\frac{1}{\Lambda!}\right)^2, \tag{5.71}$$

and therefore

$$p^s[h] = \frac{1}{\mathcal{N}} \exp\left[-\frac{\nu}{\Delta_0}\int_0^b dx\ (\partial_x h)^2\right]. \tag{5.72}$$

The structure of the normalization factor $\mathcal{N}$ from (5.71) again highlights the need to introduce a finite upper cutoff in the Fourier spectrum, as otherwise for $\Lambda \to \infty$, a normalization of the probability density functional would no longer be possible. Similarly, an infinite substrate, i.e., $b \to \infty$, also leads to a diverging $\mathcal{N}$ (see also the observations in [103]). With (5.72) we can explicitly calculate steady state equal-time correlation functions of the Fourier coefficients $h_k(t)$ by a functional integration, where $\langle\cdot\rangle_{p^s[h]} \equiv \int \mathcal{D}[h]\,(\cdot)p^s[h]$ is understood as the expectation value with respect to the stationary probability distribution. In particular

$$\langle h_k(t)\, h_l(t)\rangle_{p^s[h]} = -\frac{\Delta_0\, b^{-1}}{\mu_k + \mu_l}\,\delta_{k,-l}, \tag{5.73}$$

with $\mu_k = -4\pi^2\nu k^2/b^2$ from (3.56). Note, that

$$\lim_{t\to\infty} \langle(\cdot)(t)\rangle = \langle(\cdot)(t)\rangle_{p^s[h]}\,, \tag{5.74}$$

is expected to hold, where $\langle\cdot\rangle$ denotes averages with respect to the noise history. We will show this explicitly in the case of $\langle\Psi(t)\rangle$ and $\langle\Delta s_{\text{tot}}\rangle$ below.

5.4.2 Exact Stationary Current and Entropy Production Rate

For the steady state current J, where $\langle\Psi(t)\rangle = J\,t$, we get

$$J = \langle\partial_t\Psi(t)\rangle_{p^s[h]} = \frac{\lambda}{2}\int_0^b dx\,\left\langle(\partial_x h(x,t))^2\right\rangle_{p^s[h]} = \frac{\Delta_0\,\lambda}{2\,\nu}\,\Lambda. \tag{5.75}$$

The second step follows from a spatial integration of (3.3) with a subsequent averaging with respect to $p^s[h]$ and the last step uses Parseval's identity and (5.73). The result in (5.75) has already been derived in (5.15) as lowest order approximation of a perturbation expansion in λ_{eff} where the l.h.s. of (5.74) was used for calculating expectation values (see also [20]). It is instructive, to examine why the lowest order approximation is in fact exact. This can be seen by studying the structure of the perturbation expansion of $\langle\partial_t\Psi(t)\rangle$. Terms with an even power of λ_{eff} vanish as they represent odd moments of the Gaussian noise η, whereas terms with odd power greater than 1 vanish by exact cancellation of the involved moments.

For the steady-state entropy production rate σ, with $\langle\Delta s_{\text{tot}}\rangle = \sigma\,t$, it is found with

(5.69), using Wick's theorem and (5.73) that

$$\begin{aligned}\sigma &= \frac{\lambda^2}{2\,\Delta_0}\int_0^b dx\,\left\langle\left|(\partial_x h(x,t))^2\right|^2\right\rangle_{p_s[h]}\\ &= \frac{8\pi^4\lambda^2}{\Delta_0\,b^3}\sum_{k\in\mathfrak{R}}\sum_{l,n\in\mathfrak{R}_k\setminus\{0,k\}} l(k-l)n(k-n)\,\langle h_l(t)h_{k-l}(t)h_{-n}(t)h_{n-k}(t)\rangle_{p_s[h]}\\ &= \frac{\Delta_0\,\lambda^2}{2\,b\,\nu^2}\left[\Lambda^2+\frac{3\Lambda^2-\Lambda}{2}\right] = \frac{\Delta_0\,\lambda^2}{4\,b\,\nu^2}\left[5\,\Lambda^2-\Lambda\right],\end{aligned} \tag{5.76}$$

where $\mathfrak{R}_k \equiv [\max(-\Lambda,-\Lambda+k),\min(\Lambda,\Lambda+k)]$ (see (3.85)). Again, a comparison of (5.76) with the corresponding result from (5.45) shows that the lowest order perturbational approximation is also exact for the case of the entropy production rate σ in $1d$.

Thus, by using (5.72), we can calculate for the $(1+1)$ dimensional KPZ equation the exact expressions for the stationary current J (see (5.75)) and the entropy production rate σ (see (5.76)) for arbitrary values of the coupling parameter. This implies that two of the three constituents of the TUR product $\mathcal{Q}$ are known exactly. Hence, we state the exact, however, intermediate, result

$$\mathcal{Q} = \frac{\langle\Delta s_{\text{tot}}\rangle}{\langle\Psi(t)\rangle^2}\,\text{var}[\Psi(t)] = \left(5-\frac{1}{\Lambda}\right)\frac{\text{var}[\Psi(t)]}{\Delta_0\,b\,t}. \tag{5.77}$$

While intermediate, the expression in (5.77) lends some interesting insight in the general behavior of the KPZ-TUR. Since the ratio of $\langle\Delta s_{\text{tot}}\rangle/\langle\Psi\rangle^2$ does not depend on the value of the effective coupling parameter λ_{eff} from (3.13), the only λ_{eff}-dependence is introduced by $\text{var}[\Psi(t)]$. On this regard, we have seen above (see (5.66) and (5.67)) that for $\lambda_{\text{eff}}\to 0$, $\text{var}[\Psi(t)]\to\Delta_0\,b\,t$ and thus $\mathcal{Q}\to 5-1/\Lambda$. The independence of $\mathcal{Q}$ on λ_{eff} will hold as long as the higher order contributions from, e.g., (5.66), are negligible compared to the zeroth-order expression for $\text{var}[\Psi(t)]$. As we will see below via numerical simulations, for $\lambda_{\text{eff}}\uparrow\lambda_{\text{eff}}^{\text{c}}$ from (3.51) these higher-order contributions become increasingly relevant and will lead to $\mathcal{Q}$ depending on λ_{eff}.

Thus far, we only have explicit knowledge about the dependence of $\text{var}[\Psi(t)]$ on λ_{eff} in the EW scaling regime of the KPZ equation, i.e., for $\lambda_{\text{eff}}\le\lambda_{\text{eff}}^{\text{c}}$. In Chapter 6, we therefore aim to derive an explicit expression for $\text{var}[\Psi(t)]$ for $\lambda_{\text{eff}}>\lambda_{\text{eff}}^{\text{c}}$.

Appendix 5.A Evaluation of (5.16)

Using (5.8), the first term in (5.16) reads

$$\left\langle h_k^{(0)}(t)h_l^{(0)}(t)\right\rangle = \Pi_{k,l}(t,t)\delta_{k,-l} = e^{(\mu_k+\mu_l)t}\frac{1-e^{-(\mu_k+\mu_l)t}}{\mu_k+\mu_l}\delta_{k,-l}. \tag{5.78}$$

Note that the case of $k=0$ is treated like in (5.12). The second term in (5.16) is given by

$$
\begin{aligned}
&\left\langle h_k^{(1)}(t) h_l^{(1)}(t)\right\rangle \\
&= (2\pi^2)^2 \sum_{m\in\mathfrak{R}_k\setminus\{0,k\}} m(k-m) \sum_{n\in\mathfrak{R}_l\setminus\{0,l\}} n(l-n) \int_0^t dt'\, e^{\mu_k(t-t')} \int_0^t dr\, e^{\mu_l(t-r)} \\
&\quad \times \left\langle h_m^{(0)}(t') h_{k-m}^{(0)}(t') h_n^{(0)}(r) h_{l-n}^{(0)}(r)\right\rangle \\
&= -2(2\pi^2)^2 \sum_{m\in\mathfrak{R}_k\setminus\{0,k\}} m^2(k-m)(l+m) \int_0^t dt'\, e^{\mu_k(t-t')} \int_0^t dr\, e^{\mu_l(t-r)} \\
&\quad \times \Pi_{m,m}(t',r)\Pi_{k-m,l+m}(t',r)\delta_{k,-l} \\
&\quad + (2\pi^2)^2 \sum_{m\in\mathfrak{R}_k\setminus\{0,k\}} m(k-m) \sum_{n\in\mathfrak{R}_l\setminus\{0,l\}} n(l-n) \int_0^t dt'\, e^{\mu_k(t-t')} \int_0^t dr\, e^{\mu_l(t-r)} \\
&\quad \times \Pi_{m,k-m}(t',t')\Pi_{n,l-n}(r,r)\delta_{0,k}\delta_{0,l},
\end{aligned}
\tag{5.79}
$$

where we used Wick's-theorem, (5.8) and (5.4). Note that the two Kronecker-deltas in the last term of (5.79) can also be written as $\delta_{0,k}\delta_{0,l}\delta_{k,-l}$, such that the whole expression is multiplied by $\delta_{k,-l}$. Again with Wick's-theorem, (5.8) and (5.5) we can calculate the third and forth term of (5.16) accordingly and find

$$
\begin{aligned}
&\left\langle h_k^{(0)}(t) h_l^{(2)}(t)\right\rangle \\
&= 4(2\pi^2)^2 \sum_{m\in\mathfrak{R}_l\setminus\{0,l\}} ml(l-m)(m-l) \int_0^t dt'\, e^{\mu_l(t-t')} \int_0^{t'} dr\, e^{\mu_m(t'-r)} \\
&\quad \times \Pi_{k,l}(t,r)\Pi_{l-m,l-m}(t',r)\delta_{k,-l}, \\
&\left\langle h_k^{(2)}(t) h_l^{(0)}(t)\right\rangle \\
&= 4(2\pi^2)^2 \sum_{m\in\mathfrak{R}_k\setminus\{0,k\}} mk(k-m)(m-k) \int_0^t dt'\, e^{\mu_k(t-t')} \int_0^{t'} dr\, e^{\mu_m(t'-r)} \\
&\quad \times \Pi_{k,l}(t,r)\Pi_{k-m,k-m}(t',r)\delta_{k,-l}.
\end{aligned}
\tag{5.80}
$$

As can be seen from (5.78) to (5.80), all four terms in (5.16) contain a $\delta_{k,-l}$ and thus (5.16) reduces to

$$
\begin{aligned}
\left\langle (\Psi_g(t))^2\right\rangle = \sum_{k\in\mathfrak{R}} |g_k|^2 \Big[&\left\langle h_k^{(0)}(t) h_{-k}^{(0)}(t)\right\rangle + \lambda_{\text{eff}}^2 \Big(\left\langle h_k^{(1)}(t) h_{-k}^{(1)}(t)\right\rangle \\
&+ \left\langle h_k^{(0)}(t) h_{-k}^{(2)}(t)\right\rangle + \left\langle h_k^{(2)}(t) h_{-k}^{(0)}(t)\right\rangle\Big) + O(\lambda_{\text{eff}}^4)\Big]
\end{aligned}
\tag{5.81}
$$

The first term of (5.81) is readily evaluated with (5.78) as

$$\left\langle h_k^{(0)}(t)h_{-k}^{(0)}(t)\right\rangle = \Pi_{k,-k}(t,t)\delta_{k,k} = \frac{e^{2\mu_k t}-1}{2\mu_k} = \begin{cases} t & \text{for } k=0, \\ -\frac{1}{2\mu_k} & \text{for } k\neq 0 \text{ and } t\gg 1. \end{cases} \tag{5.82}$$

The second term of (5.81) reads with (5.79):

$$\begin{aligned} &\left\langle h_k^{(1)}(t)h_{-k}^{(1)}(t)\right\rangle \\ &= 2(2\pi^2)^2 \sum_{m\in\mathfrak{R}_k\setminus\{0,k\}} m^2(k-m)^2 \int_0^t dt'\, e^{\mu_k(t-t')} \int_0^t dr\, e^{\mu_k(t-r)} \\ &\quad\times \Pi_{m,m}(t',r)\Pi_{k-m,k-m}(t',r) \\ &\quad+ (2\pi^2)^2 \sum_{m\in\mathfrak{R}\setminus\{0\}} m^2 \sum_{n\in\mathfrak{R}\setminus\{0\}} n^2 \int_0^t dt'\,\Pi_{m,m}(t',t') \int_0^t dr\,\Pi_{n,n}(r,r) \end{aligned} \tag{5.83}$$

Hence, with $\left\langle h_k^{(1)}(t)\right\rangle$ from (5.12), the expression in (5.83) becomes

$$\begin{aligned} &\left\langle h_k^{(1)}(t)h_{-k}^{(1)}(t)\right\rangle \\ &= 2(2\pi^2)^2 e^{2\mu_k t} \sum_{m\in\mathfrak{R}_k\setminus\{0,k\}} \frac{m^2(k-m)^2}{4\mu_m\mu_{k-m}} \int_0^t dt' \int_0^t dr\, e^{(\mu_m+\mu_{k-m}-\mu_k)(t'+r)} \\ &\quad\times \left(1-e^{-2\mu_m(t'\wedge r)}-e^{-2\mu_{k-m}(t'\wedge r)}+e^{-2(\mu_m+\mu_{k-m})(t'\wedge r)}\right) + \left\langle h_k^{(1)}(t)\right\rangle^2. \end{aligned} \tag{5.84}$$

Here the choice of the minimum of $(t'\wedge r)$ is arbitrary, since for $(t'\wedge r)=r$ the other case is obtained by simply interchanging $r\leftrightarrow t'$ under the integral and vice versa; thus the results for both choices are equivalent. In the following $(t'\wedge r)=r$ is chosen. Hence, the integral expression in (5.84) can be evaluated as twice the expression

$$\begin{aligned} &e^{2\mu_k t}\int_0^t dt'\, e^{(\mu_m+\mu_{k-m}-\mu_k)t'} \int_0^{t'} dr \\ &\quad\times\left(e^{(\mu_m+\mu_{k-m}-\mu_k)r}-e^{(-\mu_m+\mu_{k-m}-\mu_k)r}-e^{(\mu_m-\mu_{k-m}-\mu_k)r}+e^{-(\mu_m+\mu_{k-m}+\mu_k)r}\right) \\ &\simeq \begin{cases} -\frac{t}{2\mu_m} & \text{for } k=0 \\ \frac{1}{2\mu_k(\mu_m+\mu_{k-m}+\mu_k)} & \text{for } k\neq 0 \end{cases} \quad \text{for } t\gg 1. \end{aligned} \tag{5.85}$$

Thus, with (5.84) and (5.85), the long time behavior of $\left\langle h_k^{(1)}(t)h_{-k}^{(1)}(t)\right\rangle$ is given by

$$\begin{aligned}&\left\langle h_k^{(1)}(t)h_{-k}^{(1)}(t)\right\rangle\\ &\simeq \left\langle h_k^{(1)}(t)\right\rangle^2 + 2(2\pi^2)^2 \times \begin{cases}\left[-\sum_{l\in\mathfrak{R}\setminus\{0\}} \frac{l^4}{4\mu_l^3}\right] t & \text{for } k=0,\\ \sum_{l\in\mathfrak{R}_k\setminus\{0,k\}} \frac{l^2(k-l)^2}{4\mu_l\mu_{k-l}} \frac{1}{\mu_k(\mu_l+\mu_{k-l}+\mu_k)} & \text{for } k\neq 0,\end{cases}\end{aligned} \tag{5.86}$$

where we changed $m \to l$. To save computational effort, rewrite the last two terms of (5.81) in the following way

$$\left\langle h_k^{(0)}(t)h_{-k}^{(2)}(t)\right\rangle + \left\langle h_k^{(2)}(t)h_{-k}^{(0)}(t)\right\rangle = 2\,\mathrm{Re}\left[\left\langle h_k^{(0)}(t)\overline{h_k^{(2)}}(t)\right\rangle\right]. \tag{5.87}$$

Hence, it suffices to calculate one of the two expectation values. With (5.80) we see that

$$\begin{aligned}&\left\langle h_k^{(0)}(t)\overline{h_k^{(2)}}(t)\right\rangle\\ &= -16\pi^4 e^{\mu_k t}\int_0^t dt'\, e^{-\mu_k t'} \sum_{m\in\mathfrak{R}_k\setminus\{0,k\}} km^2(k-m)e^{\mu_{k-m}t'}\int_0^{t'} dr\, e^{-\mu_{k-m}r}\\ &\quad\times \Pi_{k,k}(t,r)\Pi_{m,m}(t',r),\end{aligned} \tag{5.88}$$

where we substituted $m \to k-m$ and used the symmetry of $\Pi_{k,l}(t,t')$ from (5.7). Note that for $k=0$, the above expression in (5.88) vanishes. Thus in the following calculations $k\neq 0$ is assumed. In this setting, (5.88) reads with (5.8)

$$\begin{aligned}&-16\pi^4 e^{\mu_k t}\int_0^t dt'\, e^{-\mu_k t'} \sum_{l\in\mathfrak{R}_k\setminus\{0,k\}} kl^2(k-l)e^{\mu_{k-l}t'}\int_0^{t'} dr\, e^{-\mu_{k-l}r}\Pi_{k,k}(t,r)\Pi_{l,l}(t',r)\\ &= -16\pi^4 \sum_{l\in\mathfrak{R}_k\setminus\{0,k\}} \frac{kl^2(k-l)}{4\mu_k\mu_l}\frac{1}{2\mu_k(\mu_l+\mu_k+\mu_{k-l})} \qquad \text{for } k\neq 0 \text{ and } t\gg 1,\end{aligned} \tag{5.89}$$

where we changed summation index $m\to l$. Thus, with the results from (5.82), (5.86), (5.87) and (5.89), the expectation value of (5.16) reads in the long-time asymptotics

$$\left\langle(\Psi_g(t))^2\right\rangle \simeq g_0^2\left[1-2(2\pi^2)^2\lambda_{\text{eff}}^2\sum_{l\in\mathfrak{R}\setminus\{0\}}\frac{l^4}{4\,\mu_l^3}\right]t + g_0^2\lambda_{\text{eff}}^2\sum_{k\in\mathfrak{R}}\left|\left\langle h_k^{(1)}(t)\right\rangle\right|^2 + O(\lambda_{\text{eff}}^4). \tag{5.90}$$

Appendix 5.B Expectation of the Total Entropy Production

The Fokker-Planck equation for the KPZ equation from (3.10) reads, like in Section 5.2.4,

$$\partial_t p[h] = -\int_0^1 dx\, \frac{\delta}{\delta h}\left[\left(\partial_x^2 h + \frac{\lambda_{\text{eff}}}{2}\left(\partial_x h\right)^2\right) p[h] - \frac{1}{2}\frac{\delta p[h]}{\delta h}\right]. \tag{5.91}$$

Due to the conservation of probability, there is a current $j_p[h]$ given by

$$\begin{aligned} j_p[h] &= \left(\partial_x^2 h + \frac{\lambda_{\text{eff}}}{2}\left(\partial_x h\right)^2\right) p[h] - \frac{1}{2}\frac{\delta p[h]}{\delta h} \\ &= \left(\partial_x^2 h + \frac{\lambda_{\text{eff}}}{2}\left(\partial_x h\right)^2\right) p[h] - \frac{1}{2}\frac{\delta \ln p[h]}{\delta h} p[h] \\ &= \left[\left(\partial_x^2 h + \frac{\lambda_{\text{eff}}}{2}\left(\partial_x h\right)^2\right) - \frac{1}{2}\frac{\delta \ln p[h]}{\delta h}\right] p[h] \qquad (5.92) \\ &\equiv v[h]p[h]. \qquad (5.93) \end{aligned}$$

Following [25], expectation values of expressions like $\left\langle \dot{h}\mathcal{G}[h]\right\rangle$ are interpreted as

$$\left\langle \dot{h}\mathcal{G}[h]\right\rangle = \langle v[h]\mathcal{G}[h]\rangle = \int \mathcal{D}[h]\, v[h]\mathcal{G}[h]p[h] \tag{5.94}$$

$$\Leftrightarrow \quad \left\langle \dot{h}\mathcal{G}[h]\right\rangle = \int \mathcal{D}[h]\, j[h]\mathcal{G}[h]. \tag{5.95}$$

Since the goal is to find an expression for the expectation value of the total entropy production in the stationary state, Δs_{tot}, it is sensible to choose $p[h]$ as being the stationary solution $p^s[h]$ of the one-dimensional Fokker-Planck equation, which is given by

$$p^s[h] \sim \exp\left[-\left\|\partial_x h\right\|_0^2\right]. \tag{5.96}$$

Inserting this in (5.92) yields for the stationary probability current

$$j_p^s[h] = \frac{\lambda_{\text{eff}}}{2}(\partial_x h)^2 p^s[h], \tag{5.97}$$

where it was used that

$$\frac{\delta p^s[h]}{\delta h} = 2p^s[h]\partial_x^2 h. \tag{5.98}$$

Using the result from (5.95) and (5.97) leads to

$$\left\langle \dot{h}\mathcal{G}[h]\right\rangle = \int \mathcal{D}[h]\, j_p^s[h]\mathcal{G}[h] = \frac{\lambda_{\text{eff}}}{2}\int \mathcal{D}[h]\,(\partial_x h)^2\mathcal{G}[h]p^s[h] = \frac{\lambda_{\text{eff}}}{2}\left\langle(\partial_x h)^2\mathcal{G}[h]\right\rangle. \tag{5.99}$$

Here it is understood that $\langle \cdot \rangle$ now denotes the expectation value with regard to the stationary distribution $p^s[h]$.
The total stationary entropy production Δs_{tot} is given by (see (5.37)),

$$\Delta s_{\text{tot}} = \lambda_{\text{eff}} \int_0^t dt' \int_0^1 dx\, \dot{h}(x,t')(\partial_x h(x,t'))^2. \tag{5.100}$$

Hence its expectation value reads,

$$\langle \Delta s_{\text{tot}} \rangle = \lambda_{\text{eff}} \int_0^t dt' \int_0^1 dx\, \left\langle \dot{h}(x,t')(\partial_x h(x,t'))^2 \right\rangle, \tag{5.101}$$

which is evaluated with the aid of (5.99),

$$\langle \Delta s_{\text{tot}} \rangle = \frac{\lambda_{\text{eff}}^2}{2} \int_0^t dt' \left\langle \left\| \left(\partial_x h(x,t')\right)^2 \right\|_0^2 \right\rangle. \tag{5.102}$$

Appendix 5.C Regularity Results for the One-Dimensional KPZ Equation

By means of an eigenfunction expansion and perturbation theory, we have constructed in the preceding sections a solution to the KPZ equation driven by the restriction of space-time white noise to the subspace spanned by the eigenfunctions with $|k| \leq \Lambda$ (see, e.g., (3.81)). In other words, Λ is the finite cutoff of the Fourier spectrum. Due to the poor regularity of the KPZ equation (see Appendix 3.A.5), we could not use our approximation to the KPZ solution as a spectral Galerkin scheme letting $\Lambda \to \infty$, as this limit would have led to divergences. Instead, we chose a fixed Λ, arbitrarily large but finite, which is a common regularization method in physics [104]. From a mathematical point of view, in [49] a complete existence and regularity theory for the KPZ equation driven by space-time white noise has been developed (see also [105, 106] and for further reading on the so-called regularity structures introduced in [49] see [51]). In [49] it is shown that the solutions of the KPZ equation with mollified noise converge after a suitable renormalization to the solution of a renormalized KPZ equation with space-time white noise, when removing the regularization. It is due to this renormalization procedure (where a divergent quantity needs to be subtracted) and the poor regularity of the solution, that at present it is not obvious how the method developed in [49] can be of use for constructing a TUR.
On the other hand, considering the KPZ equation driven by spatially more regular noise, there is a plenty of applicable results available. In fact, dealing with the one-dimensional KPZ equation allows us to make use of the equivalence to the stochastic Burgers equation (see Section 3.1.1) and adapt the regularity results for the latter from [84, 86, 87, 107, 108]. In Appendix 3.A.5, we found that our operators $\hat{L}$ and $\hat{K}$ share the

same set of eigenfunctions, which simplifies the results obtained by the authors of [86,87] to the following. Under the assumption that

$$\sum_{k\in\mathbb{N}} k^{2\rho-2}(\alpha_k^{\mathrm{B}})^2 < \infty \qquad \text{for some } \rho > 0, \tag{5.103}$$

it is guaranteed almost surely that the mild solution $u(x,t)$ of the one-dimensional noisy Burgers equation $u \in \mathcal{C}([0,T],H)$, $T > 0$, with $H = \mathcal{L}_2([0,1])$ and the spectral Galerkin approximation converges in H to the solution u. Utilizing the mapping from KPZ to Burgers via $u(x,t) \equiv -\partial_x h(x,t)$, with h solution to the KPZ equation, which implies

$$\eta^{\mathrm{B}}(x,t) = -\partial_x \eta^{\mathrm{KPZ}}(x,t), \tag{5.104}$$

and therefore,

$$\alpha_k^{\mathrm{B}} \sim k\, \alpha_k^{\mathrm{KPZ}}, \tag{5.105}$$

we get the following result for the 1d-KPZ equation,

$$\sum_{k\in\mathbb{N}} k^{\chi}(\alpha_k^{\mathrm{KPZ}})^2 < \infty \quad (\chi = 2\rho > 0) \qquad \Rightarrow \qquad h \in \mathcal{C}\left([0,T], H^1([0,1])\right). \tag{5.106}$$

Here $H^1([0,1])$ denotes the Sobolev space of order one on $[0,1]$, i.e. $f \in H^1([0,1]) \Leftrightarrow \|f\|_{\mathcal{L}_2([0,1])} < \infty$ and $\|f'\|_{\mathcal{L}_2([0,1])} < \infty$, where f' is understood as the weak derivative of f (see also Appendix 3.A.5).
Note, that the condition on the Fourier coefficients of the noise from (5.106) is trivially fulfilled by setting $\alpha_k^{\mathrm{KPZ}} = 1$, $k \leq \Lambda$ and $\alpha_k^{\mathrm{KPZ}} = 0$, otherwise.

6 Thermodynamic Uncertainty Relation for the 1D-KPZ Equation – Dynamic Renormalization Group Results

To derive an expression for the variance of $\Psi(t)$ that is valid for $\lambda_{\mathrm{eff}} > \lambda_{\mathrm{eff}}^{\mathrm{c}}$ the perturbative approach from Chapter 5 is no longer feasible. We thus employ dynamic renormalization group (DRG) theory, which allows for values of $\lambda_{\mathrm{eff}} > \lambda_{\mathrm{eff}}^{\mathrm{c}}$. As it turns out, the analysis via DRG of the KPZ equation itself proofs to be more cumbersome than the analysis of the equivalent Burgers equation driven by KPZ noise. Hence, in the following we present the derivation of an explicit expression for $\mathrm{var}[\Psi(t)]$ based on the well known DRG approach to the one-dimensional stochastic Burgers equation.

6.1 The 1D-KPZ-Burgers Equation and var$[\Psi(t)]$

We use the equivalence of the $1d$ KPZ equation to the stochastic Burgers equation (see Section 3.1.1), given by the transformation $u(x,t) = -\partial_x h(x,t)$, with $u(x,t)$ the velocity field of the Burgers equation

$$\partial_t u(x,t) + \frac{\lambda}{2}\partial_x u^2(x,t) = \nu \partial_x^2 u(x,t) + f(x,t), \tag{6.1}$$

where $f(x,t) = -\partial_x \eta(x,t)$. In terms of the Burgers velocity field $u(x,t)$ the expression for $\dot{\Psi}(t)$ from (5.55) reads

$$\dot{\Psi}(t) = \frac{\lambda}{2}\int_0^b dx\, u^2(x,t) + \int_0^b dx\, \eta(x,t). \tag{6.2}$$

In principle, the derivation of the expression for the variance of $\Psi(t)$ is analogous to the one shown in Chapter 5. However, here we will use the continuous Fourier transform instead of the discrete Fourier series as above, since a continuous wavenumber spectrum is needed for implementing the DRG scheme. In particular, we define

$$u(q,\omega) = \int dx \int dt\, u(x,t)\, e^{-i(qx-\omega t)}, \quad u(x,t) = \int \frac{dq}{2\pi}\int \frac{d\omega}{2\pi}\, u(q,\omega)\, e^{i(qx-\omega t)}, \tag{6.3}$$

as the forward and backward Fourier transform of the velocity field $u(x,t)$, respectively. To apply (6.3) to (6.2), we use the b-periodicity of $u(x,t)$ due to the periodic boundary conditions in (3.3). In particular we have

$$\begin{aligned}\int_0^b dx\, u^2(x,t) &= \int_{-b/2}^{b/2} dx\, u^2(x,t) \\ &\approx \int_{-\infty}^{\infty} dx\, u^2(x,t) = \frac{1}{2\,\pi}\int_{-\infty}^{\infty} dq\, u(q,t)\, u(-q,t),\end{aligned} \tag{6.4}$$

where the second step holds for $b \gg 1$ and in the last step we used the partial Fourier transform (6.3) in the spatial variable x. We thus obtain

$$\langle \Psi(t)\rangle \approx \frac{\lambda}{2}\int_0^t dt' \int \frac{dq}{2\pi}\left\langle u(q,t')\, u(-q,t')\right\rangle, \tag{6.5}$$

$$\begin{aligned}\left\langle \Psi^2(t)\right\rangle \approx \langle \Psi(t)\rangle^2 + \Delta_0\, b\, t + \frac{\lambda^2}{4}\int_0^t dt' \int_0^t dt'' \int \frac{dq}{2\pi}\int \frac{dq'}{2\pi} \\ \times \left[\left\langle u(q,t')u(q',t'')\right\rangle \left\langle u(-q,t')u(-q',t'')\right\rangle \right. \\ \left. + \left\langle u(q,t')u(-q',t'')\right\rangle \left\langle u(-q,t')u(q',t'')\right\rangle\right],\end{aligned} \tag{6.6}$$

and therefore, similar to (5.54),

$$\begin{aligned}\mathrm{var}[\Psi(t)] \approx \Delta_0\, b\, t + \frac{\lambda^2}{4}\int_0^t dt' \int_0^t dt'' \int \frac{dq}{2\pi}\int \frac{dq'}{2\pi} \\ \times \left[\left\langle u(q,t')u(q',t'')\right\rangle \left\langle u(-q,t')u(-q',t'')\right\rangle \right. \\ \left. + \left\langle u(q,t')u(-q',t'')\right\rangle \left\langle u(-q,t')u(q',t'')\right\rangle\right].\end{aligned} \tag{6.7}$$

The expressions in (6.6) and (6.7) again rely on the quasi-normality hypothesis [62, 101].

6.2 Two-Point Correlation Function via DRG

Instead of calculating the two-point correlation functions in (6.7) perturbatively as in Chapter 5, we here use the DRG method described in e.g. [43, 109], where we have noise correlations corresponding to Gaussian white noise for the KPZ equation, i.e.,

$$\left\langle f(q,\omega) f(q',\omega')\right\rangle = -(2\pi)^2\, \Delta_0\, q\, q'\, \delta(q+q')\, \delta(\omega+\omega'), \tag{6.8}$$

($y = -2$ in [43, 109]). The starting point of the DRG procedure is the Fourier-space representation of (6.1), namely

$$u(q,\omega) = G_0(q,\omega) f(q,\omega) - iq\frac{\lambda}{2} G_0(q,\omega)\int \frac{dq'}{2\pi}\int \frac{d\omega'}{2\pi} u(q',\omega') u(q-q',\omega-\omega'), \tag{6.9}$$

where we define the bare propagator

$$G_0(q,\omega) \equiv \frac{1}{-i\,\omega + \nu\, q^2}. \tag{6.10}$$

The next step will be to split the velocity field in (6.9) into large-wavenumber modes, $u^>$, and small-wavenumber modes, $u^<$, where it holds that (see e.g. [43, 101])

$$u(q,\omega) = \begin{cases} u^<(q,\omega) & \text{for} \quad 0 < q < \Lambda_0\, e^{-l}, \\ u^>(q,\omega) & \text{for} \quad \Lambda_0\, e^{-l} < q < \Lambda_0, \end{cases} \tag{6.11}$$

with l the renormalization parameter and Λ_0 an ultraviolet wavenumber cutoff. An analogous splitting applies to the noise $f(q,\omega)$ as well. Averaging the ensuing equations with respect to the noise history of the $f^>$-modes and integrating out the contributions of the large-wavenumber modes $u^>$ yields corrections to the terms of the small-wavenumber modes $u^<$. As these steps are well known and explained in detail in e.g. [43, 101], we will simply state the results, which are the renormalization equations for ν and Δ_0,

$$\nu_{\mathrm{R}} = \nu \left[1 + \frac{\lambda^2\,\Delta_0}{8\pi\,\nu^3}\frac{e^l - 1}{\Lambda_0}\right], \tag{6.12}$$

$$\Delta_{0,\mathrm{R}} = \Delta_0 \left[1 + \frac{\lambda^2\,\Delta_0}{8\pi\,\nu^3}\frac{e^l - 1}{\Lambda_0}\right], \tag{6.13}$$

obtained after one elimination step. This mode elimination process is iterated using infinitesimally small wavenumber increments ($l \to dl$) which causes parameter changes $d\nu$ and $d\Delta_0$. One thus arrives at differential equations for $\nu(l)$ and $\Delta_0(l)$, given respectively by

$$\frac{\mathrm{d}\,\nu(l)}{\mathrm{d}l} = \nu(l)\,\frac{\overline{\lambda}^2}{8\,\pi}, \tag{6.14}$$

$$\frac{\mathrm{d}\,\Delta_0(l)}{\mathrm{d}l} = \Delta_0(l)\,\frac{\overline{\lambda}^2}{8\,\pi}, \tag{6.15}$$

where

$$\overline{\lambda} \equiv \lambda \left(\frac{\Delta_0(l)}{\nu^3(l)\Lambda'(l)}\right)^{1/2}, \tag{6.16}$$

with $\Lambda'(l) \equiv \Lambda_0 e^{-l}$ (see e.g. [109]). $\overline{\lambda}(l)$ denotes the renormalized coupling constant characteristic for the eliminated modes. Up to a constant numerical prefactor, $\overline{\lambda}(0)$ equals λ_{eff} from (3.13). At this point we adopt a DRG scheme introduced in [110, 111] and analyzed in [112], which has been recently applied in [113, 114]. It implies that the next step of the scheme consists in solving (6.14) and (6.15) for ν and Δ_0 explicitly, making their scale dependence transparent. It follows directly that,

$$\frac{\Delta_0(l)}{\nu(l)} = \frac{\Delta_0}{\nu} = \text{const.} \quad \forall\, l > 0\,, \tag{6.17}$$

with ν, Δ_0 and Λ_0 the unrenormalized parameters from (6.1) and (6.8). The finding in (6.17) reflects the fluctuation-dissipation theorem, known to hold for the $1d$ Burgers-KPZ system (see e.g. [20, 43, 54]). Using (6.16) and (6.17), the integration of (6.14) yields

$$\nu(l) = \nu \left(1 + \frac{\lambda^2 \Delta_0}{4\pi\nu^3} \frac{e^l - 1}{\Lambda_0}\right)^{1/2}. \tag{6.18}$$

As a last step we make the common identification $|q| = \Lambda_0 e^{-l}$ (see e.g. [43,101,109–111, 113,114]) and obtain asymptotically for large values of l (i.e., $|q| \ll 1$)

$$\nu(q) \simeq \frac{\lambda}{2\sqrt{\pi}} \left(\frac{\Delta_0}{\nu}\right)^{1/2} |q|^{-1/2}, \tag{6.19}$$

$$\Delta_0(q) = \frac{\Delta_0}{\nu}\,\nu(q) \simeq \frac{\lambda}{2\sqrt{\pi}} \left(\frac{\Delta_0}{\nu}\right)^{3/2} |q|^{-1/2}. \tag{6.20}$$

Equivalently, $\bar{\lambda}(l)$ converges for $l \to \infty$ (i.e. after all large wavenumber modes are eliminated) to a finite stable fixed point, the KPZ fixed point of the RG-flow. This fixed point is associated with the dynamical scaling exponent $z = 3/2$.
According to [109], the expressions from (6.19) and (6.20) allow for the introduction of a renormalized effective propagator

$$G(q,\omega) = \frac{1}{-i\,\omega + \nu(q)\,q^2}, \tag{6.21}$$

and a renormalized effective noise with

$$\big\langle f(q,\omega)\, f(q',\omega')\big\rangle = (2\pi)^2\, \Delta_0(q)\, q^2\, \delta(q+q')\, \delta(\omega+\omega'), \tag{6.22}$$

such that the nonlinear equation from (6.9) may be replaced by an effective linear Langevin equation

$$u(q,\omega) \simeq G(q,\omega)\, f(q,\omega). \tag{6.23}$$

Note, that in (6.23), as opposed to (6.9), the right hand side now depends on $\nu(q)$ and $\Delta_0(q)$ from (6.19) and (6.20), respectively. A justification of this step is given in [109–112] via the so-called ε-expansion. In the present case, a further justification may be given by the fact that for large times the fluctuations of $h(x,t)$ become Gaussian distributed. This indicates that their dynamics may be described by a linear Langevin equation as in (6.23). An analogous conclusion has been drawn for a slightly different setting in [114]. Using (6.21) and (6.22), we give an explicit approximation for the two-point correlation $\langle u(q,\omega) u(q',\omega')\rangle$,

$$\begin{aligned}\big\langle u(q,\omega)\, u(q',\omega')\big\rangle &\simeq G(q,\omega)\, G(q',\omega')\, \big\langle f(q,\omega)\, f(q',\omega')\big\rangle \\ &= (2\pi)^2\, q^2\, \Delta_0(q)\, G(q,\omega)\, G(q',\omega')\, \delta(q+q')\, \delta(\omega+\omega') \\ &\equiv (2\pi)^2\, C(q,\omega)\, \delta(q+q')\, \delta(\omega+\omega').\end{aligned} \tag{6.24}$$

Here we have introduced the correlation function $C(q,\omega)$ (see e.g. [109]) according to

$$C(q,\omega) \equiv q^2\,\Delta_0(q)\,G(q,\omega)\,G(-q,-\omega) = q^2\,\Delta_0(q)\;|G(q,\omega)|^2\,, \tag{6.25}$$

with $\Delta_0(q)$ from (6.20) and $G(q,\omega)$ from (6.21). Inserting the explicit expressions from (6.19) and (6.20) into (6.25) we arrive at (see also [109] for $\lambda = 1$)

$$C(q,\omega) \approx \left(\frac{\Delta_0}{\nu}\right)^{1/2} \frac{2\pi^{1/2}}{\lambda}\,\frac{|q|^{-3/2}}{1+\left(\left(\frac{\nu}{\Delta_0}\right)^{1/2}\frac{2\pi^{1/2}}{\lambda}\,\frac{\omega}{|q|^{3/2}}\right)^2}. \tag{6.26}$$

Obviously, (6.26) is in accordance with the well known scaling result for the correlation function of the Burgers equation in one spatial dimension (see e.g. [43, 109]),

$$C(q,\omega) \sim |q|^{-3/2}\Phi\left(\frac{\omega}{|q|^{3/2}}\right), \tag{6.27}$$

with Φ as a universal scaling function.

6.3 DRG Results for var$[\Psi(t)]$

Performing a Fourier backward transformation in frequency on both sides of (6.24) and inserting for $C(q,\omega)$ the expression from (6.26) leads to

$$\begin{aligned}\big\langle u(q,t)\,u(q',t')\big\rangle &= 2\pi\,C(q,t-t')\,\delta(q+q') \\ &\approx 2\pi\,\frac{\Delta_0}{2\,\nu}\,\exp\left[-\left(\frac{\Delta_0}{2\,\nu}\right)^{1/2}\frac{\lambda}{(2\pi)^{1/2}}\,|q|^{3/2}\,|t-t'|\right]\,\delta(q+q'),\end{aligned} \tag{6.28}$$

as the approximate two-point correlation of $u = -\partial_x h$ in wavenumber space. With (6.28) we now have the necessary means to calculate the product of two-point correlation functions in (6.7). In particular,

$$\begin{aligned}&\int\frac{dq}{2\pi}\int\frac{dq'}{2\pi}\,\langle u(q,t')\,u(q',t'')\rangle\,\langle u(-q,t')\,u(-q',t'')\rangle \\ &= \int dq\int dq'\,C(q,t'-t'')\,C(-q',t'-t'')\,\delta(q+q')\,\delta(-q-q') \\ &= \int dk\int dk'\,C\left(\frac{2\pi}{b}\,k,t'-t''\right)\,C\left(-\frac{2\pi}{b}\,k',t'-t''\right)\,\delta(k+k') \\ &= \frac{b}{4\pi}\,\left(\frac{\Delta_0}{\nu}\right)^{5/3}\frac{\Gamma(5/3)\,\pi^{1/3}}{\lambda^{2/3}}\,\frac{1}{|t'-t''|^{2/3}},\end{aligned} \tag{6.29}$$

where we substituted in the second step $q = 2\pi k/b$ to attribute for the fact that we operate on a finite system-size, $x \in [0, b]$, which implies an explicit length scale, and Γ is the Euler-Gamma function. Analogously, the second term in (6.7) becomes

$$\begin{aligned} &\int \frac{dq}{2\pi} \int \frac{dq'}{2\pi} \left\langle u(q,t')\, u(-q',t'') \right\rangle \left\langle u(-q,t')\, u(q',t'') \right\rangle \\ &= \frac{b}{4\pi} \left(\frac{\Delta_0}{\nu}\right)^{5/3} \frac{\Gamma(5/3)\, \pi^{1/3}}{\lambda^{2/3}} \frac{1}{|t'-t''|^{2/3}}. \end{aligned} \tag{6.30}$$

Inserting (6.29) and (6.30) into (6.7) yields

$$\begin{aligned} \mathrm{var}[\Psi(t)] &\approx \Delta_0\, b\, t + \frac{\Gamma(5/3)}{8\,\pi^{2/3}}\, b\, \frac{\lambda^{4/3}\,\Delta_0^{5/3}}{\nu^{5/3}} \int_0^t dt' \int_0^t dt''\, |t'-t''|^{-2/3} \\ &= \Delta_0\, b\, t + \frac{3\,\Gamma(2/3)}{8\,\pi^{2/3}}\, b\, \lambda^{4/3} \left(\frac{\Delta_0}{\nu}\right)^{5/3} t^{4/3}. \end{aligned} \tag{6.31}$$

Therefore in the long-time limit,

$$\mathrm{var}[\Psi(t)] \simeq \frac{3\,\Gamma(2/3)}{8\,\pi^{2/3}}\, b\, \lambda^{4/3} \left(\frac{\Delta_0}{\nu}\right)^{5/3} t^{4/3}, \tag{6.32}$$

which indicates superdiffusive behavior for the variance of $\Psi(t)$. This expression is in accordance with the scaling form predicted in [20] for the transient KPZ regime (see also (3.47)). Moreover, the present DRG approach yields the explicit amplitude factors as well. We use (6.32) in the time range $t^{\mathrm{EW}\to\mathrm{KPZ}} < t < t_{\mathrm{c}}^{\mathrm{KPZ}}$ (see (3.42), (3.44)) and check in the following for consistency with known results at the endpoints of this time interval. For times $t \geq t_{\mathrm{c}}^{\mathrm{KPZ}}$, the variance of $\Psi(t)$ behaves as $\mathrm{var}[\Psi(t)] = \mathcal{C}\, t$ (see Figure 3.2), with $\mathcal{C}$ a parameter to be determined. Hence, we have the matching condition

$$\mathrm{var}[\Psi(t_{\mathrm{c}}^{\mathrm{KPZ}})] \simeq \frac{3\,\Gamma(2/3)}{8\,\pi^{2/3}}\, b\, \lambda^{4/3} \left(\frac{\Delta_0}{\nu}\right)^{5/3} (t_{\mathrm{c}}^{\mathrm{KPZ}})^{4/3} \stackrel{!}{=} \mathcal{C}\, t_{\mathrm{c}}^{\mathrm{KPZ}}. \tag{6.33}$$

Inserting $t_{\mathrm{c}}^{\mathrm{KPZ}}$ from (3.44) into (6.33) and solving for $\mathcal{C}$ yields (with $c_2 \approx 0.4$, see, e.g., Section 3.2.2)

$$\mathcal{C} = \frac{\Gamma(2/3)}{(128\,\pi^2)^{1/3}} \sqrt{\frac{3}{c_2}} \left(\frac{\Delta_0}{2\,\nu}\right)^{3/2} \lambda\, b^{3/2} \approx 0.34 \left(\frac{\Delta_0}{2\,\nu}\right)^{3/2} \lambda\, b^{3/2}. \tag{6.34}$$

This expression may be compared with a result in [20] for the center of mass dispersion $W_c^2 = \left\langle \left(\overline{h} - \langle \overline{h} \rangle\right)^2 \right\rangle$, with $\overline{h} = \int_0^b dx\, h(x,t)/b$ the spatial mean, which is related via $\mathrm{var}[\Psi(t)] = b^2\, W_c^2$ to the variance of our observable $\Psi(t)$. The center of mass dispersion is given by

$$W_c^2 = c_0 \left(\frac{\Delta_0}{2\,\nu}\right)^{3/2} \lambda\, b^{-1/2}\, t, \tag{6.35}$$

with c_0 a universal scaling amplitude. Apart from the prefactor c_0 the result in (6.34) is the same as the one in (6.35), in particular with respect to the anomalous scaling in b. Regarding c_0, this was determined in [115] for the ASEP-process and then adopted in [20] relying on the universality hypothesis. The exact value of c_0 reads

$$c_0 = \frac{\sqrt{\pi}}{4} \approx 0.44. \tag{6.36}$$

We thus deviate from the exact result for c_0 by roughly 20%, which we regard satisfactory for our consistency check. Moreover we note that our numerical simulations in Chapter 7 indicate a correlation time that differs from the one in (3.44) by roughly a factor of 2 (see Section 7.4.3). Reiterating the steps from (6.33) and (6.34) with the numerically obtained correlation time (see (7.39)), leads to a significant improvement of our result for the universal amplitude c_0 (see (7.40)).
At the left endpoint of the transient KPZ regime, i.e., at $t = t^{\mathrm{EW}\to\mathrm{KPZ}}$, consistency may be checked by comparing (6.32) with the perturbation expansion from (5.67) for $\lambda_{\mathrm{eff}} \approx \lambda_{\mathrm{eff}}^{\mathrm{c}}$. To be precise, we compute (6.32) at the crossover time (3.42) and compare this result to (5.67) evaluated at the critical coupling parameter $\lambda_{\mathrm{eff}}^{\mathrm{c}}$. This makes sense, since on the one hand we know that $t_{\mathrm{c}}^{\mathrm{KPZ}} \gtrapprox t^{\mathrm{EW}\to\mathrm{KPZ}}$ provided that $\lambda_{\mathrm{eff}} \gtrapprox \lambda_{\mathrm{eff}}^{\mathrm{c}}$, which implies that var[$\Psi(t)$] shows transient behavior for $t \gtrapprox t^{\mathrm{EW}\to\mathrm{KPZ}}$. On the other hand the expansion from (5.67) is expected to be valid for $\lambda_{\mathrm{eff}} \lessapprox \lambda_{\mathrm{eff}}^{\mathrm{c}}$. Therefore, at $\lambda_{\mathrm{eff}} \approx \lambda_{\mathrm{eff}}^{\mathrm{c}}$ the expression for the transient KPZ variance of $\Psi(t)$ from (6.32) should match with the perturbative result from (5.67) at the EW to KPZ crossover time $t^{\mathrm{EW}\to\mathrm{KPZ}}$. With (6.32) and (3.42) we get ($c_2 \approx 0.4$)

$$\begin{aligned}
\mathrm{var}[\Psi(t^{\mathrm{EW}\to\mathrm{KPZ}})] &\simeq \frac{3\,\Gamma(2/3)}{8\,\pi^{2/3}}\, b\,\lambda^{4/3} \left(\frac{\Delta_0}{\nu}\right)^{5/3} (t^{\mathrm{EW}\to\mathrm{KPZ}})^{4/3} \\
&= \frac{\Gamma(2/3)}{(16\,\pi^5)^{1/3}}\,\frac{3}{c_2^2}\,\Delta_0\, b\, t^{\mathrm{EW}\to\mathrm{KPZ}} \\
&\approx 1.50\,\Delta_0\, b\, t^{\mathrm{EW}\to\mathrm{KPZ}},
\end{aligned} \tag{6.37}$$

whereas evaluating (5.67) at $\lambda_{\mathrm{eff}} = \lambda_{\mathrm{eff}}^{\mathrm{c}} \approx 12.3$ ($c_2 \approx 0.4$) from (3.51) results in

$$\mathrm{var}[\Psi(t^{\mathrm{EW}\to\mathrm{KPZ}})] \approx 1.57\,\Delta_0\, b\, t^{\mathrm{EW}\to\mathrm{KPZ}}. \tag{6.38}$$

Hence, the respective results differ by just 5%. Taking into consideration that both results in (5.67) and (6.32) are approximations, this seems to be a reasonable match.
To sum up, this section was devoted to the derivation of an analytical expression approximating var[$\Psi(t)$] in the transient and steady state KPZ regime, respectively. Whereas the result for the latter is essentially known from [20], there seems to be no comparable explicit result for the former in the KPZ literature. In the context of driven diffusive systems a similar result has been derived via mode-coupling theory in [39]. Let us stress,

that all amplitude factors are determined by analytic calculations for a generic KPZ system, i.e., without invoking specific model problems of the KPZ universality class. Furthermore, our approximation from (6.28) for the two-point correlation of $u = -\partial_x h$ in wavenumber space may be of some interest in itself. This is since the exact scaling function found in [60] for the $1d$ KPZ equation is given via the solution of certain differential equations (Painlevé II), which can be solved only by quite involved numerical methods. Especially, an exact analytic expression seems to be out of reach. A qualitative comparison of $\hat{g}(k) \equiv C(k,t)/C(0,t)$, with $C(k,t)$ from (6.28) to $\hat{f}(k)$ from Fig. 4 in [60] shows an altogether quite satisfying agreement.
To be more precise, for small k $(0 < k \lessapprox 2)$ the approximate scaling function $\hat{g}(k)$ decays a little faster than $\hat{f}(k)$ (Fig. 4 in [60]). For $2 \lessapprox k \lessapprox 5$, $\hat{g}(k)$ tends to zero somewhat slower than $\hat{f}(k)$ in Fig. 4 in [60]. Both deviations are, however, rather small. One feature that $\hat{g}(k)$ is missing is the oscillatory manner in which $\hat{f}(k)$ decays to zero; $\hat{g}(k)$ decays monotonously. This lacking of $\hat{g}(k)$ does not seem to be of practical importance for our purposes as the oscillations of $\hat{f}(k)$ are rapidly damped with growing k.

6.4 Thermodynamic Uncertainty Relation

Before we formulate the TUR for an arbitrary value of the coupling parameter, let us collect what we have so far derived for the variance of $\Psi(t)$. Consider first the parameter regime where $\lambda_{\text{eff}} < \lambda_{\text{eff}}^{\text{c}}$. Here we know from (5.66) that for times $t > t_{\text{c}}^{\text{EW}}$

$$\text{var}[\Psi(t)] \simeq \Delta_0\, b\, t \left[1 + \frac{\lambda_{\text{eff}}^2}{16\pi^2}\,\zeta(2) - \frac{\lambda_{\text{eff}}^4}{256\pi^4}\,(1.814\,\zeta(3) - \zeta(4)) + O(\lambda_{\text{eff}}^6)\right], \tag{6.39}$$

whereas for $t \ll t_{\text{c}}^{\text{EW}}$, $\text{var}[\Psi(t)] \simeq \Delta_0\, b\, t$ holds.
On the other hand for a parameter set with $\lambda_{\text{eff}} \gg \lambda_{\text{eff}}^{\text{c}}$ we have shown in (6.31) that

$$\text{var}[\Psi(t)] \simeq \begin{cases} \Delta_0\, b\, t\,, & t \ll t^{\text{EW}\to\text{KPZ}}, \\ \frac{3\,\Gamma(2/3)}{8\,\pi^{2/3}}\, b\, \lambda^{4/3} \left(\frac{\Delta_0}{\nu}\right)^{5/3} t^{4/3}\,, & t^{\text{EW}\to\text{KPZ}} \lessapprox t \lessapprox t_{\text{c}}^{\text{KPZ}}, \\ \frac{\sqrt{\pi}}{4} \left(\frac{\Delta_0}{2\,\nu}\right)^{3/2} \lambda\, b^{3/2}\, t\,, & t_{\text{c}}^{\text{KPZ}} \ll t, \end{cases} \tag{6.40}$$

where, for $t_{\text{c}}^{\text{KPZ}} \ll t$, the exact numerical value of $\sqrt{\pi}/4$ for the universal amplitude c_0 has been chosen [20]. The behavior for $t \ll t^{\text{EW}\to\text{KPZ}}$ may be obtained in various ways. For one, we could take the short-time limit of (6.31). Alternatively, we know from the scaling arguments presented in Figure 3.2 that for these times the system is governed by the EW-scaling regime, which implies normal diffusive behavior according to the EW equation.

Hence, with the exact results in Section 5.4 (see (5.77)) and the approximations for the variance we can formulate the TUR product $\mathcal{Q}$ in the long-time limit as

$$\mathcal{Q} \simeq \left(5 - \frac{1}{\Lambda}\right) \begin{cases} \left(1 + \frac{\lambda_{\text{eff}}^2}{32\pi^2}\, \mathcal{S}_1(\Lambda) - \frac{\lambda_{\text{eff}}^4}{256\pi^4}\, \mathcal{S}_2(\Lambda) + O(\lambda_{\text{eff}}^6)\right), & \text{for } \lambda_{\text{eff}} \lessapprox \lambda_{\text{eff}}^{\text{c}}, \\ \frac{\sqrt{\pi}}{8\sqrt{2}}\, \lambda_{\text{eff}}, & \text{for } \lambda_{\text{eff}}^{\text{c}} \ll \lambda_{\text{eff}}. \end{cases} \tag{6.41}$$

Here we state the Λ-dependent result from (5.59) in anticipation of the comparison to numerical simulations for a fixed system-size, which also implies a fixed value of Λ.

Appendix 6.A Weight-Function Independent Precision

To show that the precision ϵ^2 is independent of the choice of the weight function $g(x)$ in the limit of large times with $g(x) \in \mathcal{L}^2(0,1)$ and $\int_0^1 dx\, g(x) \neq 0$ we argue as follows. We begin with the expectation value of $\Psi_g(t) = \int_0^1 dx\, g(x)\, h(x,t)$, given by

$$\langle \Psi_g(t) \rangle = \sum_{|k|\leq\Lambda} \langle \overline{g}_k\, h_k(t) \rangle = g_0\, \langle h_0(t) \rangle + \sum_{k\neq 0} \overline{g}_k\, \langle h_k(t) \rangle = g_0\, \langle \Psi(t) \rangle + \sum_{k\neq 0} \overline{g}_k\, \langle h_k(t) \rangle\,, \tag{6.42}$$

where g_k and $h_k(t)$ are the Fourier coefficients of the respective Fourier series $g(x) = \sum_{|k|\leq\Lambda} g_k\, e^{2\pi i k x}$ and $h(x,t) = \sum_{|k|\leq\Lambda} h_k(t)\, e^{2\pi i k x}$, and $\overline{g}_k$ denotes the complex conjugate. Squaring (6.42) thus leads to

$$\langle \Psi_g(t) \rangle^2 = g_0^2\, \langle \Psi(t) \rangle^2 + \mathcal{T}_1 + \mathcal{T}_2, \tag{6.43}$$

with $\mathcal{T}_1 = 2 g_0\, \langle \Psi(t) \rangle \sum_{k\neq 0} \overline{g}_k\, \langle h_k(t) \rangle$ and $\mathcal{T}_2 = \sum_{k,l\neq 0} \overline{g}_k \overline{g}_l\, \langle h_k(t) \rangle\, \langle h_l(t) \rangle$. Similarly, we get for the expectation value of $\Psi_g^2(t)$

$$\begin{aligned} \left\langle \Psi_g^2(t) \right\rangle &= \sum_{|k|,|l|\leq\Lambda} \overline{g}_k \overline{g}_l\, \langle h_k(t) h_l(t) \rangle \\ &= \sum_{|k|\leq\Lambda} |g_k|^2\, \langle h_k(t) h_{-k}(t) \rangle \\ &= g_0^2 \left\langle \Psi^2(t) \right\rangle + \mathcal{T}_3, \end{aligned} \tag{6.44}$$

where $\mathcal{T}_3 = \sum_{k\neq 0} |g_k|^2\, \langle h_k(t) h_{-k}(t) \rangle$. In the second step we used the periodic boundary conditions and the therefore ensuing translational invariance, which implies that $\langle h_k(t) h_l(t) \rangle \sim \delta_{k,-l}$. Hence, the variance of $\Psi_g(t)$ reads

$$\text{var}[\Psi_g(t)] = \left\langle \Psi_g^2(t) \right\rangle - \langle \Psi_g(t) \rangle^2 = g_0^2 \text{var}[\Psi(t)] + \mathcal{T}_3 - \mathcal{T}_1 - \mathcal{T}_2. \tag{6.45}$$

Evaluating (6.45) divided by time t in the limit of large times leads to

$$\begin{aligned}\lim_{t\to\infty}\frac{\mathrm{var}[\Psi_g(t)]}{t} &= g_0^2\lim_{t\to\infty}\frac{\mathrm{var}[\Psi(t)]}{t}+\lim_{t\to\infty}\frac{\mathcal{T}_3-\mathcal{T}_1-\mathcal{T}_2}{t}\\ &= g_0^2\,\mathcal{V}_{\mathrm{EW,KPZ}}+\lim_{t\to\infty}\frac{\mathcal{T}_3-\mathcal{T}_1-\mathcal{T}_2}{t},\end{aligned} \tag{6.46}$$

where $\mathcal{V}_{\mathrm{EW,KPZ}}$ denotes the linear and non-linear constant of $\mathrm{var}[\Psi(t)]=\mathcal{V}_{\mathrm{EW,KPZ}}\,t$, respectively (see, e.g., Chapters 5 and 6 and [20]). We proceed with showing that the last limit in (6.46) is equal to zero. Therefore, we analyze $\lim_{t\to\infty}\mathcal{T}_3/t$ and use the inequalities

$$\begin{aligned}0\le\mathcal{T}_3 &= \sum_{k\neq0}|g_k|^2\left\langle h_k(t)h_{-k}(t)\right\rangle\\ &\le \max_{\substack{|k|\le\Lambda\\k\neq0}}|g_k|^2\sum_{k\neq0}\left\langle h_k(t)h_{-k}(t)\right\rangle\\ &= \max_{\substack{|k|\le\Lambda\\k\neq0}}|g_k|^2W^2(t),\end{aligned} \tag{6.47}$$

where $W^2(t)$ is the square of the surface width according to (3.18). Dividing (6.47) by $t>0$ and taking the limit of $t\to\infty$ results in

$$0\le\lim_{t\to\infty}\frac{\mathcal{T}_3}{t}\le\max_{\substack{|k|\le\Lambda\\k\neq0}}|g_k|^2\lim_{t\to\infty}\frac{W^2(t)}{t}, \tag{6.48}$$

It is well known that $\lim_{t\to\infty}W^2(t)=\text{const.}$ and thus $\lim_{t\to\infty}W^2(t)/t=0$ (see, e.g., Section 3.2.1). Hence, (6.48) yields that $\lim_{t\to\infty}\mathcal{T}_3/t=0$.
We further know from Section 5.4 that $\lim_{t\to\infty}\langle h_k(t)\rangle=\langle h_k(t)\rangle_{p^s[h]}=0$ for $k\neq0$, which implies straightforwardly that also $\lim_{t\to\infty}\mathcal{T}_{1,2}/t=0$, respectively[1]. Thus, (6.46) becomes

$$\mathrm{var}[\Psi_g(t)]=g_0^2\,\mathrm{var}[\Psi(t)]\qquad\text{for } t\to\infty, \tag{6.49}$$

and analogously in the limit of $t\to\infty$, (6.42) reads

$$\langle\Psi_g(t)\rangle=g_0\,\langle\Psi(t)\rangle\,. \tag{6.50}$$

Combining (6.49) and (6.50) yields for the precision

$$\epsilon_g^2=\frac{\mathrm{var}[\Psi_g(t)]}{\langle\Psi_g(t)\rangle^2}=\frac{g_0^2\mathrm{var}[\Psi(t)]}{g_0^2\,\langle\Psi(t)\rangle^2}=\epsilon^2\qquad\text{for } t\to\infty, \tag{6.51}$$

and thus the precision is in the long-time limit independent of the choice of the weight function $g(x)$.

[1] For determining $\lim_{t\to\infty}\mathcal{T}_1/t$ additionally (5.75) has been used.

7 Numerical Simulation of the 1D Kardar-Parisi-Zhang Equation

This chapter is devoted to the numerical simulation of the above derived theoretical results for the constituents of the TUR product and the TUR product itself. The comparison between the numerical and theoretical results is divided into two parts, one for the EW scaling regime and one for the KPZ scaling regime of the KPZ equation. Prior to that, we introduce the numerical scheme employed and further discuss and analyze analytically and numerically the delicate matter of the spatial discretization of the KPZ non-linearity. Especially, the impact of this discretization on the numerical results for the physical observables is highlighted.

7.1 Discretization of the 1D-KPZ Equation

We use a direct numerical integration technique to simulate the height $h(x,t)$ of the Kardar-Parisi-Zhang equation. There are various approaches regarding spatial and temporal discretization (see, e.g., [89, 104, 106, 116–122]). In the following we present the details and reasoning of our approach.

7.1.1 Spatial Discretization

We consider a one-dimensional grid with grid-points x_l subject to periodic boundary conditions with lattice-spacing δ given by

$$\delta = \frac{b}{L}, \tag{7.1}$$

where b is the fixed length of the grid and L is the number of grid-points. At each grid-point we have for a fixed time t the value of the height field $h_l(t) \equiv h(x_l,t) = h(l\delta,t)$, with $x_l = l\delta$ and $l = 0,\ldots,L-1$. The time evolution of $h_l(t)$ is then governed by (3.3), i.e.,

$$\partial_t h_l(t) = \nu\mathcal{L}_l(t) + \frac{\lambda}{2}\mathcal{N}_l(t) + \eta_l(t), \tag{7.2}$$

where $h_L(t) = h_0(t)$ due to the periodic boundary conditions. Furthermore, $\mathcal{L}_l$ and $\mathcal{N}_l$ denote the discretizations of the linear and nonlinear term at the grid-point x_l, respectively, and $\eta_l(t) \equiv \eta(x_l,t) = \eta(l\delta,t)$ represents the discretized noise. Regarding the diffusive term $\mathcal{L}_l$ in (7.2), we choose the standard discretization, namely the nearest-neighbor discrete Laplacian,

$$\mathcal{L}_l(t) = \mathcal{L}_l[\{h_j(t)\}] = \frac{1}{\delta^2}\left[h_{l+1}(t) - 2h_l(t) + h_{l-1}(t)\right], \tag{7.3}$$

see, e.g., [104, 116, 118, 121, 123]. The discretization of the nonlinear term $\mathcal{N}_l$ is more subtle. During the last few decades different discretizations of the nonlinear term have been proposed for numerically integrating the KPZ equation [116, 118, 121, 123]. In the case of one spatial dimension, they all belong to the family of so-called generalized discretizations [118],

$$\begin{aligned}\mathcal{N}_l(t) &\equiv \mathcal{N}_l^{(\gamma)}[\{h_j(t)\}] \\ &= \frac{1}{2(\gamma+1)\delta^2}\Big[\left(h_{l+1}(t) - h_l(t)\right)^2 + 2\gamma\left(h_{l+1}(t) - h_l(t)\right) \\ &\times \left(h_l(t) - h_{l-1}(t)\right) + \left(h_l(t) - h_{l-1}(t)\right)^2\Big],\end{aligned} \tag{7.4}$$

with $\gamma \in \mathbb{R}$ and $0 \leq \gamma \leq 1$. In the following, we will highlight the cases $\gamma = 0$, $\gamma = 1$ and $\gamma = 1/2$.
For $\gamma = 0$, this discretization reads

$$\mathcal{N}_l^{(0)}[\{h_j(t)\}] = \frac{1}{2}\left[\left(\frac{h_{l+1}(t) - h_l(t)}{\delta}\right)^2 + \left(\frac{h_l(t) - h_{l-1}(t)}{\delta}\right)^2\right], \tag{7.5}$$

which is simply the arithmetic mean of the forward and backward taken squared slope, respectively, of the height field at the grid-point x_l [118].
The case $\gamma = 1$ yields

$$\mathcal{N}_l^{(1)}[\{h_j(t)\}] = \left(\frac{h_{l+1}(t) - h_{l-1}(t)}{2\delta}\right)^2. \tag{7.6}$$

This is the square of the central difference discretization of $\partial_x h$, which is a commonly used choice for numerically integrating the KPZ equation, see, e.g., [116, 121].
Finally, $\gamma = 1/2$ leads to

$$\begin{aligned}\mathcal{N}_l^{(1/2)}[\{h_j(t)\}] = \frac{1}{3\delta^2}\Big[&\left(h_{l+1}(t) - h_l(t)\right)^2 + \left(h_{l+1}(t) - h_l(t)\right) \\ &\times \left(h_l(t) - h_{l-1}(t)\right) + \left(h_l(t) - h_{l-1}(t)\right)^2\Big].\end{aligned} \tag{7.7}$$

This form was applied to the KPZ equation in, e.g., [116, 117, 123]. It is closely related to the discretized non-linearity proposed in [104, 106, 120] of the 1d-Burgers equation equivalent to (7.2). Following [116], we will call (7.7) the improved discretization (ID), for the following reasons. It has been shown analytically in [116] using (7.7) that the discrete Fokker-Planck equation corresponding to (7.2) possesses a steady state probability distribution for all $\lambda > 0$, which is equal to the linear (Edwards-Wilkinson, $\lambda = 0$) steady state distribution. It was further shown that the stationary solution of the Fokker-Planck equation is reached for a non-vanishing conserved probability current, which indicates a genuine non-equilibrium steady state in the discretized system. This implies that the case $\gamma = 1/2$ accurately mimics the NESS-behavior of the continuous case, with the exact form of the total entropy production $\langle \Delta s_{\mathrm{tot}} \rangle$ from (5.38). The above mentioned properties of the operator $\mathcal{N}_l^{(1/2)}$ distinguish the case $\gamma = 1/2$ from, e.g., $\gamma = 1$, which does not fulfill the fluctuation-dissipation relation in $(1+1)$ dimensions that is essential for obtaining the discrete NESS probability distribution equivalent to the continuous case. Furthermore, the choice $\gamma = 1/2$ in (7.4) is the only one that displays the above behavior [118].

We note that for spatially smooth enough functions h, any discretization from (7.4) $(0 \leq \gamma \leq 1)$ has an approximation error $O(\delta^2)$. This implies that for sufficiently small δ the differences between their respective outcomes can be made arbitrarily small. However, the solution $h(x,t)$ of (3.3) is at every time t a very rough function in space (see also Appendices 3.A.5 and 5.C). The various discretizations in (7.4) thus lead to significantly different results, e.g., with respect to the surface width in [89, 116, 123] and in the present paper with respect to certain integral norms of the KPZ non-linearity being essential for the KPZ-TUR (see Appendix 7.A).

7.1.2 Temporal Discretization

Regarding the temporal discretization of (7.2), we choose the stochastic Heun method (see, e.g., [119,124]), as its predictor-corrector nature reflects the Stratonovich discretization used in Chapters 2 and 4. To be specific, the predictor step applies the forward Euler method to (7.2), which yields the predictor $y_l(t+\Delta t)$ according to

$$y_l(t+\Delta t) = h_l(t) + \Delta t \left[\nu \mathcal{L}_l[\{h_j(t)\}] + \frac{\lambda}{2} \mathcal{N}_l^{(\gamma)}[\{h_j(t)\}] \right] + \sqrt{\frac{\Delta_0 \Delta t}{\delta}}\, \xi_l(t). \tag{7.8}$$

Here, $l = 0, \dots, L-1$ like above and $\{\xi_l(t)\}$ are stochastically independent $N(0,1)$-distributed random variables (see, e.g., [119, 121, 124]). The prefactor in front of $\xi_l(t)$ ensures that the noise has the prescribed variance according to (3.3). The predictor from (7.8) is then used in the subsequent corrector step as

$$\begin{aligned} h_l(t+\Delta t) = h_l(t) + \frac{\Delta t}{2} \Big[&\nu \left(\mathcal{L}_l[\{h_j(t)\}] + \mathcal{L}_l[\{y_j(t+\Delta t)\}] \right) \\ &+ \frac{\lambda}{2} \left(\mathcal{N}_l^{(\gamma)}[\{h_j(t)\}] + \mathcal{N}_l^{(\gamma)}[\{y_j(t+\Delta t)\}] \right) \Big] + \sqrt{\frac{\Delta_0 \Delta t}{\delta}}\, \xi_l(t). \end{aligned} \tag{7.9}$$

The form in (7.9) displays the above mentioned Stratonovich time discretization. For the sake of simplicity, we start at $t = 0$ from a flat profile, in particular $h_l(0) = 0$, $l = 0, \dots, L-1$, and we impose periodic boundary conditions, i.e., $h_L(t) = h_0(t)$. We slightly reformulate the expressions in (7.8) and (7.9) by introducing a set of effective input parameters $\{\widetilde{\nu}, \widetilde{\Delta_0}, \widetilde{\lambda}\}$ given by

$$\widetilde{\nu} \equiv \frac{\nu}{\delta^2}, \qquad \widetilde{\Delta_0} \equiv \frac{\Delta_0}{\delta}, \qquad \text{and} \qquad \widetilde{\lambda} \equiv \frac{\lambda}{\delta^2}, \tag{7.10}$$

with δ from (7.1). Hence, the predictor-corrector Heun method reads

$$\begin{aligned} y_l(t+\Delta t) &= h_l(t) + \Delta t \left[\widetilde{\nu} \widetilde{\mathcal{L}}_l[\{h_j(t)\}] + \frac{\widetilde{\lambda}}{2} \widetilde{\mathcal{N}_l}^{(\gamma)}[\{h_j(t)\}] \right] + \sqrt{\widetilde{\Delta_0} \Delta t}\, \xi_l(t), \\ h_l(t+\Delta t) &= h_l(t) + \frac{\Delta t}{2} \Big[\widetilde{\nu} \left(\widetilde{\mathcal{L}}_l[\{h_j(t)\}] + \widetilde{\mathcal{L}}_l[\{y_j(t+\Delta t)\}] \right) \\ &\quad + \frac{\widetilde{\lambda}}{2} \left(\widetilde{\mathcal{N}_l}^{(\gamma)}[\{h_j(t)\}] + \widetilde{\mathcal{N}_l}^{(\gamma)}[\{y_j(t+\Delta t)\}] \right) \Big] + \sqrt{\widetilde{\Delta_0} \Delta t}\, \xi_l(t), \end{aligned} \tag{7.11}$$

where we set

$$\begin{aligned} \widetilde{\mathcal{L}}_l &\equiv h_{l+1}(t) - 2h_l(t) + h_{l-1}(t), \\ \widetilde{\mathcal{N}_l}^{(\gamma)} &\equiv \frac{1}{2(\gamma+1)} \Big[(h_{l+1}(t) - h_l(t))^2 + 2\gamma \, (h_{l+1}(t) - h_l(t)) \\ &\quad \times (h_l(t) - h_{l-1}(t)) + (h_l(t) - h_{l-1}(t))^2 \Big]. \end{aligned} \tag{7.12}$$

The effective spatial step-size Δx in the simulation is now simply given by

$$\Delta x = 1, \tag{7.13}$$

which is a common choice, e.g., [117, 119, 121, 123]. From the parameter set $\{\widetilde{\nu}, \widetilde{\Delta_0}, \widetilde{\lambda}\}$, which enters the simulation, the physical parameter set $\{\nu, \Delta_0, \lambda\}$ can be obtained from (7.10).

Finally, the calculation of the constituents of the TUR requires expectation values, denoted by $\langle \cdots \rangle$. Those are approximated by ensemble-averaging over a certain number E of independent realizations.

7.2 Approximation and Expected Scaling of the TUR Constituents

7.2.1 Regularizations

Since the KPZ equation is strictly speaking a singular SPDE (see, e.g., [89, 90, 106] and Appendices 3.A.5 and 5.C), it has to be regularized in some way. From a physical point of view, this can be done by either introducing a smallest length-scale (e.g., in form of a lattice-spacing δ [104]) or, in Fourier-space, by defining an upper cutoff wave number [123]. In the course of the analytical derivation of a KPZ-TUR in Chapters 5 and 6, we took the second approach and introduced the cutoff wave number $2\pi\Lambda/b$. This caused the physical entities like the NESS current, diffusion coefficient and entropy production rate to depend on this cutoff parameter (see (5.75), (5.66) and (5.76), respectively) and to become singular for $\Lambda \to \infty$. On the other hand, $\Lambda \to \infty$ represents the limit of spatially white noise. Thus, in order to approximate white noise as closely as possible, we have to choose Λ as large as possible. Here we use the real-space direct numerical simulation, described in Section 7.1, with lattice-spacing δ from (7.1) to calculate the relevant physical quantities, which will depend on δ and diverge for $\delta \to 0$. For comparison purposes, a relation between the cutoff parameter Λ and the lattice-spacing $\delta = b/L$ has to be established, keeping in mind that Λ has to be chosen as large as possible for the above reason. However, given a certain lattice spacing δ in real-space, Λ is limited by the following consideration. With b and δ fixed, our real-space direct simulation determines the values of $(\partial_x h)^2$ at L grid-points $x_l = l\,\delta$, $l = 0, \ldots, L-1$. Its Fourier transform is exact if it results in the corresponding Galerkin approximation of the non-linearity in Fourier space (i.e., a convolution with the correct wavenumber restriction for all modes). This is fulfilled if Λ satisfies the condition

$$\Lambda \leq \frac{L-1}{3}. \tag{7.14}$$

The above condition (7.14) is the content of the 3/2-rule by Orszag [123, 125, 126]. It is used in spectral codes, as the so-called dealiasing procedure (see, e.g., [123]). To sum up, given L, the largest value of Λ for which the Fourier transform of $(\partial_x h)^2$ is exactly represented by its Galerkin approximation reads

$$\Lambda = \frac{L-1}{3}. \tag{7.15}$$

Having this exact Galerkin approximation is relevant for determining the correct value of the TUR product in Chapter 5. Therefore, we choose Λ according to (7.15). With this relation between the number of grid-points L and the wavenumber cutoff Λ, we will now proceed with the numerical approximation of the TUR constituents and their respective scaling forms.

7.2.2 Mean and Variance of the Output Functional

For numerically approximating the output functional $\Psi(t)$ from (5.53) at any time-instance, we define

$$\Psi^{(N)}(t) \equiv \mathrm{Simp}[\{h_l(t)\}] = \frac{1}{3}\left[2\sum_{j=0}^{L/2-1} h_{2j}(t) + 4\sum_{j=1}^{L/2} h_{2j-1}(t)\right], \tag{7.16}$$

i.e., via a composite Simpson's rule, with periodic boundary conditions $h_L(t) = h_0(t)$, $\{h_l(t)\}$ obtained via (7.11) and $\Delta x = 1$ from (7.13). This implies that we approximate $L\,\Psi(t)/b$, rather than $\Psi(t)$ itself, which simplifies the comparison of the numerically obtained results with the theoretical ones.
The expected scaling of $\left\langle \Psi^{(N)}(t) \right\rangle$ is derived as follows. From (5.75) the corresponding (dimensionless) theoretical prediction $\langle \Psi_s(t_s) \rangle$ is known exactly as

$$\langle \Psi_s(t_s) \rangle = \left\langle \int_0^1 dx_s\, h_s(x_s, t_s) \right\rangle \simeq \frac{\lambda_{\text{eff}}}{2} \Lambda\, t_s, \qquad t_s \gg 1. \tag{7.17}$$

Here, variables with the subscript s are scaled dimensionless quantities with reference values according to Section 3.1.3 and λ_{eff} represents our effective dimensionless coupling constant from (3.13). Hence, after rescaling, (7.17) can also be written as

$$\left\langle \frac{L}{b} \int_0^b dx\, h(x,t) \right\rangle \simeq \frac{\widetilde{\lambda}\,\widetilde{\Delta_0}}{6\,\widetilde{\nu}} (L-1)\, t, \tag{7.18}$$

where (7.10) and (7.15) were used. The left hand side of (7.18) is what we approximate with $\left\langle \Psi^{(N)}(t) \right\rangle$ from (7.16), and thus

$$\left\langle \Psi^{(N)}(t) \right\rangle \simeq c_1(L)\, t, \qquad \text{with} \quad c_1(L) \equiv \frac{\widetilde{\lambda}\,\widetilde{\Delta_0}}{6\,\widetilde{\nu}} (L-1) \tag{7.19}$$

is the expected scaling behavior in the number of grid-points L and time t for $t \gg T$, with T from (3.9). Whereas we know the scaling behavior of $\langle \Psi(t) \rangle$ to be exact for all values of λ_{eff}, the variance of $\Psi(t)$ is known from (6.39) as a perturbation expansion up to $O(\lambda_{\text{eff}}^6)$ for $\lambda_{\text{eff}} < \lambda_{\text{eff}}^c$ and from the DRG result (6.40) for $\lambda_{\text{eff}} > \lambda_{\text{eff}}^c$. For deriving the expected scaling behavior, we choose the case $\lambda_{\text{eff}} \ll \lambda_{\text{eff}}^c$ as an example and take

$$\text{var}\left[\Psi_s(t_s)\right] \simeq t_s, \qquad t_s \gg 1, \tag{7.20}$$

to lowest non-vanishing order in λ_{eff}. Hence, by following the same steps as above, we get

$$\text{var}\left[\Psi^{(N)}(t)\right] \simeq c_2(L)\, t, \qquad \text{with} \quad c_2(L) \equiv \widetilde{\Delta_0}\, L, \tag{7.21}$$

for $t \gg T$. Using (7.19) and (7.21) the scaling form for the precision

$$(\epsilon^2)^{(N)} = \frac{\text{var}\left[\Psi^{(N)}(t)\right]}{\left\langle \Psi^{(N)}(t) \right\rangle^2} \tag{7.22}$$

is for $\lambda_{\text{eff}} \ll \lambda_{\text{eff}}^c$ given by

$$(\epsilon^2)^{(N)} \simeq c_3(L)\, \frac{1}{t}, \qquad \text{with} \quad c_3(L) \equiv \frac{36\,\widetilde{\nu}^2}{\widetilde{\lambda}^2\,\widetilde{\Delta_0}} \left[\frac{1}{L} + \frac{2}{L^2} + O\left(\frac{1}{L^3}\right) \right], \tag{7.23}$$

for $t \gg T$.

7.2.3 The Total Entropy Production

The last entity missing for formulating the numerical version of the KPZ-TUR is the total entropy production $\langle \Delta s_{\mathrm{tot}} \rangle$. It is given by, e.g., (5.38) where we note that the integrand on the r.h.s. is nothing but the square of the KPZ non-linearity $(\partial_x h)^2$ and we thus can approximate the integrand using any of the discretizations from (7.4). To be specific, by means of the composite Simpson's rule, we get the approximation

$$\int_0^b dx\ (\partial_x h(x,\tau))^4 \approx \frac{L^3}{3\,b^3}\left[2\sum_{j=0}^{L/2-1}\left(\mathcal{N}_{2j}^{(\gamma)}\right)^2 + 4\sum_{j=1}^{L/2}\left(\mathcal{N}_{2j-1}^{(\gamma)}\right)^2\right]. \tag{7.24}$$

The prefactor of L^3/b^3 arises from the fact that (7.24) uses (7.4) with $\Delta x = 1$. Lastly, the time integral in (5.38) is approximated via

$$\int_0^t d\tau \left\langle \int_0^b dx\ (\partial_x h(x,\tau))^4 \right\rangle \approx \frac{L^3}{b^3}\sum_{n=0}^{N-1}\left\langle \mathrm{Simp}\left[\left(\mathcal{N}_l^{(\gamma)}[\{h_j(t_n)\}]\right)^2\right]\right\rangle \Delta t, \tag{7.25}$$

where Δt is a discrete time-step and $t = N\Delta t$.
Proceeding similarly like in Section 7.2.2, we get from the theoretical prediction in (5.76) the expected scaling behavior for $\langle \Delta s_{\mathrm{tot}} \rangle^{(N)}$ and the TUR product with respect to the number of grid-points L and time t as

$$\langle \Delta s_{\mathrm{tot}} \rangle^{(N)} \simeq c_4(L)\, t, \qquad \text{with} \quad c_4(L) \equiv \frac{\widetilde{\Delta_0}}{36}\left(\frac{\widetilde{\lambda}}{\widetilde{\nu}}\right)^2\left[5\,L - 13 + \frac{8}{L}\right], \tag{7.26}$$

for $t \gg T$, which, according to Section 5.4, holds exactly for all values of λ_{eff}. Finally, we get with (7.23) and (7.26),

$$\mathcal{Q}^{(N)} \simeq 5 - \frac{3}{L} + O\left(\frac{1}{L^2}\right). \tag{7.27}$$

Note, since (7.23) only holds for $\lambda_{\mathrm{eff}} \ll \lambda_{\mathrm{eff}}^c$, the same applies to (7.27). For the more general treatment, see Section 7.4.

7.3 Comparison with Numerical Simulations – Edwards-Wilkinson Scaling Regime

7.3.1 Employed Input Parameters

We present the numerical results obtained from (7.11) by using three different discretizations according to (7.4). If not explicitly stated otherwise, we employ for the numerical simulations the ID discretization ($\gamma = 1/2$) from (7.7). The numerics is performed for the following set of input parameters. For all simulations we set $\widetilde{\nu} = \widetilde{\Delta_0} = 1$ and take $\widetilde{\lambda} = 0.1$ on a range of grid-points, which varies from $L = 16$ to $L = 1024$. In the range of $L = 16 \dots 64$ we use a time-step size of $\Delta t = 10^{-4}$ and an ensemble size of $E = 500$. For $L = 128 \dots 1024$ a larger time-step of $\Delta t = 10^{-2}$ and smaller ensemble size, $E = 250$, is used. This reduction is due to the strongly increasing run-time of the simulations for larger numbers of grid-points. The chosen value of $\widetilde{\lambda}$ is well within the EW scaling regime. The coupling constant λ_{eff} expressed in terms of the effective input parameters from (7.10), reads

$$\widetilde{\lambda}_{\text{eff}} = L^{1/2} \left(\frac{\widetilde{\Delta}_0}{\widetilde{\nu}^3} \right)^{1/2} \widetilde{\lambda}. \tag{7.28}$$

With $\widetilde{\nu} = \widetilde{\Delta}_0 = 1$, the critical value of the effective coupling constant $\widetilde{\lambda}$ is reached for (see (3.51) with $c_2 \approx 0.4$)

$$\widetilde{\lambda}^{\text{c}} \approx \frac{12.3}{L^{1/2}}, \tag{7.29}$$

ranging from $\widetilde{\lambda}^{\text{c}} \approx 3.08$ for $L = 16$ to $\widetilde{\lambda}^{\text{c}} \approx 0.384$ for $L = 1024$. Hence, we have $\widetilde{\lambda} \ll \widetilde{\lambda}^{\text{c}}$, which provides us with the ability to study the singular limit $\lambda_{\text{eff}} \downarrow 0$ for the TUR product.

7.3.2 Evaluation of the Numerical Data

In the following, we describe a procedure for comparing the scaling predictions of the TUR constituents from Section 7.2 to the numerical results. For the two cases, where the scaling predictions are known to be exact, this procedure further yields a way of assessing the accuracy of the numerical scheme in dependence on the grid-size L, the time-step size Δt and the number of independent ensembles E. At first, we check whether (7.19) and (7.21) is fulfilled. This is done by fitting the numerical data of $\left\langle \Psi^{(N)}(t) \right\rangle^2$ and $\text{var}\left[\Psi^{(N)}(t)\right]$ according to the fit-function f_1, with

$$f_1(L, t) \equiv a_L \, t^2, \tag{7.30}$$

and f_2, given by

$$f_2(L, t) \equiv b_L \, t, \tag{7.31}$$

respectively, where a_L and b_L are L-dependent fit-parameters. Subsequently, we compare a_L and b_L with $c_1^2(L)$ and $c_2(L)$, respectively.
The scaling prediction for the precision $(\epsilon^2)^{(N)}$ according to (7.23) is evaluated by fitting

$$f_3(L, t) \equiv \frac{d_L}{t}, \tag{7.32}$$

with fit-parameter d_L, to the numerically obtained data for the precision and comparing $c_3(L)$ to d_L for the respective values of L.
Finally, by fitting the numerical data for $\langle \Delta s_{\mathrm{tot}} \rangle^{(N)}$ according to

$$f_4(L,t) \equiv e_L\, t, \tag{7.33}$$

with e_L as the fit-parameter and subsequently comparing $c_4(L)$ to e_L, the scaling prediction for the total entropy production (7.26) is compared to the numerical results.

7.3.3 Expectation Squared and Variance for the Spatial Mean of the Height Field

Table 7.1: Scaling factors of $\left\langle \Psi^{(N)}(t) \right\rangle^2$ and var $\left[\Psi^{(N)}(t)\right]$

	L	a_L	$c_1^2(L)$	Δ_1 [%]	
$\left\langle \Psi^{(N)}(t) \right\rangle^2$	16	0.05835	0.06250	6.64	$\Delta t = 10^{-4}$, $E = 500$
	64	1.087	1.103	1.44	
	256	17.78	18.06	1.59	$\Delta t = 10^{-2}$, $E = 250$
	1024	286.7	290.7	1.37	
	L	b_L	$c_2(L)$	Δ_2 [%]	
var $\left[\Psi^{(N)}(t)\right]$	16	15.70	16.0	1.86	$\Delta t = 10^{-4}$, $E = 500$
	64	64.02	64.0	0.032	
	256	238.0	256.0	7.03	$\Delta t = 10^{-2}$, $E = 250$
	1024	1033	1024	0.846	

Comparison of the predicted scaling factors $c_1^2(L)$, $c_2(L)$ from (7.19), (7.21) to a_L, b_L from (7.30), (7.31), respectively, for the fits as shown in Figure 7.1. Here $\Delta_1 = |c_1^2(L) - a_L|/c_1^2(L)$, $\Delta_2 = |c_2(L) - b_L|/c_2(L)$ denote the absolute values of the respective relative errors in percent.

In Figure 7.1, we plot the numerical data of $\left\langle \Psi^{(N)}(t) \right\rangle^2$ and var $\left[\Psi^{(N)}\right]$. The data of $\left\langle \Psi^{(N)}(t) \right\rangle^2$ displays, by visible inspection of Figure 7.1, a power-law behavior for all L in time t for $t \geq t_{\mathrm{c}}^{\mathrm{EW}}$ from (3.32), i.e., $t \geq \pi L^2/288$. E.g., for $L = 64$, this amounts to $t \gtrapprox 45$ and for $L = 256$ to $t \gtrapprox 715$. Whereas for smaller values of L, this threshold seems to be sharp, for large values of L the NESS behavior is visibly reached much earlier. In Table 7.1 we list the results for the respective fit-parameters and scaling predictions

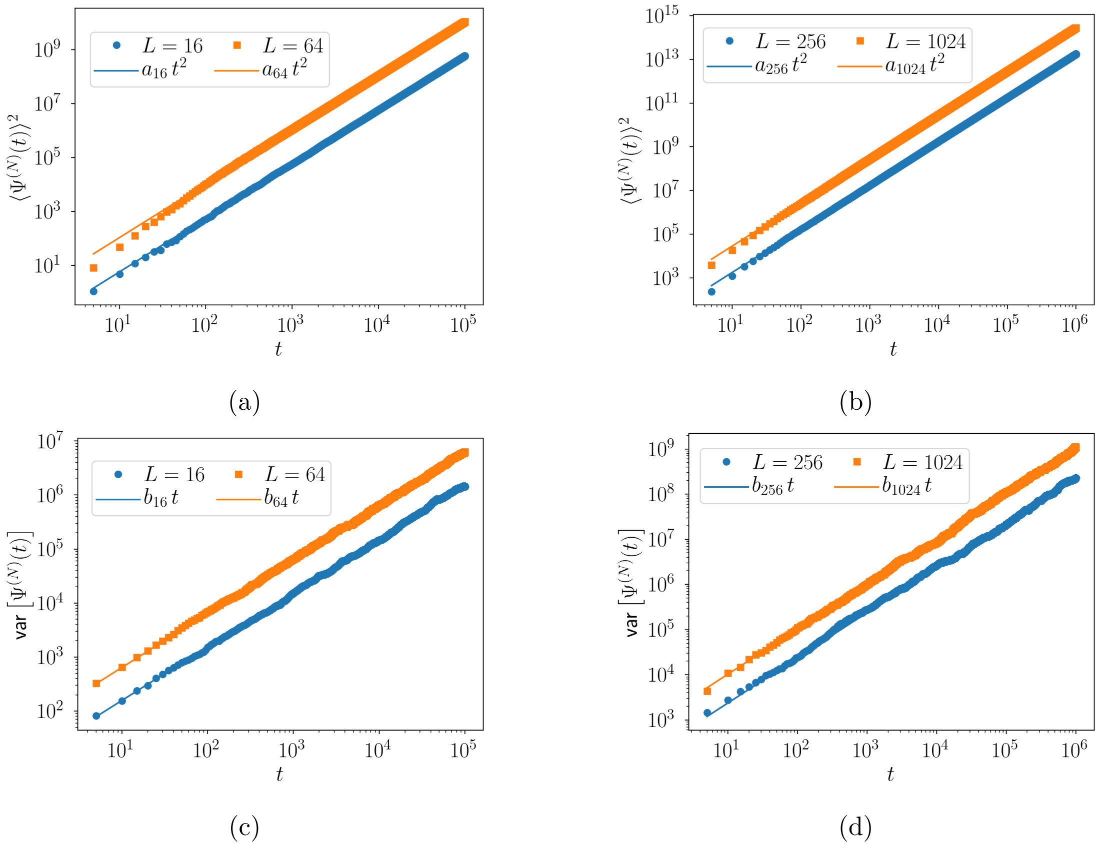

Figure 7.1: $\langle \Psi^{(N)}(t) \rangle^2$ and $\mathrm{var}\left[\Psi^{(N)}(t)\right]$ in the range of $L = 16 \ldots 1024$. The dots represent the numerical data obtained from (7.11) using (7.7), whereas the straight lines are fit-functions according to (7.30), (7.31), respectively. The graphs in (a) and (c) are obtained with the set of input-parameters $\{\widetilde{\nu}, \widetilde{\Delta_0}, \widetilde{\lambda}\} = \{1.0, 1.0, 0.1\}$, time-step size $\Delta t = 10^{-4}$ and ensemble size $E = 500$, whereas (b) and (d) show graphs with $\Delta t = 10^{-2}$ and $E = 250$ for the same set of input-parameters.

as well as their relative deviations. The values given in Table 7.1 suggest that for all L the predicted scaling form of $\left\langle \Psi^{(N)}(t) \right\rangle^2$ from (7.19) squared is indeed recovered by the numerics. The approximation becomes more accurate for a growing number of grid-points L as the relative error Δ_1 shows the clear trend of decreasing for growing L. Consequently, the larger the number of grid-points L, the better the approximation of the numerical scheme to the exact scaling behavior from (5.75) becomes. This is a clear indication that the numerical scheme works properly. The slight deviation in the above trend observed between $L = 64$ and $L = 256$ is due to the fact that we changed Δt from $\Delta t = 10^{-4}$ for $L = 64$ to $\Delta t = 10^{-2}$ for $L = 256$ as well as $E = 500$ for $L = 64$ to $E = 250$ for $L = 256$. However, as the effect is rather small, there is no need to adjust the parameters Δt and E for $L = 256 \dots 1024$ in order to achieve a higher accuracy.
We now turn to the variance of the mean height field according to (7.21). The predicted power-law behavior of var $\left[\Psi^{(N)}(t)\right]$ in (7.21) can be observed in Figs. 7.1(c) and 7.1(d). The predicted scaling factor $c_2(L)$ in (7.21) is reproduced well by the numerical data and its respective fit-functions (7.31) with fit-parameter b_L. In contrast to the results for $\left\langle \Psi^{(N)}(t) \right\rangle^2$, no clear trend in the relative error $\Delta_2 = |c_2(L) - b_L|/c_2(L)$ can be observed, i.e., Δ_2 does not become smaller with growing L. An improvement in the approximation may be obtained by an increase of the ensemble-size E and a further decrease of the time-step size Δt. This, however, would lead to a significantly longer run-time of the simulations. As in all cases the relative error is below 10%, the gain from a further improved accuracy following the above mentioned steps may be outweighed by the increasing run-time.

7.3.4 Precision and Total Entropy Production

By combining the numerical results of $\left\langle \Psi^{(N)}(t) \right\rangle^2$ and var $\left[\Psi^{(N)}(t)\right]$ according to (7.23), we obtain the data of the precision $(\epsilon^2)^{(N)}$ as shown in Figs. 7.2(a) and 7.2(b). As is to be expected considering the observations for the scaling of $\left\langle \Psi^{(N)}(t) \right\rangle^2$ and var $\left[\Psi^{(N)}(t)\right]$, both graphs display a clear power-law behavior in time t. The time elapsed in Figure 7.2 to reach the NESS behavior for the respective system-sizes and observables is in accordance to the observations made in the discussion of Figure 7.1. The compliance of the numerical data with the predicted scaling from (7.23) can be seen in Table 7.2. We will now turn to the scaling behavior of the total entropy production $\langle \Delta s_{\mathrm{tot}} \rangle^{(N)}$. In Figs. 7.2(c), 7.2(d), we show the plots of the numerically obtained data for $\langle \Delta s_{\mathrm{tot}} \rangle^{(N)}$ and the according fits. We find that the scaling behavior is recovered nicely, albeit with a significantly greater relative deviation as compared to $(\epsilon^2)^{(N)}$ (see Table 7.2). The only influence on the relative error of $\langle \Delta s_{\mathrm{tot}} \rangle^{(N)}$ is achieved by an increase in the number of grid-points L. It seems, however, that the relative errors do not become smaller than roughly 10% even for large L. In Appendix 7.A we will discuss this observation in more detail and present an analytical explanation for this discrepancy.

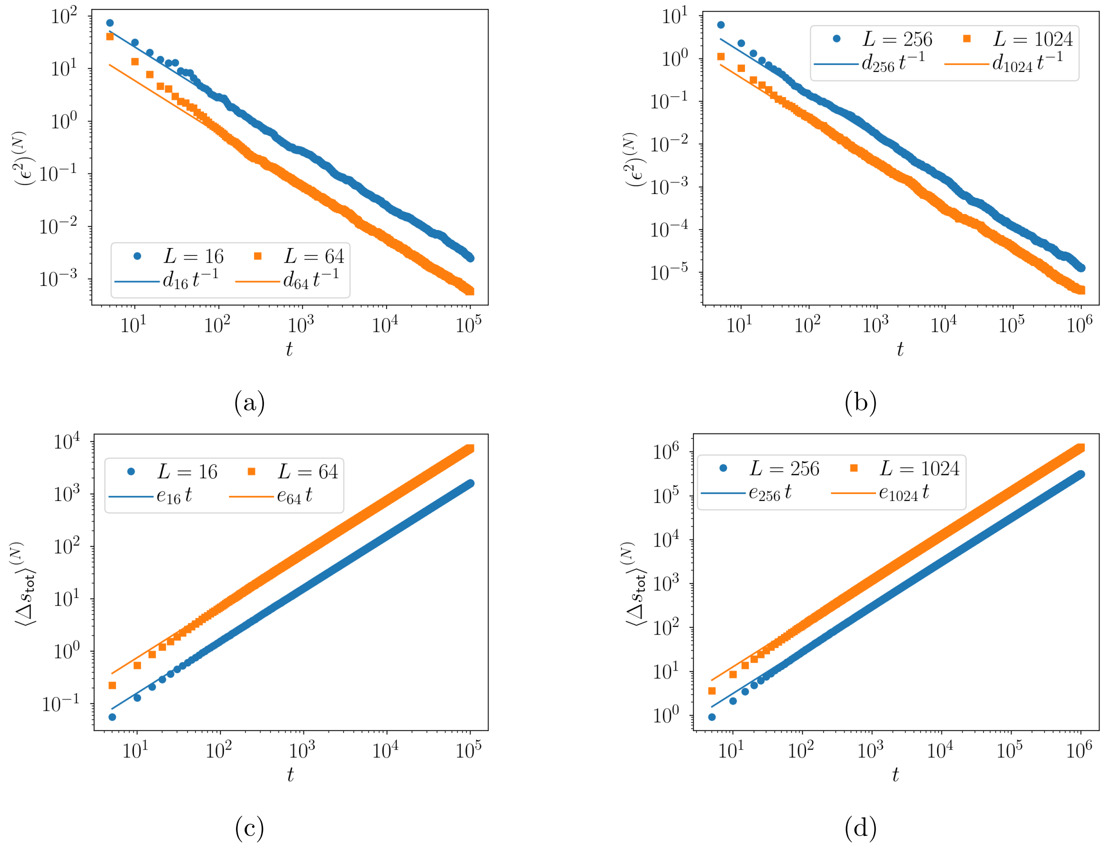

Figure 7.2: Precision $(\epsilon^2)^{(N)}$ and total entropy production $\langle \Delta s_{\mathrm{tot}} \rangle^{(N)}$ in the range of $L = 16 \ldots 1024$. The dots represent the numerical data obtained from (7.11) using (7.7), whereas the straight lines are fit-functions according to (7.32), (7.33), respectively. The graphs in (a) and (c) are obtained with the set of input-parameters $\{\widetilde{\nu}, \widetilde{\Delta_0}, \widetilde{\lambda}\} = \{1.0, 1.0, 0.1\}$, time-step size $\Delta t = 10^{-4}$ and ensemble size $E = 500$, whereas (b) and (d) show graphs with $\Delta t = 10^{-2}$ and $E = 250$ for the same set of input-parameters.

Table 7.2: Scaling factors of the precision $(\epsilon^2)^{(N)}$ and total entropy production $\langle \Delta s_{\mathrm{tot}} \rangle^{(N)}$

	L	d_L	$c_3(L)$	Δ_3 [%]	
$(\epsilon^2)^{(N)}$	16	254.9	253.1	0.686	$\Delta t = 10^{-4}$, $E = 500$
	64	58.49	58.01	0.824	
	256	14.29	14.17	0.80	$\Delta t = 10^{-2}$, $E = 250$
	1024	3.564	3.523	1.18	
	L	e_L	$c_4(L)$	Δ_4 [%]	
$\langle \Delta s_{\mathrm{tot}} \rangle^{(N)}$	16	0.01607	0.01875	14.3	$\Delta t = 10^{-4}$, $E = 500$
	64	0.07588	0.08531	11.1	
	256	0.3150	0.3520	10.5	$\Delta t = 10^{-2}$, $E = 250$
	1024	1.272	1.419	10.3	

Comparison of the predicted scaling factors $c_3(L)$, $c_4(L)$ from (7.23), (7.26) to d_L, e_L from (7.32), (7.33) for the fits as shown in Figure 7.2. Here $\Delta_3 = |c_3(L) - d_L|/c_3(L)$, $\Delta_4 = |c_4(L) - e_L|/c_4(L)$ denote the absolute values of the respective relative errors in percent.

7.3.5 Thermodynamic Uncertainty Relation

In the previous sections we have derived the scaling forms of all the TUR constituents and compared these predictions to the numerics. Here, we will combine these results for the numerical thermodynamic uncertainty product $\mathcal{Q}^{(N)} = \langle \Delta s_{\text{tot}} \rangle^{(N)} (\epsilon^2)^{(N)}$. In Figure 7.3, we plot the TUR product $\mathcal{Q}^{(N)}$. It can be seen that it approaches a stationary value. Since in the stationary state the data of $\mathcal{Q}^{(N)}$ fluctuates stochastically around a certain value, we introduce $\overline{\mathcal{Q}}_\tau^{(N)}$, i.e., the temporal mean of $\mathcal{Q}^{(N)}$ for times $t \geq \tau$. This yields a quantity that can be compared to $\mathcal{Q}$ from (7.27) shown as dashed lines in Figure 7.3. Note that the value of $\tau = 10^3$ is chosen heuristically based on the observations from Figure 7.3. From Table 7.3, it can be seen that $\overline{\mathcal{Q}}_\tau^{(N)}$ ranges from 4.16 to 4.58. Hence, for all calculated configurations the TUR product is significantly greater than 2 and thus the numerical calculations support the theoretical prediction from (7.27) well, in the sense that the TUR product is not saturated. It can be further inferred from Table 7.3 that all the $\overline{\mathcal{Q}}_\tau^{(N)}$'s underestimate the theoretically predicted values.

We have shown that for $\left\langle \Psi^{(N)}(t) \right\rangle^2$ and var $\left[\Psi^{(N)}(t)\right]$ the predicted scaling forms from

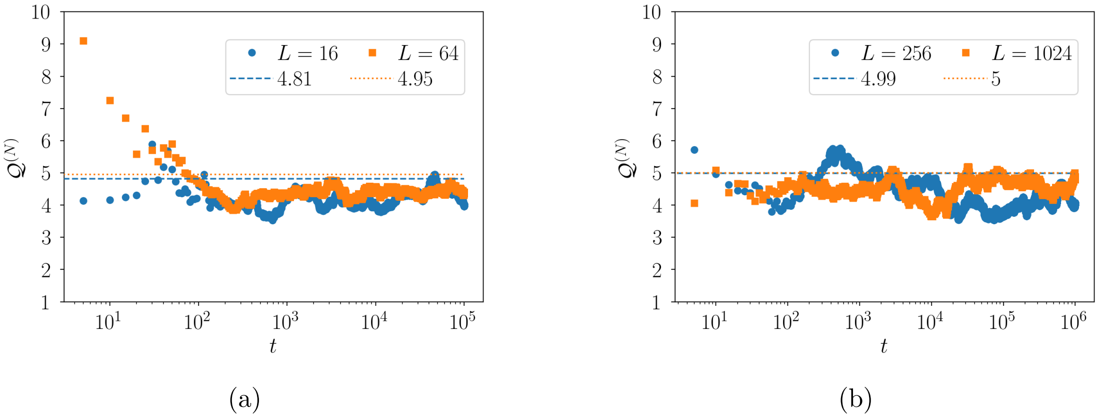

Figure 7.3: TUR product $\mathcal{Q}^{(N)}$ in the range of $L = 16 \dots 1024$. The dots represent the numerical data obtained from (7.11) using (7.7), whereas the dashed lines are the theoretically expected values of $\mathcal{Q}$ according to (7.27). In (a) the set of input-parameters $\{\widetilde{\nu}, \widetilde{\Delta_0}, \widetilde{\lambda}\} = \{1.0, 1.0, 0.1\}$, time-step size $\Delta t = 10^{-4}$ and ensemble size $E = 500$ is used, whereas in (b) we use a time-step size of $\Delta t = 10^{-2}$ and an ensemble size of $E = 250$ for the same set of input-parameters.

(7.19) and (7.21), respectively, fit the numerically obtained data for these two quantities very well. Especially for large values of the number of grid-points L, we observed for $\left\langle \Psi^{(N)}(t) \right\rangle^2$ a clear decrease in the relative error between the theoretical predictions

Table 7.3: Scaling values of $\mathcal{Q}^{(N)} = \langle \Delta s_{\mathrm{tot}} \rangle^{(N)} \, (\epsilon^2)^{(N)}$

L	$\overline{\mathcal{Q}}_\tau^{(N)}$	$\mathcal{Q}$	Δ [%]	
16	4.33	4.81	10	$\Delta t = 10^{-4}$, $E = 500$, $\tau = 10^3$
64	4.44	4.95	10	
256	4.16	4.99	17	$\Delta t = 10^{-2}$, $E = 250$, $\tau = 10^3$
1024	4.58	5.00	8	

Comparison of the predicted values of $\mathcal{Q}$ from (7.27) to $\overline{\mathcal{Q}}_\tau^{(N)}$ from Figs. 7.3(a) and 7.3(b). Here $\Delta = |\mathcal{Q} - \overline{\mathcal{Q}}_\tau^{(N)}|/\mathcal{Q}$ denotes the absolute value of the relative error in percent.

and the numerical results, i.e., $\Delta_1 \to 0$ (see Table 7.1). The relative error Δ_2 of the variance var $\left[\Psi^{(N)}(t)\right]$ did not depend on L and seems to be solely caused by stochastic fluctuations due to the limited ensemble size E (see Table 7.1). With the above two quantities, both components of the precision $(\epsilon^2)^{(N)}$ from (7.23) were found to follow the predicted scaling forms and thus also the numerically obtained precision behaves as expected (see Table 7.2). In Table 7.2 we have seen for $\langle \Delta s_{\mathrm{tot}} \rangle^{(N)}$, that the scaling of the numerical data fits well with the theoretically predicted one from (7.26). It was observed, however, that even for large L the relative error did not get smaller than roughly 10%. We conclude that this is an inherent issue with the numerical scheme from (7.11) with the non-linearity according to (7.7). Further in-depths discussion of this point will be presented in Appendix 7.A.

For the TUR product we observe that all simulated systems tend to a stationary value for $\mathcal{Q}^{(N)}$ (see Figure 7.3). However, for the above quoted reasons, the numerical value is underestimating the theoretically expected one in all cases (see Table 7.3). Nevertheless, the numerical data shows clearly that the TUR product is well above the value of 2 and ranges for our simulations roughly between 4 and 5, which supports the analytically predicted limit of $\mathcal{Q} = 5 - 1/\Lambda = 5 - 3/L$ for $\lambda_{\mathrm{eff}} \downarrow 0$ from, e.g., (6.41) and (7.27).

7.4 Comparison with Numerical Simulations – Arbitrary Coupling Strength

7.4.1 Employed Input Parameters

For the numerical simulation for arbitrary coupling strength λ_{eff}, we focus on the system-size $L = 256$. Like in Section 7.3 we set $\widetilde{\nu} = \widetilde{\Delta_0} = 1$ and employ an ensemble-size of $E = 250$ but use a time-step size of $\Delta t = 10^{-3}$. The effective coupling constant $\widetilde{\lambda}$ is taken to be $\widetilde{\lambda} = 0.1$, $\widetilde{\lambda} = 0.768$ and $\widetilde{\lambda} = 4.0$ with the exception of Figure 7.9. According to (7.29), the second choice, $\widetilde{\lambda} = 0.768$, represents the critical value $\widetilde{\lambda}^c$ for $L = 256$. Hence, $\widetilde{\lambda} = 0.1$ belongs to the EW scaling regime and is shown again for comparison purposes over an extended time-range, whereas $\widetilde{\lambda} = 4.0$ lies well within the genuine KPZ scaling regime.

7.4.2 Expected Spatial Mean of the Height Field and Total Entropy Production

In Figure 7.4 we show for two values of $\widetilde{\lambda}$ a comparison of numerical data for both $\langle \Psi(t) \rangle^2$ and $\langle \Delta s_{\text{tot}} \rangle$ with the respective theoretical predictions according to (7.19) and (7.26). In the case of $\widetilde{\lambda} = 0.1$ the system is in the EW scaling regime and thus the relevant time-scale is the EW correlation time t_{c}^{EW}, which is indicated by the vertical line in Figs. 7.4(a) and (b). As can be seen well, for times $t > t_{\text{c}}^{\text{EW}}$ the numerical data follows the theoretical prediction for both $\langle \Psi(t) \rangle^2$ and $\langle \Delta s_{\text{tot}} \rangle$. For $\widetilde{\lambda} = 4.0$ the system is in its KPZ scaling regime, which implies that the numerical data is expected to converge to the theoretical predictions for times $t > t_{\text{c}}^{\text{KPZ}}$, i.e., the KPZ correlation time. In Figs. 7.4(c) and (d) this convergence can be well observed. Thus, the results in Figure 7.4 are additional support for the fact that the expressions for $\langle \Psi(t) \rangle$ and $\langle \Delta s_{\text{tot}} \rangle$ obtained analytically in (7.19) and (7.26), respectively, hold for an arbitrary coupling constant.

7.4.3 Variance of $\Psi(t)$ and Universal Scaling Amplitude

Using the same steps as in Section 7.2 and referring to (5.59) and (6.40), respectively, we obtain the following scaling expression for var$[\Psi(t)]$. For parameter sets with $\lambda_{\text{eff}} \lessapprox \lambda_{\text{eff}}^c$,

$$\text{var}[\Psi(t)] \simeq \widetilde{\Delta}_0 \, L \, t \left(1 + L \, \frac{\widetilde{\Delta}_0 \, \widetilde{\lambda}^2}{\widetilde{\nu}^3} \, \frac{\mathcal{S}_1(L)}{32 \, \pi^2} - L^2 \, \frac{\widetilde{\Delta}_0^2 \, \widetilde{\lambda}^4}{\widetilde{\nu}^6} \, \frac{\mathcal{S}_2(L)}{256 \, \pi^4} + O(\lambda_{\text{eff}}^6) \right), \tag{7.34}$$

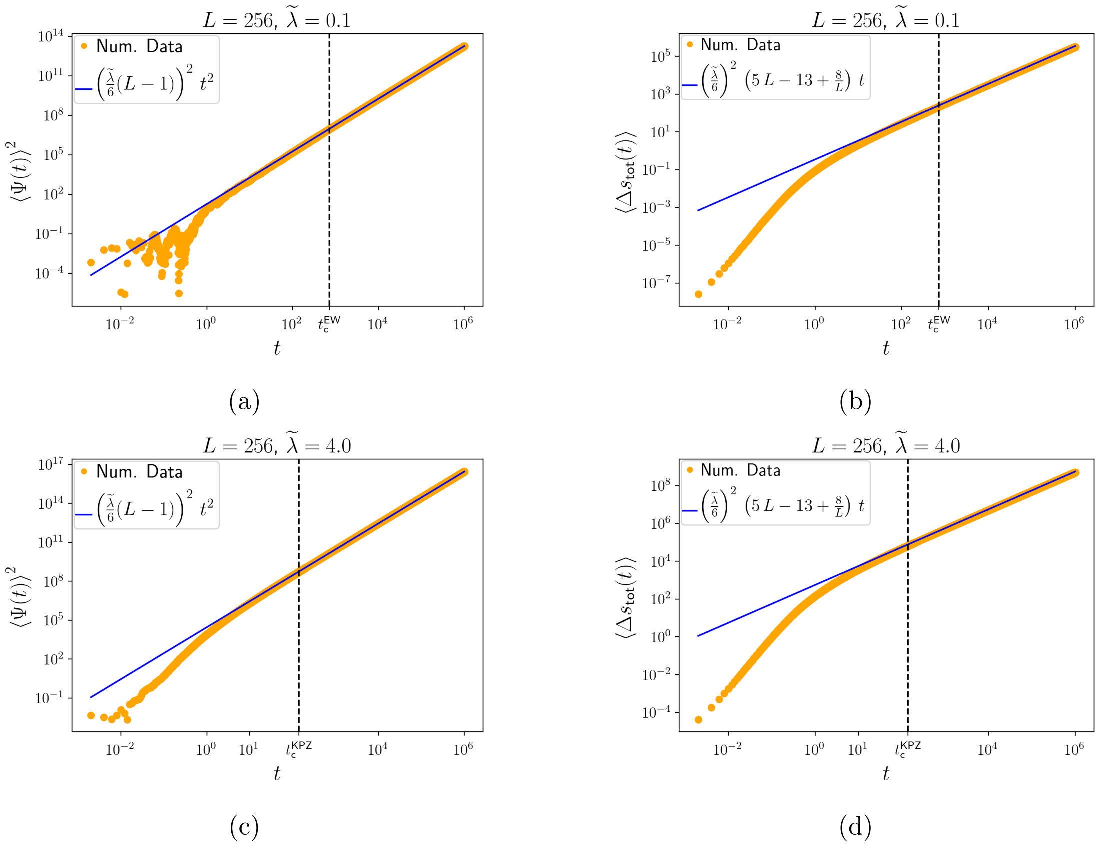

Figure 7.4: Comparison of the numerical data obtained for a system-size of $L = 256$ to $\langle \Psi(t) \rangle^2$ from (7.19) in (a) and (c) and to $\langle \Delta s_{\mathrm{tot}} \rangle$ from (7.26) in (b) and (d), respectively. In (a) and (b) we simulate a system with $\widetilde{\lambda} = 0.1 < \widetilde{\lambda}^{\mathrm{c}}$, i.e., in the EW scaling regime of the KPZ equation, whereas in (c) and (d) we simulate a system with $\widetilde{\lambda} = 4 > \widetilde{\lambda}^{\mathrm{c}}$, which puts the system in the KPZ scaling regime. The vertical lines indicate the respective correlation times $t_{\mathrm{c}}^{\mathrm{EW}}$ from (3.53) and $t_{\mathrm{c}}^{\mathrm{KPZ}}$ from (3.44).

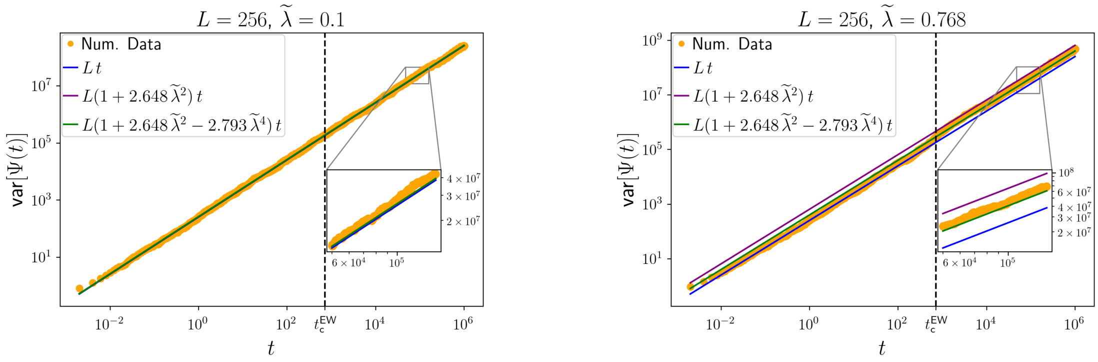

(a) (b)

Figure 7.5: Comparison of numerical data obtained for $L = 256$ with $\widetilde{\lambda} = 0.1$ in (a) and $\widetilde{\lambda} = 0.768 \approx \widetilde{\lambda}^{\mathrm{c}}$ in (b) with the theoretical prediction from (7.34) of the variance of $\Psi(t)$ in the EW scaling regime. We show three orders of approximation, i.e., $\widetilde{\lambda}^0$, $\widetilde{\lambda}^2$ and $\widetilde{\lambda}^4$, for var[$\Psi(t)$] to demonstrate the effect of including higher order terms. The vertical line indicates the EW correlation time $t_{\mathrm{c}}^{\mathrm{EW}}$ from (3.53).

with

$$\begin{aligned} \mathcal{S}_1(L) &= 2 \sum_{k=1}^{\lceil \frac{L-1}{3} \rceil} \frac{1}{k^2}\,, \\ \mathcal{S}_2(L) &= 2 \sum_{k=1}^{\lceil \frac{L-1}{3} \rceil} \frac{1}{k^3} \sum_{m=-\lceil \frac{L-1}{3} \rceil + k}^{\lceil \frac{L-1}{3} \rceil} \frac{m}{k^2 + (k-m)^2 + m^2} - \sum_{k=1}^{\lceil \frac{L-1}{3} \rceil} \frac{1}{k^4}\,. \end{aligned} \tag{7.35}$$

On the other hand for parameter sets with $\lambda_{\mathrm{eff}}^{\mathrm{c}} \ll \lambda_{\mathrm{eff}}$ we have with (6.40)

$$\mathrm{var}[\Psi(t)] \simeq \begin{cases} \widetilde{\Delta}_0\, L\, t\,, & t \ll t^{\mathrm{EW}\to\mathrm{KPZ}}, \\ \frac{3\,\Gamma(2/3)}{8\,\pi^{2/3}}\, L\, \widetilde{\lambda}^{4/3} \left(\frac{\widetilde{\Delta}_0}{\widetilde{\nu}}\right)^{5/3} t^{4/3}\,, & t^{\mathrm{EW}\to\mathrm{KPZ}} \lessapprox t \lessapprox t_{\mathrm{c}}^{\mathrm{KPZ}}, \\ \frac{\sqrt{\pi}}{4} \left(\frac{\widetilde{\Delta}_0}{2\,\widetilde{\nu}}\right)^{3/2} \widetilde{\lambda}\, L^{3/2}\, t\,, & t_{\mathrm{c}}^{\mathrm{KPZ}} \ll t\,. \end{cases} \tag{7.36}$$

Figure 7.5 shows numerically obtained data of the variance of $\Psi(t)$ for $\widetilde{\lambda} = 0.1$ (see Figure 7.5(a)), $\widetilde{\lambda} = 0.768 \approx \widetilde{\lambda}^{\mathrm{c}}$ (see Figure 7.5(b)). To demonstrate the effect of including higher order terms in the approximation of var[$\Psi(t)$] in the EW scaling regime, we show in Figure 7.5 each partial sum of the expansion in (7.34) separately in increasing order. As can be seen clearly in Figure 7.5(a), there is no discernible difference between the lowest and highest order perturbation result for $\widetilde{\lambda} = 0.1$. In Figure 7.5(b), for $\widetilde{\lambda} = 0.768$, however, the difference between the three approximation orders becomes apparent. Here the zero-order approximation ($\widetilde{\lambda}^0$) underestimates the numerical data and the first-order approximation ($\widetilde{\lambda}^2$) is a slight overestimation, whereas the second-order result ($\widetilde{\lambda}^4$) matches the numerical data well. For values $\widetilde{\lambda} > \widetilde{\lambda}^{\mathrm{c}}$, we leave the region in which the perturbation expansion from Chapter 5 is expected to be valid, which is reflected in a rapid decline in the quality of the highest-order approximation (not shown explicitly), as is to be expected. The numerical values in the legend of Figure 7.5 are obtained by evaluating (7.35) and inserting these results into (7.34) for $L = 256$ (i.e., $\lceil (L-1)/3 \rceil = 85$).

For the case of $\lambda_{\mathrm{eff}}^{\mathrm{c}} < \lambda_{\mathrm{eff}}$, we show in Figure 7.6 numerical data of the variance of $\Psi(t)$.

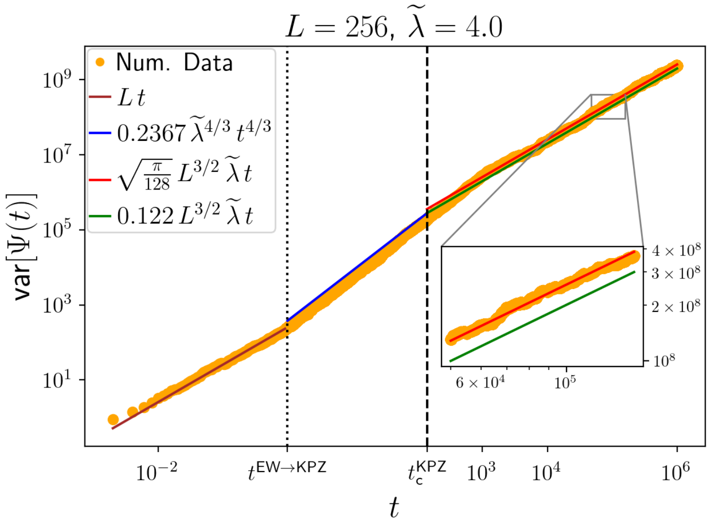

Figure 7.6: Numerical data of var[$\Psi(t)$] for $\widetilde{\lambda} = 4.0 > \widetilde{\lambda}^{\mathrm{c}}$, i.e., in the KPZ regime. For $t < t^{\mathrm{EW}\to\mathrm{KPZ}}$ we plot the variance according to the first line in (7.36). In the transient regime, i.e., for $t^{\mathrm{EW}\to\mathrm{KPZ}} < t < t_{\mathrm{c}}^{\mathrm{KPZ}}$, the variance according to the second line in (7.36) is shown. For $t > t_{\mathrm{c}}^{\mathrm{KPZ}}$, i.e., in the stationary KPZ regime, we plot for one the third line from (7.36) and on the other hand $\mathcal{C}\,t$ with $\mathcal{C}$ from (6.34).

As can be seen clearly, the variance displays the expected scaling behaviors (see (7.36)), namely, on the one hand, for times $t < t^{\mathrm{EW}\to\mathrm{KPZ}}$ scaling according to the EW scaling regime of the KPZ equation. On the other hand, for times $t > t^{\mathrm{EW}\to\mathrm{KPZ}}$ Figure 7.6 shows the typical KPZ scaling regime behavior, namely for $t^{\mathrm{EW}\to\mathrm{KPZ}} < t < t_{\mathrm{c}}^{\mathrm{KPZ}}$ the transient regime with its super-diffusivity and for $t_c^{\mathrm{KPZ}} < t$ the stationary KPZ regime. In regard of the EW to KPZ crossover time from (3.42), we see very good agreement between the theoretical prediction, indicated by the left vertical line in Figure 7.6 and the numerical data. However, the theoretical prediction for the KPZ correlation time from (3.44), shown as the right vertical line in Figure 7.6 seems to be too small, as the superdiffusive behavior continues beyond t_c^{KPZ}. We will investigate this in more detail below. This discrepancy aside, we find good agreement in all three sub-regimes of the variance between the numerical data and the theoretical predictions from (6.34) and (7.36).

In Figure 7.7 we show our approach to determining the numerical KPZ correlation

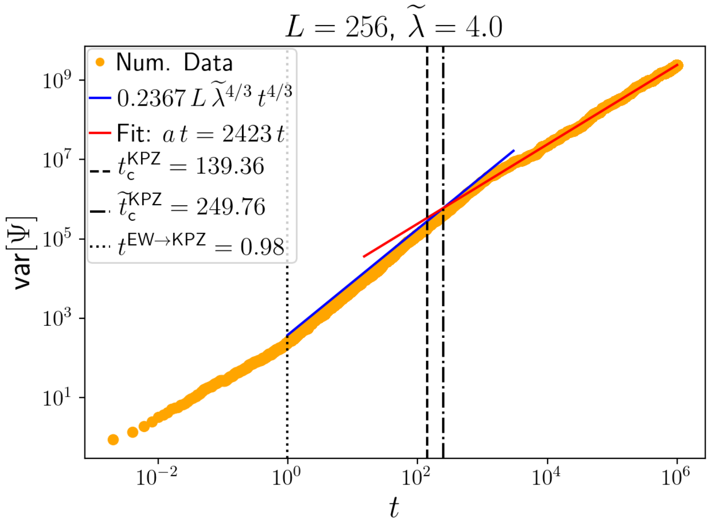

Figure 7.7: Exemplary determination of the numerical KPZ correlation time $\widetilde{t}_c^{\mathrm{KPZ}}$ for $\widetilde{\lambda} = 4.0$.

time $\widetilde{t}_c^{\mathrm{KPZ}}$. In particular, we search the time at which the transient behavior according to (7.36) becomes equal to the stationary branch. Here we determine the latter by fitting the numerical data in the stationary KPZ regime via a fit-function $a\,t$, with a the fit-parameter. Hence, we find for $\widetilde{t}_c^{\mathrm{KPZ}}$,

$$\widetilde{t}_c^{\mathrm{KPZ}} = \left(\frac{8\,\pi^{2/3}\,\widetilde{\nu}^{5/3}\,a}{3\,\Gamma(2/3)\,\widetilde{\Delta}_0^{5/3}\,\widetilde{\lambda}^{4/3}\,L} \right)^3 . \tag{7.37}$$

Table 7.4 shows the numerically obtained $\widetilde{t}_c^{\mathrm{KPZ}}$ and t_c^{KPZ} from (3.44) in dependence of $\widetilde{\lambda}$. For all values of $\widetilde{\lambda}$ the numerically obtained correlation time $\widetilde{t}_c^{\mathrm{KPZ}}$ is roughly a factor of 2 larger than the one from (3.44). To be precise

$$\widetilde{t}_{\mathrm{c}}^{\mathrm{KPZ}} = (2.18 \pm 0.46)\, t_{\mathrm{c}}^{\mathrm{KPZ}}, \tag{7.38}$$

where the factor is the mean of the right hand column of Table 7.4 and the error the standard deviation of the mean. The numerical result in (7.38) is compatible with the one obtained by equating (6.32) with (6.35) and solving for the correlation time. The discrepancy between $\widetilde{t}_{\mathrm{c}}^{\mathrm{KPZ}}$ and $t_{\mathrm{c}}^{\mathrm{KPZ}}$ may, at least qualitatively, be explained by finite size effects. In particular, $t_{\mathrm{c}}^{\mathrm{KPZ}}$ from (3.44) uses the universal amplitude c_2 with the numerically determined value $c_2 \approx 0.4$ and $0.21 \approx 1/(12\, c_2)$ (see Section 3.2.1). This numerical value of c_2, however, results for $b \to \infty$ from the integral $c_2(b) = \int_{2\pi\xi/b}^{\infty} ds g(s)/s^2$ with ξ the KPZ correlation length and $g(s)$ the scaling function of the surface width (see Section 3.2.1). Evaluating this integral for any finite value of b (e.g., $b = L = 256$) with its finite lower integration limit would lead to a value $c_2 < 0.4$ and thus to a larger correlation time $t_{\mathrm{c}}^{\mathrm{KPZ}}$. We expect this consideration to qualitatively resolve the discrepancy between $t_{\mathrm{c}}^{\mathrm{KPZ}}$ and $\widetilde{t}_{\mathrm{c}}^{\mathrm{KPZ}}$. The general, explicit evaluation of this integral seems to be out of reach, however.
Let us use (7.38) to reevaluate the universal scaling amplitude c_0 from (6.35) according to the calculation in (6.34), which leads to

$$\begin{aligned} \mathcal{A}\, \widetilde{t}_{\mathrm{c}}^{\mathrm{KPZ}} &= \frac{3\,\Gamma(2/3)}{8\,\pi^{2/3}}\, \frac{\widetilde{\Delta_0}^{5/3}\, \widetilde{\lambda}^{4/3}}{\widetilde{\nu}^{5/3}}\, L\, \left(\widetilde{t}_{\mathrm{c}}^{\mathrm{KPZ}}\right)^{4/3}, \\ \mathcal{A} &= (0.45 \pm 0.03) \left(\frac{\widetilde{\Delta}_0}{2\,\widetilde{\nu}}\right)^{3/2} \widetilde{\lambda}\, L^{1/2}\,. \end{aligned} \tag{7.39}$$

Hence, we get for the universal scaling amplitude c_0,

$$c_0 = (0.45 \pm 0.03), \tag{7.40}$$

where the theoretically predicted value from [20, 115] is $\sqrt{\pi}/4 \approx 0.44$, which is well inside the error bars of (7.40). Thus, by using the numerically obtained value of the KPZ correlation time, $\widetilde{t}_{\mathrm{c}}^{\mathrm{KPZ}}$ from (7.38), and the DRG result for the variance of $\Psi(t)$ from (7.36) in the transient regime with the matching condition from (6.33) we are able to obtain the universal scaling amplitude from (6.35) to good accuracy (see (7.40)). The result in (7.40) is a considerable improvement of (6.34) which used $t_{\mathrm{c}}^{\mathrm{KPZ}}$ from (3.44).

Table 7.4: Numerical Estimation of $\widetilde{t}_{\mathrm{c}}^{\mathrm{KPZ}}$

$\widetilde{\lambda}$	$t_{\mathrm{c}}^{\mathrm{KPZ}}$	$\widetilde{t}_{\mathrm{c}}^{\mathrm{KPZ}}$	$\widetilde{t}_{\mathrm{c}}^{\mathrm{KPZ}}/t_{\mathrm{c}}^{\mathrm{KPZ}}$
0.87	640.74	1839.26	2.87
1.0	557.45	1446.18	2.59
1.25	445.96	745.42	1.67
1.5	371.63	1032.80	2.78
1.75	318.54	584.15	1.83
2.0	278.72	524.67	1.88
2.5	222.98	496.44	2.23
3.0	185.82	363.50	1.96
4.0	139.36	249.76	1.79

Numerical values of the theoretically predicted KPZ correlation time $t_{\mathrm{c}}^{\mathrm{KPZ}}$ from (3.44) and the numerically obtained $\widetilde{t}_{\mathrm{c}}^{\mathrm{KPZ}}$ (see Figure 7.7) in dependence of $\widetilde{\lambda}$ and for $L = 256$. The right column shows the ratio of the two correlation times.

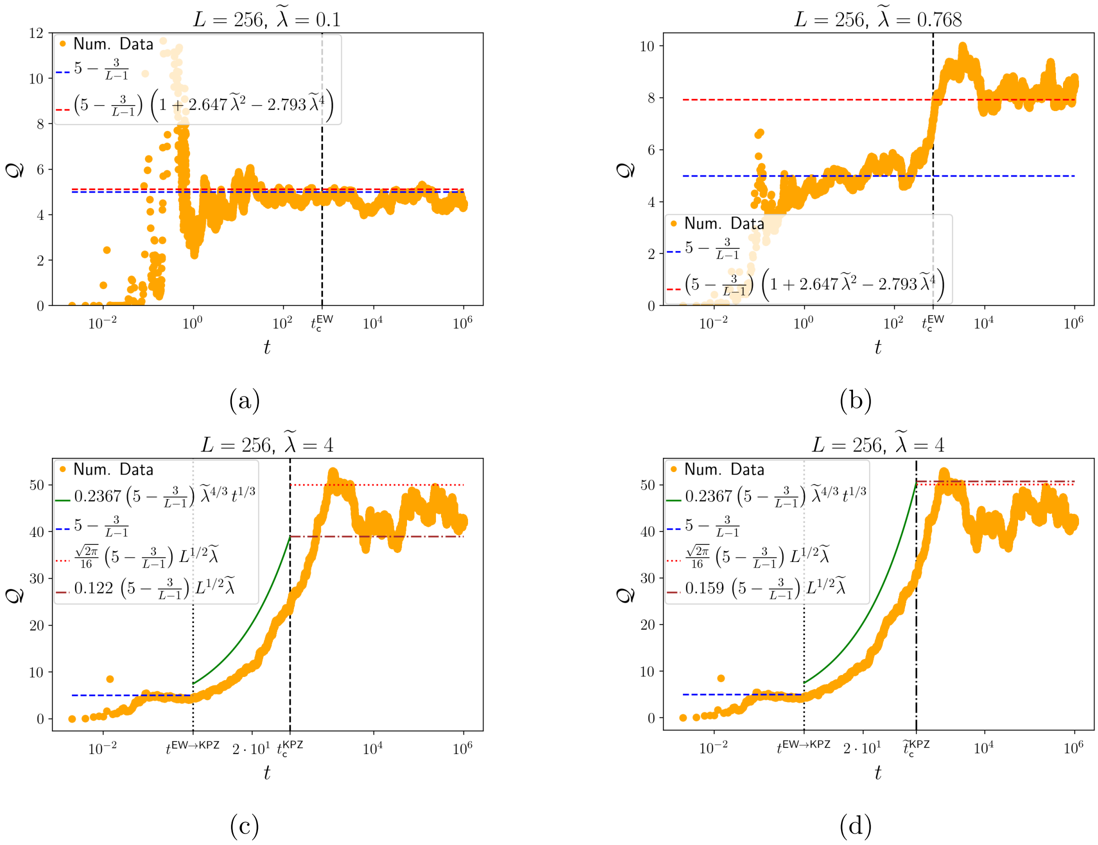

Figure 7.8: Comparison of numerical data obtained for $L = 256$ and $\widetilde{\lambda} = 0.1$, $\widetilde{\lambda} = 0.768 \approx \widetilde{\lambda}^{\mathrm{c}}$ and $\widetilde{\lambda} = 4.0$ with the theoretical prediction of the TUR product $\mathcal{Q}$ both in the EW scaling regime of the KPZ equation, (a) and (b), as well as in the KPZ regime, (c), (d). Note, that in (d) we use the numerically obtained values for $\widetilde{t}_{\mathrm{c}}^{\mathrm{KPZ}}$ from (7.38) and for c_0 from (7.40).

7.4.4 TUR Product $\mathcal{Q}$

For the scaling form of the TUR product $\mathcal{Q}$, we obtain via (7.19), (7.26), (7.34) and (7.36),

$$\mathcal{Q} \simeq \left(5 - \frac{3}{L-1}\right) \begin{cases} \left(1 + L\,\frac{\widetilde{\Delta}_0\,\widetilde{\lambda}^2}{\widetilde{\nu}^3}\,\frac{\mathcal{S}_1(L)}{32\,\pi^2} - L^2\,\frac{\widetilde{\Delta}_0^2\,\widetilde{\lambda}^4}{\widetilde{\nu}^6}\,\frac{\mathcal{S}_2(L)}{256\,\pi^4}\right), & \text{for } \lambda_{\text{eff}} \lessapprox \lambda_{\text{eff}}^{\text{c}}, \\ \frac{\sqrt{\pi}}{8\sqrt{2}}\,\frac{\widetilde{\Delta}_0^{1/2}\,\widetilde{\lambda}}{\widetilde{\nu}^{3/2}}\,L^{1/2}, & \text{for } \lambda_{\text{eff}}^{\text{c}} \ll \lambda_{\text{eff}}. \end{cases} \tag{7.41}$$

In Figure 7.8 we show for the three specific values of $\widetilde{\lambda}$ from Section 7.4.1 the time-evolution of the TUR product $\mathcal{Q}$. As can be seen for the two cases of $\widetilde{\lambda} \leq \widetilde{\lambda}^{\text{c}}$, Figure 7.8(a), (b), the perturbation expansion from (7.41) yields convincing agreement with the numerical data for times $t \geq t_{\text{c}}^{\text{EW}}$. To demonstrate the effect of the higher order contributions in the perturbation scheme, we also plot the zero-order result for reference. In Figure 7.8(c), (d), i.e., in the KPZ scaling regime, we find that for times $t \leq t^{\text{EW}\to\text{KPZ}}$ the TUR product $\mathcal{Q}$ converges to the EW scaling result, namely $\mathcal{Q} = 5 - 3/(L-1)$. For times $t \geq t_{\text{c}}^{\text{KPZ}}$ we see the final convergence to the KPZ steady state result of $\mathcal{Q}$, where in Figure 7.8(c) the upper horizontal line indicates $\mathcal{Q}$ according to (7.41) and the lower line represents the result one obtains by using (6.34). Both can be seen as reasonable approximations to the steady state value of $\mathcal{Q}$, however, in the light of the results regarding the numerical correlation time $\widetilde{t}_{\text{c}}^{\text{KPZ}}$ and the then resulting universal scaling amplitude in (7.40), we regard the upper line as the more reliable one. This is further supported by the observation in Sections 7.3.4 and 7.3.5 and Appendix 7.A that the numerical scheme intrinsically underestimates the TUR product $\mathcal{Q}$. For the theoretical prediction in the transient regime of the KPZ equation in Figure 7.8(c) we rely on the assumption that the steady-state results of $\langle\Psi(t)\rangle^2$ from (7.19) and $\langle\Delta s_{\text{tot}}\rangle$ from (7.26) yield reasonable approximations even for times t smaller than the KPZ correlation time $t_{\text{c}}^{\text{KPZ}}$. This is to some extent justified by the findings in Figure 7.4. We thus expect for $t^{\text{EW}\to\text{KPZ}} < t < t_{\text{c}}^{\text{KPZ}}$ using (7.36),

$$\mathcal{Q} = \left(5 - \frac{3}{L-1}\right) \frac{3\,\Gamma(2/3)}{8\,\pi^{2/3}}\,\frac{\widetilde{\Delta}_0^{2/3}}{\widetilde{\nu}^{5/3}}\,\widetilde{\lambda}^{4/3}\,t^{1/3}, \tag{7.42}$$

which is what we plotted in Figure 7.8(c). As can be seen, the expression in (7.42) predicts the transient time-behavior well. The slight offset may either be a result of the intrinsic numerical underestimation of $\mathcal{Q}$ or originate in a minor error in the DRG result from (7.36) in terms of the numerical prefactor c_0. In Figure 7.8(d), we show the same graphs as in Figure 7.8(c). However, here we use the numerically obtained value of the KPZ correlation time, $\widetilde{t}_{\text{c}}^{\text{KPZ}}$ from (7.38), and the corresponding reevaluated universal scaling amplitude from (7.40), which replaces the numerical prefactor in (6.34). This

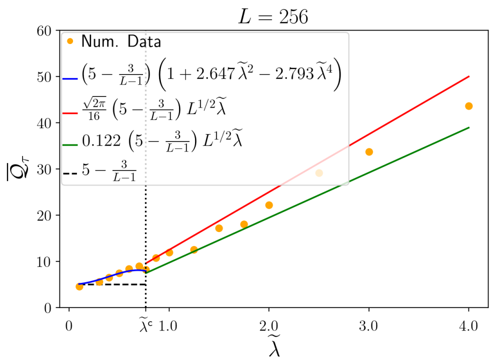

(a)

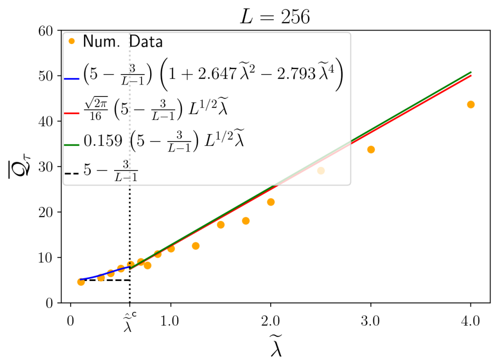

(b)

Figure 7.9: Display of the numerical steady state values of the TUR product $\overline{\mathcal{Q}}_\tau$, obtained as time averages for times $t \geq \tau = 10^4$ in dependence of $\widetilde{\lambda}$. The solid lines represent the theoretical predictions in the two scaling regimes. In (a), these are taken from (6.34) and (7.41), whereas in (b) we used (7.38) and (7.40) to reevaluate (6.34).

leads to closing the gap between the two stationary results in the KPZ regime and thus smoothes the transition between the two branches of (7.36) for times $t > t^{\mathrm{EW}\to\mathrm{KPZ}}$. In Figure 7.9 we show the TUR product in dependence of $\widetilde{\lambda}$. The values for $\overline{\mathcal{Q}}_\tau$ are obtained by calculating the temporal average in the KPZ stationary state of $\mathcal{Q}$ for times $t \geq \tau = 10^4$. We expect the numerical data to follow the prediction in (7.41), which it does with good agreement as can be seen in Figure 7.9. Here the solid line below $\widetilde{\lambda}^{\mathrm{c}}$ represents the perturbative result and is compared to the zero-order result depicted as the horizontal dashed line. In Figure 7.9(a) we show for $\widetilde{\lambda} > \widetilde{\lambda}^{\mathrm{c}}$, with $\widetilde{\lambda}^{\mathrm{c}}$ from (7.29) for $L = 256$, the theoretical predictions according to (6.34) and (7.41), i.e., for the KPZ correlation time from (3.44). On the other hand, Figure 7.9(b) displays the same theoretical predictions, reevaluated with the numerically obtained KPZ correlation time from (7.38) and the ensuing c_0 from (7.40). Using the KPZ correlation time $\widetilde{t}_{\mathrm{c}}^{\mathrm{KPZ}}$ from (7.38) demands also a reevaluation of the critical value of the coupling parameter. Repeating the calculation of (3.51) in Section 6.3, we obtain for the numerically determined KPZ correlation time $\widetilde{t}_{\mathrm{c}}^{\mathrm{KPZ}}$ an effective critical coupling parameter of

$$\hat{\lambda}_{\mathrm{eff}}^{\mathrm{c}} \approx 9.47, \tag{7.43}$$

and thus for a system size of $L = 256$

$$\hat{\widetilde{\lambda}}^{\mathrm{c}} \approx 0.592, \tag{7.44}$$

which is shown in Figure 7.9(b). As can be seen and is to be expected, using (7.38), (7.40) and (7.44) causes the two solid lines in Figure 7.9(b) for $\widetilde{\lambda} > \hat{\widetilde{\lambda}}^{\mathrm{c}}$ to almost coincide and shrinks the jumps at the critical $\widetilde{\lambda}$ significantly in comparison to Figure 7.9(a) (see also Figure 7.8(c), (d)). Another effect of introducing $\hat{\widetilde{\lambda}}^{\mathrm{c}}$ is that for $\widetilde{\lambda} < \hat{\widetilde{\lambda}}^{\mathrm{c}}$ the 4th-order perturbation expansion from (7.41) is cut off before it reaches its local maximum (as opposed to Figure 7.9(a)), which seems to be a physically more reasonable behavior.

Appendix 7.A Analytical Test of the Generalized Discretization for the KPZ–Non-Linearity

7.A.1 Implications of Poor Regularity

In Appendix 3.A.5 we have shown that $\left\langle \|\partial_x h^{(0)}\|^2_{\mathcal{L}^2} \right\rangle = \left\langle \int dx\, (\partial_x h^{(0)})^2 \right\rangle$ is not a well-defined quantity. Using Hölders inequality for the expectation, one gets

$$\left\langle \int dx\, (\partial_x h^{(0)})^2 \right\rangle \leq \left(\left\langle \int dx\, (\partial_x h^{(0)})^4 \right\rangle \right)^{1/2}, \tag{7.45}$$

which shows that $\left\langle \int dx\, (\partial_x h^{(0)})^4 \right\rangle = \left\langle \|(\partial_x h^{(0)})^2\|^2_{\mathcal{L}^2} \right\rangle$ is not well defined either. These two expressions do, however, play an important role in determining the TUR constituents. Hence, some form of regularization is needed to make these expressions well-defined. In Chapter 5, this was accomplished by introducing a cutoff Λ of the Fourier-spectrum, i.e., $|k| \leq \Lambda$.

Here, we will follow a different path. Since the solution of the Edwards-Wilkinson equation given by

$$h^{(0)}(x,t) \equiv \sum_{k\in\mathbb{Z}} h_k^{(0)}(t) e^{2\pi i k x} \tag{7.46}$$

is expected to be a reasonable approximation to the solution of the KPZ equation (3.3) for $\lambda \ll 1$, we approximate the KPZ non-linearity $(\partial_x h)^2$ by $(\partial_x h^{(0)})^2$. The Fourier-coefficients $h_k^{(0)}$ are given by

$$h_k^{(0)}(t) = e^{\mu_k t} \int_0^t dr\, e^{-\mu_k r} \eta_k(r), \tag{7.47}$$

where $\mu_k = -4\pi^2 k^2$ (see (5.3)) and η_k is the k-th Fourier-coefficient of $\eta(x,t) = \sum_k \eta_k e^{2\pi i k x}$, i.e., the Fourier-series of the KPZ noise from (3.3). This procedure is equivalent to solving the KPZ equation by a low order perturbation solution with respect to λ, which was performed in Chapter 5. We then replace in $\left\langle \int_0^1 dx\, (\partial_x h^{(0)})^2 \right\rangle$ and $\left\langle \int_0^1 dx\, (\partial_x h^{(0)})^4 \right\rangle$ the non-linearity $(\partial_x h^{(0)})^2$ with any of its generalized discretizations

$\mathcal{N}_\delta^{(\gamma)}[h^{(0)}]$,

$$\left\langle \int_0^1 dx\, \mathcal{N}_\delta^{(\gamma)}[h^{(0)}(x,t)] \right\rangle, \tag{7.48}$$

$$\left\langle \int_0^1 dx\, \left(\mathcal{N}_\delta^{(\gamma)}[h^{(0)}(x,t)]\right)^2 \right\rangle, \tag{7.49}$$

where we have defined

$$\begin{aligned} &\mathcal{N}_\delta^{(\gamma)}[h^{(0)}(x)] \\ &\equiv \frac{1}{2(\gamma+1)\delta^2}\left[\left(h^{(0)}(x+\delta)-h^{(0)}(x)\right)^2 + 2\gamma\left(h^{(0)}(x+\delta)-h^{(0)}(x)\right)\right. \\ &\left.\times\left(h^{(0)}(x)-h^{(0)}(x-\delta)\right) + \left(h^{(0)}(x)-h^{(0)}(x-\delta)\right)^2\right] \end{aligned} \tag{7.50}$$

as the continuum variant of (7.4). For simplicity, as the operator only acts on x we omit the time t in the above equation. Of course, the expressions from (7.48), (7.49) will diverge for $\delta \to 0$. The necessary regularization of these expressions is performed by introducing a smallest $\delta > 0$.
Both ways of regularization are based on the physical idea of introducing a smallest length scale [104], here in real space and in Chapter 5 in Fourier space, so their respective results are directly comparable to one another.

7.A.2 Expected Integral Norms of the Non-Linearity

The expectation of the $\mathcal{L}^1$-norm of $\mathcal{N}_\delta^{(\gamma)}[h^{(0)}]$ from (7.48) is evaluated for $t \gg 1$ and $\delta \ll 1$ as

$$\left\langle \int_0^1 dx\, \mathcal{N}_\delta^{(\gamma)}[h^{(0)}(x,t)] \right\rangle \simeq \frac{1}{2(\gamma+1)\delta}, \tag{7.51}$$

where the details of the calculation are given in Appendix 7.B. Similarly, the expectation of the $\mathcal{L}^2$-norm squared from (7.49) reads

$$\left\langle \int_0^1 dx\, \left(\mathcal{N}_\delta^{(\gamma)}[h^{(0)}(x,t)]\right)^2 \right\rangle \simeq \frac{2+\gamma^2}{4\,(\gamma+1)^2\,\delta^2}, \tag{7.52}$$

as shown in Appendix 7.C. The expressions in (7.51) and (7.52) being divergent for $\delta \to 0$ reflect the regularity issues from above.

7.A.3 Approximations of the TUR Constituents

We now establish how the expressions in (7.48) and (7.49) are related to the respective constituents of the thermodynamic uncertainty relation.

The Output Functional

Consider the dimensionless form of the KPZ equation from (3.3) (see, e.g., (3.10)). Performing a spatial integration within the boundaries $(0, 1)$ yields with the definition of the output functional $\Psi(t)$ from (5.53)

$$\begin{aligned}
&\partial_{t_s}\Psi_s(t_s) \\
&= \int_0^1 dx_s\, \partial_{x_s}^2 h_s(x_s,t_s) + \frac{\lambda_{\text{eff}}}{2}\int_0^1 dx_s\; (\partial_{x_s} h_s(x_s,t_s))^2 + \int_0^1 dx_s\, \eta_s(x_s,t_s).
\end{aligned} \tag{7.53}$$

Due to the periodic boundary conditions the diffusive term vanishes. A subsequent averaging leads to

$$\langle \partial_{t_s}\Psi_s(t_s)\rangle = \frac{\lambda_{\text{eff}}}{2}\left\langle \int_0^1 dx_s\; (\partial_{x_s} h_s(x_s,t_s))^2 \right\rangle. \tag{7.54}$$

In the NESS, (7.54) becomes

$$\partial_{t_s}\langle \Psi_s(t_s)\rangle = \lim_{t_s\to\infty}\frac{\lambda_{\text{eff}}}{2}\left\langle \int_0^1 dx_s\; (\partial_{x_s} h_s(x_s,t_s))^2 \right\rangle. \tag{7.55}$$

We now approximate the right hand side of (7.55) by (7.48) and thus we find with (7.51) for the output functional in lowest non-vanishing order of λ_{eff} and for $t_s \gg 1$

$$\langle \Psi_s(t_s)\rangle_\delta^{(\gamma)} \simeq \frac{\lambda_{\text{eff}}}{4}\frac{1}{(\gamma+1)\,\delta}\, t_s. \tag{7.56}$$

The Total Entropy Production

From Section 5.4, we know that in the NESS $\langle \Delta s_{\text{tot}}\rangle = \sigma\, t_s$ holds with σ as the dimensionless entropy production rate given by

$$\sigma = \lim_{t_s\to\infty}\frac{\lambda_{\text{eff}}^2}{2}\left\langle \int_0^1 dx_s\; \left[(\partial_{x_s} h_s(x_s,t_s))^2\right]^2 \right\rangle, \tag{7.57}$$

where we now approximate the right hand side of (7.57) by (7.49). Hence, with (7.52) we obtain for the entropy production rate for $t_s \gg 1$

$$\sigma_\delta^{(\gamma)} \simeq \frac{\lambda_{\text{eff}}^2}{8}\frac{2+\gamma^2}{(\gamma+1)^2\,\delta^2}. \tag{7.58}$$

The Variance

We have

$$\text{var}[\Psi_s(t_s)] = \left\langle (\Psi_s(t_s))^2\right\rangle - \langle \Psi_s(t_s)\rangle^2, \tag{7.59}$$

where

$$\Psi_s(t_s) = \int_0^1 dx_s\, h_s(x_s, t_s) = h_0(t_s), \tag{7.60}$$

with $h_0(t)$ the zero-th coefficient of the Fourier series $h(x,t) = \sum_k h_k(t)e^{2\pi ikx}$ for the KPZ solution. The h_k may be expanded in terms of the effective coupling constant λ_{eff} and to lowest non-vanishing order it reduces to $h_k(t) \approx h_k^{(0)}(t)$, where the latter corresponds to the solution of the Edwards-Wilkinson equation ($\lambda_{\text{eff}} = 0$). Hence, to lowest non-vanishing order we get from (7.60)

$$\begin{aligned}\left\langle (\Psi_s(t_s))^2 \right\rangle &\simeq \left\langle \left(h_0^{(0)}(t_s)\right)^2 \right\rangle = \left\langle \left(\int_0^{t_s} d\tau_s\, \eta_0(t_s)\right)^2 \right\rangle \\ &= \int_0^{t_s} dr_s \int_0^{t_s} ds_s\, \langle \eta_0(r_s)\eta_0(s_s)\rangle = \int_0^{t_s} d\tau_s = t_s,\end{aligned} \tag{7.61}$$

where (7.47) and the relation $\langle \eta_0(r)\eta_0(s)\rangle = \delta(r-s)$ have been used. The second term in (7.59) is known from (7.56) and thus gives no contribution to the $O(\lambda_{\text{eff}}^0)$-term from (7.61). However, for completeness we note that the next non-vanishing term in a λ_{eff}-expansion of $\left\langle (\Psi_s(t_s))^2 \right\rangle$ is $O(\lambda_{\text{eff}}^2)$ and the prefactor of λ_{eff}^2 contains the contribution $1/((\gamma+1)^2\delta^2)t_s^2$, which cancels the second term in (7.59). This is similar to the continuum case in Chapter 5. Thus, to lowest non-vanishing order in λ_{eff}, the variance is for all $0 \leq \gamma \leq 1$ given by

$$\operatorname{var}\left[\Psi_s(t_s)\right]_\delta^{(\gamma)} \simeq t_s, \tag{7.62}$$

in dimensionless form.

The Discrete TUR Product

As the variance from (7.62) is to lowest order identical to the theoretical predicted one, the TUR product as a function of γ, denoted by $\mathcal{Q}_\delta^{(\gamma)}$, reads with (7.56) and (7.58) for $\delta \ll 1$, $t_s \gg 1$

$$\begin{aligned}\mathcal{Q}_\delta^{(\gamma)} &= \langle \Delta s_{\text{tot}}\rangle_\delta^{(\gamma)} \frac{t_s}{\left(\langle \Psi_s(t_s)\rangle_\delta^{(\gamma)}\right)^2} \simeq \frac{\lambda_{\text{eff}}^2}{8} \frac{(2+\gamma^2)}{\delta^2\,(\gamma+1)^2}\, t_s\, \frac{t_s}{\frac{\lambda_{\text{eff}}^2}{16}\frac{1}{\delta^2\,(\gamma+1)^2}\, t_s^2} \\ &= 2\,(2+\gamma^2) = \begin{cases} 4 & \text{for} \quad \gamma = 0 \\ 9/2 & \text{for} \quad \gamma = 1/2 \\ 6 & \text{for} \quad \gamma = 1 \end{cases}.\end{aligned} \tag{7.63}$$

Since $\mathcal{Q}_\delta^{(\gamma)}$ is monotonously increasing with γ, the case of $\gamma = 0$ represents a lower bound on the TUR product. Hence, the TUR is clearly not saturated as was predicted in Chapter 5.

Compared to Chapter 5, we here follow an independent path in obtaining the TUR product in (7.63). Instead of using a Fourier space representation, we derive the TUR product from real space calculations. In particular, we introduce a smallest length scale δ in real space as the regularizing parameter opposed to a cutoff parameter in the Fourier spectrum in Chapter 5. In other words, we work here with the full Fourier spectrum but have to approximate the non-linearity by (7.50), whereas in Chapter 5 we calculated the exact non-linearity, but only on a finite Fourier spectrum with $|k| \leq \Lambda$. Below we connect these two approaches. We note that the divergences of $\langle \Psi(t) \rangle^2$ and $\langle \Delta s_{\text{tot}} \rangle$ are in the present representation in $1/\delta^2$ for $\delta \to 0$, whereas in Chapter 5 these expressions diverge in Λ^2 for $\Lambda \to \infty$. Thus, the analysis above may well be understood as an alternative way of calculating the thermodynamic uncertainty relation.

7.A.4 Comparison of the Approximated TUR Constituents with the Theoretical Predictions

To compare the results of the approximated TUR components in (7.56) and (7.58) to the theoretical predictions from Chapter 5, we need to express the lattice-spacing δ in terms of the Fourier-cutoff Λ used there. On the interval $(0,1)$, the lattice-spacing is given by $\delta = 1/L$, with L the number of grid-points. Using the link between L and Λ from (7.15) leads to

$$\delta = \frac{1}{L} = \frac{1}{3\Lambda + 1} \approx \frac{1}{3\Lambda}, \tag{7.64}$$

where the last step holds for large enough Λ. Thus, with the theoretical predictions for $\langle \Psi_s(t_s) \rangle^2$ and $\langle \Delta s_{\text{tot}} \rangle$ from Chapter 5 given by

$$\langle \Psi_s(t_s) \rangle^2 \simeq \frac{\lambda_{\text{eff}}^2}{4} \, \Lambda^2 \, t_s^2, \tag{7.65}$$

$$\langle \Delta s_{\text{tot}} \rangle \simeq \frac{\lambda_{\text{eff}}^2}{4} \left[5\,\Lambda^2 - \Lambda \right] \, t_s, \tag{7.66}$$

we can calculate the relative deviation Δ of $\left(\langle \Psi(t) \rangle_\delta^{(\gamma)} \right)^2$ and $\langle \Delta s_{\text{tot}} \rangle_\delta^{(\gamma)}$, respectively. For the expectation of the output functional squared we obtain for $\Lambda \gg 1$ with (7.64), (7.65) and (7.56)

$$\begin{aligned} \Delta \left[\left(\langle \Psi_s(t_s) \rangle_\delta^{(\gamma)} \right)^2 \right] &\equiv \frac{\langle \Psi_s(t_s) \rangle^2 - \left(\langle \Psi_s(t_s) \rangle_\delta^{(\gamma)} \right)^2}{\langle \Psi_s(t_s) \rangle^2} \\ &= 1 - \frac{9}{4\,(\gamma+1)^2}. \end{aligned} \tag{7.67}$$

Analogously, we get for the relative deviation of $\langle \Delta s_{\text{tot}} \rangle_\delta^{(\gamma)}$ for $\Lambda \gg 1$ and with (7.64), (7.66) and (7.58)

$$\begin{aligned} \Delta\left[\langle \Delta s_{\text{tot}} \rangle_\delta^{(\gamma)}\right] &\equiv \frac{\langle \Delta s_{\text{tot}} \rangle - \langle \Delta s_{\text{tot}} \rangle_\delta^{(\gamma)}}{\langle \Delta s_{\text{tot}} \rangle} \\ &= 1 - \frac{9}{10} \frac{2+\gamma^2}{(\gamma+1)^2}. \end{aligned} \tag{7.68}$$

With the theoretical prediction from Chapter 5,

$$\mathcal{Q} = \langle \Delta s_{\text{tot}} \rangle \, \epsilon^2 \simeq 5 - \frac{1}{\Lambda} \approx 5, \tag{7.69}$$

where the last step holds for $\Lambda \gg 1$, we calculate the relative deviation of the thermodynamic uncertainty product according to

$$\Delta\left[\mathcal{Q}_\delta^{(\gamma)}\right] = 1 - \frac{2}{5}\,(2+\gamma^2). \tag{7.70}$$

In Table 7.5 we show the relative deviations of all three quantities for some significant values of γ. As can be seen, the overall best result is obtained for $\gamma = 1/2$. For all other

Table 7.5: Relative deviations Δ

	Δ		
γ	$\left(\langle \Psi(t) \rangle_\delta^{(\gamma)}\right)^2$	$\langle \Delta s_{\text{tot}} \rangle_\delta^{(\gamma)}$	$\mathcal{Q}_\delta^{(\gamma)}$
0	$-5/4$	$-8/10$	$1/5$
0.392	-0.161	0	0.138
$1/2$	0	$1/10$	$1/10$
$1/\sqrt{2}$	0.228	0.228	0
1	$7/16$	$13/40$	$-1/5$

Overview of the relative errors of the approximated TUR components from (7.56) and (7.58) as well as of the TUR product itself from (7.63). A negative sign in Δ indicates that the respective approximated value overestimates the theoretically predicted one and vice versa for a positive sign of Δ.

choices of γ as displayed in Table 7.5, either all the relative errors are greater or, if one of the three errors is chosen to be zero, the two others turn out to be larger than the respective ones for $\gamma = 1/2$. In fact, $\gamma = 1/2$ minimizes the target function

$$F(\gamma) \equiv \left(\Delta[(\langle \Psi_s(t_s) \rangle_\delta^{(\gamma)})^2]\right)^2 + \left(\Delta[\langle \Delta s_{\text{tot}} \rangle_\delta^{(\gamma)}]\right)^2 + w\left(\Delta[\mathcal{Q}_\delta^{(\gamma)}]\right)^2, \tag{7.71}$$

for $w = 2$. Choosing, e.g., $w = 1, 3$ results in $\gamma = 0.48, 0.52$, respectively. Hence, $\gamma = 1/2$ provides in a natural sense a much better approximation than $\gamma = 0, 1$.
The main purpose of the above analysis was to confirm and explain our key numerical findings from Figure 7.1, Table 7.1 and Figure 7.2, Table 7.2. Namely, that for $\gamma = 1/2$ the error of $\left\langle \Psi^{(N)}(t) \right\rangle^2$ nearly vanishes, while $\langle \Delta s_{\mathrm{tot}} \rangle$ is underestimated by roughly 10% and consequently the TUR product is underestimated by roughly 10% as well (see Table 7.3). These findings are confirmed by the corresponding analytical results in Table 7.5 and (7.63). Furthermore, we infer from the analysis above that the deviation for $\langle \Delta s_{\mathrm{tot}} \rangle^{(N)}$ (and thus for the TUR) cannot be reduced by changing the parameters of the numerical scheme like lattice-size $\delta = \Delta x$ or the time step Δt. It is instead caused by an intrinsic property of the non-linear operator $\mathcal{N}_\delta^{(1/2)}$ which recovers the correct scaling of $\left\langle \int_0^1 dx\, (\partial_x h^{(0)})^2 \right\rangle$, but underestimates the prefactor in the scaling form of $\left\langle \int_0^1 dx\, (\partial_x h^{(0)})^4 \right\rangle$ by exactly 10%.

7.A.5 Numerical Results for the Generalized Discretization of the Non-Linearity

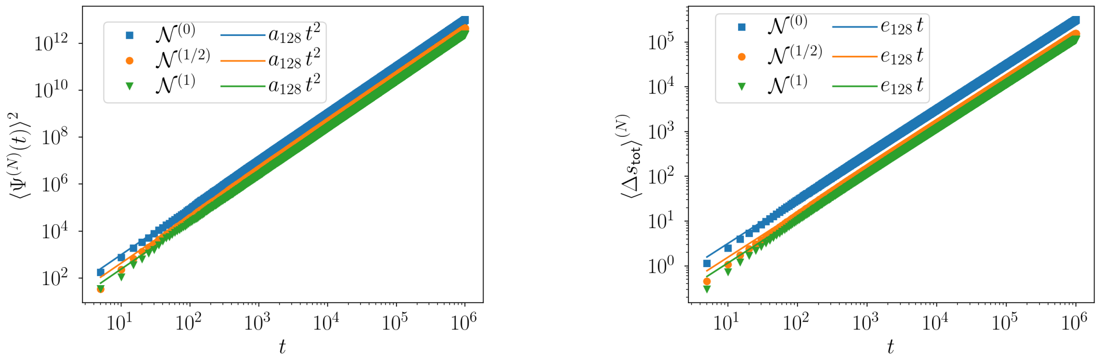

Figure 7.10: $\left\langle \Psi^{(N)}(t) \right\rangle^2$ and $\langle \Delta s_{\mathrm{tot}} \rangle^{(N)}$ from (7.19) and (7.26), respectively, for $\mathcal{N}_l^{(\gamma)}$ with $\gamma = 0,\, 1/2,\, 1$. The dots represent the numerical data for $\{\widetilde{\nu}, \widetilde{\Delta_0}, \widetilde{\lambda}\} = \{1.0, 1.0, 0.1\}$, $\Delta t = 10^{-2}$, $E = 250$ and $L = 128$. The straight lines show fits according to (7.30) and (7.33) with fit-parameters a_L and e_L, respectively.

The above analytical results from (7.63) as well as Table 7.5 are confirmed by additional numerical simulations for $\mathcal{N}_l^{(\gamma)}$ with $\gamma = 0,\, 1/2,\, 1$. Figure 7.10 shows the data for $\left\langle \Psi^{(N)}(t) \right\rangle^2$ and $\langle \Delta s_{\mathrm{tot}} \rangle^{(N)}$ from (7.19) and (7.26), respectively. We quantify the significant differences between the respective graphs in Table 7.6. A comparison of the numerically found relative errors Δ in Table 7.6 to those analytically obtained in Ta-

Table 7.6: Scaling factors of $\left\langle\Psi^{(N)}(t)\right\rangle^2$ and $\langle\Delta s_{\mathrm{tot}}\rangle^{(N)}$

γ	fit-values		Δ [%]
0	a_{128}	9.98	-123
	e_{128}	0.315	-81
1/2	a_{128}	4.39	2
	e_{128}	0.155	11
1	a_{128}	2.44	46
	e_{128}	0.116	33

Comparison of the predicted scaling factors $c_1^2(L)$ and $c_4(L)$ from (7.19) and (7.26) to a_L and e_L from (7.30) and (7.33) for the fits as shown in Figure 7.10. Here $\Delta = (c_1^2(L) - a_L)/c_1^2(L)$ (and $\Delta = (c_4(L) - e_L)/c_4(L)$) denotes the respective relative errors, where a negative sign indicates that the fitted value overestimates the theoretical value and vice versa.

ble 7.5 shows very good agreement, which supports the above analysis. As the variance is not dependent on the respective choice of γ (see (7.62)), which was also reproduced by the numerics, we refrain from explicitly showing this plot as there is no discernible difference in the three graphs. Finally, we show the TUR product $\mathcal{Q}^{(N)}$ for the three different choices of γ in Figure 7.11, indicating a clear distinction between the three different discretizations and good agreement with the analytically calculated values from (7.63) represented by the dashed lines in the plot.

Appendix 7.B Expectation of the $\mathcal{L}^1$-Norm of $\mathcal{N}_\delta^{(\gamma)}[h^{(0)}(x)]$

To obtain the result in (7.51), we define

$$D_\delta^{(p,q)} h^{(0)}(x,t) \equiv \frac{h^{(0)}(x+p\delta,t) - h^{(0)}(x-q\delta,t)}{(p+q)\delta}, \tag{7.72}$$

then the expression in (7.50) may also be written as

$$\begin{aligned}\mathcal{N}_\delta^{(\gamma)}[h^{(0)}] = \frac{1}{2(\gamma+1)} \Bigg[&\left(D_\delta^{(1,0)} h^{(0)}\right)^2 + 2\gamma \left(D_\delta^{(1,0)} h^{(0)}\right)\left(D_\delta^{(0,1)} h^{(0)}\right) \\ &+ \left(D_\delta^{(0,1)} h^{(0)}\right)^2\Bigg].\end{aligned} \tag{7.73}$$

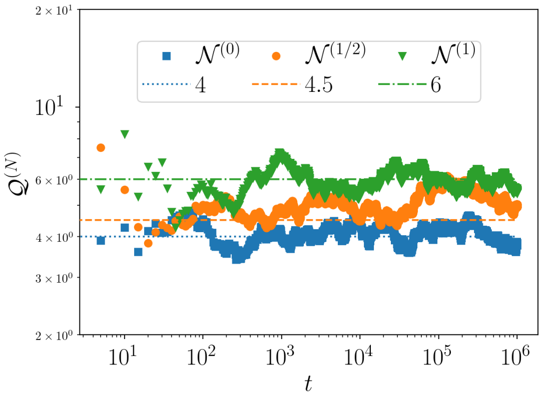

Figure 7.11: TUR product for three different discretizations of the non-linearity $\mathcal{N}_l^{(\gamma)}$ from (7.4), namely $\gamma = 0,\, 1/2,\, 1$. The dashed lines represent the analytically calculated values from (7.63) as a reference.

Using (7.73), (7.48) for $0 \le \gamma \le 1$ reads

$$\begin{aligned}
&\left\langle \int_0^1 dx\, \mathcal{N}_\delta^{(\gamma)}[h^{(0)}(x,t)] \right\rangle \\
&= \frac{1}{2(\gamma+1)} \left[\left\langle \int_0^1 dx\, \left(D_\delta^{(1,0)} h^{(0)}\right)^2 \right\rangle + \left\langle \int_0^1 dx\, \left(D_\delta^{(0,1)} h^{(0)}\right)^2 \right\rangle \right. \\
&\left. +2\gamma \left\langle \int_0^1 dx\, \left(D_\delta^{(1,0)} h^{(0)}\right) \left(D_\delta^{(0,1)} h^{(0)}\right) \right\rangle \right].
\end{aligned} \tag{7.74}$$

The first two terms in (7.74) are calculated via

$$\left\langle \int_0^1 dx\, \left(D_\delta^{(p,q)} h^{(0)}\right)^2 \right\rangle = \left\langle \int_0^1 dx\, \left(\sum_{k\in\mathbb{Z}} h_k^{(0)}(t) C_k^{(p,q)} e^{2\pi i k x} \right)^2 \right\rangle, \tag{7.75}$$

where

$$C_k^{(p,q)} \equiv \frac{e^{2\pi i k p \delta} - e^{-2\pi i k q \delta}}{(p+q)\delta}. \tag{7.76}$$

Denoting by $\overline{(\cdot)}$ the complex conjugate, the right hand side of (7.75) is evaluated as follows

$$\begin{aligned}
&\left\langle \int_0^1 dx \left(\sum_{k\in\mathbb{Z}} h_k^{(0)}(t) C_k^{(p,q)} e^{2\pi i k x} \right)^2 \right\rangle \\
&= \sum_{k,l\in\mathbb{Z}} \left\langle h_k^{(0)}(t) \overline{h^{(0)}}_l(t) \right\rangle C_k^{(p,q)} \overline{C_l^{(p,q)}} \int_0^1 dx\, e^{2\pi i (k-l) x} \\
&= \sum_{k\in\mathbb{Z}\setminus\{0\}} \left\langle h_k^{(0)}(t) \overline{h^{(0)}}_k(t) \right\rangle C_k^{(p,q)} \overline{C_k^{(p,q)}} \simeq - \sum_{k\in\mathbb{Z}\setminus\{0\}} \frac{\left| C_k^{(p,q)} \right|^2}{2\,\mu_k},
\end{aligned} \tag{7.77}$$

where we have used in the second step that $\int_0^1 dx\, e^{2\pi i(k-l)x} = \delta_{k,l}$ with $\delta_{k,l}$ the Kronecker symbol. The third step employs the two-point correlation function of $h_k^{(0)}$ from (7.85) for $t \gg 1$, with $\mu_k = -(2\pi k)^2$. Using (7.76) we get

$$- \sum_{k\in\mathbb{Z}\setminus\{0\}} \frac{\left| C_k^{(p,q)} \right|^2}{2\,\mu_k} = - \sum_{k\in\mathbb{Z}\setminus\{0\}} \frac{\left| e^{2\pi i k p \delta} - e^{-2\pi i k q \delta} \right|^2}{2\,\mu_k\,(p+q)^2\,\delta^2} = \sum_{k\in\mathbb{Z}\setminus\{0\}} \frac{1 - \cos 2\pi k(p+q)\delta}{(2\pi k(p+q)\delta)^2}. \tag{7.78}$$

With the substitution $x = 2\pi k(p+q)\delta$ and $\delta \ll 1$, we may rewrite (7.78) as

$$2 \sum_{k>0} \frac{1 - \cos 2\pi k(p+q)\delta}{(2\pi k(p+q)\delta)^2} \simeq \frac{1}{\pi(p+q)\delta} \int_0^\infty dx\, \frac{1-\cos x}{x^2}. \tag{7.79}$$

The integral in (7.79) can be evaluated by either using the residue theorem or by employing an adequate CAS, and yields $\pi/2$. Hence, the expression of (7.75) is given for $t \gg 1$ and $\delta \ll 1$ by

$$\left\langle \int_0^1 dx \left(D_\delta^{(p,q)} h^{(0)} \right)^2 \right\rangle \simeq \frac{1}{2\,(p+q)\,\delta}. \tag{7.80}$$

The last term in (7.74) is evaluated analogously. Thus by using again the property of the Fourier eigenbasis and (7.85) for $t \gg 1$ we get

$$\begin{aligned}
&\left\langle \int_0^1 dx \left(\sum_{k\in\mathbb{Z}} h_k^{(0)}(t) C_k^{(1,0)} e^{2\pi ikx} \right) \overline{\left(\sum_{l\in\mathbb{Z}} h_l^{(0)}(t) C_l^{(0,1)} e^{2\pi ilx} \right)} \right\rangle \\
&\simeq - \sum_{k\in\mathbb{Z}\setminus\{0\}} \frac{C_k^{(1,0)}\, C_{-k}^{(0,1)}}{2\,\mu_k} = \sum_{k>0} \frac{2\cos 2\pi k\delta - \cos 4\pi k\delta - 1}{(2\pi k\delta)^2} \\
&\simeq \frac{1}{2\pi\delta} \int_0^\infty dx\, \frac{2\cos x - \cos 2x - 1}{x^2} \\
&= \frac{1}{2\pi\delta} \left[\int_0^\infty dx\, \frac{1-\cos 2x}{x^2} - 2\int_0^\infty dx\, \frac{1-\cos x}{x^2} \right] = \frac{1}{2\pi\delta}\left[\pi - 2\frac{\pi}{2}\right] = 0,
\end{aligned} \tag{7.81}$$

where we have substituted $x = 2\pi k\delta$ with $\delta \ll 1$ and used the value of the integral in (7.79). Combining (7.80) and (7.81) gives (7.51).

Appendix 7.C Expectation of the $\mathcal{L}^2$-Norm Squared of $\mathcal{N}_\delta^{(\gamma)}[h^{(0)}(x)]$

To ease the calculation of (7.49), let us first rewrite (7.50) in the following way,

$$\mathcal{N}_\delta^{(\gamma)}[h^{(0)}] = \frac{1}{\gamma+1}\left[2\left(D_\delta^{(1,1)} h^{(0)}\right)^2 + (\gamma-1)\left(D_\delta^{(1,0)} h^{(0)}\right)\left(D_\delta^{(0,1)} h^{(0)}\right)\right]. \tag{7.82}$$

Hence,

$$\begin{aligned}
&\left(\mathcal{N}_\delta^{(\gamma)}[h^{(0)}]\right)^2 \\
&= \frac{1}{(\gamma+1)^2}\left[4\left[\left(D_\delta^{(1,1)} h^{(0)}\right)^2\right]^2 + (\gamma-1)^2 \left[\left(D_\delta^{(1,0)} h^{(0)}\right)\left(D_\delta^{(0,1)} h^{(0)}\right)\right]^2 \right. \\
&\left. +4(\gamma-1)\left(D_\delta^{(1,1)} h^{(0)}\right)^2 \left(D_\delta^{(1,0)} h^{(0)}\right)\left(D_\delta^{(0,1)} h^{(0)}\right)\right].
\end{aligned} \tag{7.83}$$

Consequently,

$$\begin{aligned}
&\left\langle \int_0^1 dx \left[\left(D_\delta^{(1,1)} h^{(0)}\right)^2\right]^2 \right\rangle \\
&= \sum_{\substack{k,l,n\in\mathbb{Z}\\ l,n\neq k}} \left\langle h_l^{(0)}(t) h_{k-l}^{(0)}(t) \overline{h_n^{(0)}}(t) \overline{h_{k-n}^{(0)}}(t) \right\rangle C_l^{(1,1)} C_{k-l}^{(1,1)} \overline{C_n^{(1,1)}}\, \overline{C_{k-n}^{(1,1)}},
\end{aligned} \tag{7.84}$$

where we have used (7.76). The four point correlation function can be evaluated via Wick's theorem and

$$\left\langle h_k^{(0)}(t) h_l^{(0)}(t') \right\rangle = \Pi_{k,l}(t,t')\delta_{k,-l}, \tag{7.85}$$

with

$$\Pi_{k,l}(t,t') \equiv e^{\mu_k t + \mu_l t'} \frac{1 - e^{-(\mu_l+\mu_l)(t\wedge t')}}{\mu_k + \mu_l}, \tag{7.86}$$

$\mu_k = -4\pi^2 k^2$ from (3.58). With (7.85) and (7.86), the expression in (7.84) becomes

$$\begin{aligned}
&\left\langle \int_0^1 dx \left[\left(D_\delta^{(1,1)} h^{(0)} \right)^2 \right]^2 \right\rangle \\
&= \left(\sum_{l\in\mathbb{Z}\setminus\{0\}} \Pi_{l,l}(t,t) C_l^{(1,1)} C_{-l}^{(1,1)} \right)^2 + 2 \sum_{k\in\mathbb{Z}} \sum_{l\in\mathbb{Z}\setminus\{0,k\}} \Pi_{l,l}(t,t)\Pi_{k-l,k-l}(t,t) \\
&\times C_l^{(1,1)} C_{k-l}^{(1,1)} \overline{C_l^{(1,1)}}\, \overline{C_{k-l}^{(1,1)}},
\end{aligned} \tag{7.87}$$

i.e., (7.87) results in

$$\begin{aligned}
&3 \left(\sum_{l\in\mathbb{Z}\setminus\{0\}} \Pi_{l,l}(t,t) C_l^{(1,1)} C_{-l}^{(1,1)} \right)^2 \simeq \frac{3}{4} \left(\sum_{l\in\mathbb{Z}\setminus\{0\}} \frac{\sin^2 2\pi l\delta}{(2\pi l\delta)^2} \right)^2 \\
&\simeq \frac{3}{(2\pi\delta)^2} \left(\int_0^\infty dx\, \frac{\sin^2 x}{x^2} \right)^2 = \frac{3}{(2\pi\delta)^2} \left(\frac{\pi}{2} \right)^2 = \frac{3}{16\,\delta^2},
\end{aligned} \tag{7.88}$$

where we have substituted $x = 2\pi l\delta$ for $\delta \ll 1$ and used (7.86) for $t \gg 1$. Next, we will calculate

$$\begin{aligned}
&\left\langle \int_0^1 dx \left(D_\delta^{(1,1)} h^{(0)} \right)^2 \left(D_\delta^{(1,0)} h^{(0)} \right) \left(D_\delta^{(0,1)} h^{(0)} \right) \right\rangle \\
&= \sum_{l\in\mathbb{Z}\setminus\{0\}} \Pi_{l,l}(t,t) \left| C_l^{(1,1)} \right|^2 \sum_{n\in\mathbb{Z}\setminus\{0\}} \Pi_{n,n}(t,t) \overline{C_n^{(1,0)}}\, \overline{C_{-n}^{(0,1)}} \\
&+ 2 \sum_{k\in\mathbb{Z}} \sum_{l\in\mathbb{Z}\setminus\{0,k\}} \Pi_{l,l}(t,t)\Pi_{k-l,k-l}(t,t) C_l^{(1,1)} C_{k-l}^{(1,1)} \overline{C_l^{(1,0)}}\, \overline{C_{k-l}^{(0,1)}},
\end{aligned} \tag{7.89}$$

where we have again used Wick's theorem and (7.85) with (7.86) as well as an index shift $k-l \leftrightarrow l$ to obtain the prefactor of two in the second term. The first term in (7.89) reads for $t \gg 1$

$$\begin{aligned}
&\sum_{l\in\mathbb{Z}\setminus\{0\}} \Pi_{l,l}(t,t) \left| C_l^{(1,1)} \right|^2 \sum_{n\in\mathbb{Z}\setminus\{0\}} \Pi_{n,n}(t,t) \overline{C_n^{(1,0)}}\, \overline{C_{-n}^{(0,1)}} \\
&\simeq \sum_{l\in\mathbb{Z}\setminus\{0\}} \Pi_{l,l}(t,t) \left| C_l^{(1,1)} \right|^2 \sum_{n>0} \frac{2\cos 2\pi n\delta - \cos 4\pi n\delta - 1}{(2\pi n\delta)^2} \simeq 0,
\end{aligned} \tag{7.90}$$

since the second sum in (7.90) has the same form like the one in (7.81). The second term in (7.89) may be evaluated with (7.86) for $t \gg 1$ by substituting $x = 2\pi l\delta$ for $\delta \ll 1$ according to

$$\begin{aligned}
&\sum_{k\in\mathbb{Z}}\sum_{l\in\mathbb{Z}\setminus\{0,k\}} \Pi_{l,l}(t,t)\Pi_{k-l,k-l}(t,t)C_l^{(1,1)}C_{k-l}^{(1,1)}\overline{C_l^{(1,0)}}\,\overline{C_{k-l}^{(0,1)}} \\
&\simeq \sum_{l\neq 0}\frac{C_l^{(1,1)}\overline{C_l^{(1,0)}}}{2\mu_l}\sum_{n\neq 0}\frac{C_n^{(1,1)}\overline{C_n^{(0,1)}}}{2\mu_n} \\
&= \frac{1}{4}\left(\sum_{l>0}\frac{1-\cos 4\pi l\delta}{(2\pi l\delta)^2}\right)^2 \simeq \frac{1}{4(2\pi\delta)^2}\left(\int_0^\infty dx\,\frac{1-\cos 2x}{x^2}\right)^2 = \frac{1}{16\,\delta^2}.
\end{aligned} \tag{7.91}$$

where we have again used the value of the integral in (7.79). Lastly, with Wick's theorem, (7.85), (7.86) and (7.76) we get

$$\begin{aligned}
&\left\langle \int_0^1 dx\,\left(\left(D_\delta^{(1,0)}\right)\left(D_\delta^{(0,1)}\right)\right)^2\right\rangle = 2\left(\sum_{l\in\mathbb{Z}\setminus\{0\}}\Pi_{l,l}(t,t)C_l^{(1,0)}C_{-l}^{(0,1)}\right)^2 \\
&+\sum_{k\in\mathbb{Z}}\sum_{l\in\mathbb{Z}\setminus\{0,k\}}\Pi_{l,l}\Pi_{k-l,k-l}\left|C_l^{(1,0)}\right|^2\left|C_{k-l}^{(0,1)}\right|^2.
\end{aligned} \tag{7.92}$$

Here, we used again an index shift $k-l \leftrightarrow l$ to obtain the factor of two in front of the first sum of (7.92). The first term in (7.92) has, after inserting (7.86) for $t \gg 1$ and substituting $x = 2\pi l\delta$ the same form as the second sum in (7.90) and thus vanishes. The second term in (7.92) becomes for $t \gg 1$

$$\begin{aligned}
&\sum_{k\in\mathbb{Z}}\sum_{l\in\mathbb{Z}\setminus\{0,k\}}\Pi_{l,l}\Pi_{k-l,k-l}\left|C_l^{(1,0)}\right|^2\left|C_{k-l}^{(0,1)}\right|^2 \simeq \left(\frac{1}{2}\sum_{l\neq 0}\frac{\sin^2\pi l\delta}{(\pi l\delta)^2}\right)^2 \\
&\simeq \frac{1}{4\pi^2\delta^2}\left(\int_{-\infty}^\infty dx\,\frac{\sin^2 x}{x^2}\right)^2 = \frac{1}{4\pi^2\delta^2}\pi^2 = \frac{1}{4\delta^2},
\end{aligned} \tag{7.93}$$

where we substituted in the second step $x = \pi l\delta$. Hence, combining (7.88), (7.90), (7.91) and (7.93) leads to

$$\begin{aligned}
\left\langle\int_0^1 dx\,\left(\mathcal{N}_\delta^{(\gamma)}[h^{(0)}(x,t)]\right)^2\right\rangle &\simeq \frac{1}{(\gamma+1)^2}\left[\frac{12}{16\delta^2}+\frac{(\gamma-1)^2}{4\delta^2}+\frac{8(\gamma-1)}{16\delta^2}\right] \\
&= \frac{2+\gamma^2}{4(\gamma+1)^2\delta^2},
\end{aligned} \tag{7.94}$$

which is the result given in (7.52).

8 Thermodynamic Uncertainty Relation for the KPZ Equation in Higher Dimensions

In this chapter, we will discuss an approach to calculate the TUR product $\mathcal{Q}$ for the KPZ equation in higher dimensions. To this end, like in Chapter 6, we rely on DRG techniques now generalized to spatial dimensions $d > 2$.

8.1 Higher-Dimensional DRG

8.1.1 The Renormalization Equations

The derivation of the d-dimensional renormalization equation for the RG-parameters ν, Δ_0 and $\overline{\lambda}$ follows the same steps as discussed in Chapter 6. In particular, we use the relation between the KPZ equation and the stochastic Burgers equation (see Section 3.1.1) with noise correlations given by

$$\left\langle f_i(\mathbf{q}, \omega)\, f_j(\mathbf{q}', \omega) \right\rangle = -(2\,\pi)^{d+1}\, q_i\, q_j\, \Delta_0\, \delta^d(\mathbf{q} + \mathbf{q}')\, \delta(\omega + \omega'), \tag{8.1}$$

in analogy to (6.8). We obtain the following RG differential equations depending on the spatial dimension d,

$$\frac{d\,\nu(l)}{dl} = \frac{\varepsilon}{d}\,\frac{K_d}{8}\,\nu(l)\,\overline{\lambda}^2(l), \tag{8.2}$$

$$\frac{d\,\Delta_0(l)}{dl} = \frac{K_d}{8}\,\Delta_0(l)\,\overline{\lambda}^2(l), \tag{8.3}$$

$$\frac{d\,\overline{\lambda}^2(l)}{dl} = \overline{\lambda}^2(l)\left(\varepsilon - \frac{3-2d}{d}\frac{K_d}{4}\,\overline{\lambda}^2(l)\right). \tag{8.4}$$

Here, we have set $\varepsilon = 2-d$ and $K_d = (2^{d-1}\pi^{d/2}\Gamma(d/2))^{-1}$ with Γ the Euler-Gamma function, see, e.g., [43, 109]. It is important to realize that the definition of the dimensionless coupling parameter $\overline{\lambda}(l)$ depends on the spatial dimension d via

$$\overline{\lambda}(l) = \lambda\sqrt{\frac{\Delta_0(l)}{\nu^3(l)\,(\Lambda'(l))^{\varepsilon}}}, \tag{8.5}$$

where again $\Lambda'(l) = \Lambda_0\, e^{-l}$. For $d = 1$, (8.5) reduces to (6.16). From (8.4) we infer the d-depending fixed-point structure by setting the l.h.s. of (8.4) to zero and solve for $\overline{\lambda}_*^2$, which yields

$$\overline{\lambda}_*^2 = \begin{cases} 0, & \text{Gaussian fixed-point,} \\ \frac{4\,d}{K_d}\,\frac{\varepsilon}{3-2\,d}, & \text{KPZ fixed-point.} \end{cases} \tag{8.6}$$

The results of a linear stability analysis of the fixed-points in (8.6) are given in Table 8.1. The stability analysis in Table 8.1 and its graphic representation in Figure 3.3 shows the

Table 8.1: Fixed-Point Stability

	Gaussian	KPZ
$0 < d < 3/2$	unstable	stable
$2 < d$	stable	unstable

Linear stability analysis of the two respective fixed-points from (8.6) in dependence of the spatial dimension d.

well-known fact that the DRG formalism cannot be used to obtain the strong coupling KPZ fixed-point for spatial dimensions beyond the lower critical dimension $d = 2$ (see, e.g., [54, 68]). In particular, for all $d > 2$ and $\overline{\lambda}$ above the phase-separation line (i.e., the curve $\overline{\lambda}_*(d) = \sqrt{4d\varepsilon/(K_d(3-2d))}$, see Figure 3.3), the RG-flow starting with $\overline{\lambda}$ tends to a strong coupling fixed-point at infinity. However, for $d > 2$ and $\overline{\lambda}$ below the phase-separation line in Figure 3.3, the RG-flow is attracted by the Gaussian fixed-point. This allows for the application of the DRG scheme in the smooth phase of the KPZ equation, i.e., in its EW-scaling regime.

Thus, the task is to derive the DRG corrections to the bare propagator $G_0(\mathbf{q}, \omega)$ and to the correlation function $C(\mathbf{q}, \omega)$ for the case of $d > 2$, which will be obtained via the same steps as in Chapter 6. We begin by stating the d-dimensional equivalent to the relation between $\nu(l)$ and $\Delta_0(l)$ from (6.17). To this end, we divide (8.2) by (8.3) and find

$$\frac{\nu(l)}{\nu} = \left(\frac{\Delta_0(l)}{\Delta_0}\right)^{\varepsilon/d}. \tag{8.7}$$

For the case of $d = 1$, (8.7) results in the fluctuation-dissipation theorem from (6.17). Inserting (8.7) into (8.2) and using (8.5) allows for a solution $\nu(l)$, given by

$$\nu(l) = \nu \left(1 + \frac{3\varepsilon - d}{\varepsilon}\,\frac{K_d}{8\,d}\,\frac{\lambda^2\,\Delta_0}{\nu^3\,\Lambda_0^\varepsilon}\,(e^{\varepsilon\,l} - 1)\right)^{\varepsilon/(3\varepsilon - d)}. \tag{8.8}$$

Hence, for large values of the renormalization parameter l we have

$$\nu(l) \simeq \nu \left(1 - \frac{3\varepsilon - d}{\varepsilon}\,\frac{K_d}{8\,d}\,\overline{\lambda}^2\right)^{\varepsilon/(3\varepsilon - d)}, \tag{8.9}$$

since, for $d > 2$, $\varepsilon < 0$. Expanding the r.h.s. of (8.9) with respect to $\overline{\lambda}^2$ leads for $\overline{\lambda}^2 \ll 1$ to

$$\nu(l) \simeq \nu \left(1 - \frac{K_d}{8\,d}\,\overline{\lambda}^2\right), \tag{8.10}$$

where the dependence on ε has dropped out. With the relation from (8.7) the solutions of (8.2) and (8.3) are given for $\overline{\lambda}^2 \ll 1$ and $d > 2$ by

$$\nu(q) = \nu(l) \simeq \nu \left(1 - \frac{K_d}{8\,d}\,\overline{\lambda}^2\right), \tag{8.11}$$

$$\Delta_0(q) = \Delta_0(l) \simeq \Delta_0 \left(1 - \frac{K_d}{8\,d}\,\overline{\lambda}^2\right)^{d/\varepsilon}, \tag{8.12}$$

respectively, where we have set $q = |\mathbf{q}| = \Lambda_0 e^{-l}$ (see also Section 6.2). Contrary to the case $\varepsilon > 0$, see, e.g., Section 6.2 for $d = 1$, the results (8.11) and (8.12) do not explicitly depend on scale q but show nevertheless corrections in $O(\overline{\lambda}^2)$ compared to the bare values ν and Δ_0.

8.1.2 The Correlation Tensor

We proceed with the generalization of (6.24) to $d > 2$ spatial dimensions. Whereas for $d = 1$ the correlation $\langle u(q,\omega)\, u(q',\omega')\rangle$ is a scalar, for any $d > 1$ this correlation becomes a tensor of the form

$$\frac{\langle u_i(\mathbf{q},\omega)\, u_j(\mathbf{q}',\omega')\rangle}{(2\pi)^{d+1}\,\delta^d(\mathbf{q}+\mathbf{q}')\,\delta(\omega+\omega')} = C_{ij}(\mathbf{q},\omega) = q_i\, q_j\, \Delta_0(q)\, |G(q,\omega)|^2. \tag{8.13}$$

Here, $\Delta_0(q)$ is taken from (8.12), $G(q,\omega)$ denotes the renormalized propagator given by

$$G(q,\omega) = \frac{1}{-i\,\omega + \nu(q)\, q^2}, \tag{8.14}$$

with $\nu(q)$ from (8.11), and the indices i, j are the respective components of the solution vector $\mathbf{u}(\mathbf{q},\omega)$ for the d-dimensional Burgers equation. After a Fourier backward transformation with respect to ω we obtain for $\varepsilon < 0$,

$$\big\langle u_i(\mathbf{q},t)\, u_j(\mathbf{q},t')\big\rangle = (2\pi)^d\, C_{ij}(\mathbf{q},|t-t'|)\, \delta^d(\mathbf{q}+\mathbf{q}'), \tag{8.15}$$

with

$$C_{ij}(\mathbf{q},t) = \frac{\Delta_0}{2\,\nu^{d/\varepsilon}}\, \frac{q_i\, q_j}{q^2}\, (\nu(q))^{d/\varepsilon - 1}\, e^{-\nu(q)\, q^2\, t}. \tag{8.16}$$

From the argument of the exponential function in (8.16), the dynamical exponent $z = 2$ associated with the Gaussian fixed-point can be inferred. Like in Chapter 6, we will use the results from (8.15) and (8.16) to calculate the TUR constituents for the case of $d > 2$.

8.2 Calculation of the Higher-Dimensional TUR Constituents

8.2.1 $\langle\Psi(t)\rangle$ and var$[\Psi(t)]$

The d-dimensional expression for the expectation value of $\Psi(t)$ is obtained along the same lines as for the one-dimensional case, i.e., via spatial integration of (3.1) subject to periodic boundary conditions and subsequent averaging. For vanishing initial condition $h(\mathbf{r},0)=0$, it is given by

$$\langle\Psi(t)\rangle = \frac{\lambda}{2}\int_0^t dt' \int_0^b d\mathbf{r}\,\left\langle\left(\nabla h(\mathbf{r},t')\right)^2\right\rangle, \tag{8.17}$$

where we abbreviate $\int_0^b dr_1 \int_0^b dr_2 \cdots \int_0^b dr_d \equiv \int_0^b d\mathbf{r}$. With $\mathbf{u}(\mathbf{r},t) = -\nabla h(\mathbf{r},t)$ and a Fourier transform in the spatial coordinates we rewrite (8.17) analogously to (6.4) as

$$\begin{aligned}
\langle\Psi(t)\rangle &= \frac{\lambda}{2}\int_0^t dt' \int_0^b d\mathbf{r} \int \frac{d\mathbf{q}}{(2\pi)^d} \int \frac{d\mathbf{q}'}{(2\pi)^d} \sum_{i,j=1}^{d} \left\langle u_i(\mathbf{q},t')\, u_j(\mathbf{q}',t')\right\rangle \delta_{ij}\, e^{i(\mathbf{q}+\mathbf{q}')\cdot\mathbf{r}} \\
&\approx \frac{\lambda}{2}\int_0^t dt' \int_{-\infty}^{\infty} d\mathbf{r} \int \frac{d\mathbf{q}}{(2\pi)^d} \int \frac{d\mathbf{q}'}{(2\pi)^d} \sum_{i,j=1}^{d} \left\langle u_i(\mathbf{q},t')\, u_j(\mathbf{q}',t')\right\rangle \delta_{ij}\, e^{i(\mathbf{q}+\mathbf{q}')\cdot\mathbf{r}} \\
&= \frac{\lambda}{2}\int_0^t dt' \int \frac{d\mathbf{q}}{(2\pi)^d} \sum_{i=1}^{d} \left\langle u_i(\mathbf{q},t')\, u_i(-\mathbf{q},t')\right\rangle \\
&= \frac{\lambda}{2}\int_0^t dt' \int_{|\mathbf{k}|<\Lambda} d\mathbf{k} \sum_{i=1}^{d} C_{ii}\left(\frac{2\pi}{b}\mathbf{k},0\right) \\
&= \frac{\lambda\, t}{2}\int_{|\mathbf{k}|<\Lambda} d\mathbf{k} \sum_{i=1}^{d} C_{ii}\left(\frac{2\pi}{b}\mathbf{k},0\right),
\end{aligned} \tag{8.18}$$

where the second step holds for $b \gg 1$ (see also (6.4)) and the fourth includes the substitution $\mathbf{q} = 2\pi\mathbf{k}/b$ to reflect the finite system size, (8.15) and the assumption that the Fourier cutoff $\Lambda \gg 1$. Inserting the result for the correlation tensor for $\varepsilon < 0$ from

(8.16) leads to

$$
\begin{aligned}
\langle\Psi(t)\rangle &= \frac{\lambda\, t}{4}\,\frac{\Delta_0}{\nu^{d/\varepsilon}}\int_{|\mathbf{k}|<\Lambda} d\mathbf{k}\sum_{i=1}^{d}\frac{k_i\,k_i}{|\mathbf{k}|^2}\left(\nu\left(\frac{2\pi}{b}\mathbf{k}\right)\right)^{d/\varepsilon-1} \\
&= \frac{\lambda\, t}{4}\,\frac{\Delta_0}{\nu}\left(1-\overline{\lambda}^2\frac{K_d}{8\,d}\right)^{d/\varepsilon-1} S_d\int_0^{\Lambda} dk\, k^{d-1} \\
&= \frac{\Delta_0\,\lambda}{2\,\nu}\,\frac{\pi^{d/2}\,\Lambda^d}{d\,\Gamma(d/2)}\left(1-\overline{\lambda}^2\frac{K_d}{8\,d}\right)^{d/\varepsilon-1} t \\
&\simeq \frac{\Delta_0\,\lambda}{2\,\nu}\,\frac{\pi^{d/2}\,\Lambda^d}{d\,\Gamma(d/2)}\, t\,, \qquad \text{for } \overline{\lambda}\ll 1\,,
\end{aligned}
\tag{8.19}
$$

where

$$
\begin{aligned}
S_d &= \int_0^{2\pi} d\phi\prod_{n=1}^{d-2}\int_0^{\pi} d\vartheta_n\,\sin^{d-1-n}\vartheta_n \\
&= 2\pi\prod_{n=1}^{d-2}\frac{\pi^{1/2}\,\Gamma((d-k)/2)}{\Gamma((d+1-k)/2)} = \frac{2\,\pi^{d/2}}{\Gamma(d/2)}.
\end{aligned}
\tag{8.20}
$$

Similarly, the d-dimensional expression for $\langle\Psi^2(t)\rangle$ is given by

$$
\langle\Psi^2(t)\rangle = \left\langle\left(\frac{\lambda}{2}\int_0^t dt'\int_0^b d\mathbf{r}\,\left(\nabla h(\mathbf{r},t')\right)^2 + \int_0^t dt'\int_0^b d\mathbf{r}\,\eta(\mathbf{r},t')\right)^2\right\rangle. \tag{8.21}
$$

Switching again to the Fourier representation in $\mathbf{u}(\mathbf{q},\omega)$ leads for $b\gg 1$ to

$$
\langle\Psi^2(t)\rangle = \left\langle\left(\frac{\lambda}{2}\int_0^t dt'\int\frac{d\mathbf{q}}{(2\pi)^d}\sum_{i=1}^{d} u_i(\mathbf{q},t')\,u_i(-\mathbf{q},t') + \int_0^t dt'\int_0^b d\mathbf{r}\,\eta(\mathbf{r},t')\right)^2\right\rangle. \tag{8.22}
$$

Using the same assumption of quasi-normality like in Chapter 6 and the noise autocorrelation from (3.1), we arrive at

$$
\begin{aligned}
\langle\Psi^2(t)\rangle = \Delta_0\, b^d\, t + \frac{\lambda^2}{4}\int_0^t dt'\int_0^t dt''\int\frac{d\mathbf{q}}{(2\pi)^d}\int\frac{d\mathbf{q}'}{(2\pi)^d} \\
\times\sum_{i,j=1}^{d}\left\langle u_i(\mathbf{q},t')u_i(-\mathbf{q},t')u_j(\mathbf{q}',t'')u_j(-\mathbf{q}',t'')\right\rangle.
\end{aligned}
\tag{8.23}
$$

Employing Wick's theorem on the four-point correlation in (8.23) yields

$$\begin{aligned}\left\langle \Psi^2(t)\right\rangle = \langle \Psi(t)\rangle^2 + \Delta_0\, b^d\, t + \frac{\lambda^2}{2}\int_0^t dt' \int_0^t dt'' \int \frac{d\mathbf{q}}{(2\pi)^d}\int \frac{d\mathbf{q}'}{(2\pi)^d} \\ \times \sum_{i,j=1}^{d} \left\langle u_i(\mathbf{q},t')u_j(\mathbf{q}',t'')\right\rangle \left\langle u_i(-\mathbf{q},t')u_j(-\mathbf{q}',t'')\right\rangle,\end{aligned} \tag{8.24}$$

where $\langle \Psi(t)\rangle^2$ stems from the product of two-point correlations, which have equal indices i, j, respectively. Inserting (8.15) in (8.24) and substituting $\mathbf{q} = 2\pi\mathbf{k}/b$ to take the finite system size into account, leads to

$$\left\langle \Psi^2(t)\right\rangle = \langle \Psi(t)\rangle^2 + \Delta_0\, b^d\, t + \frac{\lambda^2}{2}\int_0^t dt' \int_0^t dt'' \int_{|\mathbf{k}|<\Lambda} d\mathbf{k} \sum_{i,j=1}^{d}\left[C_{ij}\left(\frac{2\pi}{b}\mathbf{k}, |t'-t''|\right)\right]^2. \tag{8.25}$$

Therefore, we obtain for the variance of $\Psi(t)$,

$$\mathrm{var}[\Psi(t)] = \Delta_0\, b^d\, t + \frac{\lambda^2}{2}\int_0^t dt' \int_0^t dt'' \int_{|\mathbf{k}|<\Lambda} d\mathbf{k} \sum_{i,j=1}^{d}\left[C_{ij}\left(\frac{2\pi}{b}\mathbf{k}, |t'-t''|\right)\right]^2. \tag{8.26}$$

With the explicit expression for C_{ij} from (8.16) we rewrite (8.26) according to

$$\begin{aligned}\mathrm{var}[\Psi(t)] = \Delta_0\, b^d\, t + \frac{\lambda^2\,\Delta_0^2}{8\,\nu^2}\left(1-\overline{\lambda}^2\frac{K_d}{8\,d}\right)^{2(d/\varepsilon-1)} \int_0^t dt' \int_0^t dt'' \int_{|\mathbf{k}|<\Lambda} d\mathbf{k} \\ \times \sum_{i,j=1}^{d} \frac{k_i^2\,k_j^2}{|\mathbf{k}|^4}\, e^{-a_d |\mathbf{k}|^2|t'-t''|},\end{aligned} \tag{8.27}$$

where $a_d \equiv 2\nu\left(1-\overline{\lambda}^2\frac{K_d}{8\,d}\right)\left(\frac{2\pi}{b}\right)^2 > 0.$

With the sum in (8.27) evaluating to 1, the momentum integral simplifies significantly and is given by

$$\begin{aligned}&\mathrm{var}[\Psi(t)] \\ &= \Delta_0\, b^d\, t + \frac{\lambda^2\,\Delta_0^2}{8\,\nu^2}\left(1-\overline{\lambda}^2\frac{K_d}{8\,d}\right)^{2(d/\varepsilon-1)} S_d \int_0^t dt' \int_0^t dt'' \int_0^\Lambda dk\, k^{d-1}\, e^{-a_d\, k^2\,|t'-t''|},\end{aligned} \tag{8.28}$$

S_d from (8.20). Relying on the aid of a computer algebra system for the evaluation of the integrations in (8.28) and collecting the time-dependent terms, yields

$$\begin{aligned}&\mathrm{var}[\Psi(t)]\\&= \Delta_0\, b^d\, t + \frac{\lambda^2\,\Delta_0^2}{8\,\nu^2}\left(1-\overline{\lambda}^2\frac{K_d}{8\,d}\right)^{2(d/\varepsilon-1)} S_d\left(\frac{2\Lambda^{d-2}\,t}{(d-2)a_d}+\Gamma\left(\frac{d}{2}-2\right)\left(\frac{t^{4/d-1}}{a_d}\right)^{d/2}\right).\end{aligned} \tag{8.29}$$

To simplify the expression in (8.29), we approximate $(1-\overline{\lambda}^2 K_d/(8d)) \approx 1$, i.e., assume $\overline{\lambda} \ll 1$, which leads after reinserting the explicit form of a_d from (8.27) and S_d from (8.20) to

$$\begin{aligned}&\mathrm{var}[\Psi(t)]\\&= \Delta_0\, b^d\left(1+\frac{\lambda_{\mathrm{eff}}^2}{16}\,\frac{\pi^{d/2-2}\,\Lambda^{d-2}}{(d-2)\,\Gamma(d/2)}\right)t + \frac{\lambda^2\,\Delta_0^2\,b^d}{2^{2+3d/2}\,\nu^{2+d/2}}\,\frac{\Gamma(d/2-2)}{\pi^{d/2}\,\Gamma(d/2)}\,t^{2-d/2},\end{aligned} \tag{8.30}$$

with λ_{eff} from (3.13). From (8.30) we recognize that the DRG scheme led to two corrections to the purely noise driven diffusive behavior of the variance. The first, linearly proportional to the time t, alters the diffusivity, whereas the second correction displays sub-diffusive behavior for $2 < d < 4$. For $d > 4$ the second contribution is dampened with growing time t. In the limit of $t \to \infty$, the sub-diffusive correction becomes irrelevant for all $d > 2$ and can be neglected for the steady state form of the variance, which therefore reads

$$\mathrm{var}[\Psi(t)] = \Delta_0\, b^d\left(1+\frac{\lambda_{\mathrm{eff}}^2}{16}\,\frac{\pi^{d/2-2}\,\Lambda^{d-2}}{(d-2)\,\Gamma(d/2)}\right)t\,, \qquad d > 2. \tag{8.31}$$

Note, that the structure of (8.31) resembles the lowest-order correction in the perturbation expansion for the variance in Chapter 5, e.g., (5.66) and (5.67).

8.2.2 Entropy Production Rate

For the d-dimensional stationary entropy production rate $\sigma = \left\langle \frac{d\,\Delta s_{\mathrm{tot}}}{dt}\right\rangle$ we obtain from (4.22), interpreted in the Stratonovich-sense and for Gaussian white noise,

$$\sigma = \frac{\lambda^2}{2\,\Delta_0}\int_0^b d\mathbf{r}\,\left\langle (\nabla h(\mathbf{r},t))^2\,(\nabla h(\mathbf{r},t))^2\right\rangle. \tag{8.32}$$

Here, we rely on the assumption that the stationary probability density functional for $d > 1$, which is not explicitly known for the KPZ equation (3.1), may be replaced by the stationary PDF of the corresponding EW equation (3.2), $p^s[h] \sim \exp\left[-\frac{\nu}{\Delta_0}\int d\mathbf{r}(\nabla\, h)^2\right]$.

The latter holds for any $d \geq 2$. This assumption implies that the height field may be treated for large times as a Gaussian distributed random variable. As the DRG scheme for $d > 2$ is applicable in the EW scaling regime of the KPZ equation only, we feel that for the calculation of the stationary entropy production rate σ the above approximation is feasible; at least in the weak-coupling limit, $\lambda_{\text{eff}} \downarrow 0$.
Following the same steps as in Section 8.2.1, namely, identifying $\mathbf{u} = -\nabla h$ and switching to Fourier space representation it follows that

$$\begin{aligned}\sigma = \frac{\lambda^2}{2\,\Delta_0} \int \frac{d\mathbf{q}}{(2\pi)^d} \int \frac{d\mathbf{q}'}{(2\pi)^d} \int \frac{d\mathbf{q}''}{(2\pi)^d} \\ \times \sum_{i,j=1}^{d} \left\langle u_i(\mathbf{q}', t) u_i(\mathbf{q} - \mathbf{q}', t) u_j(\mathbf{q}'', t) u_j(-\mathbf{q} - \mathbf{q}'', t) \right\rangle .\end{aligned} \tag{8.33}$$

Applying Wick's theorem to the four-point correlation in (8.33), inserting (8.15) and substituting $\mathbf{q} = 2\pi\mathbf{k}/b$ leads to

$$\begin{aligned}\sigma = \frac{\lambda^2}{2\,\Delta_0\, b^d} \Bigg[\left(\int_{|\mathbf{k}|<\Lambda} d\mathbf{k} \sum_{i=1}^{d} C_{ii}\left(\frac{2\pi}{b}\mathbf{k}, 0\right) \right)^2 \\ +2 \int_{|\mathbf{k}|<\Lambda} d\mathbf{k} \int_{\substack{|\mathbf{k}'|<\Lambda \\ |\mathbf{k}-\mathbf{k}'|<\Lambda}} d\mathbf{k}' \sum_{i,j=1}^{d} C_{ij}\left(\frac{2\pi}{b}\mathbf{k}', 0\right) C_{ij}\left(\frac{2\pi}{b}(\mathbf{k}-\mathbf{k}'), 0\right) \Bigg] .\end{aligned} \tag{8.34}$$

Note the involved boundaries of the second momentum integral ensure the Fourier cutoff is adequately represented (see also (3.80), (3.85) and Chapter 5). The first integral in (8.34) is, with (8.16), readily evaluated as

$$\begin{aligned}\int_{|\mathbf{k}|<\Lambda} d\mathbf{k} \sum_{i=1}^{d} C_{ii}\left(\frac{2\pi}{b}\mathbf{k}, 0\right) &= \frac{\Delta_0}{\nu} \frac{\pi^{d/2}}{d\,\Gamma(d/2)} \left(1 - \overline{\lambda}^2 \frac{K_d}{8\,d}\right)^{d/\varepsilon - 1} \Lambda^d \\ &\approx \frac{\Delta_0}{\nu} \frac{\pi^{d/2}}{d\,\Gamma(d/2)} \Lambda^d , \qquad \text{for } \overline{\lambda}^2 \ll 1 .\end{aligned} \tag{8.35}$$

For the second one we find with (8.16) and again $\overline{\lambda}^2 \ll 1$

$$\begin{aligned}&\int_{|\mathbf{k}|<\Lambda} d\mathbf{k} \int_{\substack{|\mathbf{k}'|<\Lambda \\ |\mathbf{k}-\mathbf{k}'|<\Lambda}} d\mathbf{k}' \sum_{i,j=1}^{d} C_{ij}\left(\frac{2\pi}{b}\mathbf{k}', 0\right) C_{ij}\left(\frac{2\pi}{b}(\mathbf{k}-\mathbf{k}'), 0\right) \\ &= \frac{\Delta_0^2}{4\,\nu^2} \int_{|\mathbf{k}|<\Lambda} d\mathbf{k} \int_{\substack{|\mathbf{k}'|<\Lambda \\ |\mathbf{k}-\mathbf{k}'|<\Lambda}} d\mathbf{k}' \left(\frac{\mathbf{k}' \cdot (\mathbf{k} - \mathbf{k}')}{|\mathbf{k}'||\mathbf{k} - \mathbf{k}'|} \right)^2 .\end{aligned} \tag{8.36}$$

Thus, the steady state entropy production rate σ for $d > 2$ and $\overline{\lambda}^2 \ll 1$ is given by,

$$\sigma = \frac{\lambda^2\,\Delta_0}{4\,\nu^2\,b^d}\left[\frac{2\,\pi^d\,\Lambda^{2d}}{d^2\,\Gamma^2(d/2)} + \mathcal{I}_d\right], \tag{8.37}$$

with $\mathcal{I}_d$ defined as

$$\mathcal{I}_d \equiv \int_{|\mathbf{k}|<\Lambda} d\mathbf{k} \int_{\substack{|\mathbf{k}'|<\Lambda \\ |\mathbf{k}-\mathbf{k}'|<\Lambda}} d\mathbf{k}' \left(\frac{\mathbf{k}'\cdot(\mathbf{k}-\mathbf{k}')}{|\mathbf{k}'||\mathbf{k}-\mathbf{k}'|}\right)^2. \tag{8.38}$$

The expression $\mathcal{I}_d$ may be interpreted in geometrical terms of d-dimensional wavevector space. Introducing the angle γ between the wavevectors $\mathbf{k}'$ and $\mathbf{k}-\mathbf{k}'$, $\mathcal{I}_d$ is rewritten as

$$\mathcal{I}_d = \int_{|\mathbf{k}|<\Lambda} d\mathbf{k} \int_{\substack{|\mathbf{k}'|<\Lambda \\ |\mathbf{k}-\mathbf{k}'|<\Lambda}} d\mathbf{k}'\,\cos^2\gamma. \tag{8.39}$$

Hence, first, for the outer vector $\mathbf{k}$ fixed, $\cos^2\gamma$ as a function of $\mathbf{k}'$ is summed over the allowed integration domain, and subsequently a second sum is taken over all wavevectors $\mathbf{k}$ inside the ball $|\mathbf{k}| < \Lambda$. The interaction of the Fourier modes $\mathbf{k}'$ and $\mathbf{k}-\mathbf{k}'$ takes place along their mutual projection onto one another as is indicated by the $\cos\gamma$ term. Accordingly, the non-linear interaction between the above modes is weighted with $\cos^2\gamma$. Thus, (8.39) represents that amount of the entropy production rate, which is generated by the interaction of the Fourier modes $\mathbf{k}'$ and $\mathbf{k}-\mathbf{k}'$ summed over all $\mathbf{k}$, $\mathbf{k}'$ satisfying the restriction from (8.34).

8.3 Higher-Dimensional TUR Product $\mathcal{Q}$

Combining the results from (8.19), (8.31) and (8.37) yields for the TUR product $\mathcal{Q}$ from (4.24)

$$\mathcal{Q} = 2 + \frac{d^2\,\Gamma^2(d/2)}{\pi^d\,\Lambda^{2d}}\,\mathcal{I}_d. \tag{8.40}$$

With the interpretation from (8.39) in mind and with

$$V_d(\Lambda) = \frac{2\,\pi^{d/2}}{d\,\Gamma(d/2)}\,\Lambda^d, \tag{8.41}$$

denoting the volume of a d-dimensional ball with radius Λ, the excess term in (8.40) can be written as

$$4\,V_d^{-1}(\Lambda)\int_{|\mathbf{k}|<\Lambda} d\mathbf{k}\,V_d^{-1}(\Lambda)\int_{\substack{|\mathbf{k}'|<\Lambda \\ |\mathbf{k}-\mathbf{k}'|<\Lambda}} d\mathbf{k}'\,\cos^2\gamma. \tag{8.42}$$

Eq. (8.42) may be understood as a twofold average of the interaction strengths $\cos^2\gamma$, $\gamma = \gamma(\mathbf{k},\mathbf{k}')$, taken over all modes $\mathbf{k}$, $\mathbf{k}'$, respectively, inside a d-dimensional ball with

radius Λ. Therefore, it represents some kind of mean interaction strength.
Unfortunately, this geometrical interpretation does not immediately lead to a simple way of calculating the excess term in (8.40). Instead, we concern ourselves with the evaluation of $\mathcal{I}_d$ from (8.38) by introducing d-dimensional polar coordinates. To this end, we will replace the angle γ from above by a suitably chosen coordinate angle. As a first step we substitute

$$\mathbf{k}' = \mathbf{q} + \mathbf{k}/2, \tag{8.43}$$

which is a common symmetrization for this type of integrals (see, e.g., [101]). With (8.43), the integrand of $\mathcal{I}_d$ from (8.38) becomes after some algebraic manipulation

$$\left(\frac{\mathbf{k}' \cdot (\mathbf{k} - \mathbf{k}')}{|\mathbf{k}'||\mathbf{k} - \mathbf{k}'|}\right)^2 = \frac{\left(1 - 4\,\frac{|\mathbf{q}|^2}{|k|^2}\right)^2}{1 - 8\,\frac{|\mathbf{q}|^2}{|\mathbf{k}|^2}\,\cos(2\vartheta) + 16\,\frac{|\mathbf{q}|^4}{|\mathbf{k}|^4}}\,, \qquad \vartheta \equiv \measuredangle(\mathbf{k}, \mathbf{q}). \tag{8.44}$$

In Figures 8.1 and 8.2, we show the relevant entities of (8.38), (8.44), respectively,

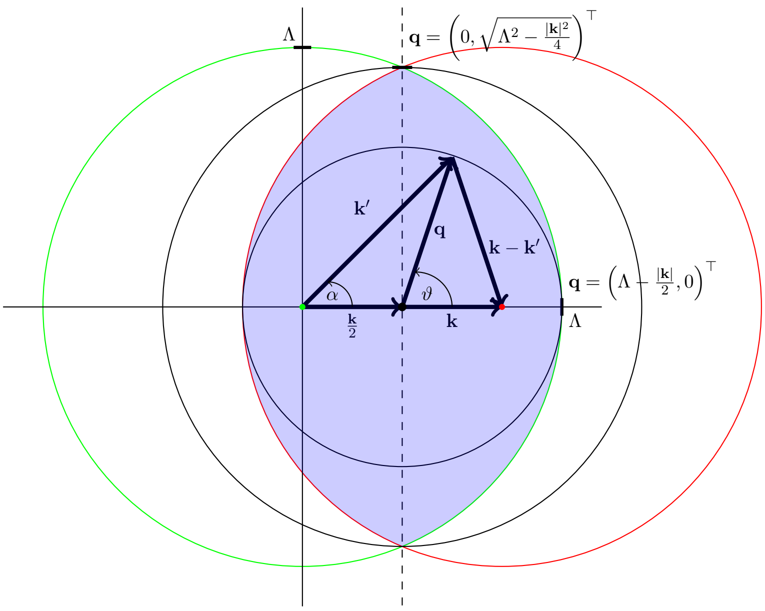

Figure 8.1: The allowed domain of integration (blue-shaded area) respecting the boundary conditions $|\mathbf{k}|$, $|\mathbf{k}'| < \Lambda$ and $|\mathbf{k} - \mathbf{k}'| < \Lambda$ (green and red circles, respectively) for $d = 2$. The symmetrization via the substitution from (8.43) is also shown.

including their boundaries for $d = 2$. To illustrate the allowed integration-domain for the inner integral over $\mathbf{q}$ in Figure 8.1, we choose the horizontal coordinate axis to be aligned with the vector $\mathbf{k}$. As the expression (8.44) is completely determined within the

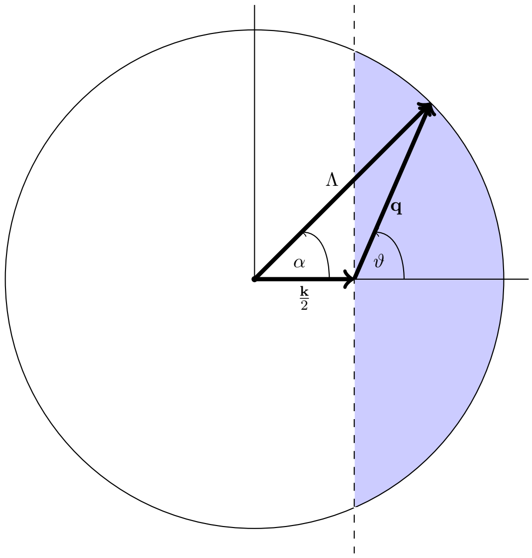

Figure 8.2: Exact boundary conditions on $\mathbf{q}$ for the case of $d = 2$.

plane spanned by the vectors $\mathbf{k}$ and $\mathbf{q}$, higher dimensions can be inferred from the 2d-case, since the relative positions of the vectors $\mathbf{k}$, $\mathbf{q}$ in higher dimensions can be projected onto the plane shown in Figure 8.1. In particular, for calculating the inner integral over $\mathbf{q}$ we may in higher dimensions choose the alignment of the coordinate system in such a way that $\mathbf{k}$ coincides with the polar axis. Hence, the angle ϑ from (8.44) becomes the polar angle ϑ of the spherical coordinate system. This has the advantage that the angle between $\mathbf{k}$ and $\mathbf{q}$ is for all dimensions given by the polar angle ϑ of the spherical coordinate system.
The green and red circles in Figure 8.1 represent the conditions $|\mathbf{k}|, |\mathbf{k}'| < \Lambda$ and $|\mathbf{k}-\mathbf{k}'| < \Lambda$, respectively. The blue-shaded intersection of these two encircled areas shows the allowed domain that fulfills the boundary conditions on $|\mathbf{k}|, |\mathbf{k}'|$ and $|\mathbf{k}-\mathbf{k}'|$. The right half of the blue-shaded domain is given by

$$|\mathbf{q}| < \frac{|\mathbf{k}|}{2}\left(\sqrt{\frac{4\,\Lambda^2}{|\mathbf{k}|^2} - \sin^2\vartheta} - \cos\vartheta\right), \qquad \text{with } \vartheta \in [-\pi/2, \pi/2]. \tag{8.45}$$

The parametrization of the boundary curve in (8.45) follows from the law of cosines applied to the triangle shown in Figure 8.2. Instead of trying to calculate the momentum integrations exactly via (8.45), which seems to be a very cumbersome task, even with the aid of a computer algebra system, we choose to make the following simplification.
In Figure 8.1 we have drawn two additional black circles. One with radius $\Lambda - |\mathbf{k}|/2$ and one with radius $\sqrt{\Lambda^2 - |\mathbf{k}|^2/4}$. As can be seen, the disk with the former radius underestimates the allowed domain of integration, whereas the disk with the latter radius

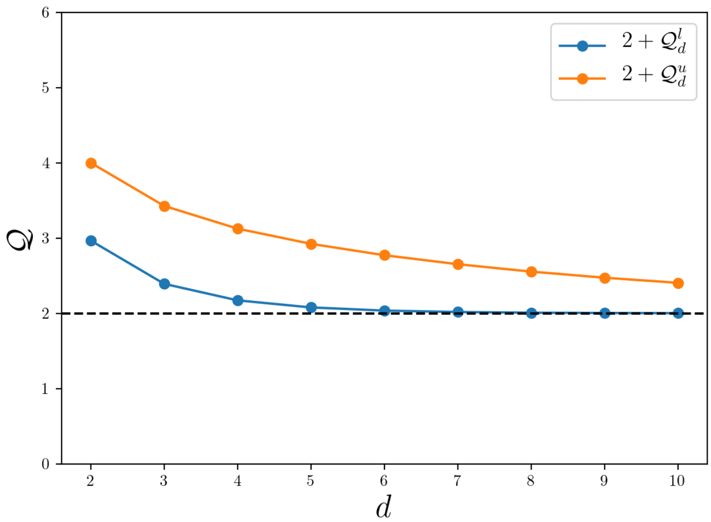

Figure 8.3: Graphs of $\mathcal{Q} = 2 + \mathcal{Q}_d^{u,l}$, respectively, from (8.50) obtained with the aid of a computer algebra system.

is an overestimation. Hence, the true value of the inner momentum integration lies between the values obtained for $|\mathbf{q}| < \Lambda - |\mathbf{k}|/2$ and $|\mathbf{q}| < \sqrt{\Lambda^2 - |\mathbf{k}|^2/4}$, respectively. In this way we construct an upper ($\mathcal{I}_d^u$) and lower ($\mathcal{I}_d^l$) bound on $\mathcal{I}_d$ from (8.38) with (8.43).

Rewriting (8.38) using (8.43) with respect to the approximated boundaries of the $\mathbf{q}$-integration and, for the sake of simplicity, substituting $|\mathbf{q}|/|\mathbf{k}| = \rho$ leads to

$$\mathcal{I}_d^{u,l} = S_d \int_0^\Lambda dk\, k^{2d-1}\, S_{d-1} \int_0^{\mathcal{G}_{u,l}(k)} d\rho \int_0^\pi d\vartheta\, \sin^{d-2}\vartheta\, \frac{\left(1-4\,\rho^2\right)^2}{1-8\,\rho^2\,\cos(2\vartheta)+16\,\rho^4}, \tag{8.46}$$

where

$$\mathcal{G}_{u,l}(k) \equiv \begin{cases} \sqrt{\frac{\Lambda^2}{k^2} - \frac{1}{4}} & (u) \\ \frac{\Lambda}{k} - \frac{1}{2} & (l) \end{cases}, \tag{8.47}$$

S_n from (8.20), and the term $\sin^{d-2}\vartheta$ stems from the d-dimensional Jacobian. Inserting the values for S_d, S_{d-1} from (8.20) we have

$$\mathcal{I}_d^{u,l} = \frac{4\,\pi^{d-1/2}}{\Gamma(d/2)\,\Gamma((d-1)/2)}\,\mathcal{B}_d^{u,l}(\Lambda), \tag{8.48}$$

where

$$\mathcal{B}_d^{u,l}(\Lambda) \equiv \int_0^\Lambda dk\, k^{2d-1} \int_0^{\mathcal{G}_{u,l}(k)} d\rho \int_0^\pi d\vartheta\, \frac{\sin^{d-2}\vartheta\, \left(1-4\,\rho^2\right)^2}{1-8\,\rho^2\,\cos(2\vartheta)+16\,\rho^4}. \tag{8.49}$$

Hence, we find for the TUR product from (8.40),

$$\mathcal{Q} = 2 + \mathcal{Q}_d^{u,l}, \qquad \mathcal{Q}_d^{u,l} \equiv \frac{4\,\Gamma(d/2)\,d^2}{\pi^{1/2}\,\Gamma((d-1)/2)\,\Lambda^{2d}}\mathcal{B}_d^{u,l}(\Lambda). \tag{8.50}$$

In Figure 8.3 we show the evaluation of (8.50), where the values for the respective integrals in (8.49) were obtained with the aid of a computer algebra system. As can be seen clearly, both the upper and lower bounds (u and l, respectively) to the true value decrease with growing dimension d. Further, the difference between the upper and lower bound also decreases with increasing d. Consequently, the higher the dimension, the tighter the approximation via (8.46) to the exact expression from (8.45) becomes. In regard to the value of the TUR product $\mathcal{Q}$, Figure 8.3 suggests that for $d \to \infty$ the TUR will be saturated, i.e. $\mathcal{Q} = 2$ for $d \to \infty$.
Like in the one-dimensional case (see (5.43)) the convolution term $\mathcal{I}_d$ from (8.37), (8.40) is responsible for exceeding the saturation value $\mathcal{Q} = 2$. This excess can be traced back to the amount of entropy production generated by the interaction of the feasible Fourier modes due to the non-linearity. But there is numerical evidence that the mean interaction strength from (8.42) tends to zero from above for $d \to \infty$.

9 Concluding Remarks and Perspectives

Two highly active fields of statistical physics at the present time are stochastic thermodynamics, in particular the thermodynamic uncertainty relation (TUR) for current-like variables, and stochastic field theories like the Kardar-Parisi-Zhang (KPZ) equation. The former has led in recent years to a deep understanding of the thermodynamics of processes on a molecular level. The latter has evolved into a paradigmatic example of non-linear stochastic field theories due to its rich dynamical properties and its far encompassing universality class.
So far, only few connections between stochastic thermodynamics and stochastic field theories have been made. In, e.g., [127, 128], concepts of stochastic thermodynamics have been applied to turbulence and in particular fluctuation theorems were used to gain insight into enstrophy and energy cascades, respectively. Other contributions deal with the definition of non-equilibrium steady state (NESS) entropy production in the context of active matter field theories [129] and, more generally, scalar field Langevin equations [130]. In both publications, the general approach to define entropy production in a NESS follows the same lines that is pursued in Chapter 4. Publications that address the stochastic thermodynamics of the continuous KPZ equation explicitly are [131, 132]. The former suggests a framework to formulate a non-equilibrium stationary state potential from which, e.g., fluctuation theorems are derived. The latter proposes a distinction between internal and external entropy production in the stationary state of a one-dimensional KPZ system.

The formulation of a TUR for stochastic field theories is novel and a first result of this thesis. The approach in Chapter 4 for formulating a field-theoretic TUR is based on an extension of notions like generalized currents and their precision as well as entropy production to stochastic fields. To exemplify these general concepts, we applied them to the KPZ equation. For the most part, we concerned ourselves with the one-dimensional KPZ equation on a finite substrate. In this setting we derived a main result, namely that the TUR for the KPZ equation holds but is not saturated.
In order to do so, we employed in the first part of Chapter 5 a quite general technique from the theory of stochastic partial differential equations. It comprises the following steps. (i) The space dependence of the height and noise field is represented in terms of their respective Fourier series or, more generally, eigenfunction expansions. (ii) The resulting non-linear integral equation for the time-dependent k-th Fourier coefficient of the height field is solved by means of a perturbation expansion with respect to the coupling parameter of the non-linearity. The solution constructed in that way is understood in

the mild sense [82].
Within this framework, we derived explicit expressions for stationary state generalized currents and their diffusivity as well as for the entropy production rate to lowest non-trivial order of the perturbation expansion. This allowed us to show that the TUR product for a time-integrated generalized current like the spatially averaged height field has at least the value of five with equality holding in the weak coupling limit. Moreover, we were able to pinpoint the origin of the excess in the TUR, which was shown to be caused by mode-coupling effects due to the non-linearity of the KPZ equation.
An advantage of this approach is that it does not rely on deep physical assumptions and is therefore very generally applicable. This is, at the same time, also somewhat of a drawback, especially when higher order approximations are to be calculated, which becomes quickly a cumbersome task. We thus refined our approach in the second part of Chapter 5 in the following way. On one hand we used the known stationary probability distribution functional of the height field to calculate equal-time steady state correlation functions. This enabled us to show that the lowest-order perturbative expressions for the stationary state current and entropy production rate are actually exact. On the other hand we invoked the physical assumption of quasi-normality, a concept loaned from turbulence theory [101, 102], to calculate the variance of the spatially averaged height field perturbatively to higher orders. This variance is the only TUR constituent stemming from a two-time correlation function.
Using the relevant correlation times of the one-dimensional KPZ equation on a finite substrate and their respective dependence on the effective coupling parameter, we were able to state an expected range of validity of the perturbative approach from Chapter 5. In particular, we found that there exists a certain critical value of the effective coupling constant, below which the crossover from the EW scaling regime to the KPZ scaling regime does not occur, since the system reaches its stationary EW regime beforehand. We thus assumed the perturbation expansion to be valid for all values of the effective coupling constant that are smaller than the critical one. This assumption was confirmed at a later stage of this thesis via numerical simulations.

Due to the existence of this critical effective coupling constant, the question naturally arises regarding a TUR for values of the coupling constant larger than the critical one, i.e., in the genuine KPZ scaling regime. While a lot of qualitative statements can be made already by referring to the scaling predictions for the KPZ scaling regime from, e.g., [20], we need explicit quantitative expressions for each of the constituents of the TUR. Since the exact results for the entropy production rate and the current in a non-equilibrium stationary state hold for all values of the effective coupling constant, the only constituent still to be evaluated in the KPZ scaling regime is the variance of the spatially averaged height field. To this end we used dynamic renormalization group techniques in Chapter 6 and the correspondence of the KPZ equation to the noisy Burgers equation in one spatial dimension to obtain an explicit approximate expression for its two-point correlation in wavenumber space. We derived expressions for the variance of the spatially averaged height field, both in the transient phase and stationary state of the KPZ scaling regime. Moreover, an approximation to a universal scaling amplitude could be determined analytically to satisfying accuracy from the KPZ equation directly instead of extracting it from a discrete model within the KPZ universality class as in [20]. Although these findings are byproducts of our analysis, they may be of interest on their own.

Combining the results for the TUR in the EW scaling regime from Chapter 5 and in the KPZ scaling regime from Chapter 6 allowed for establishing the TUR for all values of the effective coupling constant smaller and significantly larger than the critical one, which constitutes a further central result.

We continued our study of the TUR for the one-dimensional KPZ equation by performing direct numerical simulations in Chapter 7. For the time-discretization we used a stochastic Heun method reflecting the Stratonovich discretization. The spatial discretization is known to be a more delicate matter. Different discretizations of the non-linearity may lead to significantly different results. This is due to the poor regularity of the KPZ equation (see Appendices 3.A.5 and 5.C).

We tested three different popular discretization schemes via a combined generalized discretization operator. The best results were obtained for the so-called improved discretization of the non-linearity introduced in [116]. The overall agreement between numerical and analytical results was quite satisfying. The relative error between the numerical and theoretical results for the expectation of the spatially averaged height field and its variance would become smaller via a combined increase of the numerical system size amounting to a refinement in spatial resolution, the number of independent ensembles and a decrease of the time-step size. For the entropy production, however, it was found that the numerical scheme systematically underestimated the entropy production by roughly 10%.

Via an analytical calculation we were able to gain a deeper understanding of the interplay between the generalized discretization operator of the non-linearity and the accuracy of the ensuing numerical results. In this way, it could be shown that the best numerical approximation of the entropy production underestimates the theoretical value intrinsically by exactly 10%. On one hand, this finding solidified the confidence in the overall numerical scheme. On the other hand, the observation that a quantity like the entropy production carries an intrinsic numerical error, ought to be of interest in itself and should be kept in mind when performing direct numerical simulations of the KPZ equation. We note, that the above analysis may also be seen as an alternative derivation of the TUR in the weak-coupling limit.

As a final result, we also derived an analytic expression for the thermodynamic uncertainty relation in spatial dimensions greater than two in the linear scaling regime of the d-dimensional KPZ equation in Chapter 8. To this end we extended the dynamic renormalization group approach from Chapter 6 to higher dimensions. It is found, that the TUR in the weak coupling limit exceeds the value of two also for $d > 2$. However, with increasing dimension, the excess decreases. The analysis suggests that the TUR would indeed become saturated for infinite spatial dimension. Since the excess above the saturation value could again be attributed to mode coupling effects of the non-linearity, we concluded that the effective interaction strength of the coupled Fourier modes diminishes with growing spatial dimension in the smooth phase of the KPZ equation.

Concerning future research, the possibilities are plentiful. One interesting question is that of a possible phase transition in the TUR of the one-dimensional KPZ equation when crossing from values of the effective coupling constant below the critical one to values above. Within our analytical approach this cannot be answered, since the dynamic renormalization group applies strictly only for values of the effective coupling parameter significantly larger than the critical one and the region of validity of the perturbation expansion ends at the value of the critical effective coupling parameter.
Staying with the matter of phase transitions, another certainly intriguing topic is that of a higher dimensional thermodynamic uncertainty relation in the rough phase of the KPZ equation. Again, the dynamic renormalization group approach is not feasible due to its fixed-point structure in spatial dimensions greater than two. Two possible alternatives come to mind. One is to employ mode-coupling theory as in, e.g., [70, 133], to obtain expressions for the one- and two-time correlation functions of the TUR. Another approach could be the framework of non-perturbative dynamic renormalization group as introduced in, e.g., [71, 134, 135]. In this framework, however, the renormalization equations seem to be too involved for a purely analytical treatment and thus this approach would have to be carried out numerically from a certain point onward.
A further aspect is the question whether the exact numerical value of the TUR product of non-linear field theories is universal in the sense that a whole class of SPDEs yield the same value of the thermodynamic uncertainty product in the weak coupling limit. For example, it would be of interest to check, whether driven diffusive systems with non-linearities given by even powers of the gradient of the field variable show similar or possibly even the same behavior like the KPZ equation.
Last, but certainly not least, the application of the general formalism from Chapter 4 to, e.g., the Navier-Stokes equation seems very intriguing. For this particular case, however, a first hurdle to overcome is the determination of an explicit expression for a non-equilibrium stationary state probability density functional. To this end, a possible approach could be that of a weak noise approximation as in, e.g., [65, 66, 98, 99, 103]. While certainly cumbersome, the reward in form of a thermodynamic uncertainty relation for turbulence in fluids might very well make up for it.

Bibliography

[1] Oliver Niggemann and Udo Seifert. Field-Theoretic Thermodynamic Uncertainty Relation. *Journal of Statistical Physics*, 178:1142–1174, 2020.

[2] Oliver Niggemann and Udo Seifert. Numerical Study of the Thermodynamic Uncertainty Relation for the KPZ-Equation. *Journal of Statistical Physics*, 182:25, 2021.

[3] Oliver Niggemann and Udo Seifert. The Two Scaling Regimes of the Thermodynamic Uncertainty Relation for the KPZ-Equation. *Journal of Statistical Physics*, 186:3, 2022.

[4] Ken Sekimoto. Langevin Equation and Thermodynamics. *Progress of Theoretical Physics Supplement*, 130:17–27, 1998.

[5] Udo Seifert. Entropy Production along a Stochastic Trajectory and an Integral Fluctuation Theorem. *Phys. Rev. Lett.*, 95:040602, 2005.

[6] Andre C. Barato and Udo Seifert. Thermodynamic Uncertainty Relation for Biomolecular Processes. *Phys. Rev. Lett.*, 114:158101, 2015.

[7] Todd R. Gingrich, Jordan M. Horowitz, Nikolay Perunov, and Jeremy L. England. Dissipation Bounds All Steady-State Current Fluctuations. *Phys. Rev. Lett.*, 116:120601, 2016.

[8] Todd R Gingrich, Grant M Rotskoff, and Jordan M Horowitz. Inferring dissipation from current fluctuations. *Journal of Physics A: Mathematical and Theoretical*, 50(18):184004, 2017.

[9] J.M. Horowitz and T.R. Gingrich. Thermodynamic uncertainty relations constrain non-equilibrium fluctuations. *Nat. Phys.*, 16:15–20, 2020.

[10] L. Peliti and S. Pigolotti. *Stochastic Thermodynamics: An Introduction.* Princeton University Press, 2021.

[11] Udo Seifert. Stochastic thermodynamics: From principles to the cost of precision. *Physica A: Statistical Mechanics and its Applications*, 504:176 – 191, 2018.

[12] Mehran Kardar, Giorgio Parisi, and Yi-Cheng Zhang. Dynamic Scaling of Growing Interfaces. *Phys. Rev. Lett.*, 56:889–892, 1986.

[13] A. Ballestad, B. J. Ruck, M. Adamcyk, T. Pinnington, and T. Tiedje. Evidence from the Surface Morphology for Nonlinear Growth of Epitaxial GaAs Films. *Phys. Rev. Lett.*, 86:2377–2380, 2001.

[14] D. E Wolf and J Villain. Growth with Surface Diffusion. *Europhysics Letters (EPL)*, 13(5):389–394, 1990.

[15] C.A. Tracy and H. Widom. A Fredholm Determinant Representation in ASEP. *J Stat Phys*, 132:291–300, 2008.

[16] C.A. Tracy and H. Widom. Integral Formulas for the Asymmetric Simple Exclusion Process. *Commun. Math. Phys.*, 279:815–844, 2008.

[17] C.A. Tracy and H. Widom. Asymptotics in ASEP with Step Initial Condition. *Commun. Math. Phys.*, 290:129–154, 2009.

[18] Takayasu Iwatsuka, Yohsuke T. Fukai, and Kazumasa A. Takeuchi. Direct Evidence for Universal Statistics of Stationary Kardar-Parisi-Zhang Interfaces. *Phys. Rev. Lett.*, 124:250602, 2020.

[19] S. F. Edwards and D. R. Wilkinson. The surface statistics of a granular aggregate. *Proceedings of the Royal Society of London. A. Mathematical and Physical Sciences*, 381(1780):17–31, 1982.

[20] Joachim Krug. Origins of scale invariance in growth processes. *Advances in Physics*, 46(2):139–282, 1997.

[21] Kazumasa A. Takeuchi. An appetizer to modern developments on the Kardar–Parisi–Zhang universality class. *Physica A: Statistical Mechanics and its Applications*, 504:77–105, 2018. Lecture Notes of the 14th International Summer School on Fundamental Problems in Statistical Physics.

[22] Herbert Spohn. The 1+1 dimensional Kardar-Parisi-Zhang equation: more surprises. *Journal of Statistical Mechanics: Theory and Experiment*, 2020(4):044001, 2020.

[23] C. Jarzynski. Nonequilibrium Equality for Free Energy Differences. *Phys. Rev. Lett.*, 78:2690–2693, 1997.

[24] K. Sekimoto. *Stochastic Energetics.* Lecture Notes in Physics. Springer Berlin Heidelberg, 2010.

[25] Udo Seifert. Stochastic thermodynamics, fluctuation theorems and molecular machines. *Reports on Progress in Physics*, 75(12):126001, 2012.

[26] Vladimir Y. Chernyak, Michael Chertkov, and Christopher Jarzynski. Path-integral analysis of fluctuation theorems for general Langevin processes. *Journal of Statistical Mechanics: Theory and Experiment*, page P08001, 2006.

[27] C. W. Gardiner. *Handbook of Stochastic Methods.* Berlin: Springer, 3rd edition, 2004.

[28] U. Seifert. Stochastic thermodynamics: principles and perspectives. *The European Physical Journal B*, 64(3):423–431, 2008.

[29] Andreas Dechant and Shin ichi Sasa. Current fluctuations and transport efficiency for general Langevin systems. *Journal of Statistical Mechanics: Theory and Experiment*, 2018(6):063209, 2018.

[30] Andreas Dechant and Shin-ichi Sasa. Entropic bounds on currents in Langevin systems. *Phys. Rev. E*, 97:062101, 2018.

[31] R. Chetrite and H. Touchette. Nonequilibrium Markov Processes Conditioned on Large Deviations. *Ann. Henri Poincaré*, 16:2005–2057, 2015.

[32] Timur Koyuk and Udo Seifert. Quality of the thermodynamic uncertainty relation for fast and slow driving. *Journal of Physics A: Mathematical and Theoretical*, 54(41):414005, 2021.

[33] Arnab Pal, Shlomi Reuveni, and Saar Rahav. Thermodynamic uncertainty relation for systems with unidirectional transitions. *Phys. Rev. Research*, 3:013273, 2021.

[34] Yoshihiko Hasegawa and Tan Van Vu. Fluctuation Theorem Uncertainty Relation. *Phys. Rev. Lett.*, 123:110602, 2019.

[35] Alexander Altland and Ben D. Simons. *Condensed Matter Field Theory.* Cambridge University Press, 2 edition, 2010.

[36] Timothy Halpin-Healy and Yi-Cheng Zhang. Kinetic roughening phenomena, stochastic growth, directed polymers and all that. Aspects of multidisciplinary statistical mechanics. *Physics Reports*, 254(4):215 – 414, 1995.

[37] Hiroshi Frusawa. Stochastic dynamics and thermodynamics around a metastable state based on the linear Dean–Kawasaki equation. *Journal of Physics A: Mathematical and Theoretical*, 52(6):065003, 2019.

[38] G. I. Sivashinsky. Nonlinear analysis of hydrodynamic instability in laminar flames–I. Derivation of basic equations. *Acta Astronautica*, 4(11):1177–1206, 1977.

[39] H. van Beijeren, R. Kutner, and H. Spohn. Excess Noise for Driven Diffusive Systems. *Phys. Rev. Lett.*, 54:2026–2029, 1985.

[40] Ernesto Medina, Terence Hwa, Mehran Kardar, and Yi-Cheng Zhang. Burgers equation with correlated noise: Renormalization-group analysis and applications to directed polymers and interface growth. *Phys. Rev. A*, 39:3053–3075, 1989.

[41] David A. Huse, Christopher L. Henley, and Daniel S. Fisher. Huse, Henley, and Fisher respond. *Phys. Rev. Lett.*, 55:2924–2924, 1985.

[42] A. M. Polyakov. Turbulence without pressure. *Phys. Rev. E*, 52:6183–6188, 1995.

[43] Dieter Forster, David R. Nelson, and Michael J. Stephen. Large-distance and long-time properties of a randomly stirred fluid. *Phys. Rev. A*, 16:732–749, 1977.

[44] Mehran Kardar and Yi-Cheng Zhang. Scaling of Directed Polymers in Random Media. *Phys. Rev. Lett.*, 58:2087–2090, 1987.

[45] Stéphane Zaleski. A stochastic model for the large scale dynamics of some fluctuating interfaces. *Physica D: Nonlinear Phenomena*, 34(3):427–438, 1989.

[46] Pierre Le Doussal and Pasquale Calabrese. The KPZ equation with flat initial condition and the directed polymer with one free end. *Journal of Statistical Mechanics: Theory and Experiment*, 2012(06), 2012.

[47] L. Bertini and G. Giacomin. Stochastic Burgers and KPZ Equations from Particle Systems. *Comm Math Phys*, 183:571–607, 1997.

[48] M. Gubinelli and M. Jara. Regularization by noise and stochastic Burgers equations. *Stoch PDE: Anal Comp*, pages 325–350, 2013.

[49] Martin Hairer. Solving the KPZ equation. *Annals of Mathematics*, 178, 2013.

[50] P. Gonçalves and M. Jara. Nonlinear Fluctuations of Weakly Asymmetric Interacting Particle Systems. *Arch Rational Mech Anal*, 212:597–644, 2014.

[51] M. Hairer. A theory of regularity structures. *Inventiones mathematicae*, 198(2):269–504, 2014.

[52] M. Gubinelli and N. Perkowski. KPZ Reloaded. *Commun. Math. Phys.*, 349:165–269, 2017.

[53] M. Gubinelli and N. Perkowski. Energy solutions of KPZ are unique. *J. Amer. Math. Soc.*, 31:427–471, 2018.

[54] Erwin Frey and Uwe Claus Täuber. Two-loop renormalization-group analysis of the Burgers–Kardar-Parisi-Zhang equation. *Phys. Rev. E*, 50:1024–1045, 1994.

[55] Oliver Niggemann and Haye Hinrichsen. Sinc noise for the Kardar-Parisi-Zhang equation. *Phys. Rev. E*, 97:062125, 2018.

[56] Tamás Vicsek and Fereydoon Family. Dynamic Scaling for Aggregation of Clusters. *Phys. Rev. Lett.*, 52:1669–1672, 1984.

[57] Family F. and Vicsek T. Scaling of the active zone in the Eden process on percolation networks and the ballistic deposition model. *J. Phys. A: Math. Gen.*, 18:L75–L81, 1985.

[58] Timothy Halpin-Healy and Yi-Cheng Zhang. Kinetic roughening phenomena, stochastic growth, directed polymers and all that. Aspects of multidisciplinary statistical mechanics. *Physics Reports*, 254(4):215 – 414, 1995.

[59] U.C. Täuber. *Critical Dynamics: A Field Theory Approach to Equilibrium and Non-Equilibrium Scaling Behavior.* Cambridge University Press, 2014.

[60] M. Prähofer and H. Spohn. Exact Scaling Functions for One-Dimensional Stationary KPZ Growth. *Journal of Statistical Physics*, 115:255–279, 2004.

[61] Joachim Krug, Paul Meakin, and Timothy Halpin-Healy. Amplitude universality for driven interfaces and directed polymers in random media. *Phys. Rev. A*, 45:638–653, 1992.

[62] Joachim Krug. 1/f noise for driven interfaces. *Phys. Rev. A*, 44:R801–R804, 1991.

[63] Leonard M. Sander and Hong Yan. Temporal characteristics in nonequilibrium surface-growth models. *Phys. Rev. A*, 44:4885–4892, 1991.

[64] Matthew P. A. Fisher and G. Grinstein. Nonlinear transport and $1/f^{\alpha}$ noise in insulators. *Phys. Rev. Lett.*, 69:2322–2325, 1992.

[65] Hans C. Fogedby. Kardar-Parisi-Zhang equation in the weak noise limit: Pattern formation and upper critical dimension. *Phys. Rev. E*, 73:031104, 2006.

[66] Hans C. Fogedby. Patterns in the Kardar-Parisi-Zhang equation. *Pramana*, 71(2):253–262, 2008.

[67] Michael Lässig. On the renormalization of the Kardar-Parisi-Zhang equation. *Nuclear Physics B*, 448(3):559–574, 1995.

[68] K.J. Wiese. On the Perturbation Expansion of the KPZ Equation. *Journal of Statistical Physics*, 93:143–154, 1998.

[69] Yuhai Tu. Absence of Finite Upper Critical Dimension in the Spherical Kardar-Parisi-Zhang Model. *Phys. Rev. Lett.*, 73:3109–3112, 1994.

[70] M. A. Moore, T. Blum, J. P. Doherty, M. Marsili, J-P. Bouchaud, and P. Claudin. Glassy Solutions of the Kardar-Parisi-Zhang Equation. *Phys. Rev. Lett.*, 74:4257–4260, 1995.

[71] Thomas Kloss, Léonie Canet, and Nicolás Wschebor. Nonperturbative renormalization group for the stationary Kardar-Parisi-Zhang equation: Scaling functions and amplitude ratios in 1+1, 2+1, and 3+1 dimensions. *Phys. Rev. E*, 86:051124, 2012.

[72] Michael Lässig and Harald Kinzelbach. Upper Critical Dimension of the Kardar-Parisi-Zhang Equation. *Phys. Rev. Lett.*, 78:903–906, 1997.

[73] Jin Min Kim. Phase Transition of the Kardar-Parisi-Zhang Equation in Four Substrate Dimensions. *Phys. Rev. Lett.*, 80:888, 1998.

[74] Jin Min Kim. Phase transition of directed polymer in random potentials on 4+1 dimensions. *Physica A: Statistical Mechanics and its Applications*, 270(3):335–341, 1999.

[75] L. Canet and M. A. Moore. Universality Classes of the Kardar-Parisi-Zhang Equation. *Phys. Rev. Lett.*, 98:200602, 2007.

[76] Moshe Schwartz and Ehud Perlsman. Upper critical dimension of the Kardar-Parisi-Zhang equation. *Phys. Rev. E*, 85:050103, 2012.

[77] Yen-Liang Chou, Michel Pleimling, and R. K. P. Zia. Changing growth conditions during surface growth. *Phys. Rev. E*, 80:061602, 2009.

[78] Yen-Liang Chou and Michel Pleimling. Characterization of non-equilibrium growth through global two-time quantities. *Journal of Statistical Mechanics: Theory and Experiment*, 2010(08):P08007, 2010.

[79] Yen-Liang Chou and Michel Pleimling. Kinetic roughening, global quantities, and fluctuation–dissipation relations. *Physica A: Statistical Mechanics and its Applications*, 391(13):3585 – 3593, 2012.

[80] Malte Henkel, Jae Dong Noh, and Michel Pleimling. Phenomenology of aging in the Kardar-Parisi-Zhang equation. *Phys. Rev. E*, 85:030102, 2012.

[81] A.-L. Barabási and H. E. Stanley. *Fractal Concepts in Surface Growth.* Cambridge University Press, Cambridge, 1995.

[82] Giuseppe Da Prato and Jerzy Zabczyk. *Stochastic equations in infinite dimensions.* Encyclopedia of mathematics and its applications; 45. Cambridge Univ. Press, Cambridge, 1. publ. edition, 1992.

[83] Lawrence C. Evans. *Partial differential equations.* Graduate studies in mathematics; 19. American Mathematical Society, Providence, Rhode Island, reprint. with corr. edition, 2002.

[84] Guiseppe Da Prato, Arnaud Debussche, and Roger Temam. Stochastic Burgers' equation. *Nonlinear Differential Equations and Applications NoDEA*, 1(4):389–402, 1994.

[85] Giuseppe Da Prato and Jerzy Zabczyk. *Ergodicity for infinite dimensional systems.* London Mathematical Society lecture note series; 229. Cambridge University Press, New York; Cambridge, 1996.

[86] B. Goldys and B. Maslowski. Exponential ergodicity for stochastic Burgers and 2D Navier-Stokes equations. *Journal of Functional Analysis*, 226(1):230 – 255, 2005.

[87] Dirk Blömker, Minoo Kamrani, and S. Mohammad Hosseini. Full discretization of the stochastic Burgers equation with correlated noise. *IMA Journal of Numerical Analysis*, 33(3):825–848, 2013.

[88] C. Foias, O.P. Manley, R. Rosa, and R Temam. *Navier-Stokes equations and turbulence.* Encyclopedia of mathematics and its applications; 83. Cambridge University Press, Cambridge, 1. publ. edition, 2001.

[89] M. Hairer and J. Voss. Approximations to the Stochastic Burgers Equation. *Journal of Nonlinear Science*, 21:897–920, 2011.

[90] Ivan Corwin and Hao Shen. Some recent progress in singular stochastic PDEs. *Bull. Am. Math. Soc. (N. S.)*, 57(3):409–454, 2020.

[91] Diogo Poças and Bartosz Protas. Transient growth in stochastic Burgers flows. *Discrete & Continuous Dynamical Systems - B*, 23:2371, 2018.

[92] R Kubo. The fluctuation-dissipation theorem. *Reports on Progress in Physics*, 29(1):255–284, 1966.

[93] Hans-Karl Janssen. On a Lagrangean for classical field dynamics and renormalization group calculations of dynamical critical properties. *Zeitschrift für Physik B Condensed Matter*, 23(4):377–380, 1976.

[94] C. De Dominicis. TECHNIQUES DE RENORMALISATION DE LA THÉORIE DES CHAMPS ET DYNAMIQUE DES PHÉNOMÈNES CRITIQUES. *Journal de Physique Colloques*, 37(C1):C1–247–C1–253, 1976.

[95] P. C. Martin, E. D. Siggia, and H. A. Rose. Statistical Dynamics of Classical Systems. *Phys. Rev. A*, 8:423–437, 1973.

[96] David Hochberg, Carmen Molina-París, Juan Pérez-Mercader, and Matt Visser. Effective potential for the massless KPZ equation. *Physica A: Statistical Mechanics and its Applications*, 280(3):437 – 455, 2000.

[97] C. Maes, K. Netocny, and B Wynants. On and Beyond Entropy Production: the Case of Markov Jump Processes. *Markov Processes And Related Fields*, 14:445–464, 2008.

[98] Hans C Fogedby. Nonequilibrium dynamics of a growing interface. *Journal of Physics: Condensed Matter*, 14(7):1557–1569, 2002.

[99] Hans C. Fogedby. Soliton approach to the noisy Burgers equation: Steepest descent method. *Phys. Rev. E*, 57:4943–4968, 1998.

[100] F. Hayot and C. Jayaprakash. Structure functions in the stochastic Burgers equation. *Phys. Rev. E*, 56:227–230, 1997.

[101] W.D. McComb. *The Physics of Fluid Turbulence*. Number 25 in Oxford Engineering Science Series. Oxford University Press, 2003.

[102] Pierre Sagaut and Claude Cambon. *Homogeneous Turbulence Dynamics*. Springer International Publishing AG, 2nd edition, 2018.

[103] Baruch Meerson, Pavel V Sasorov, and Arkady Vilenkin. Nonequilibrium steady state of a weakly-driven Kardar–Parisi–Zhang equation. *Journal of Statistical Mechanics: Theory and Experiment*, 2018(5):053201, 2018.

[104] T. Sasamoto and H. Spohn. Superdiffusivity of the 1D Lattice Kardar-Parisi-Zhang Equation. *Journal of Statistical Physics*, 137:917, 2009.

[105] Massimiliano Gubinelli and Nicolas Perkowski. KPZ Reloaded. *Communications in Mathematical Physics*, 349(1):165–269, 2017.

[106] G. Cannizzaro and K. Matetski. Space–Time Discrete KPZ Equation. *Communications in Mathematical Physics*, 358(2):521–588, 2018.

[107] D. Blömker and A. Jentzen. Galerkin Approximations for the Stochastic Burgers Equation. *SIAM Journal on Numerical Analysis*, 51(1):694–715, 2013.

[108] Dirk Blömker and Minoo Kamrani. Numerical Solution of Stochastic Partial Differential Equations with Correlated Noise. *arXiv e-prints*, page arXiv:1311.2207, 2013.

[109] Victor Yakhot and Z.-S. She. Long-time, large-scale properties of the random-force–driven Burgers equation. *Phys. Rev. Lett.*, 60:1840–1843, 1988.

[110] Victor Yakhot and Steven A. Orszag. Renormalization-Group Analysis of Turbulence. *Phys. Rev. Lett.*, 57:1722–1724, 1986.

[111] Victor Yakhot and Steven A. Orszag. Renormalization group analysis of turbulence. I. Basic theory. *J Sci Comput*, 1:3–51, 1986.

[112] Leslie M. Smith and Stephen L. Woodruff. Renormalization-Group Analysis of Turbulence. *Annual Review of Fluid Mechanics*, 30(1):275–310, 1998.

[113] Tapas Singha and Malay K. Nandy. Skewness in (1+1)-dimensional Kardar-Parisi-Zhang–type growth. *Phys. Rev. E*, 90:062402, 2014.

[114] Enrique Rodríguez-Fernández and Rodolfo Cuerno. Non-KPZ fluctuations in the derivative of the Kardar-Parisi-Zhang equation or noisy Burgers equation. *Phys. Rev. E*, 101:052126, 2020.

[115] B. Derrida, M.R. Evans, and D. Mukamel. Exact diffusion constant for one-dimensional asymmetric exclusion models. *J. Phys. A: Math. Gen.*, 26:4911, 1993.

[116] Chi-Hang Lam and F. G. Shin. Improved discretization of the Kardar-Parisi-Zhang equation. *Phys. Rev. E*, 58:5592–5595, 1998.

[117] Rafael Gallego, Mario Castro, and Juan M. López. Pseudospectral versus finite-difference schemes in the numerical integration of stochastic models of surface growth. *Phys. Rev. E*, 76:051121, 2007.

[118] R. C. Buceta. Generalized discretization of the Kardar-Parisi-Zhang equation. *Phys. Rev. E*, 72:017701, 2005.

[119] A. Greiner, W. Strittmatter, and J. Honerkamp. Numerical integration of stochastic differential equations. *Journal of Statistical Physics*, 51:95–108, 1988.

[120] J. Krug and H. Spohn. Kinetic Roughening of Growing Surfaces. In C. Godrèche, editor, *Solids Far From Equilibrium.* Cambridge University Press, Cambridge, 1991.

[121] Keye Moser, János Kertész, and Dietrich E. Wolf. Numerical solution of the Kardar-Parisi-Zhang equation in one, two and three dimensions. *Physica A: Statistical Mechanics and its Applications*, 178(2):215 – 226, 1991.

[122] Vladimir G. Miranda and Fábio D. A. Aarão Reis. Numerical study of the Kardar-Parisi-Zhang equation. *Phys. Rev. E*, 77:031134, 2008.

[123] Lorenzo Giada, Achille Giacometti, and Maurice Rossi. Pseudospectral method for the Kardar-Parisi-Zhang equation. *Phys. Rev. E*, 65:036134, 2002.

[124] Peter E. Kloeden and Platen Eckhard. *Numerical Solution of Stochastic Differential Equations*. Number 23 in Stochastic Modelling and Applied Probability. Springer-Verlag Berlin Heidelberg, 1992.

[125] Steven A. Orszag. On the Elimination of Aliasing in Finite-Difference Schemes by Filtering High-Wavenumber Components. *Journal of the Atmospheric Sciences*, 28(6):1074–1074, 1971.

[126] C Basdevant, M Deville, P Haldenwang, J.M Lacroix, J Ouazzani, R Peyret, P Orlandi, and A.T Patera. Spectral and finite difference solutions of the Burgers equation. *Computers & Fluids*, 14(1):23–41, 1986.

[127] Marco Baiesi and Christian Maes. Enstrophy dissipation in two-dimensional turbulence. *Phys. Rev. E*, 72:056314, 2005.

[128] Amilcare Porporato, Milad Hooshyar, Andrew D. Bragg, and Gabriel Katul. Fluctuation theorem and extended thermodynamics of turbulence. *Proceedings of the Royal Society A: Mathematical, Physical and Engineering Sciences*, 476(2243):20200468, 2020.

[129] Cesare Nardini, Étienne Fodor, Elsen Tjhung, Frédéric van Wijland, Julien Tailleur, and Michael E. Cates. Entropy Production in Field Theories without Time-Reversal Symmetry: Quantifying the Non-Equilibrium Character of Active Matter. *Phys. Rev. X*, 7:021007, 2017.

[130] Yuting I Li and Michael E Cates. Steady state entropy production rate for scalar Langevin field theories. *Journal of Statistical Mechanics: Theory and Experiment*, 2021(1):013211, 2021.

[131] Horacio S. Wio, Miguel A. Rodríguez, and Rafael Gallego. Variational approach to KPZ: Fluctuation theorems and large deviation function for entropy production. *Chaos: An Interdisciplinary Journal of Nonlinear Science*, 30(7):073107, 2020.

[132] Miguel A. Rodriguez, Rafael Gallego, and Horacio S. Wio. Stochastic entropies and fluctuation theorems for a generic 1D KPZ system: Internal and external dynamics. *Europhysics Letters*, (Accepted Manuscript), 2021.

[133] J. P. Doherty, M. A. Moore, J. M. Kim, and A. J. Bray. Generalizations of the kardar-parisi-zhang equation. *Phys. Rev. Lett.*, 72:2041–2044, 1994.

[134] Steven Mathey, Elisabeth Agoritsas, Thomas Kloss, Vivien Lecomte, and Léonie Canet. Kardar-Parisi-Zhang equation with short-range correlated noise: Emergent symmetries and nonuniversal observables. *Phys. Rev. E*, 95:032117, 2017.

[135] Davide Squizzato and Léonie Canet. Kardar-Parisi-Zhang equation with temporally correlated noise: A nonperturbative renormalization group approach. *Phys. Rev. E*, 100:062143, 2019.

Danksagungen

Zuerst möchte ich Herrn Prof. Dr. Udo Seifert für die Anregung zu dieser Arbeit sowie für die stets hilfreichen Gespräche und daraus resultierenden Denkanstößße danken. Zudem bin ich für die Möglichkeit der mehrmaligen Vorlesungsvertretung dankbar.
Des weiteren danke ich Herrn Prof. Dr. Siegfried Dietrich für seine Bereitschaft zur Übernahme des Mitberichts und Herrn Prof. Dr. Ronny Nawrodt für den Prüfungsvorsitz.
Ein freundliches Dankeschön gebührt auch Frau Anja Steinhauser für ihre Hilfsbereitschaft bezüglich aller Themen rund um die Lehre und sonstiger organisatorischer Belange.
Herrn Manuel Petzi und Herrn Philipp Neufeld danke ich für die gute Zusammenarbeit während der Betreuung ihrer jeweiligen Abschlussarbeiten.
Für das sehr angenehme Arbeitsklima während unserer gemeinsamen Zeit am II. Institut für Theoretische Physik danke ich allen früheren und derzeitigen Mitarbeitern.
Bedanken möchte ich mich auch bei meiner Familie für ihre Unterstützung nicht nur während der Promotion, sondern über mein gesamtes Studium hinweg.

Ehrenwörtliche Erklärung

Ich erkläre, dass ich diese Arbeit selbständig verfasst und keine anderen als die angegebenen Quellen und Hilfsmittel verwendet habe.

Stuttgart, den 02.02.2022 Oliver Niggemann